國立交通大學
土木工程學系
碩士論文

反復扭轉剪力夯實造成之砂土密度及體積變化

Change of Density and Volume in Sand Due to

Cyclic Torsional Shear Compaction

研究生：黃湘銘

指導教授：方永壽 博士

中 華 民 國 一 〇 二 年 八 月

反復扭轉剪力夯實造成之砂土密度及體積變化

Change of Density and Volume in Sand Due to Cyclic Torsional Shear Compaction

研 究 生: 黃湘銘　　　Student：Xiang-Ming Huang

指導教授：方永壽 博士　Advisor：Dr. Yung-Show Fang

國 立 交 通 大 學

土 木 工 程 學 系

碩 士 論 文

A Thesis

Submitted to the Department of Civil Engineering

College of Engineering

National Chiao Tung University

in Partial Fulfillment of the Requirements

for the Degree of

Master of Engineering

in Civil Engineering

August, 2013

Hsinchu, Taiwan, Republic of China

中華民國一○二年八月

反復扭轉剪力夯實造成之砂土密度及體積變化

研究生：黃湘銘　　　指導教授：方永壽 博士

國立交通大學土木工程學系碩士班

摘要

本論文以實驗方法探討反復扭轉剪力夯實造成砂質填土土體內相對密度的改變及沉陷量。本研究使用自行設計建造直徑為 0.45 m 之剪力盤之反復扭剪夯實儀，在土層表面施加靜態垂直應力與反復剪應力。本研究以氣乾之渥太華砂為填土，填入整層高度為 1.5 m 或 5 層高度 0.3 m 之疏鬆砂土。填土初始相對密度為 36 %。本研究採用雷射測距儀來量測土體表面沉陷量，採用密度控制盒埋置於試體內部以量測各點土壤相對密度。根據實驗結果，本研究可獲得以下幾項結論。在最初 5 次的反復扭轉夯實次數 (N = 5)，表面沉陷量明顯地增加。進行反復扭轉剪力夯實 20 次後 (N = 20)，土壤顆粒排列趨於緊密，土體達到主要地表沉陷量，後續扭剪造成之地表沉陷量趨緩。對 5 層厚度各 0.3 m 的土體分別進行反復扭轉剪力夯實後 20 次後，各層之平均體積應變量為 9.77 %、10.53 %、10.37 %、10.05 % 與 10.32 %，顯示反復扭轉剪力夯實對各土層造成之體積變化是相對地均勻。而整層的相對密度值都被成功的增加到大於 70 %。對 5 層土層施作分層夯實，改良土體平均相對密度值為 76.3 %，標準差為 6.2 %。證明此反復扭轉剪力夯實方法成功的將整層土層改良。

關鍵字：土壤夯實；反復扭轉剪力；相對密度；砂；地表沉陷；體積應變

Change of Volume and Density in Sand Due to Cyclic Torsional Shear Compaction

Student: Xiang-Ming Huang   Advisor: Dr. Yung-Show Fang

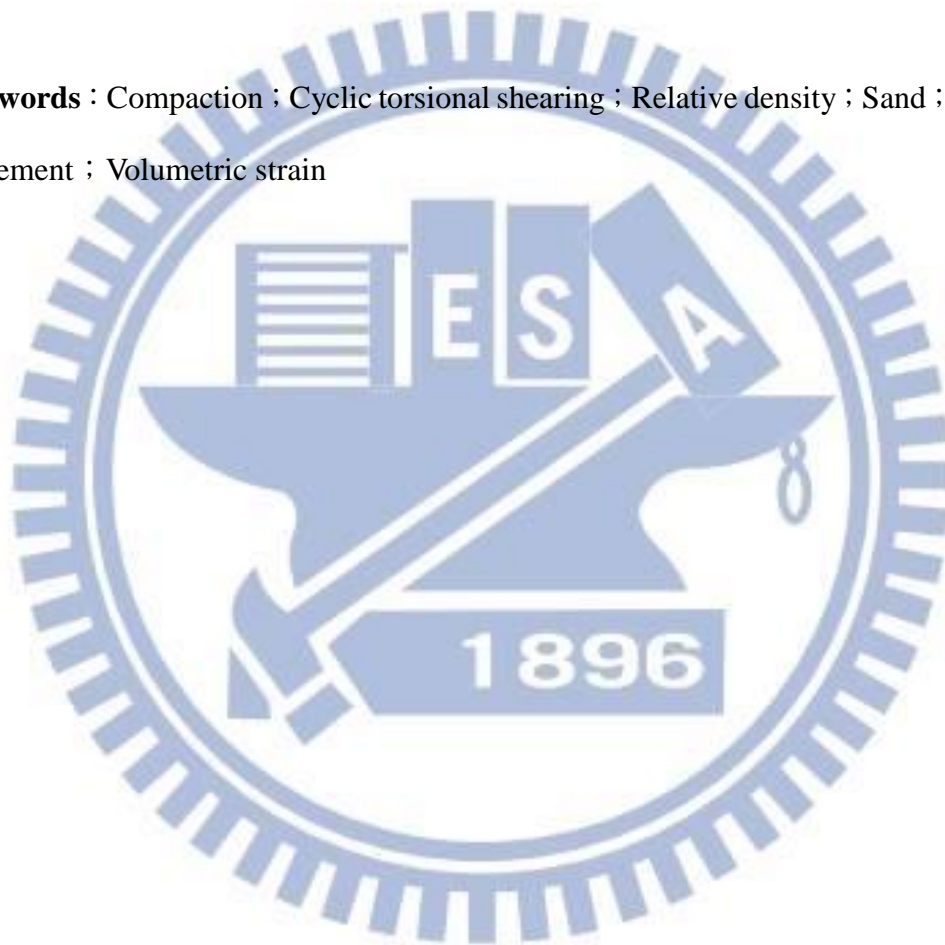Department of Civil Engineering

National Chiao Tung University

Abstract

This paper presents experimental data on the change of volume and relative density in a cohesionless soil mass due to static vertical load and cyclic torsional shearing compaction. A cyclic torsional shearing compactor was with a 0.45 m-diameter circular shearing disc was designed and constructed at National Chiao Tung University. Air-dry Ottawa sand was used as fill material. The initial relative density of the fill was 36 %. The static vertical load and cyclic torsional shearing were applied on the surface of a 1.5 m-thick lift, and then on another specimen with five 0.3 m-thick lifts, with the rotation angles be $\pm 5°$. Surface settlement of the fill was measured with a laser distance meter. Soil density cups were buried in the cohesionless specimen to monitor the distribution of relative density of with depth soil. Based on the test results, the following conclusions were drawn.

In the first 5 cycles of cyclic torsional shearing application, the surface settlement increased significantly. However, after 20 cycles, the major part of settlement was accomplished, soil particle were sheared and reached a densely-packed condition. As a result, it was difficult to increase the surface settlement any further with more cyclic shear application. For shearing compaction on five 0.3 m-thick lifts, after 20 cycles of torsional shearing with the torsional angle of $\theta = \pm 5°$, the average volumetric strain for the lift 1, 2, 3, 4, and 5 was 9.77, 10.53, 10.37, 10.05 and 10.32 %, respectively. It was

clear that the cyclic torsional shearing compaction in each lift was relatively uniform.

Most of the relative density measured in compacted fill were greater than 70 %. The

entire soil body was successfully compacted with cyclic torsional shearing compaction.

For five compacted lifts, the mean relative density was 76.3 % with a standard deviation

of 6.2 %. It was obvious that the entire soil body was successfully compacted with this

ground improvement technique.

Keywords：Compaction；Cyclic torsional shearing；Relative density；Sand；Surface

settlement；Volumetric strain

Acknowledgements

Table of Contents

List of Tables

List of Figures

List of Symbols

C_u = Uniformity Coefficient

D_r = Relative Density

D_{10} = Diameter of Ottawa Sand whose Percent finer is 10%

D_{60} = Diameter of Ottawa Sand whose Percent finer is 60%

e_{max} = Maximum Void Ratio of Soil

e_{min} = Minimum Void Ratio of Soil

f = Frequency

G_s = Specific Gravity

N = Number of Cycle

T = Torque

z = Depth from Surface

σ = Normal Stress

γ = Unit Weight of Soil

τ_{max} = Maximum Torsional Shear Stress

θ = Disc Rotation Angle

ϕ = Angle of Internal Friction of Soil

δ_i = Angle of Interface Friction

δ_{sw} = Angle of Side-Wall Friction

δ_w = Angle of Wall Friction

Chapter 1

INTRODUCTION

In the construction of highway embankments, earth dams, and many other engineering structures, engineers are often required to compact loose soils to increase their densities. The purpose of the compaction operation is to improve the engineering properties of soil such as increasing shear strength, reducing permeability and compressibility. Various techniques had been used to increase the bearing capacity of shallow foundations, to increase the factor of safety against possible slope failure of embankments and earth dams, and to reduce the shrinkage and swelling of soils.

1.1 Objectives of Study

In the past commonly methods used for soil improvement included compaction, vibroflotation, dynamic compaction, compaction sand pile, blasting method, vibro rod, and stone columns. Most of these engineering methods may produce loud noise and vibration during compaction, thus not suitable for use in the metropolitan area. In this study, the cyclic torsional shear compaction was introduced as an alternative construction method. With this compaction method, the relative density of sand could increase from 36% up 85%. This method produced low noise and no low vibration. The purpose of this study is to investigate the change of volume and relative density in the soil mass due to cyclic torsional shear compaction.

1.2 Research Outline

This research utilizes the nonyielding soil bin facility at NCTU and the cyclic torsional shear compactor (CTSC) to investigate the relative density.

Previous studies by Chen (2011) and Liu (2012) indicated that for the CTSC with a 0.3m diameter shear disc could compact the loose sand to achieve a relative density of 70 to 75%. However, the effectively depth of compaction was only 0.15 m-thick. In NAVFAC DM7.2 (US Navy 1982), the compaction thickness of 0.2-0.3 m was generally recommended. To achieve the suggested compaction thickness, a new CTSC with a 0.45m-diameter shearing disc was designed, constructed and test in this study.

Air-dry Ottawa sand was used as fill material. The soil specimen used was 1.5m-long, 1.5m-wide, and 1.5-high.

This paper reports experimental data associated with the volume and relative density change due to the cyclic torsional shearing compaction.

1.3 Organization of Thesis

This thesis was divided into the following parts:

1. Review of past investigations regarding cyclic torsional shear compaction of cohesionless soils (Chapter 2)

2. Description of the National Chiao Tung University soil bin, and cyclic torsional shear compactor (Chapter 3)

3. Soil characteristic and soil density control technique (Chapter 4)

4. Testing procedure (Chapter 5)

5. Experimental results of surface settlement, volume change, and relative density distribution due to compaction (Chapter 6)

6. Conclusions (Chapter 7)

Chapter 2

Literature Review

Das (2010) stated that the soil at a construction site may not always be totally suitable for supporting structures such as buildings, bridges, highways, and dams. For example, in granular soil deposits, the in situ soil may be very loose and perform a large settlement under loading. In such a case, the soil needs to be improved to decrease it deformability.

Sometimes the top soil layers are undesirable and must be removed and replaced with better soils on which the structural foundation can be built. The soil used as fill should be well compacted to sustain the desired structural load. Compacted fills may also be required in low-lying areas to raise the ground elevation for the construction of foundation.

To improve its engineering properties, contractors are generally required to compact the loose soils to increase their unit weights and reducing settlements. Previous studies associated with the compaction-induced effects such as the change of soil density, the volume change in the soil mass and mechanism of soils under compaction are discussed in this chapter.

2.1 Soil Improvement with Densification

Kramer (1996) defined the common soil improvement techniques to mitigate seismic hazards. Soil improvement methods were divided into four categories including, (1) densification techniques (vibrofloatation, vibro rod, dynamic compaction, blasting,

and compaction grouting); (2) reinforcement techniques (stone columns, compaction piles, and drilled inclusions); (3) grouting and mixing techniques (permeation grouting, intrusion grouting, soil mixing, and jet grouting), and (4) drainage techniques. In this thesis, only the densification of cohesionless soil was discussed.

2.1.1 Densification Techniques

Fig. 2.1 shows two of the many possible ways that a system of equal-sized spheres can be packed. The simple cubic packing in Fig. 2.1 (a) is the loosest of the stable arrangements. The dense packings in Fig. 2.1 (b) represent the densest possible state for such a system. A dense packing of soil spheres can be reached by soil densification techniques.

2.1.2 Soil Densification with Vibratory Compactor

D'Appolonia et al. (1969) proposed the vibratory rollers are particularly useful for compacting granular soils. Fig. 2.2 shows the effects of compaction of a 8-ft lift dune sand after five passes by a vibratory roller. The low unit weight that remains in the uppermost zone is due to vibration and lack of confinement in sand. Fig. 2.3 shows the compacted unit-weight profiles for the same dune sand after 2, 5, 15, and 45 roller passes. For field compaction work, the specification requires that the granular soil be compacted to a certain minimum relative density at all depths. Determination of the height of each lift depends on the type of roller and the economic number of passes. The method for determination of the lift height is shown in Fig. 2.4. For soils at all depths to reach a minimum relative density $D_r = 75\%$, the lift thickness should be controlled to be less than 18 inch.

2.2 Cyclic Simple Shear Test

The cyclic simple shear test is a convenient method for determining the shear modulus and damping ratio of soils. It is also a convenient device for studying the liquefaction behavior of saturated cohesion less soils. In Fig.2.5, Airey and Wood (1987) showed the NGI cyclic simple shear apparatus. In the cyclic simple shear test, a soil specimen, usually 20-30 mm high with a diameter of 60-80 mm, is subjected to a vertical effective stress σ_v and a cyclic shear stress τ, as shown in Fig. 2.6. The horizontal load necessary to deform the specimen is measured by the horizontal load cell (Fig. 2.5), and the shear deformation of the specimen is measured by the linear variable differential transformer (LVDT).

2.2.1 Study of Youd

Youd (1972) reported the experimental results regarding the void-ratio reduction of sand due to cyclic simple shearing. Fig. 2.7 shows the gradual densification of sand by repeated shear displacement in a simple shear test. Each cycle of shear straining reduces the void ratio of the soil by a certain amount, although at a decreasing rate. Decrease in volume of the sand, as shown in Fig. 2.7, can take place only if drainage occurs freely. In the figure, after 10,000 cycles, the void ratio of sand was reduced from 0.54 to 0.42. It is obvious from the figure that cyclic shearing is an effect measure to densify the cohesionless soil.

2.2.2 Study of Hsu and Vucetic

Hsu and Vucetic (2004) studied the volume decrease of dry or partially saturated sands subjected to several cycles of cyclic shear strain amplitudes γ_c. If the cyclic shear strain amplitudes γ_{c1} are smaller than a certain threshold value called the volumetric cyclic threshold shear strain γ_{tv} ($\gamma_{c1} < \gamma_{tv}$), their volume will not change. Such cyclic behavior is depicted schematically in Fig. 2.8. In the figure the results of three cyclic strain-controlled direct simple shear (DSS) tests conducted on dry or partially saturated specimens are sketched. The variations of shear strain γ over time t are presented in Fig. 2.8(a). The resulting variations of vertical strain ε_v are presented in Fig. 2.8(b). The relationship between γ_c, the permanent cyclic vertical strain ε_{vc}, and the number of cycles N, is presented in Fig. 2.8(c). The cyclic vertical strain ε_{vc} in Fig. 2.8(c) is taken as ε_v at the end of cycle N, and it is also called the cyclic settlement strain.

It can be seen in Fig. 2.8(c) how below certain γ_{tv} the soil does not settle ($\varepsilon_{vc} = 0$), while above it, it settles significantly ($\varepsilon_{vc} > 0$). Accordingly, the amplitude γ_{tv} represents the boundary between two fundamentally different types of volume change behavior. Below γ_{tv}, the soil particles are not displaced with respect to each other and the soil's mineral skeleton and volume remain practically unchanged during cycling loading. When the soil is subjected to $\gamma_c > \gamma_{tv}$, the particles are displaced with respect to each other irreversibly, resulting in permanent changes of the soil's volume and microstructure. It is clear in Fig. 2.8 that the cyclic shearing is an effective method to reduce the vertical strain of soil, and to densify the soil mass.

2.3 Cyclic Torsional Simple Shear Test

Fig. 2.9 shows the cyclic torsional simple shear device proposed by Ishibashi et al. (1985). In this device, with a hollow cylindrical specimen 71.1 mm in outside diameter,

50.8 mm in inside diameter, and 142.2 mm in height, can be subjected to independent variations of axial stress, inner and outer confining pressure, and torsional shear stress or strain. The device could closely simulates the in-situ stress condition.

2.3.1 Study of Ishibashi et al.

Ishibashi et al. (1985) studied the volume change of a hollow cylindrical Ottawa sand specimen subjected to cyclic torsional shearing in drained conditions. The experiments were conducted under uniform cyclic shear strains and the following conclusions were drawn. In Fig. 2.10, relationships between the induced cyclic volumetric strain the uniform cyclic shear strain γ_{cyc} for a given number of cycle is nearly linear. It is clear in Fig. 2.10 that the volume reduction of the soil specimen is significantly influenced by the cyclic shear strain γ_{cyc} and the number of cyclic shear stress application N.
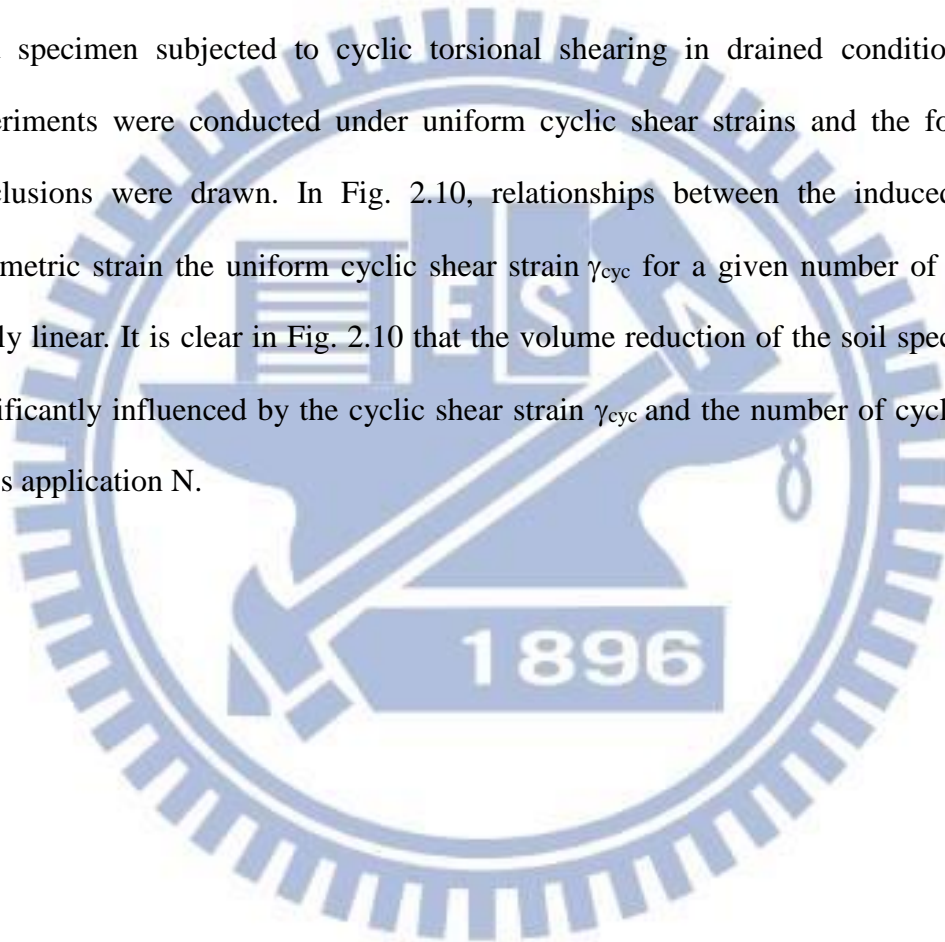
2.4 Densification with Cyclic Torsional Shearing

2.4.1 Study of Yang

Yang (2002) used the disc-shearing instrument (Fig. 2.11(a)) at Chung-Yuan University to study the soil settlement due to cyclic torsional shearing. The diameter of the circular shearing disc was 198 mm. The diameter of the cylindrical sandy specimen was 200 mm, and the height of the soil specimen was 105 mm. The cyclic shear tests were carried out with initial relative densities from 30 % to 50 %, and normal stresses applied from 7 kPa to 150 kPa. One-way and cyclic (N=1) shear stresses were applied on Mailiao sand, Vietnam sand, and Ottawa sand. Fig. 2.11(b) shows the relative density increase ΔD_r due to cyclic shearing (N=1) was about twice that due to one-way shearing.

2.4.2 Study of Ren

Ren (2006) studied the soil densification due to cyclic torsional shearing. The diameter of the sandy specimen was 200 mm and the height was 105 mm. The diameter of the shear disc was 198 mm. Mailiao sand, Ottawa sand and Vietnam sand were tested with an initial relative density of 30 %. Normal stresses of 20, 60 and 100 kPa, and the shear angle 10˚, 20˚, 30˚, 60˚ and 90˚ were used for testing.

Fig. 2.12 showed the relative density of sand increased with increasing number of cyclic shear stress application N. The first 6 cycles of τ_{cyc} application was most effective. Fig. 2.13 showed a greater relative density increment was achieved at a shallow depth. Less D_r increment due to the cyclic shear stress was observed at a deeper depth.

2.4.3 Study of Huang

To reduce the boundary effects due to a small soil tank, Huang (2008) used a 600

mm-diameter, 150 mm-high soil bin. The diameter of the shearing disc was 200 mm, and the (tank diameter)/ (disc diameter) ratio was 3.0.

To include two different grain characteristics, Mailiao sand and Ottawa sand were selected as soil specimen. The initial relative density of the soil sample before shearing was 50 %. The applied vertical normal stress varied 10 to 90 kPa, the cyclic shearing angle varied from 5° to 45°. Fig. 2.14 indicated, for both Mailiao and Ottawa sand, the relative density of sand increased with increasing normal stress σ.

2.4.4 Study of Chen

Chen (2011) presents experimental data on the settlement and relative density change due to cyclic torsional shearing compaction. A new cyclic torsional shearing compactor was designed and constructed at NCTU. The thickness (T) of the soil after compaction was 0.6 m. The initial relative density was 34.5% ± 2.3% and the vertical pressure on the surface loading was 9.2 kPa. Fig. 2.15 showed the soil surface settlements after 1, 2, 5, 10, 20, 30 and 40 cycles of cyclic torsional shearing. It was obvious that the soil settlement increased with increasing number of cycles (N) of torsional shearing.

In the first 2 cycles of torque application, surface settlement increased significantly. However, after N = 20, the major part of settlement has accomplished, soil particles were sheared and reached a densely-packed condition. Therefore, it was difficult to increase the settlement any further with more cyclic shear application.

Fig. 2.16 showed the relative density distributions of the compacted specimen for N = 1, 2, 5, 10, 20 and 40. Test results showed that the density distribution increased with increasing number of cycles of torsional shearing.

In Fig. 2.17, cyclic torsional shearing was applied on the surface of each 0.15m-

thick lift, and the distribution of relative density in Lifts 1 to 4. Test results revealed that the trend of pressure distribution in each 0.15 m-thick lift was similar. The average relative density achieved in each lift was greater than the required value of 70 %~75% (US Navy DM-7 1982).

2.4.5 Study of Liu

Liu (2012) presents experimental data on the settlement, relative density and earth pressure due to cyclic torsional shearing compaction (CTSC). The CTSC was designed and constructed by Chen (2011) at NCTU. The vertical static load (q = 9.2 kPa) and cyclic torsional shearing were applied on the surface of the four 150 mm-thick lifts. Then cyclic shearing was applied with rotation angles of $\pm1°$, $\pm3°$, $\pm5°$, $\pm7°$ and $\pm10°$ for 20 cycles. It was obvious that the soil surface settlement increased with increasing rotation angles (θ) of torsional shearing. A cone penetrometer was used to measure cone resistance q_c with depth in the compacted soil mass. Based on the test results, the following conclusions were drawn.

Fig. 2.18 showed that the variation of surface settlement with the disc rotation angle from 0° to $\pm10°$. After 20 cycles of torsional shearing with the rotation angle of $\theta = \pm10°$ on the surface of the four 150 mm-thick lifts, the average surface settlement was 38.2 mm (volumetric strain = 6.4%). The surface settlement due to the static load q was 19.0mm. The extra surface settlement due to the torsional shearing compaction was about 19.2 mm. It is obvious that the cyclic torsional shearing compaction (static plus cyclic loads) is an effective method to densify loose soil.

Fig. 2.19 showed that relative density distribution for $\theta = 0°$ to $\pm10°$. In the figure, the relative density of compacted fill increased with increasing disc rotation angle θ. With static load q = 9.2 kPa and the lift thickness of 150 mm, after 20 cycles of torsional

shearing with angle θ of ±5°, the relative density achieved was 72 to 84%. The compacted relative density increased with increasing θ angle.

Fig 2.20 showed the distribution of normalized q_c for the compacted fill. For the loose fill, the $q_c/q_{c,loose}$ was 1.0. In Fig 2.20, the cone resistance ratio $q_c/q_{c,loose}$ increased from 4.6 to about 9.0 due to cyclic torsional shear compaction. Test results showed the effect of static vertical load and the cyclic torsional shearing on the cone resistance of soil were quite obvious.

2.5 Requirements of Soil Improvement

ASTM Test Designation D-4253 (2007) provide a procedure for determining the minimum and maximum dry unit weights of granular soils. These unit weights can be used to determine the relative density of soil compacted in the field. The term relative density is commonly used to indicate the in situ denseness or looseness of a granular soil. The relative density of soil is defined as :

$$D_r = \frac{e_{max} - e}{e_{max} - e_{min}} \quad \text{x } 100\% \qquad (\ 2.1\ )$$

where e = in situ void ratio of the soil, e_{max} = void ratio of the soil in the loosest state, e_{min} = void ratio of the soil in the densest state.

Das (2010) reported that the value of D_r may vary from a minimum of 0 % for very loose soils to a maximum of 100 % for very dense soils. Soils engineers qualitatively describe the granular soil deposits according to their relative densities. In-place soils seldom have relative densities less than 20 to 30 %. Compacting a granular soil to a relative density greater than about 85 % is difficult. Lambe and Whitman (1969)

reported that for dense soils the value of D_r was 65 to 85 % as shown in Table. 2.1. In the compaction requirements and procedure, US Navy Design Manual NAVFAC DM-7 (1982) reported that 70 to 75 % relative density can be obtained by proper compaction procedures. For coarse-grained, granaler well-graded soil, vibratory compaction generally is the most effective procedure.

2.6 Maximum Index Density and Unit Weight of Soils Using a Vibratory Table

ASTM Test Designation D 4253 – 93 (2007) provided a test method for determining the maximum index density/unit weight of cohesionless, free-draining soils using a vertical vibrating table.

The maximum index density/unit weight of a given free-draining soil is determined by placing either oven-dried or wet soil in a mold, applying a 2-lb/in^2 (13.78 kPa) surcharge (dead weight) to the surface of soil, and then vertically vibrating the mold, soil, and surcharge (see Fig. 2.21). Without the surcharge on the soil surface, a low unit weight zone might remain in the upper most part of the compacter soil due to lack of confinement in sand. Use either an electromagnetic, eccentric, or cam-driven vibrating table having a sinusoid-like time-vertical displacement relationship at a double amplitude of vertical vibration (peak-to-peak) of about 0.013 in. (0.33 mm) for 8 min at 60 Hz, or 0.019 in. (0.48 mm) for 10 min at 50 Hz. The maximum index density/weight is calculated by dividing the oven-dried mass/weight of the densified soil by it volume (average height of densified soil times area of mold).

Chapter 3

Experimental Apparatus

To investigate the effects of cyclic torsional shear compaction on the relative density of a cohesionless soil mass, the instrumented non-yielding model retaining wall facility at National Chiao Tung University (NCTU) was used. All soil improvement experiments described in this chapter were conducted in the soil bin of the NCTU non-yielding model retaining wall facility. This chapter introduces the soil bin, cyclic torsional shear compactor used for laboratory experiments.

3.1 Soil Bin

The soil bin shown in Fig. 3.1, which was fabricated with steel plates with inside dimensions of 1,500 mm $\times$ 1,500 mm $\times$ 1,600 mm. The model wall in Fig. 3.1. is 1.5 m-wide, 1.6 m-high, and 45 mm-thick. To achieve an at-rest condition, the wall material should be nearly rigid. It is hoped that the deformation of the walls could be neglected when the soil bin is filled with cohesionless soil. In Fig. 3.1, twenty-four 20 mm-thick steel columns were welded to the four sidewalls to reduce any lateral deformation during loading. In addition, twelve C-shaped steel beams were welded horizontally around the box to further increase the stiffness of the box.

Assuming a 1.5 m-thick cohesionless backfill with a unit weight $= 17.1$ kN/m^3, and an internal friction angle $= 41^o$ was pluviated into the soil bin. A 45 mm-thick solid steel plate with a Young's modulus of 210 GPa was chosen as the model wall material. The estimated deflection of the model wall would be only 1.22×10^{-3} mm.

Therefore, it can be concluded that the lateral movement of the wall is negligible.

The end-wall and sidewalls of the soil bin were made of 35 mm-thick steel plates. Outside the steel walls, vertical steel columns and horizontal steel beams were welded to increase the stiffness of the end-wall and sidewalls. If the soil bin was filled with dense sand, the estimated maximum deflection of the sidewall would be 1.86×10^{-3} mm. From a practical point of view, the deflection of the four walls around the soil bin can be neglected.

3.2 Cyclic Torsional Shear Compactor

In previous studies Chen (2011), and Liu (2012) showed that cyclic torsional shearing compaction is an effective method to improve the engineering properties of loose sand. However, since the diameter of the shearing, disc was only 300mm, the compaction was effective for only the relatively-thin top soil layer.

Fig 3.2 shows, under the application of the same vertical pressure p, the settlement S_1 of a full sized footing of width b_1 in a structure will always be greater than the settlement S_2 of a smaller test plate of width b_2. This is because the depth to which vertical pressure of the same intensity p will penetrate is a function of the width b of the footing.

The effective depth of compaction plays an important role in field earthwork. The effects of compaction with a smooth-wheel vibratory roller can easily reach an effective depth of 0.3 m. In this study, the effective depth of compaction was increased by adjusting the diameter of the shearing disc D up to 450 mm.

To enhance an effective soil compactor with less noise, and less vibration, a cyclic torsional shear compactor (CTSC) was developed at National Chiao Tung University (NCTU). To increased effective compaction depth, the diameter of the shearing disc

was enlarge to 450 mm. Fig 3.3. and Fig 3.4. show the cyclic torsional shear compactor. The entire cyclic torsional shear compactor consists of four components, namely: (1) shearing disc; (2) surcharge weight; and (3) torque loading device.   The design and construction of cyclic torsional shear compactor is introduced as follows. The new compactor was designed by the author of thesis.

3.2.1 Shearing Disc

Fig. 3.3 shows the disc diameter is 450 mm, and the steel base disc is 25 mm-thick. To efficiently carry the applied cyclic shear stress from the disc to the soil, 12 radial steel fins were carved on the bottom of the shearing disc as shown in Fig. 3.5. Fig. 3.6 shows the steel radial fin was 3 mm-thick, 6 mm-wide and the wedge angle of the fin was $90°$. Under the vertical pressure, the steel fin would bite into the soil mass. To provide adequate friction between the disc and the soil, the bottom of the shearing disc was covered with a layer of anti-slip frictional material called Safety-Walk (3M). The slip resistant tape was attached to the disc bottom on the fan-shaped areas between the steel fins as shown in Fig. 3.7.

3.2.2 Surcharge Weight

1. Ultimate Bearing Capacity of a Circular Footing

Vesic (1973) proposed three failure modes of shallow foundations, which included general shear failure, local shear failure and punching shear failure. Fig. 3.8 showed a strip foundation with a width of B resting on the surface of soil, and the nature of bearing capacity failures Fig 3.8 illustrated the relationship between the load per unit area q and the foundation settlement for three failure modes. The load per unit area of

foundation at which shear failure in soil occurred was called the ultimate bearing capacity.

Vesic (1973) proposed a relationship for the mode of bearing capacity failure of foundations on resting on sands (shown in Fig. 3.9). The mode of failure was affected by the relative density of sand, depth of foundation embedment and the effective footing width. In this study, the initial relative density of loose sand was 36 % (see Fig. 4.12 in chapter 4), the static was applied on the surface of sand (D_f = 0). To determine the failure mode of the circular loading disc used in this study, with D_r = 36%, D_f = 0, and B* = B = the diameter of shearing disc. In fig. 3.9, the point was located between the punching and local shear failure zone.

Terzaghi (1943) suggested that for a continuous foundation, the failure surface in soil at the ultimate load may be assumed to be similar to that shown in Fig. 3.10. The effect of soil above the bottom of the foundation may be replaced by an equivalent surcharge, $q = \gamma D_f$, where γ is a unit weight of soil and D_f is the depth of embedment of the footing.

Using the equilibrium analysis, Terzaghi expressed the ultimate bearing capacity q_u in the form

$$q_u = c'N_c + qN_q + \frac{1}{2}\gamma BN_\gamma \tag{3.1}$$

where c' = cohesion of soil

γ = unit weight of soil

N_c, N_q, N_r = bearing capacity factors that are non-dimensional and are functions only of the soil friction angle $\emptyset'$.

To estimate the ultimate bearing capacity of a circular foundation, Eq. (3.1) may be modified to:

$$q_u = 1.3c'N_c + qN_q + 0.3\gamma BN_\gamma \tag{3.2}$$

16

In Eq. (3.2), B equals the diameter of foundation. In this study, B equals the diameter of the shearing disc of the CTSC. For the foundations that exhibited the local shear failure mode in soils, Terzaghi suggested the following modification to Eq. (3.2)

$$q_u = 0.867c'N'_c + qN'_q + 0.3\gamma BN'_\gamma \tag{3.3}$$

N'_c, N'_q, and N'_γ, the modified bearing capacity factors, can be calculated by using the bearing capacity of factors equations (for N_c, N_q, N_r, respectively) by replacing $\phi = \tan^{-1}(\frac{2}{3}\tan^{-1}\phi')$. The variation of N_c, N_q and N_r with the soil friction angle ϕ' is given in Table 3.1.

Ho (1999) conducted the direct shear tests to establish the relationship between the internal angle ϕ and unit weight γ of Ottawa sand used for this study, as shown in Fig. 3.11. For the air-pluviated fill, the empirical relationship between soil unit weight γ and ϕ angle was formulated by Chang (2000) as follows

$$\phi = 6.43\gamma - 68.99 \tag{3.4}$$

where

ϕ = angle of internal friction of soil (degree)

γ = unit weight of fill (kN/m^3)

Eq. (3.4) is applicable for γ = 15.45 ~ 17.45 k/m^3 only.

Based on equation (3.4), corresponding to γ = 15.6 kN/m^3 for loose sand, the corresponding internal friction angle ϕ = 31.3˚.

To calculate the ultimate bearing capacity of the circular loading disc eqn. (3.3) was rearranged.

For a circular disc with diameter 0.45m (B = 0.45 m), acting on the surface (q = γD_f = 0) of a cohesionless soil (C' = 0), Equation (3.3) became:

$$q_u = 0.3\gamma BN_\gamma$$

For ϕ = 31.3˚, from Table 3.1, Nγ=1.569, and the ultimate bearing capacity q$_u$ =

3.30 kPa.

ASTM Test Designation D 4253 – 93 (2007) provided a test method for determining the maximum index density/unit weight of cohesionless, free-draining soils using a vertical vibrating table. In this method, a 2-lb/in^2 (13.78 kPa) surcharge (dead weight) was applied to the surface of soil, then vertically vibrating was applied. Without the surcharge vertical stress of 13.78kPa on the soil surface, a low unit weight zone might remain in the upper most part of the compacter soil due to lack of confinement.

In this study, a surcharge pressure of q = 10.35 kPa was applied on the soil surface during the cyclic shearing process. This q = 10.35 kPa was about 3.1times the ultimate bearing capacity of circular disc on loose sand (q_u = 3.30 kPa). This q=10.35 kPa was only about 75% of the surcharge pressure suggested by the ASTM D4235-93. This loading was selected because the shear stress applied was directly proportion to the normal stress applied. A light normal stress would induce a low cyclic shear stress, which might be hard to compact the loose fill. A heavy stress would induce a high cyclic shear stress, which might make it impossible to operate the CTSC test manually. It should be mentioned that the effects of compaction might be strongly affected by the applied surcharge stress. It was assumed that the contact pressure between the load disc and the soil was uniform. For this study, the vertical surcharge pressure of 10.35 kPa was used throughout the investigation.

2. Design of Surcharge Weight

The surcharge weight of the CTSC is loaded by normal loading discs. Table 3.2 shows the mass, thickness, and radius of the normal loading discs available for this study. As shown Fig 3.12, the outside-diameter steel disc is 290 mm. The diameter of the screw rod hole is 21.6 mm, the diameter of the torque shaft hole is 43 mm, and the

diameter of the hoist screw hole is 10.25 mm.

3.2.3 Torque Loading Device

The entire torque loading device consists of two components, namely: (1) Torque shaft and connecting frame, and (2) Torque wrench.

1. Torque Shaft and Connecting Frame

Fig. 3.13 and 3.14 show the dimensions of the torque loading frame at the top of the torsional shear device. The hoist ring was placed on top of the frame so that torsional shear compactor be lifted and lowered by the overhead crane in the laboratory. Two hexagon caps were fixed on the arms of the connecting frame, which enable the torque wrench to be hooked up to the connecting frame. The applied torque was transmitted from the torque wrench, to the connecting frame, then to the torque shaft and shear disc as illustrated in Fig. 3.2

Fig 3.15 (a) and Fig 3.15 (b) the show the dimensions of the extension tube. It can use to connect the CTSC and the connecting frame to lengthen the height of the CTSC. The mass of extension tube is 4.80 kg, which can be the surcharge weight of the CTSC. Fig 3.16 show the CTSC is connected by the extension tube. It can use to compact the deep of the soil bin when the CTSC cannot shear with two torque wrenches.

2. Torque Wrench

Fig. 3.17 (a) shows, the torque wrench is 430 mm long. Fig. 3.17 (b) shows the torque wrench made of stainless steel. During testing, proper wrench length was selected so that no collision between the torque wrench with the sidewall of the soil bin would occur. The torque wrench was attached to the torque loading frame to induce torsional shear on the loose fill.

The digital torque wrench shown in Fig. 3.18 and Fig. 3.19 was used to measure torque applied to the soil. The digital torque wrench has a digital torque value readout.

Accuracy in the clockwise direction was +/- 1%, and the accuracy in the counterclockwise direction was +/- 2%. Readout units included N-m, ft-lb, in-lb and kg-cm. The digital torque wrench made by OLY SCIENTIFIC Equipment Ltd. (model 921/200E) was 530 mm. The maximum operation range is 200 N-m. The square drive is 12.7 mm x 12.7 mm.

Without any normal loading disc, the mass of the CTSC frame is 49.4 kg. Adding 5 pieces of 19.80 kg, 1 piece of 9.6 kg, 1piece of 4.8 kg, 1 piece of 1.55 kg, 3 pieces of 1.05 kg and 1 piece of 0.5 kg loading normal discs, the total mass of the entire CTSC became 168.0 kg.

The weight of the entire CTSC is equal to 1.65 kN. The diameter of the shearing disc is 0.45 m, and the area of the bottom of the shearing disc is 0.159 m^2. The vertical pressure acting on the surface of the fill due to the weight of the CTSC is q = weight / area = 10.35 kPa. For all tests, the vertical pressure of 10.35 kPa, which is equal to the ultimate bearing capacity of the loose sand under circular shearing disc, was used throughout the investigation. It should be mentioned that this thesis is intended to report the preliminary experimental results obtained from a light-weight cyclic torsional shear compactor.

Chapter 4

Soil Characteristics

This chapter introduces the properties of the fill, and the reduction of friction between the soil and lubricated side wall. The control and measurement of soil density distribution in the fill are also introduced.

4.1 Soil Properties

Air-dry Ottawa sand (ASTM C-778) was used throughout this investigation. Table 4.1. showed that physical properties of the soil include G_s = 2.65, e_{max} = 0.76, e_{min} = 0.50, D_{60} = 0.39 mm, and D_{10} = 0.26 mm. Grain-size distribution of the soil is shown in Fig. 4.1. Major factors considered in choosing Ottawa sand as the fill material are summarized as follows.

1. Its round shape, which avoids the effect of angularity of soil grains.

2. Uniform distribution of grain size (coefficient of uniformity C_u = 1.5), which avoids the effects due to soil gradation.

3. High rigidity of solid grains, which reduces possible disintegration of soil particles under loading.

4. Its high permeability, which allows fast drainage and therefore reduces water pressure behind the wall.

4.2 Side-wall Friction

To simulate the field condition of a infinite half space for compaction, the shear stress between the fill and the side walls of the soil bin should be minimized to nearly frictionless. To reduce the friction between sidewall and fill Fang et al. (2004) suggested to use a lubrication layer fabricated with plastic sheets. Two types of plastic sheeting, one thick and two thin plastic sheets, were adopted to reduce the interface friction. All plastic sheets were hung vertically on the side walls before the soil was deposited as shown in Fig. 4.2.

In this study, two thin (0.009 mm-thick) and one thick (0.152 mm-thick) plastic sheets were adopted for the soil improvement experiments. Fig. 4.3 shows the variation of side-wall friction angle δ_{sw} as a function of the normal stress σ_v for the plastic sheet method (1 thick + 2 thin sheeting) reported by Fang et al. (2004). The measured side-wall friction angle with this method was about 7.5°. For all experiments in this paper, the lubrication layers were applied on four side walls of the soil bin.

4.3 Control of Soil Density

4.3.1 Air-Pluviation of Loose Sand

To achieve a uniform soil density in the fill, Ottawa sand was deposited by air-pluviation method into the soil bin. The air-pluviation method had been widely used for a long period of time to reconstitute laboratory sand specimens. Rad and Tumay (1987) reported that pluviation is the method that provides reasonably homogeneous specimens with desired relative density. Lo Presti et al. (1992) reported that the pluviation method could be performed for greater specimens in less time.

Das (2010) suggested that, for granular soil deposits, the relative density D_r of 15~50% is defined as loose, $D_r = 50~70\%$ is defined as medium, and $D_r = 70~85\%$ is defined as dense. For the air-pluviation method, Fig. 4.4 shows the soil hopper let the sand flow through a calibrated slot opening at the lower end. A picture of the soil pluviating processes is shown in Fig. 4.5. To achieve a loose fill, Chen (2003) adopted the drop height of 1.0 m and hopper slot opening of 15 mm. In this study, the drop height of 1.0 m and the hopper slot-opening of 15 mm were also selected to achieve the loose fill. In Fig. 4.6, under such a condition, Ho(1999) indicated that the expected relative density of soil was about 35%.

4.3.2 Measurement of Soil Density

To observe the distribution of soil density in the soil bin, soil density cups were made. The soil density cup made of acrylic is illustrated in Fig. 4.7. The cylindrical cup wall was only 10 mm-high, so that the shear deformation and volume reduction could occur in the cup during testing. A picture of the soil density cup is shown in Fig. 4.8. During the preparation of the 1.5 m-thick loose soil specimen, density cups were buried in the soil mass at different elevations and different locations in the fill as shown in Fig. 4.9 and Fig. 4.10. After the loose soil had been filled up to 1.5 m from the bottom of the soil bin by air-pluviation, density cups were dug out from the soil mass carefully. Fig. 4.11 shows the mass of the cup and soil in the cap was measured with an electrical scale.

For a 1.5 m-thick air-pluviated Ottawa sand layer, the distribution of soil density with depth is shown in Fig. 4.12. For the loose sand, the mean unit weight γ is 15.6 kN/m^2, the mean relative density is $D_r = 36$ % with the standard deviation of 2.0 %. Das (2010) suggested that for the granular soil deposit with a relative density 15% $\leq D_r \leq$

50% is defined as loose sand. The loose relative density $D_r = 36$ % achieved by the air-pluviation method is this study (Fig. 4.12.) was quite loose and uniform with depth.
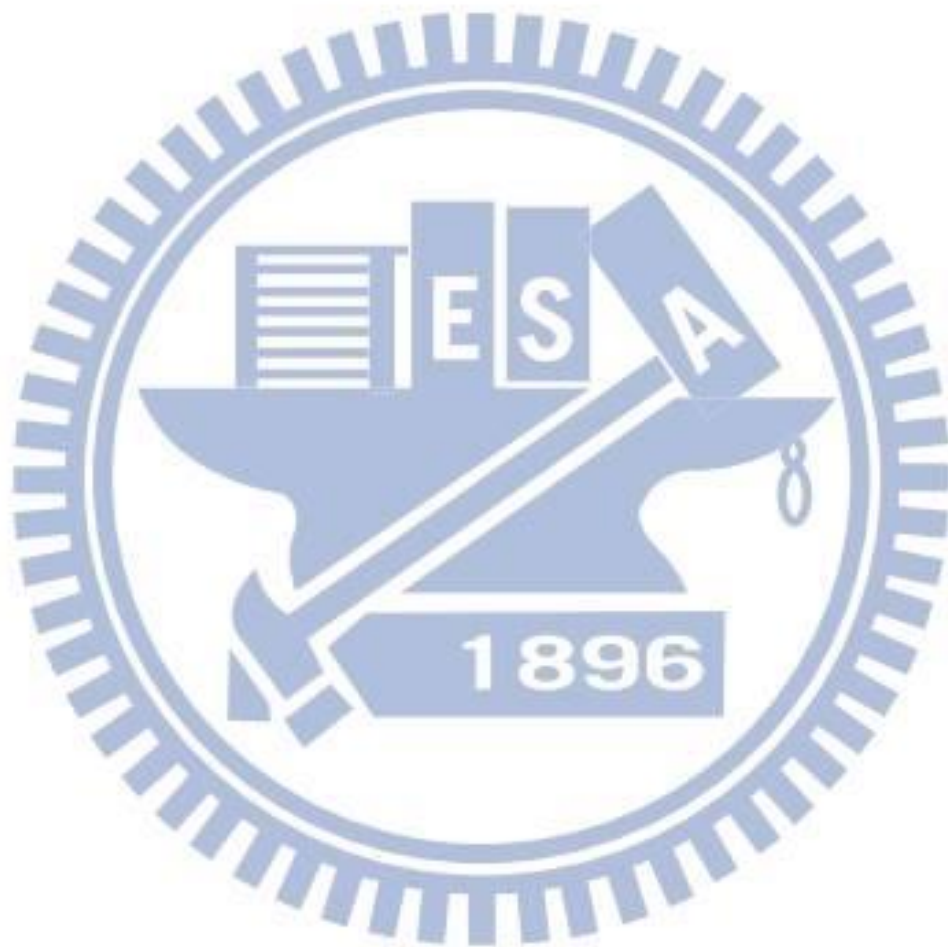
Chapter 5

Testing Procedure

The procedure to conduct the cyclic torsional shear test is introduced in this chapter. The testing procedure can be divided into three parts: (1) specimen preparation; (2) application of vertical static load; and (3) application of cyclic torsional shearing. These parts will are illustrated in the following sections with pictures.

5.1 Specimen Preparation

Fig. 5.1 shows air-dry Ottawa sand in the soil storage. The soil was shoveled from the soil storage to the sand hopper, and the mass of the fill was measured with an electrical scale (Fig 5.2). Fig. 5.3 shows the sand hopper was lifted by the overhead crane in the laboratory. Fig. 5.4 shows Ottawa sand was deposited by air-pluviation method into the soil bin. To achieve the loose backfill, the drop height was controlled to be 1.0 m and the hopper slot-opening of 15 mm were selected. The 1.0 m-long rope next to the hopper was used to control the drop distance. Fig. 5.5 (a) and (b) show portable ladders were placed on top of the sidewalls, and a bridge board was placed between the ladders. Throughout the test, the operator stayed on the bridge board to avoid any unexpected surcharge on the soil specimen.

Fig. 5.6 shows the leveling of the pluviated soil surface by the student with a brush. Fig. 5.7 shows density cups were buried in the soil mass at different elevations in the fill. Fig. 5.8 shows how check the density cup horizontal with a bubble level. The empty eight density cups were placed on the surface of the soil layer. The air-pluviation of soil

and density cup placement operations were repeated unit a fill thickness T = 1.5 m was reached.

5.2 Application of Vertical Static Load

The procedure to apply the vertical static load on top of the air-pluviated loose sand is introduced. The cyclic torsional shear compactor (Fig. 3.4) used to apply static load has a footing diameter of 0.45 m and the vertical static load q = 10.35 kPa. Fig. 5.9 (a), (b), (c), and (d) illustrates the loading pattern on soil surface. For applying four times of vertical static load, the 3x3 loading formation is based four points A, B, C, and D.

Fig. 5.10 shows the CTSC was hoisted with overhead crane into the soil bin. Fig. 5.11 shows the vertical static load was applied on the loose sand with four different loading pattern shown in Fig. 5.9 (a) to (d). The combination of static load footprint caused a uniform surcharge on the soil structure. Fig. 5.12 shows the soil surface of the 4 patterns of vertical static load.

5.3 Application of Cyclic Torsional Shearing

In this study, the cyclic torsional shear was applied on the soil surface with a rotation angle of +5° to -5°. Fig. 5.13 show that applied the CTSC with the rotation angle controller on the loose fill. In Fig. 5.14, 5.15 and 5.16, with a rotation angle indicator and controller, the rotation angle of the shearing disc could be effectively controlled to be from 0° to +5° and -5°. The application of cyclic torsional shear to loose sand is shown in Fig. 5.17.

For the test with N = 20, the soil surface after the torsional shear for the 3x3 loading formation (Fig. 5.9 (a)) for the first 5 cycles is shown in Fig. 5.18 (a). To prevent disc penetration due to continuous shearing at the same location, the shearing was moved to

another 3x3 formation (Fig. 5.9 (b)) for N = 6 to 10. The soil surface after shearing

compaction for N = 6 to 10 is shown in Fig.5.18 (b). Fig. 5.18 (c) and (d) show that the

soil surface after the loading pattern for N = 11 to 15 (Fig. 5.9(c)) and N = 16 to 20 (Fig.

5.9 (d)).

To determine the relative density of soil in the cup, Fig. 5.19 shows the density

cup was carefully dug out of compacted soil mass. Fig. 5.20 (a) to (c) show the scraping

of soil toward the edge of the density cup with a spatula. Fig. 5.21 shows the brush

away of soil particles from the base plate of cup. Soil mass in the cup was measured

with an electrical scale and the relative density of the compacted soil could be

calculated.
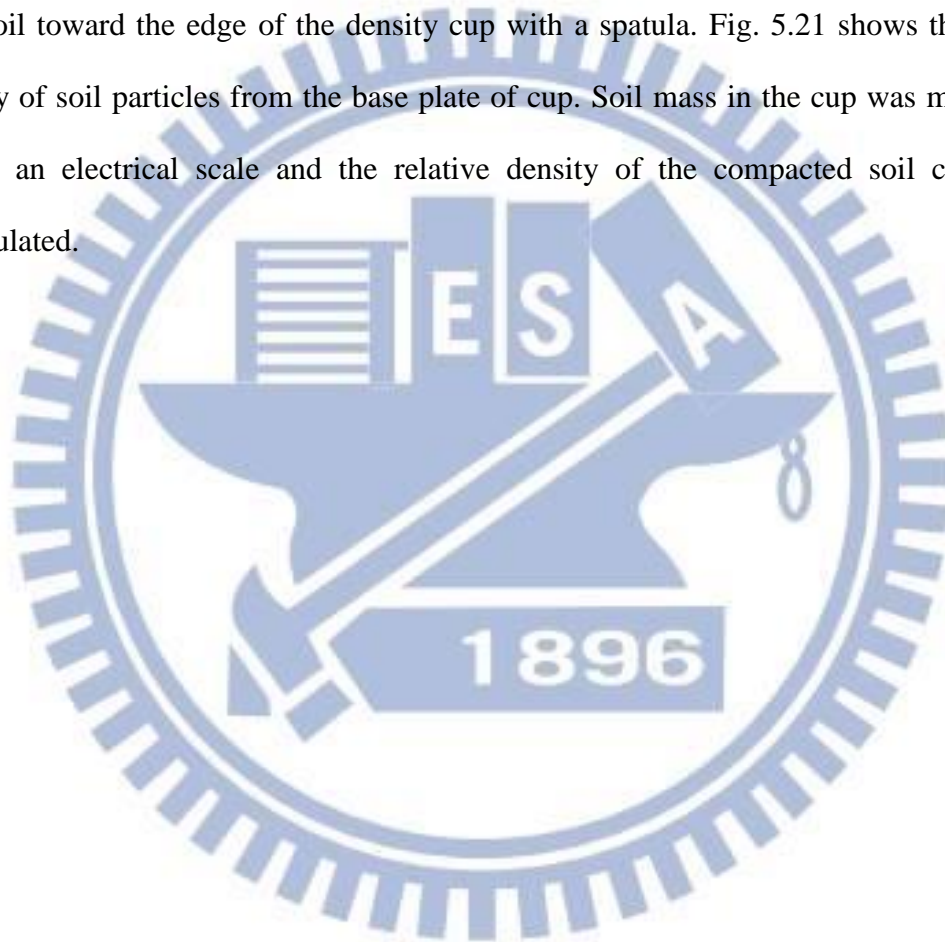
Chapter 6

Test Results

This chapter showed experimental results regarding soil densification due to static load and cyclic torsional shearing. The vertical static load applied of the fill was q = 10.35 kPa. The cyclic torque T and shear stress τ_{max} applied on the soil surface was measured and calculated, respectively. Experiments were first conducted on the surface of a 1.5 m-thick soil lift. The surface settlement S and relative density D_r distribution of the soil layer due to the static load and cyclic torsional shear were measured. The rotation angle θ of the shearing disc varied between +5° and -5° , and the number of loading cycle N varied from 1 to 40. In the second part of this chapter, to obtain a soil mass with a relative density greater than 70 to 75%, experiments were applied on the fill for five 0.30 m-thick lifts. Each lift was compacted with the cyclic torsional shear compactor with q = 10.35 kPa, θ = ±5° , and N = 20.

6.1 Static Load Tests on a 1.5 m-thick Lift

To separate the densification effects due to static and cyclic loadings, in this section, the surface of a 1.5 m-thick soil lifts was compressed with the static vertical loading q only. Effects of soil densification such as the volume change, change of relative density in the compressed fill were investigate.

For this test, a 1.5 m-thick lift was prepared by air-pluviation method. Fig 6.1 (a) and (b) showed that the density cups were buried in the soil mass at different elevations and locations in a 1.5 m-thick fill. Fig 6.2 showed that measure points A to I for surface

settlement. The surface settlements of a 1.5 m-thick compressed soil lift due to the static load of the compactor were investigated. The initial relative density of the loose fill was 36 ± 2% (see Fig. 4.12.) The applied static normal stress was q = 10.35 kPa. To achieve a uniform settlement, the vertical loading was applied on the surface with four different 3x3 formations as indicated in Fig. 5.9.

6.1.1 Volume Change Due to Static Load

Fig. 6.3 showed the settlement measurement was carried out with the laser distance meter placed between two steel beams. The surface settlements were measured at measure at points A to I indicated in Fig 6.2. Fig. 6.4 (a) showed that surface settlement of Lift1 due to static load, the minimum and maximum values were 14.1 mm and 17.4 mm. The average of surface settlement was 15.4 mm.

To express the dimensional volume change characteristics, the volume change data was normalized by dividing the volume change ΔV by the original volume V_0 to obtain the volumetric strain ε_v. The fill in the soil bin does not allow any lateral deformation. Only vertical compression was allowed for volume change. The horizontal cross-section of soil mass was kept a constant A. The volumetric strain ε_v of the soil mass is defined as:

$$\varepsilon_v, \% = \frac{\Delta V}{V_0} \times 100 = \frac{\Delta H \times A}{H_0 \times A} \times 100 = \frac{\Delta H}{H_0} \times 100 \qquad (6.1)$$

Fig. 6.4 (b) showed the volumetric strain of Lift 1 due to static loading. The induced volumetric strain ε_v was about 1.02 %. It is obvious that static vertical loading is an effective method to compress the loose fill. To limit the scope of thesis, only the vertical stress q = 10.35 kPa was used throughout this study.

6.1.2 Relative Density after Static Load

To investigate the relative density distribution in the compressed fill, density cups were buried in soil mass at different elevations and locations as shown in Fig. 6.1. (a) and (b). For the un-compacted loose soil, the initial relative density was about 36 % (see Fig 4.12). Fig. 6.5 showed the distribution of relative density with depth due to the application static vertical load = 10.35 kPa on the 1.5 m-thick lift. The segmental line was obtained by connecting data point closet to the average D_r for at the depth. It is obvious show that the relative density increase at the top of the lift. The relative density increase was most apparent in the upper 0.45m of the lift, was equal to the diameter of the shearing disc. However, in the lower part the lift the relative density did not enough to reach the target value of D_r = 70 to 75 % required by NAVFAC DM-7 (US Navy 1982).

6.1.3 Relative Density Increase Ratio

To investigate the effects of the cyclic torsional shear compaction, the relative density increment $\Delta D_r = D_{r,N} - D_{r,loose}$ is defined, where $D_{r,N}$ = the relative density due to compaction with N cycles of shearing, $D_{r,loose}$ = the relative density of loose sand. Fig 6.6 (a) showed that the distribution of relative density increment due to static load with depth. In the figure, near on the top of the fill, the relative density increased significantly. Little D_r increase was observed near the bottom of the 1.5 m-thick fill.

To study the effects due to cyclic torsional shearing compaction, a new index was defined in this section. The relative density increment was normalized by the relative density of loose sand. The Relative Density Increase Ratio, RDIR, was defined as:

$$\text{RDIR} = \frac{\Delta D_r}{D_{r,loose}} = \frac{D_{r,N} - D_{r,loose}}{D_{r,loose}} \qquad (6.2)$$

where $D_{r,loose}$ = relative density of loose sand, $D_{r,N}$ = relative density of soil after N cycles of shearing compaction.

NAVFAC DM-7 (1982) reported that the relative density of 70% to 75% can be obtained by proper compaction procedures. In this study, the initial relative density of the loose fill is 36% (see Fig 4.12). Based on Eqn. (6.2), the target of range of soil improvement corresponding to D_r = 70% and 75 % would be 0.94 to 1.08, respectively, the RDIR due to static load was far from the required relative density increase ratios.

6.2 Cyclic Torsional Shear Compaction on a 1.5 m-thick Lift

In the experiments, the surface of a 1.5 m-thick single soil lift was first compressed with the static vertical load (dead-load of the compactor), and then compacted with cyclic torsional shearing. The effects of soil densification were demonstrated with the surface settlement and relative density change of the compacted fill.

6.2.1 Measurement of Applied Torque

Fig. 6.7 showed the torque applied on the soil surface was measured with a digital torque meter. Fig 6.8 showed that relationship between the measured torque T' and applied torque T. Fig 6.9 showed the difference between the CTSC with extension tube or without extension tube. For the rotation angle θ of shearing disc changing from +5 ° to -5° , the torques measured at N = 1, 5, 10, 15, and 20 were shown in Fig. 6.10, 6.11, and 6.12, respectively. In Fig.6.8, for N = 1 the applied torque varied between 67.8 to -65.8 N-m. In Fig. 6.12 (b), for N = 20 the applied torque varied between 69.7

31

to -70.2 N-m. Fig 6.13 showed the applied torque T as a function of the number of cycle of cyclic torsional shearing. Test results indicated that the applied torque did not change with increasing number of shearing cycles. Test Results also indicated that the application extension tube (see Fig. 6.5 (b)) did not affect the transmission of torque the torque loading device to the shearing disc.

Fig. 6.14 showed the how to determine the maximum torsional shear stress τ_{max} at the edge of the shearing disc due to the applied torque T. A linear distribution of shear stress from the center to the edge of the disc was assumed. Fig. 6.15 showed the maximum shear stress with increasing number of cycle of torsional shearing.

6.2.2 Volume Change Due to Cyclic Torsional Shear Compaction

Fig 6.16 showed that, after the application of the static loading, cyclic torsional shear was applied on the surface of soil fill with the 3x3 formation for N = 1, 2, 3, 4, 5, 10, 15, 20, 30, 40. The applied vertical stress was 10.35 kPa. The rotation angle of the shearing disc varied between +5° to-5°. The diameter of the shearing disc was 0.45 m. The cyclic torsional shear was applied on the 3x3 loading pattern. Fig. 6.17 (a) showed the surface settlement after the first cycle of torsional shearing application. The measured surface settlement varied from 17.6 to 21.6 mm, the average value of surface settlement was 19.4 mm. Fig. 6.26 (a) showed the surface settlement after 40 cycles of cyclic torsional shearing application. The measured surface settlement varied from 34.3 to 39.8 mm, and the average value was 37.4 mm. The extra settlement due to the cyclic torsional shearing compaction was about 22 mm, which was more than the settlement due to static vertical loading. Fig 6.27 (a) show the measured surface settlement of the 1.5 m-thick fill after the application cyclic torsional shearing cycles of 1, 2, 3, 4, 5, 10,

15, 20, 30 and 40 cycles. In the figure, the surface settlement increased with increasing number of τ_{max} application. Fig. 6.28 (a) showed the variation of surface settlement from 19.4 to 37.4 mm with increasing value from static load to N = 40.

Fig 6.17 (b) showed the volumetric strain after the first of cycles of torsional shearing application. The volume change was normalized by the initial soil volume by Eq. (6.1), the value of the volumetric strain due to the first cycle of τ_{max} varied from 1.17 % to 1.44%, the average value was 1.29 %. Fig. 6.26 (b) showed the volumetric strain after 40 cycles of varied from 2.28 % to 2.65 %, the average value was 2.49 %. Fig 6.27 (b) showed the volumetric strain of the 1.5 m-thick fill after application of cycle shearing for 1, 2, 3, 4, 5, 10, 15, 20, 30 and 40 cycles. In the figure, the volumetric strain increased with increasing number of cycles of cyclic torsional shearing. Fig 6.28 (b) showed the variation of surface settlement and volumetric strain with number of cycle N of shearing. It should be mentioned that, for 1.5 m-thick soil fill, the densification due to shearing compaction occurred only at the upper most part of the soil mass. Little volume change occurred at the lower part of the fill. Therefore, the volumetric strain of the entire soil body may not be very significant.

In Fig 6.28 (a), in the first 5 cycles of cyclic torsional shearing application, the surface settlement was increased significantly. However, after 20 cycles, the major part of settlement was accomplished, soil particles were sheared and reached a densely-packed condition. As a result, it was difficult to increase the surface settlement any further with more cyclic shear application. Thus, N = 20 may be the optimal number for cyclic torsional shearing construction.

6.2.3 Relative Density Distribution after Change Due to Surface Compaction

Fig 6.29, 6.30, 6.31 showed the distribution of relative density due to cyclic torsional shearing for N = 5, 10 and 20, respectively. It is clear in these figures, the soil density increase due to static load and shearing compaction was most obvious in the upper of the lift. There was little density increase at the bottom of the 1.5 m-thick lift. To achieve the required relative density D_r = 70 to 75 %, for the entire soil mass, several strategies were proposed: (1) enlarging the diameter of shearing disc D (to influenced depth); (2) reducing the lift thickness of fill layers, (for example, from T = 1.5 m to T = 0.3 m); (3) increase the applied torque T and the cyclic torsional applied shear stress τ_{max} accordingly.

Fig. 6.32 showed the distribution of relative density after the application of cyclic torsional shearing for N = 0 (static load), 5, 10, 20. In the figure, the relative density of the compacted fill increased with increasing number of cycles of torsional shearing application. The US Navy design manual (NAVFAC DM-7.2 1982) described that for coarse-grained, granular well-graded soils, 70 to 75 % relative density can be obtained by proper compaction procedures. In this study, the range D_r = 70 to 75 % is selected as the minimum required relative density. In Fig. 6.31, N = 20 was selected as suggested by Fig. 6.28 (a), the corresponding effective-depth of compaction would be about 0.30 m. The effective depth of compaction and the the number of cycles of compaction during construction could be reduced by properly adjusting the applied rotation angle θ, and the normal load q. Further study should be carried out regarding these factors.

6.2.4 Relative Density Increase Ratio

Fig 6.33 (a), 6.34 (a), and 6.35(a) showed that the distributions of the relative density increment with depth after cyclic compaction for N = 5, 10 and 20, respectively.

In these figures, the relative density increment ΔD_r observed near the top of the fill were greater than that near the bottom. Fig 6.36 (a) showed that the distributions of the relative density increment ΔD_r with depth for various number of shearing cycles. In Fig. 6.33 (a) for N = 5, at the depth z = 0.3 m, the relative density increment ΔD_r after 20 cycles of cyclic torsional shearing compaction was 22 to 28 %. These values were less than the required relative density D_r = 70 to 75 %. However, after 20 cycles of shearing application, in Fig.6.35 (a), the relative density of compacted soil reached the required values. Thus test results indicated that cyclic torsional shearing was an effective method for compacting the upper 0.3 m fill.

Fig. 6.33 (b), 6.34 (b), and 6.35 (b) showed that the distribution of the relative density increase ratio with depth after cyclic torsional shearing compaction. On the top of lift (depth = 0 to 0.3m), the ratio reached the range of RDIR = 0.94 to 1.08. This means that, the relative density of the loose fill must increase about 94 to 108 % to reach the required state. In Fig. 6.35 (b), after 20 cycles of shearing loading, the RDIR varied from 0.94 to 1.03.   Fig. 6.36 showed that at different depth, that RDIR mostly increased with increasing number of cycles of shearing compaction.

6.3 Compaction on Five 0.30 m-thick Lifts

In the field, it is often necessary to compact the entire soil mass to a requirement minimum relative density. In this study, a 1.5 m-thick fill was accomplished by compacting five 0.30 m-thick lifts with the cyclic torsional shear compactor (CTSC). The applied vertical load q was 10.35 kPa, and the number of cycle shear stress application N was 20.

6.3.1 Compaction of Lift One

Fig. 6.37 illustrated the thickness of soil fill was 0.3 m and soil density cups were buried at different elevations in Lift 1. Fig. 6.38 showed the surface settlement and volumetric strain after the application of the static load on lift 1. In Fig. 6.38 (b), the minimum and the maximum of volumetric strain of the soil were 4.4 and 7.6 %, and the average value was 5.9 %. Fig. 6.39 shows the surface settlement and volumetric strain after 20 cycles of shearing compaction. In Fig. 6.39 (b), the minimum and the maximum of the volumetric strain were 8.9 and 11.3 %, and the average value was 9.8%. It apparently indicated that cyclic torsional shearing compaction is an effective method to compact the soil in Lift 1. The extra volumetric strain due to the cyclic torsional shearing compaction on Lift 1 was 3.9 %. Test results indicated that static compression alone was not sufficient to compact the soil fill.

The distribution of relative density after 20 cycles of shearing compaction was shown in Fig. 6.40. After the static compression and cyclic torsional shearing compaction, the relative density increased significantly. The relative density in Lift 1 increased from about 36 % values mostly to above 70 %.

Fig. 6.41 showed the relative density increment and relative density increase ratio after 20 cycles of shearing compaction. Fig. 6.41 (a) showed the relative density increment successfully increased reached the target zone (for $D_r = 70 \sim 75\%$)

6.3.2 Compaction of Lift Two

Fig. 6.42 showed soil density cups were buried at different elevations in lifts 1 and 2. Both lifts were compacted on the surface with the CTSC. Fig. 6.43 (a) and Fig.6.44 (a) showed the accumulated settlement after static load and cyclic torsional shearing compaction, respectively. In Fig 6.44 (b), the accumulated volumetric strain after 20

cycles of shearing compaction range from 9.8 to 11.4 %, the average volumetric strain was 10.5 %.

Fig. 6.45 showed that distribution of relative density with depth after 20 cycles of shearing compaction on the top of lift 2. In the figure, the relative density in the lift 2 obviously reached the target zone of $D_r = 70$ to 75 %. In the two 0.3 m-thick compacted lifts, most of the measured relative densities were above to 70 %. The relative density increment ΔD_r and relative density increase ratio RDIR after 20 cycles of shearing compaction on the top of lift 2 were shown in Fig. 6.45 (a) and (b). Test results indicated that cyclic torsional shear compaction was an effective method to compacte the cohesionless soil fill.

6.3.3 Compaction of Lift Three

Fig. 6.47 showed soil fill and soil density cups buried at different elevations in lifts. After static load and shearing compaction on the surface of Lift 3, the accumulated settlement and the volumetric strain were shown in Fig. 6.48 and Fig. 6.49. The accumulated volumetric strain after 20 cycles of shearing compaction on Lift 3 varied from 9.4 to 11.0 %.

Fig. 6.50 illustrated the distribution of relative density with depth after 20 cycles of shearing compaction on Lift 3. In the figure, the measured relative density values were mostly above to 70 %. Some of the relative densities measured near the top of each lift were even greater than 80 %. Fig. 6.51 (a) and (b) showed the variation of relative density increment and relative density increase ratio with depth. In Fig 6.51 (a) and (b), the measured values were mostly above the shaded target zone, especially the values measured near the top of each lift.

6.3.4 Compaction of Lift Four

Fig. 6.52 showed the soil density cups buried in lifts 1 to 4. After the static load and cyclic shearing compaction on the surface of each lift, the accumulated settlement and the volumetric strain were shown in Fig. 6.53 and Fig. 6.54. Fig. 6.54 (b) showed the accumulated volumetric strain after 20 cycles of shearing compaction varied from 9.54 to 10.7 %.

The distribution of the relative density with depth after 20 cycles of shearing compaction were applied on top of lift 1 to 4 were shown in Fig. 6.55. In the figure, the most of the relative densities were above 70 %. The distributions of ΔD_r and RDIR with depth were shown in Fig. 6.56 (a) and (b).

6.3.5 Compaction of Lift Five

Fig. 6.57 showed the density cups buried at different elevations in lifts 1 to 5. After static compression and cyclic compaction on the surface of each lift, the accumulated settlement and the volumetric strain were shown in Fig. 6.58 and Fig. 6.59. For the five 0.3 m-thick compacted soil lifts, the accumulated settlements varied from 147.4 mm to 166 mm. The average settlement was 154.8 mm. In Fig. 6.59 (b), the accumulated volumetric strain varied from 9.84 % to 11.0 %, the average value was 10.3 %. In Fig. 6.39 (b), Fig 6.44 (b), Fig 6.49 (b), Fig. 6.54 (b) and Fig 6.59 (b), the average volumetric after cyclic shearing on top of lift 1, 2, 3, 4 and 5 strain were 9.77 %, 10.53 %, 10.37 %, 10.05 % and 10.32 %,respectively. It indicated that the volume change due to the cyclic torsional shearing compaction on each lift was quite uniformly.

Fig. 6.60 showed that distribution of relative density with depth after 20 cycles of shearing compaction on lift 5. At this stage, the cyclic shearing compaction for the entire soil body was completed. In Fig 6.60, most of the measured relative densities

were greater than 70%. Fig 6.61 showed the mean relative density of the compacted

soil mass was 76.39 with a standard deviation of 6.2%. It is clear in Fig 6.61 that the

entire soil body was successfully compacted with this ground improvement technique.

Fig 6.62 showed the ΔD_r and RDIR with depth after 20 cycles of cyclic shearing.

6.4 Cyclic Torsional Shear Compaction with Different Shearing Angles

To discuss the effects due to variation of shearing angles, test were conducted for

the shearing angle of $\pm 1°$, $\pm 2°$, $\pm 3°$, $\pm 5°$, $\pm 10°$, $\pm 15°$, $\pm 20°$ and $\pm 30°$, and the number

of loading cycles were set to be N = 20. Compaction was applied on the fill surface for

a 1.5 m-thick lift.

6.4.1 Applied Torque for Different Shearing Angles

Fig. 6.63 showed the controller used for different shearing angle with angle. At N

= 20, the torque measured T for $\theta = \pm 1°$, $\pm 2°$, $\pm 3°$, $\pm 5°$, $\pm 10°$, $\pm 15°$, $\pm 20°$ and $\pm 30°$

were shown in Fig. 6.64. For $\theta = \pm 1°$ the applied torque varied between -53.9 to 52.6

N-m. For $\theta = \pm 30°$ the applied torque varied between -89.5 to 92.3 N-m. Fig. 6.65

showed the applied torque T as a function of the shearing angle θ. Test results indicated

that the applied torque increased with increasing shearing angle θ.

Fig. 6.66 showed the maximum shear stress as a function of the shearing angle θ.

Test results indicated that maximum shear stress τ_{max} increased with increasing shearing

angle θ.

6.4.2 Volume Change of Soil with Shearing Angles

Fig. 6.68 (a) showed the surface settlement after 20 cycles of shearing application with the shearing angle $\theta = \pm1°$. The measured surface settlement varied from 20.6 to 27.6 mm, the average value was 23.2 mm. Fig. 6.75 (a) showed the surface settlement after 20 cycles of shearing application with the shearing angle $\theta = \pm30°$. The measured surface settlement varied from 34.4 to 47.6 mm, the average value was 42.2 mm. Fig. 6.76 (a) showed the measured surface settlement for a 1.5 m-thick fill after 20 cycles of shearing application for shearing angles of $\theta = \pm1°$, $\pm2°$, $\pm3°$, $\pm5°$, $\pm10°$, $\pm15°$, $\pm20°$ and $\pm30°$. In the Fig. 6.76 (a), the surface settlement increased with increasing shearing disc angle. Fig. 6.77 (a) showed the variation of surface settlement from 18.1 to 43.1 mm with increasing shearing angle θ from 0 to $\pm30°$.

Fig. 6.76 (b) showed the volumetric strain of the 1.5 m-thick fill after 20 cycles of application of shearing angle for $\theta = \pm1°$, $\pm2°$, $\pm3°$, $\pm5°$, $\pm10°$, $\pm15°$, $\pm20°$ and $\pm30°$. In Fig. 6.76 (b), the volumetric strain increased with increasing shearing disc angle. It should be mentioned that, for 1.5 m-thick soil fill, the densification due to shearing compaction occurred only at the upper-most part of the soil mass.

Chapter 7

CONCLUSIONS

In this study, the change of volume and relative density in the soil due to static vertical loading, and cyclic torsional shearing compaction were investigated. Based on the experiment results, the following conclusions were drawn.

A. For the 1.5 m-thick lift:

1. Under the static load of q = 10.35 kPa, the relative density increase was most apparent in the upper 0.45 m of lift. However, in the lower part of the lift, little relative density change occurred.

2. The densification due to cyclic shearing compaction occurred only at the upper part of the soil mass. Little volume change occurred at the lower part of the fill.

3. In the first 5 cycles of cyclic torsional shearing application, the surface settlement increased significantly. However, after 20 cycles, the major part of settlement was accomplished, soil particle were sheared and reached a densely-packed condition. As a result, it was difficult to increase the surface settlement any further with more cyclic shear application.

4. The relative density distribution after the application of cyclic torsional shearing for N = 0 (static load), 5, 10, and 20 increased with increasing number of cycles of shearing application.

5. After 20 cycles of shearing application with rotation angle $\theta = \pm 5°$ the relative density of the compacted soil reached the required $D_r = 70$ to 75 %. Test results indicated that cyclic torsional shearing was an effective method for compacting the upper 0.3 m of fill.

B. For five 0.3 m-thick lifts

    1. For shearing compaction on five 0.3 m-thick lifts, after 20 cycles of torsional shearing with the torsional angle of $\theta = \pm 5°$, the average volumetric strain for the lift 1, 2, 3, 4, and 5 was 9.77, 10.53, 10.37, 10.05 and 10.32 %, respectively. It was clear that the cyclic torsional shearing compaction in each lift was relatively uniform.

    2. Most of the relative density measured in compacted fill were greater than 70 %. The entire soil body was successfully compacted with cyclic torsional shearing compaction.

    3. For five compacted lifts, the mean relative density was 76.3 % with a standard deviation of 6.2 %. It was obvious that the entire soil body was successfully compacted with this ground improvement technique.
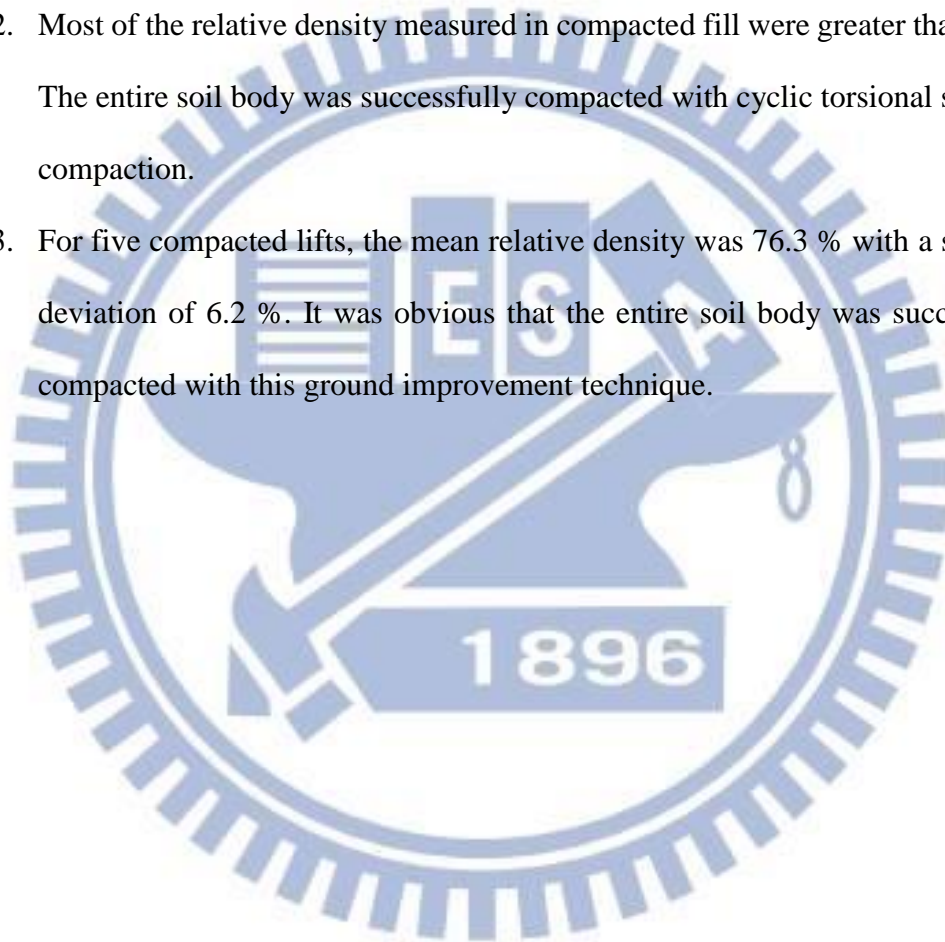
References

1. Airey, D.W. and Wood, D.M. (1987). "An evaluation of direct simple shear tests on clay," Geotechnique, Vol. 37, No.1, pp. 25-35

2. ASTM D4253-93 (2007). "Standard Test Methods for Maximum Index Density and Unit Weight oUsing a Vibratory Table," Section four, Construction, Volume 04.08, Soil and Rock (I): D420-D5779 Annual Bf Soils ook of ASTM Standards, ASTM, Conshohocken, PA, USA.

3. Burgess, G. P. (1999). "Performance of Two Full-scale Model Geosynthetic Reinforced Segmental Retaining Walls," MS thesis, Royal Military College of Canada, Kingston, Ontario, 207.

4. Chang, S. Y., (2000), "Effect of Backfill Density on Active Earth Pressure," Master of Engineering Thesis, Dept. of of Civil Engineering, National Chiao Tung University, Hsinchu, Taiwan.

5. Chen, T. J., (2003). "Earth Pressures Due to Vibratory Compaction." Ph.D. Dissertation, National Chiao Tung University, Hsinchu, Taiwan.

6. Chen, T. J., and Fang, Y. S, (2008). "Earth Pressure Due to Vibratory Compaction", Journal of Geotechnical and Geoenvironmental Engineering, ASCE, 134 (4), 1-8.

7. Das, B. M., (2010), "Principles of Geotechnical Engineering.", 7th Ed., Cengage Learning, Stamford, CT, USA.

8. Chen, K.Y., (2011). "Densification of Sand Due to Cyclic Torsional Shear Compaction." Master of Engineering Thesis. Dissertation, National Chiao Tung University, Hsinchu, Taiwan.

9. Das, B. M., (2011), "Principles of Soil Dynamics.", 2nd Ed., Cengage Learning, Stamford, CT, USA.

10. Das, B. M. (2011), "Principles of Foundation Engineering", 7th Ed., Cengage Learning, Stamford, CT, USA.

11. D'Appolonia, D. J., Whitman, R. V., and D'Appolonia, E. (1969). "Sand Compaction with Vibratory Rollers." *Journal of the Soil Mechanics and*

Foundations Division, ASCE, 95(SM1), 263-284.

12. Duncan, J. M., and Seed, R. B. (1986). "Compaction-induced Earth Pressures under K_o-conditions." *Journal of Geotechnical Engineering*, ASCE, 112(1), 1-22

13. Duncan, J. M, Williams, G. W., Sehn, A. L,, and Seed, R. B. (1991). "Estimation Earth Pressure Due to Compaction," *Journal of Geotechnical Engineering*, ASCE, 117 (12), 1833-1847.

14. Fang, Y. S., Chen, T. J., Holtz, R. D., and Lee, W. F., (2004). "Reduction of Boundary Friction in Model Tests," *Geotechnical Testing Journal*, ASTM, 27(1), 1-10.

15. Holtz, R. D., and Kovacs, W. D. (1981) "An Introduction to Geotechnical Engineering," Prentice-Hall, Inc., Englewood Cliffs, N.J. USA.

16. Ho, Y. C., (1999), "Effects of Backfill Compaction on Passive Earth Pressure," Master of Engineering Thesis, National Chiao Tung University, Hsinchu, Taiwan.

17. Hsu, C. C., and Vucetic, M., (2004), "Volumetric Threshold Shear Strain for Cyclic Settlement," Journal of Geotechnical and Geoenvironmental Engineering, ASCE, 130 (11), 58-70.

18. Huang, Y. X., (2008) "A Study on the Disc Shearing Behavior of Sand in a Mid-size Soil Tank," Master of Engineering Thesis, Chung Yuan Christian University, Chungli, Taiwan.

19. Ishibashi, I., and Sherif, M. A., (1974), "Soil Liquefaction by Torsional Simple Shear Device," Journal of the Geotechnical Engineering Division, ASCE, 100 (8), 871-888.

20. Ishibashi, I., Kawamura, M., and Bhatia, S. K., (1985), "Effect of Initial Shearing on Cyclic Drained and Undrained Characteristics of Sand." Geotechnical Engineering Report 85-2, School of Civil and Environmental Engineering, Cornell University, Ithaca, New York, USA.

21. Kramer, S. L., (1996), "Geotechnical Earthquake Engineering", Prentice-Hall, Inc., Upper Saddle River, New Jersey.

22. Lambe T. W. and Whitman R. V. (1969) "Soil Mechanics," JOHN WILEY &

SONS, New York.

23. Liu, C., (2012). "Change of Density and Stress in Sand Due to Cyclic Torsional Shear Compaction," Master of Engineering Thesis. Dissertation, National Chiao Tung University, Hsinchu, Taiwan.

24. Lo Presti, D. C. F., Pedroni, S., and Crippa, V. (1992). "Maximum Dry Density of Cohesionless Soils by Pluviation and by ASTM D 4253-83: A comparative study." *Geotechnical Testing Journal*, ASTM, 15(2), 180-189.

25. McElroy, J. A. (1997). "Seismic Stability of Geosynthetic Reinforced Slopes: A shaking table study." MS thesis, University of Washington, Seattle, 286.

26. Miura, K., Tsukada, Y., Tsubokawa, Y., Ishito, M., Nishimura, N., Ohtani, Y., and You, G. L., (2000), "Bearing capacity during earthquake of the spread footing reinforced with micropiles." Proceedings, 12th World Conference on Earthquake Engineering, pp. 1-8.

27. Rad, N. S., and Tumay, M. T. (1987). "Factors affecting sand specimen preparation by raining." *ASTM Geotechnical Testing Journal*, 10(1), 31-37.

28. Ren, F. Y., (2006) "A Study on the Influence of Type of Plate Shearing on the Relative Density of Loose Sand," Master of Engineering Thesis, Chung Yuan Christian University, Chungli, Taiwan.

29. Terzaghi K. (1943) "Theoretical Soil Mechanics," John Wiley and Sons

30. Tschebotarioeff G. P. (1973) "Foundations, retaining, and earth structures, " McGRAW-HILL BOOK CO., New York.

31. US NAVY. (1982), "Foundations and Earth Structures," *NAVFAC Design Manual DM-7.2*. Naval Facilities Engineering Command, U.S. Government Printing Office, Washington, D. C., 60.

32. Vesic, A. S., (1973), "Analysis of Ultimate Loads of Shallow Foundations," Journal of the Soil Mechanics and Foundations Division, ASCE, 99 (1), 45-73.

33. Yang, C. T., (2002) "A Study on Plate Shear to Improve Relative Density of Sand," Master of Engineering Thesis, Chung Yuan Christian University, Chungli, Taiwan.

34. Youd, T. L., (1972), "Compaction of Sand by Repeated Straining," Journal of the Soil Mechanics and Foundations Division, ASCE, 98 (7), 709-725.
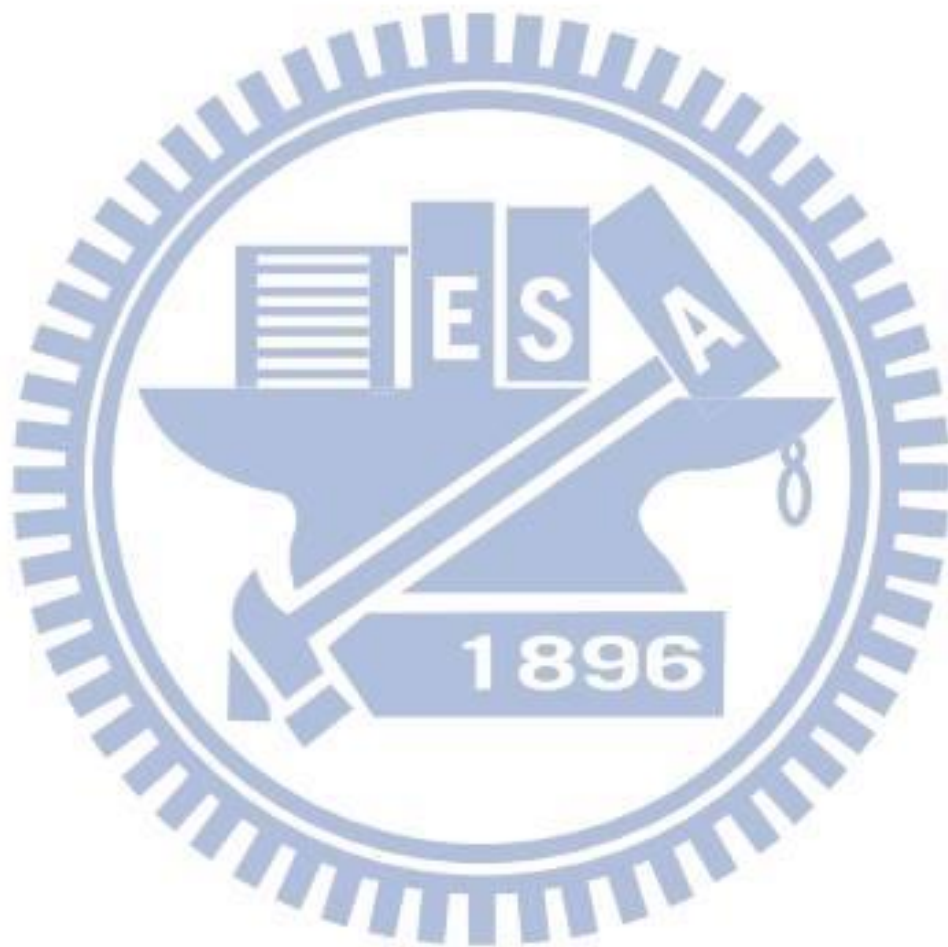
Table. 2.1. Qualitative description of granular soil deposits

Relative density (%) Das (2010)	Relative density (%) Lambe and Whitman (1969)	Description of soil deposit
0 - 15	0 - 15	Very loose
15 - 50	15 – 35	Loose
50 - 70	35 - 65	Medium
70 - 85	65 - 85	Dense
85 - 100	85 - 100	Very dense
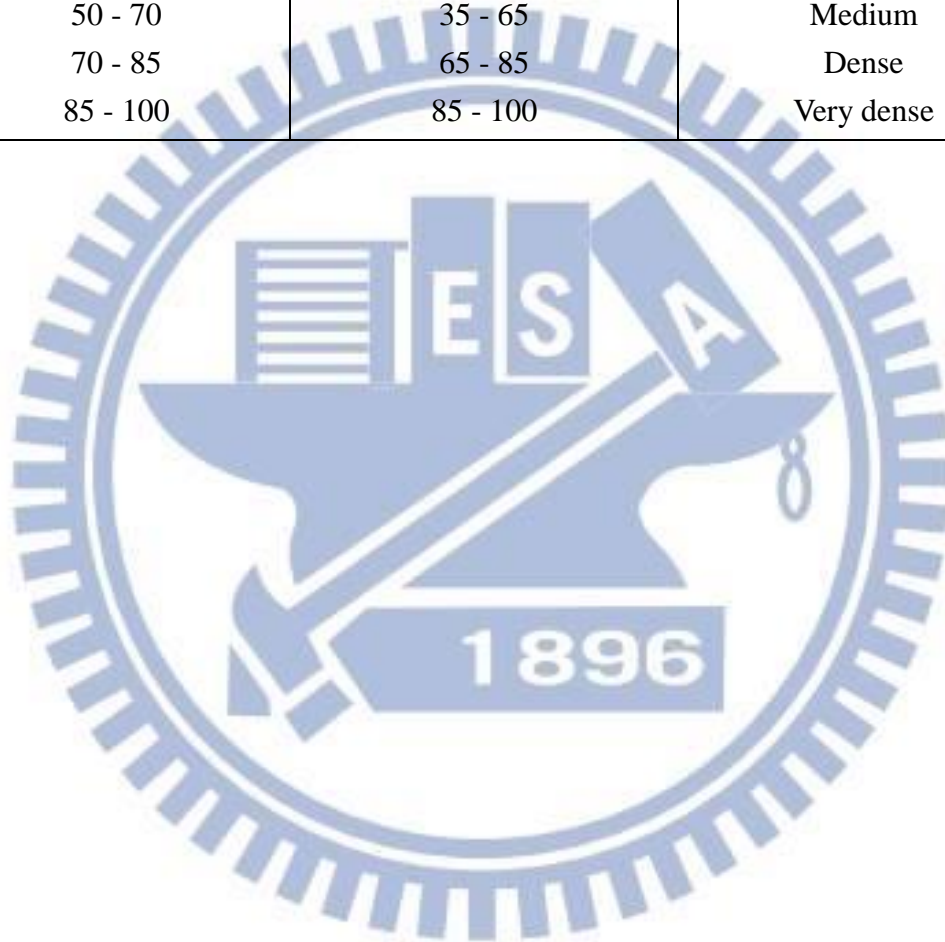
Table 3.1. Terzaghi's Modified Capacity Factors N'_c, N'_q, and N'_γ

ϕ'	N'_c	N'_q	N'_γ	ϕ'	N'_c	N'_q	N'_γ
0	5.70	1.00	0.00	26	15.53	6.05	2.59
1	5.90	1.07	0.005	27	16.30	6.54	2.88
2	6.10	1.14	0.02	28	17.13	7.07	3.29
3	6.30	1.22	0.04	29	18.03	7.66	3.76
4	6.51	1.30	0.055	30	18.99	8.31	4.39
5	6.74	1.39	0.074	31	20.03	9.03	4.83
6	6.97	1.49	0.10	32	21.16	9.82	5.51
7	7.22	1.59	0.128	33	22.39	10.69	6.32
8	7.47	1.70	0.16	34	23.72	11.67	7.22
9	7.74	1.82	0.20	35	25.18	12.75	8.35
10	8.02	1.94	0.24	36	26.77	13.97	9.41
11	8.32	2.08	0.30	37	28.51	15.32	10.90
12	8.63	2.22	0.35	38	30.43	16.85	12.75
13	8.96	2.38	0.42	39	32.53	18.56	14.71
14	9.31	2.55	0.48	40	34.87	20.50	17.22
15	9.67	2.73	0.57	41	37.45	22.70	19.75
16	10.06	2.92	0.67	42	40.33	25.21	22.50
17	10.47	3.13	0.76	43	43.54	28.06	26.25
18	10.90	3.36	0.88	44	47.13	31.34	30.40
19	11.36	3.61	1.03	45	51.17	35.11	36.00
20	11.85	3.88	1.12	46	55.73	39.48	41.70
21	12.37	4.17	1.35	47	60.91	44.45	49.30
22	12.92	4.48	1.55	48	66.80	50.46	59.25
23	13.51	4.82	1.74	49	73.55	57.41	71.45
24	14.14	5.20	1.97	50	81.31	65.60	85.75
25	14.80	5.60	2.25				

Table. 3.2. Characteristics of normal loading discs

Mass (kg)	19.80	9.60	4.80	1.55	1.05	0.50
Thickness Disc (mm)	37.5	20.0	10.0	3.0	2.0	1.0
Disc Diameter (mm)	290	290	290	290	290	290
Quantity Available	13	3	1	2	3	5
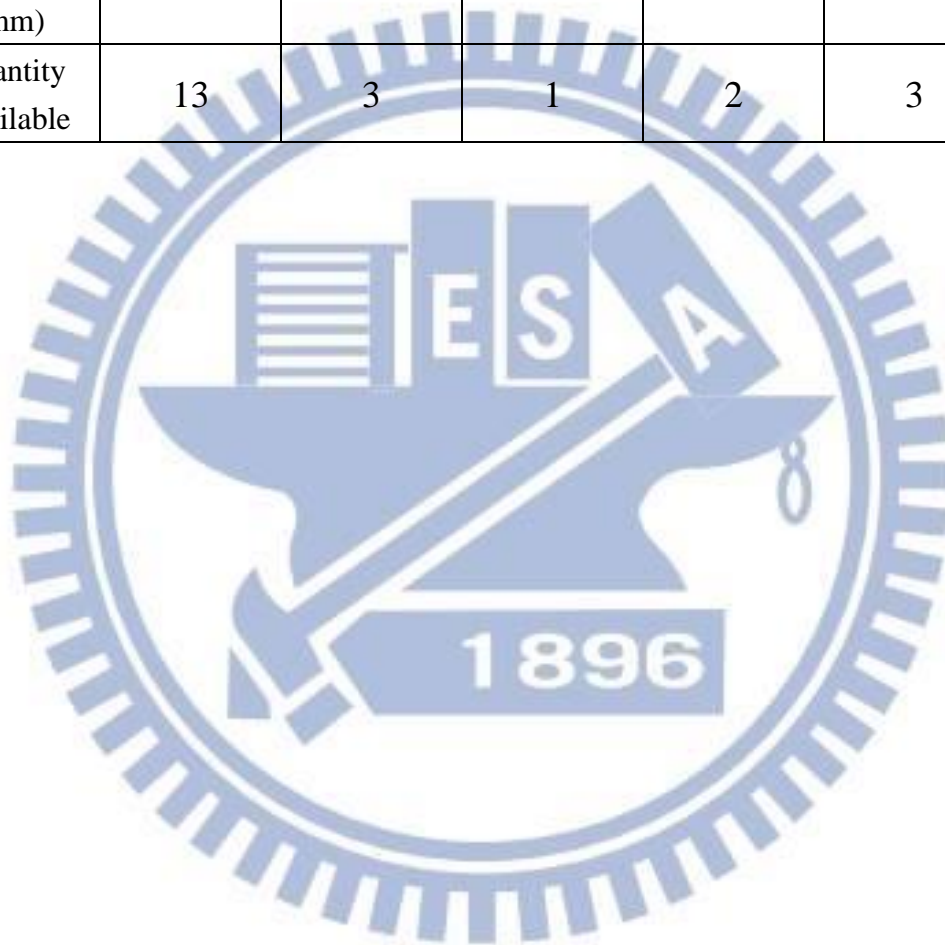
Table. 4.1. Physical properties of Ottawa sand

Shape	Rounded
e_{max}	0.76
e_{min}	0.50
G_s	2.65
D_{60}, (mm)	0.39
D_{60}, (mm)	0.26
C_u	1.50
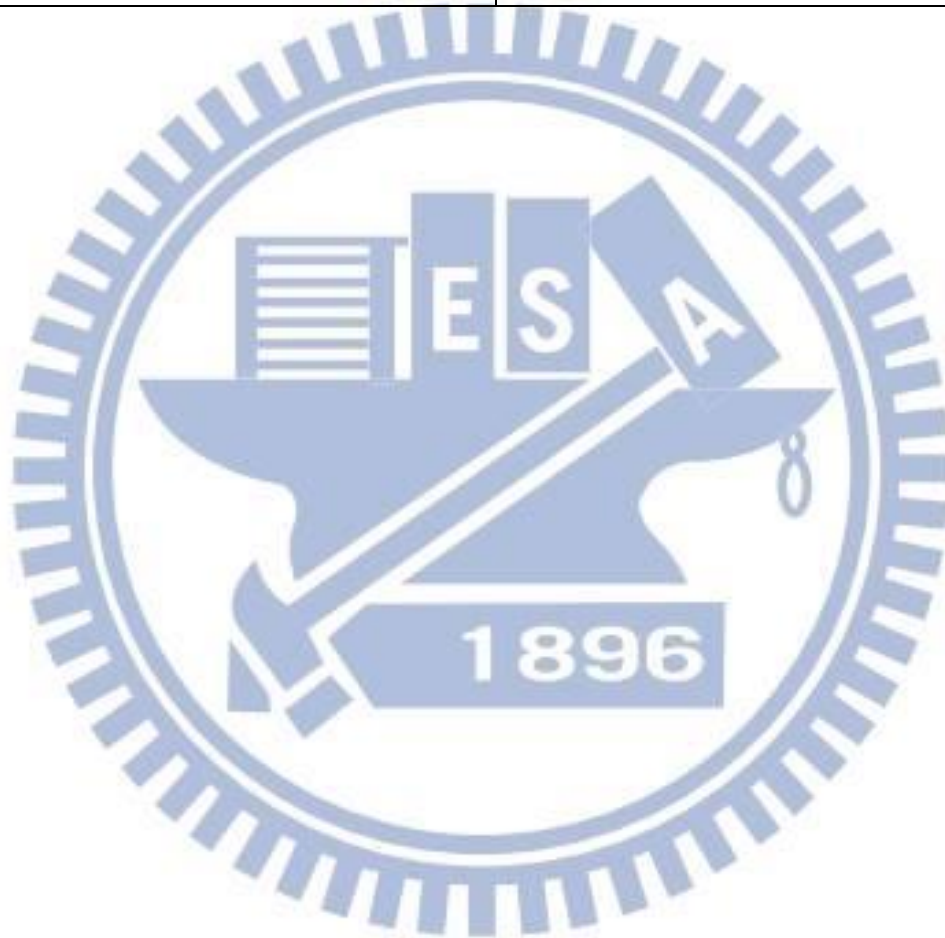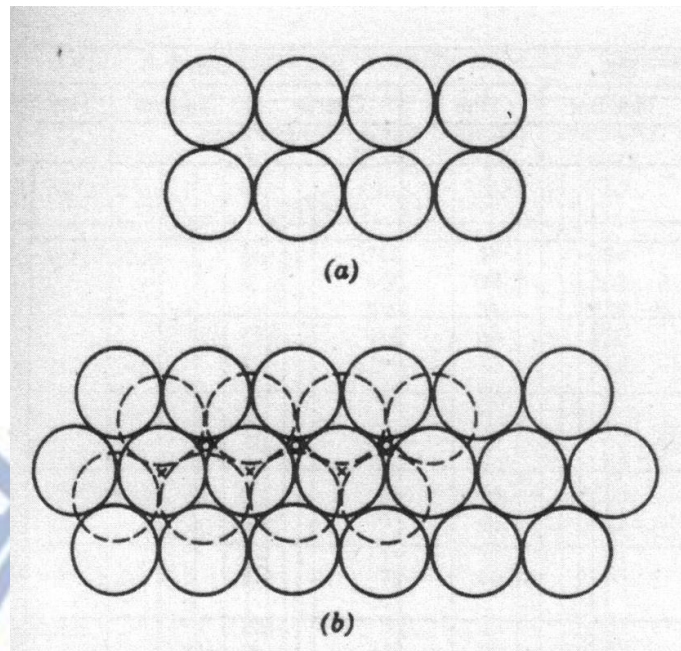
Fig. 2.1. Arrangement of uniform spheres (after Deresiewicz, 1958)
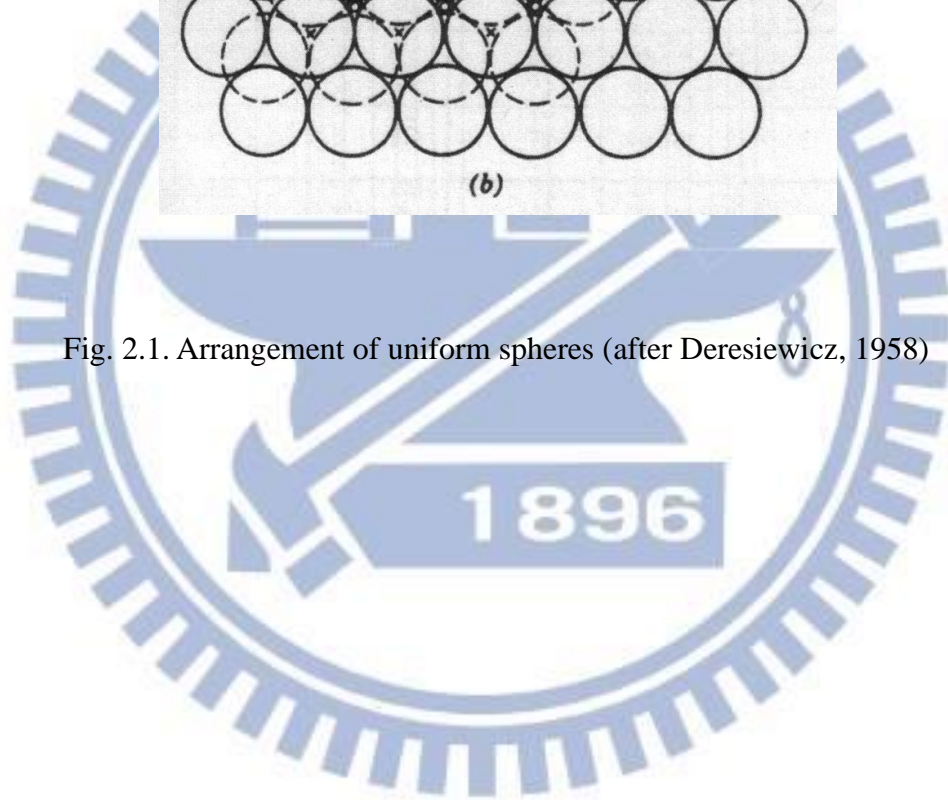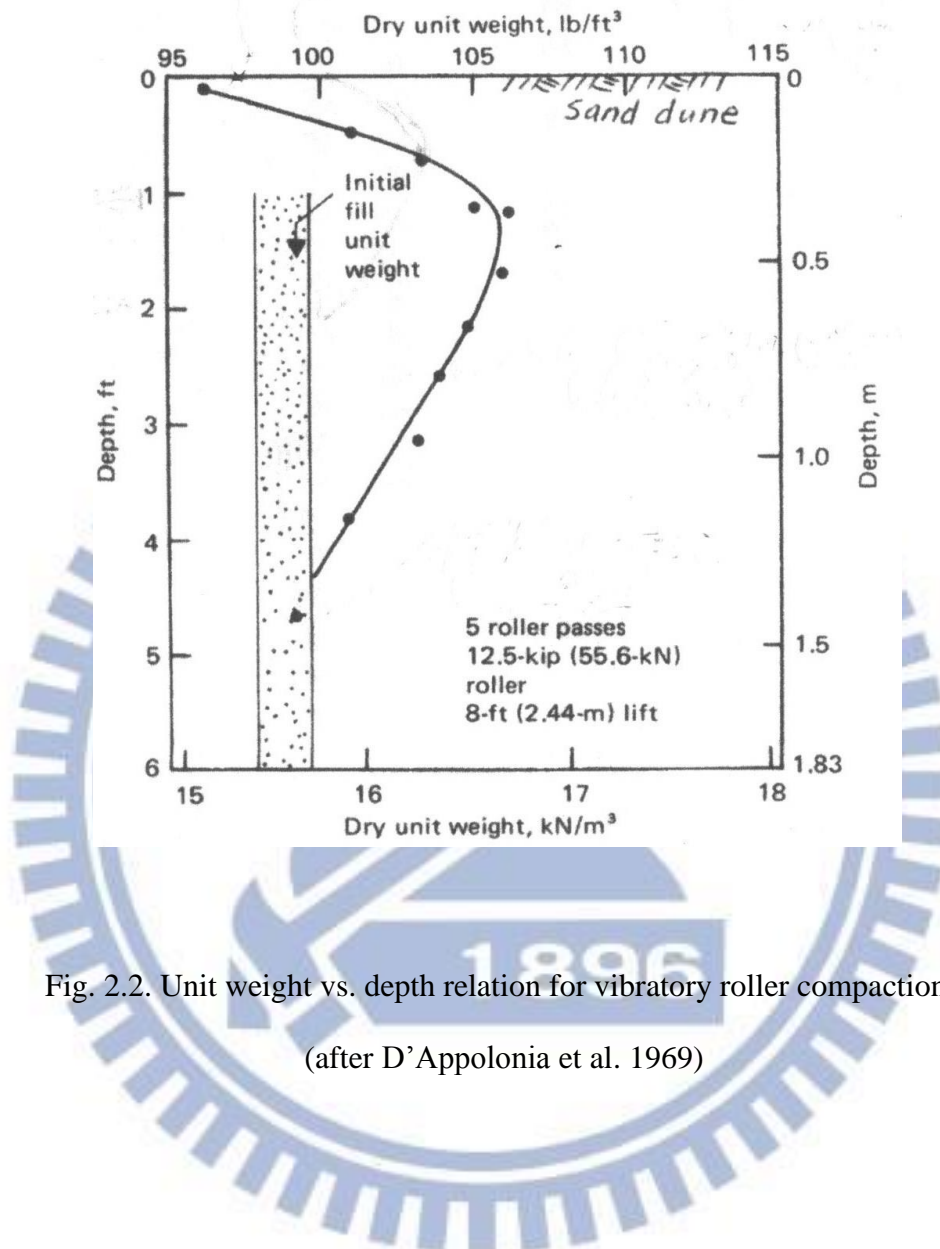
Fig. 2.2. Unit weight vs. depth relation for vibratory roller compaction

(after D'Appolonia et al. 1969)
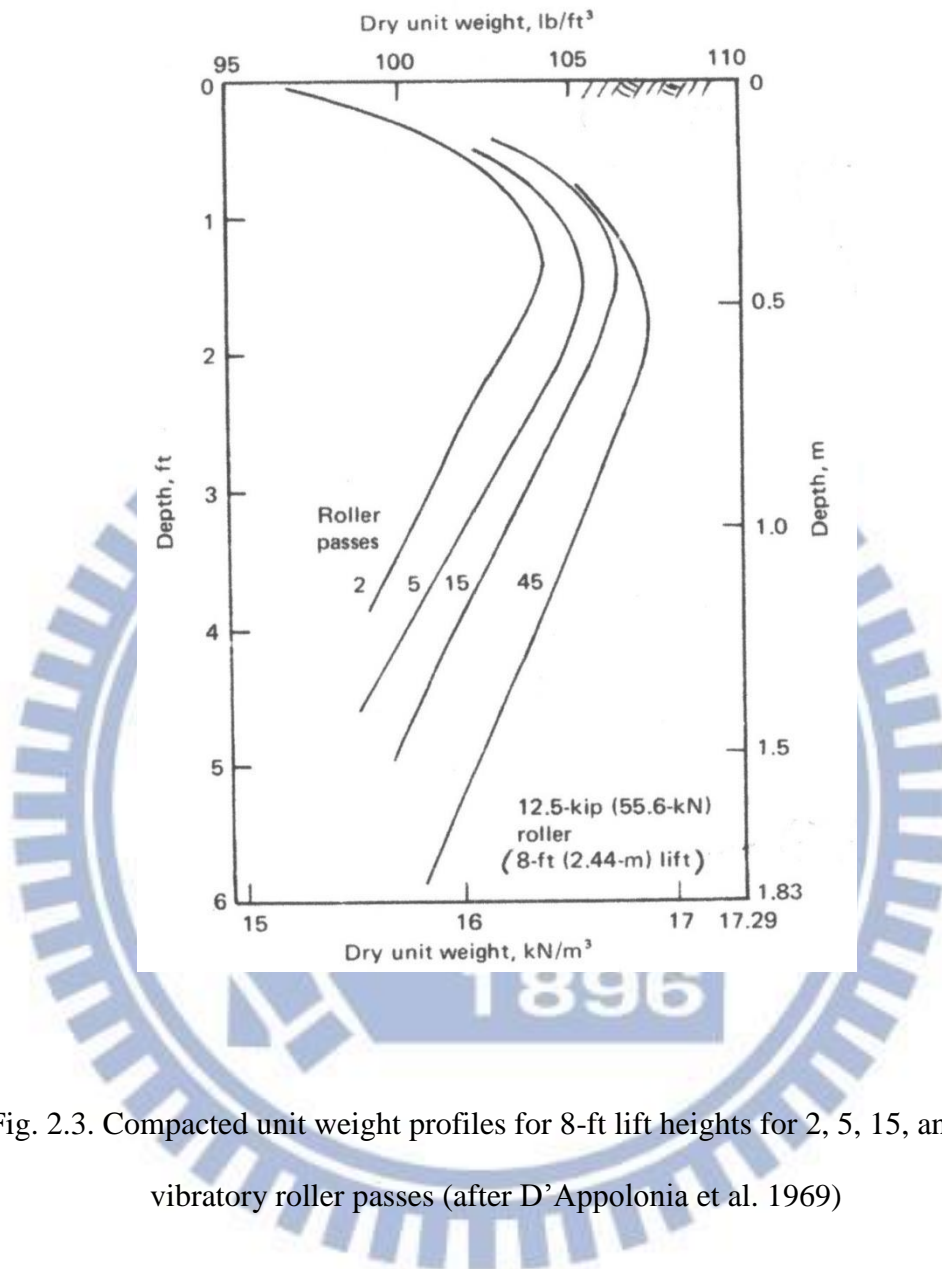
Fig. 2.3. Compacted unit weight profiles for 8-ft lift heights for 2, 5, 15, and 45
vibratory roller passes (after D'Appolonia et al. 1969)

53
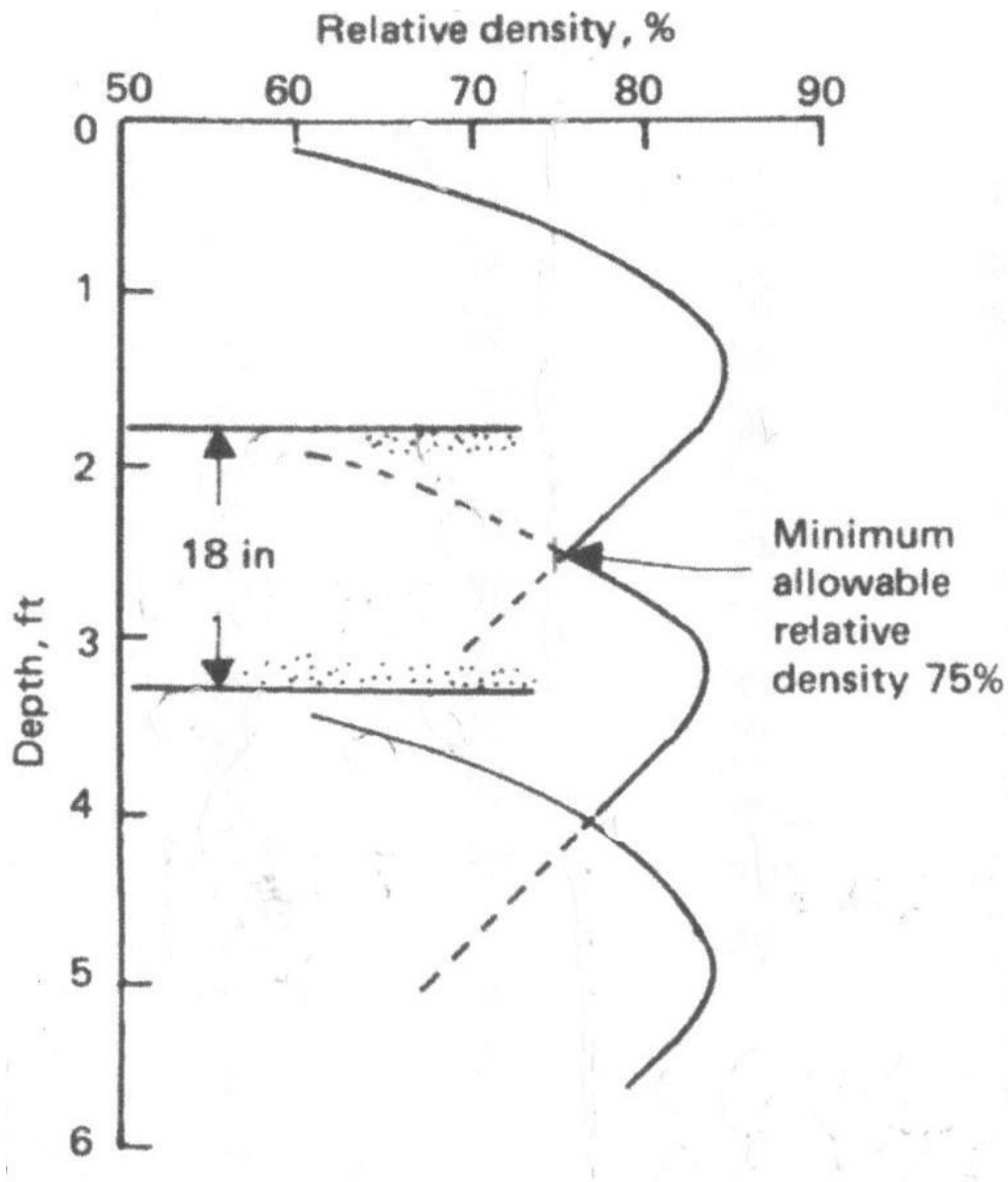
Fig. 2.4. Approximate method for determining lift height required to achieve a minimum compacted relative density of 75% with five roller passes using data for a large lift height(after D'Appolonia et al. 1969)
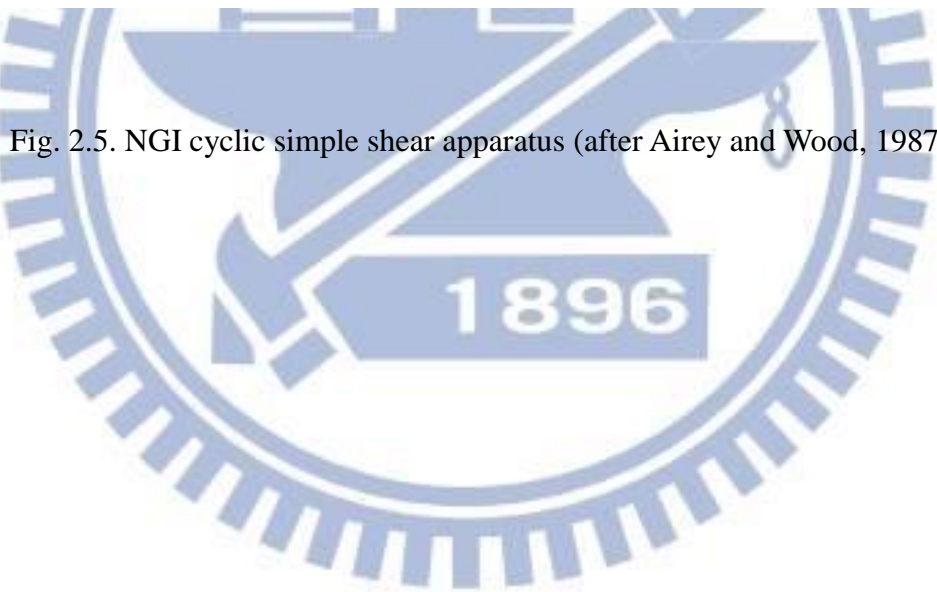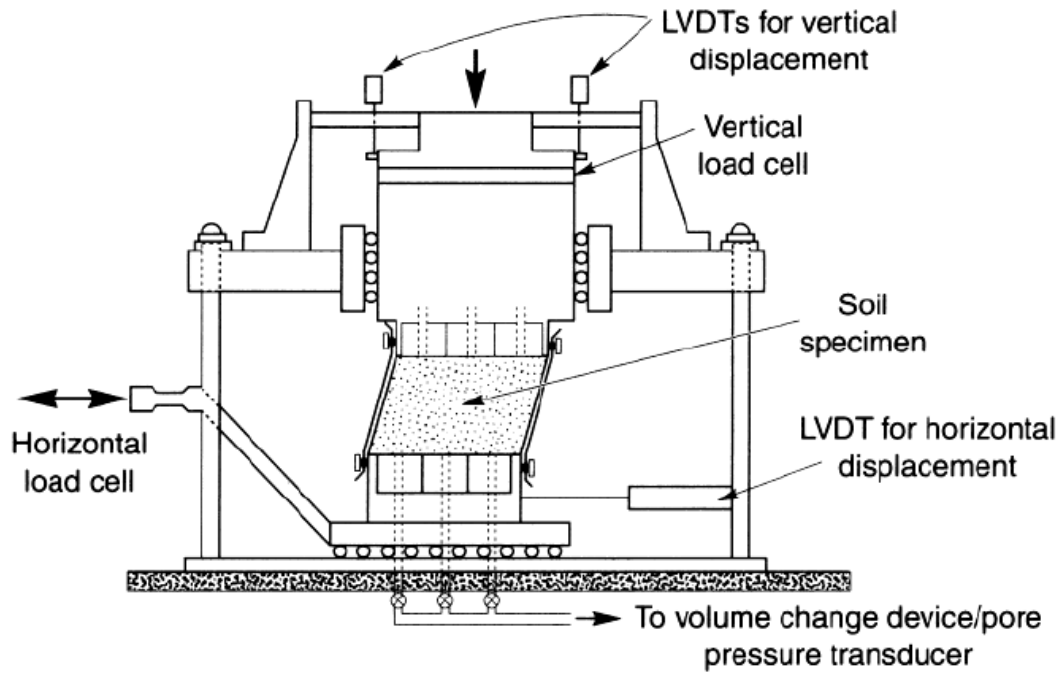
Fig. 2.5. NGI cyclic simple shear apparatus (after Airey and Wood, 1987)
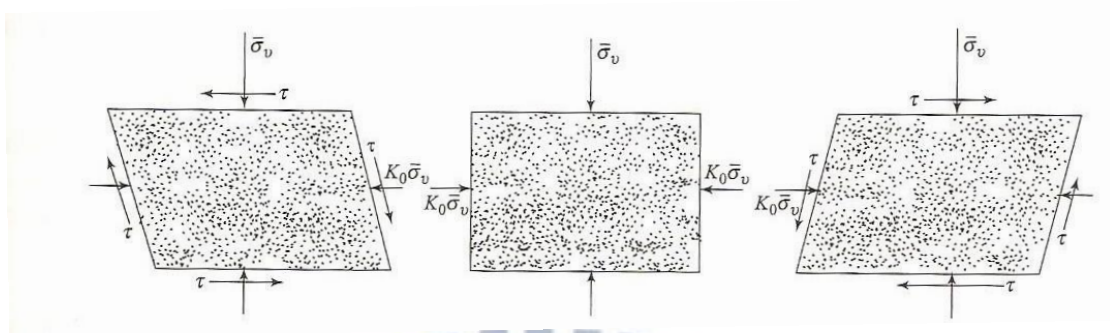
Fig. 2.6. Stress conditions of a soil specimen cyclic horizontal shear stress
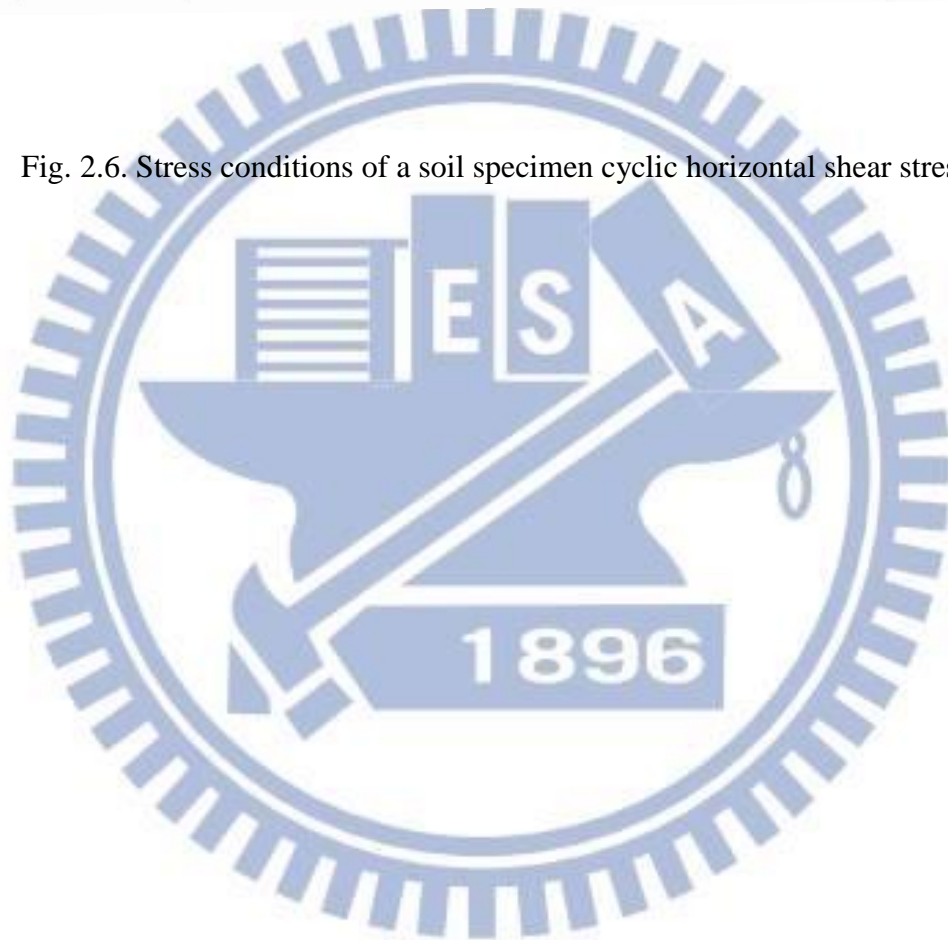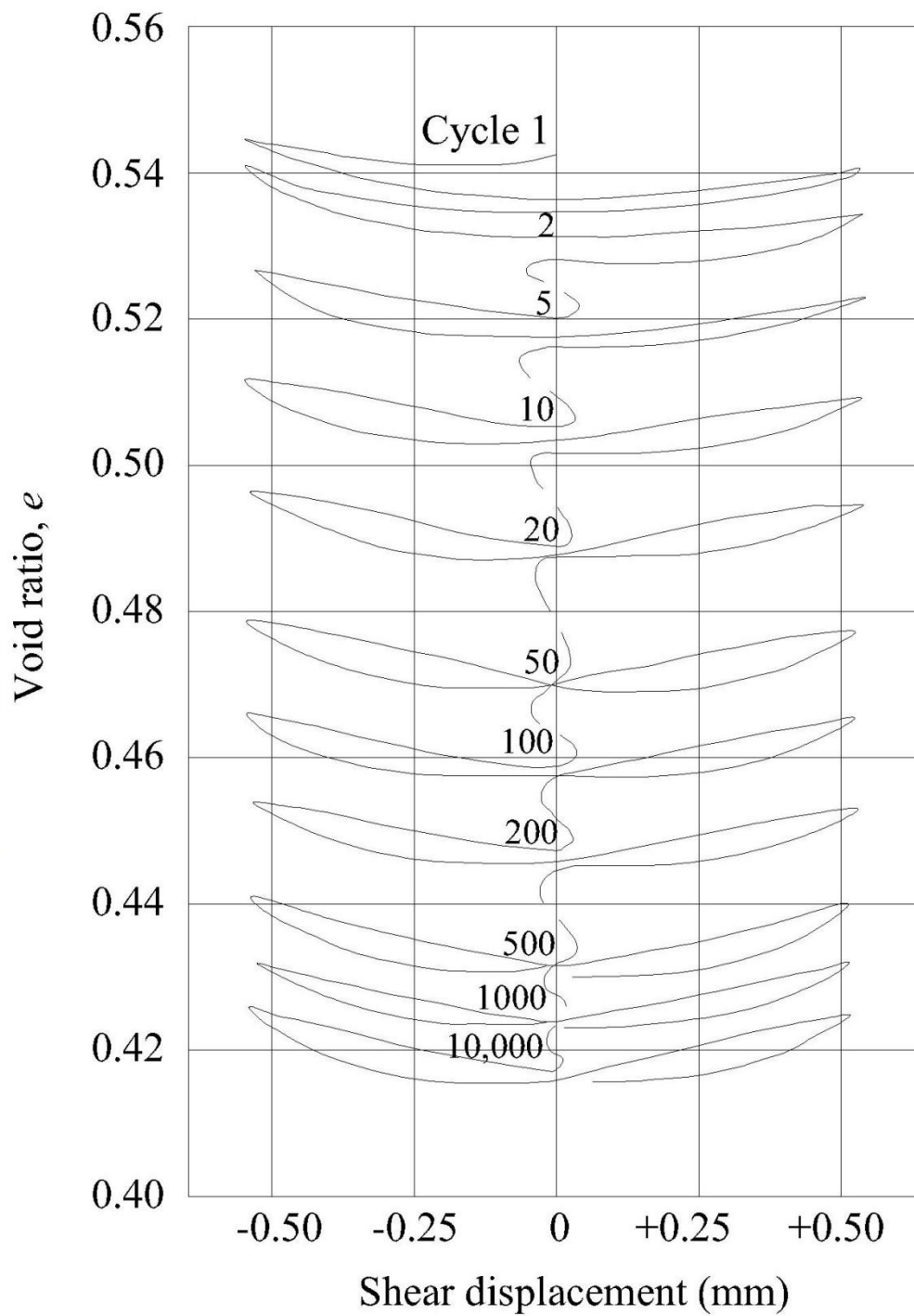
Fig. 2.7. Void ratio versus cyclic displacement for densification of a sand with successive cycles of shear (after Youd, 1972)
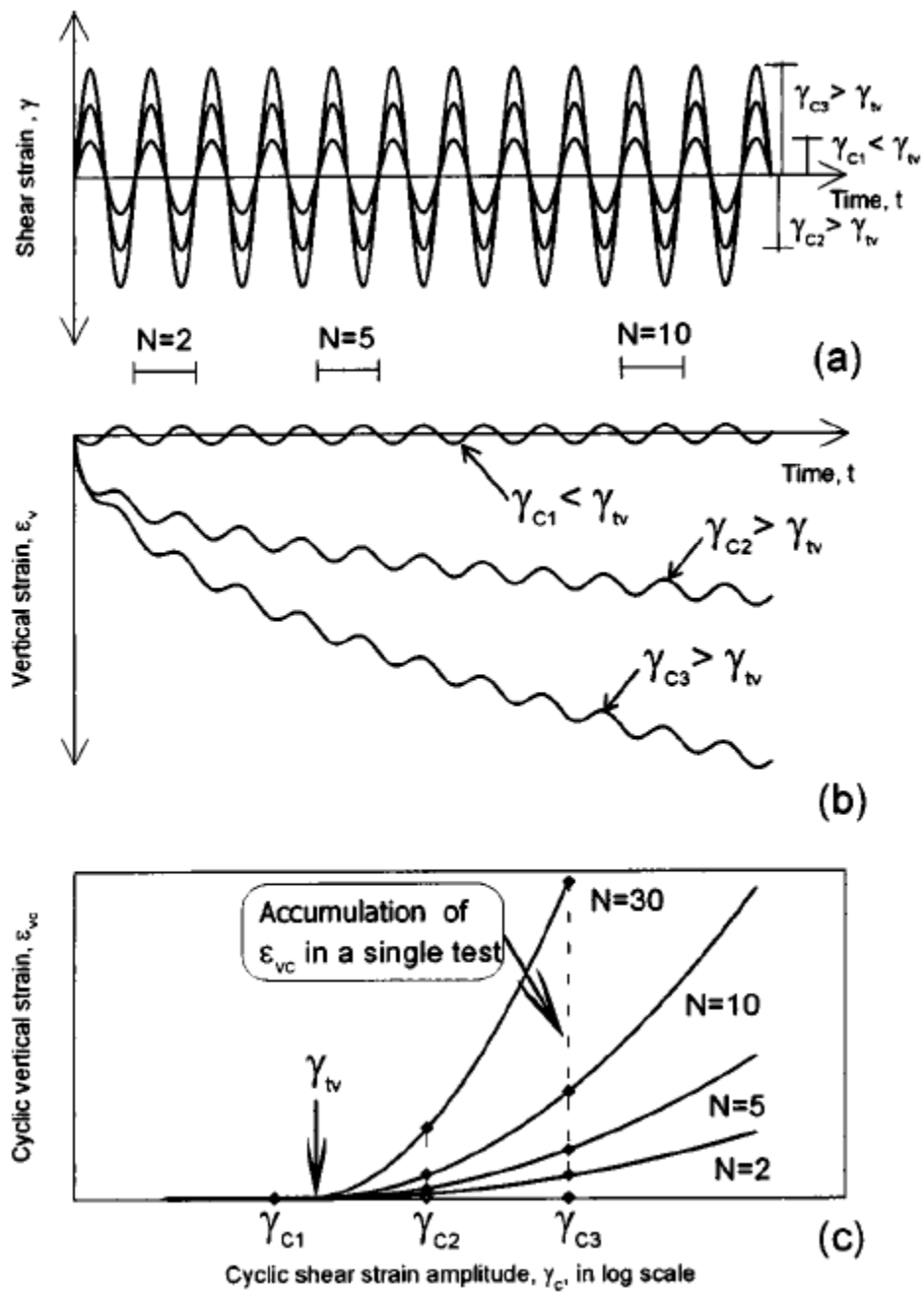
Fig. 2.8. Sketch of typical results of cyclic simple shear strain-controlled tests with

definitions of volumetric cyclic threshold strain (after Hsu and Vucetic, 2004)
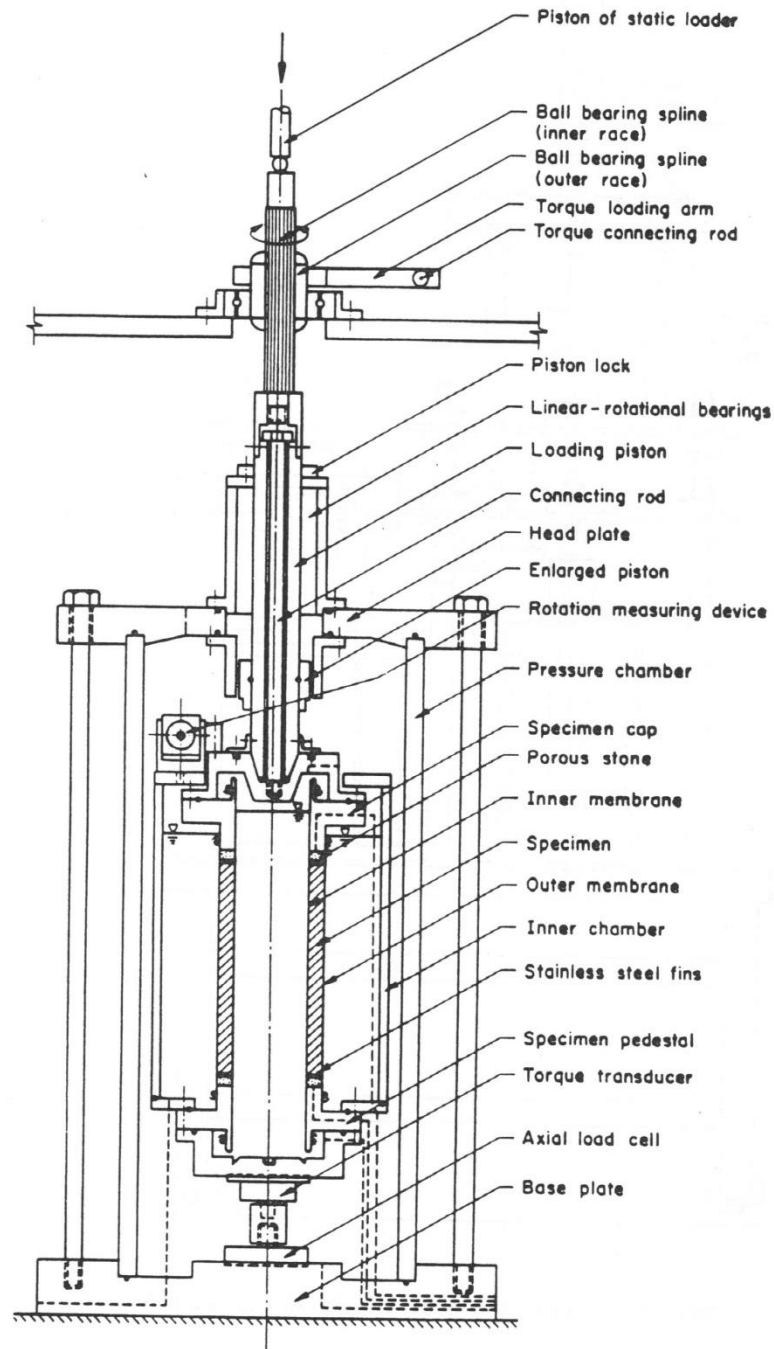
Fig. 2.9. Torsional simple shear device (after Ishibashi et al. 1985)
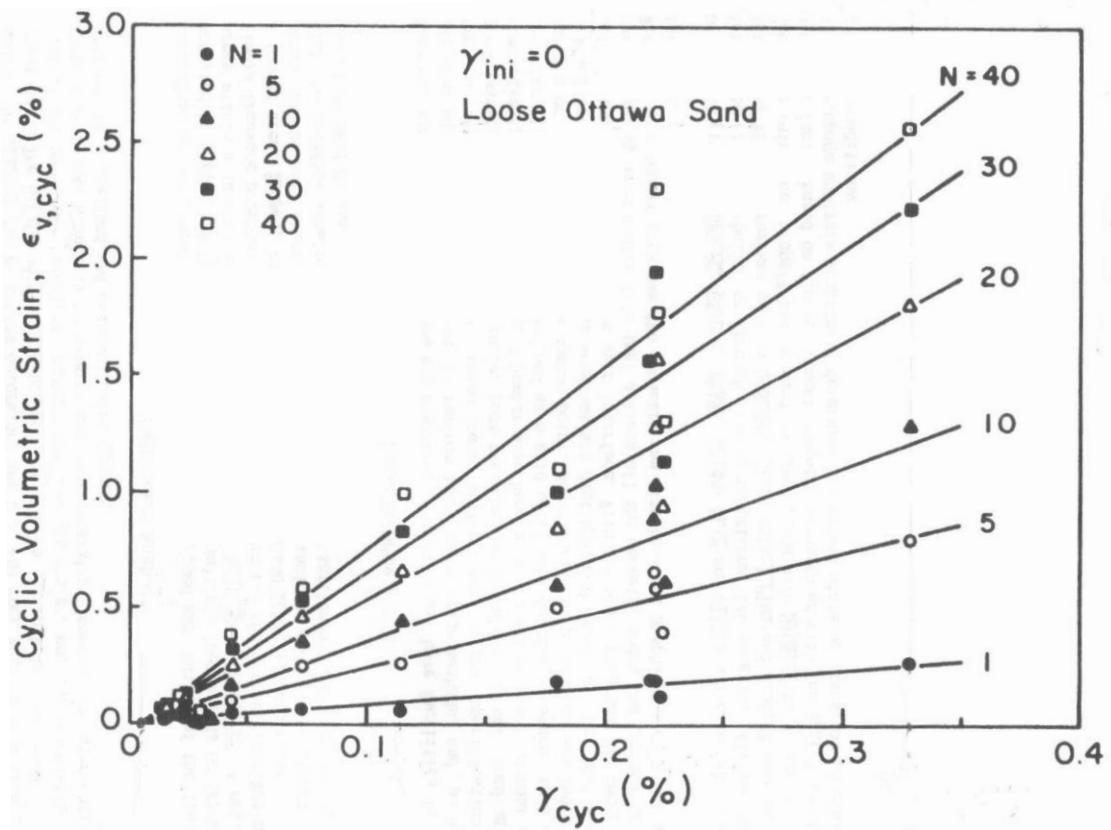
Fig. 2.10. Variation of cyclic volumetric strain as a function of cyclic shear strain

(after Ishibashi et al., 1985)

(a)
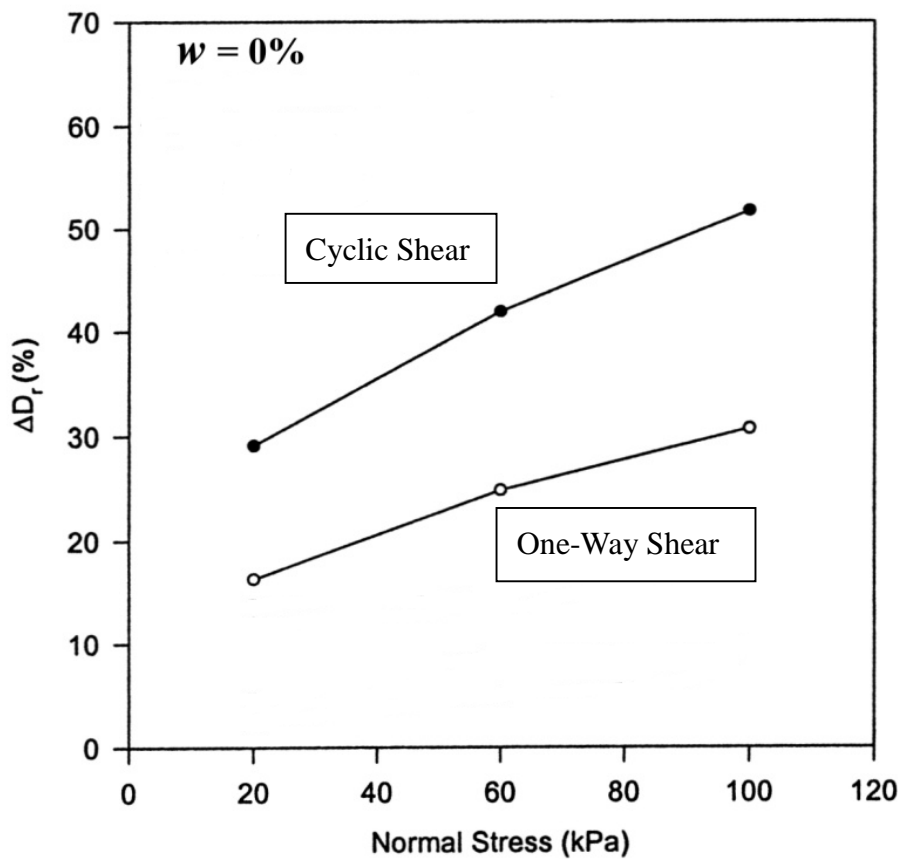
(b)

Fig. 2.11. Change of relative density with one-way and cyclic disc shearing versus normal stress (after Yang, 2002)
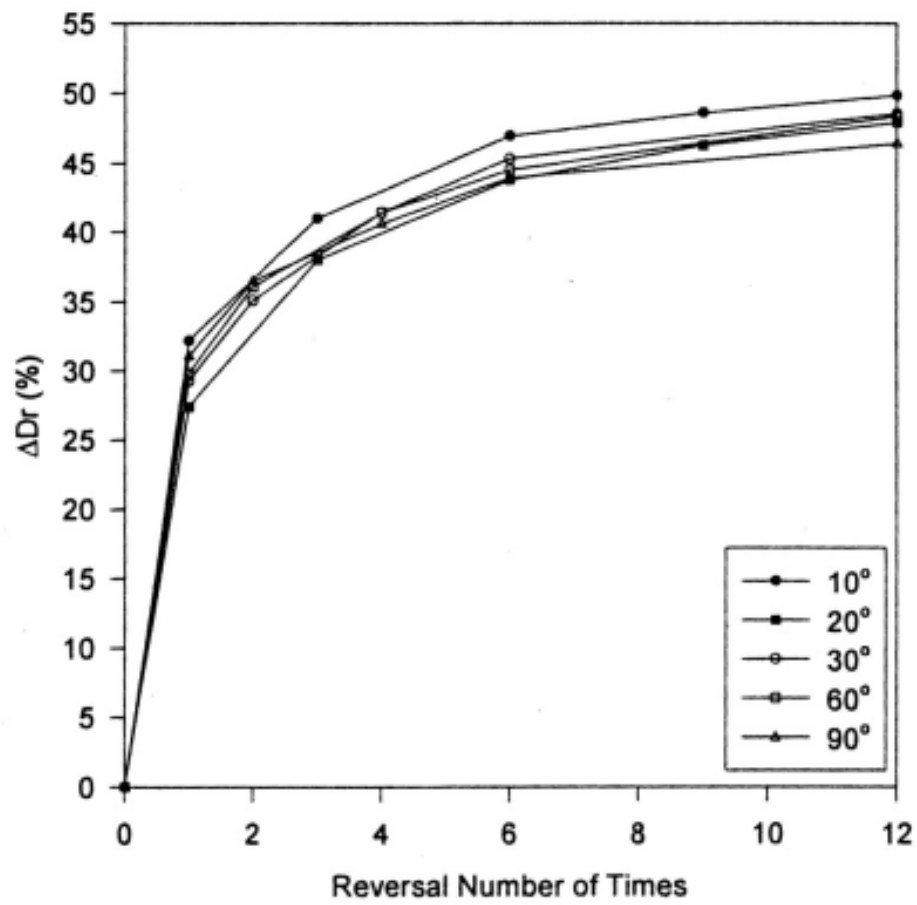
Fig. 2.12. Change of relative density due to cyclic disc shear with number of cycles

(after Ren, 2006)
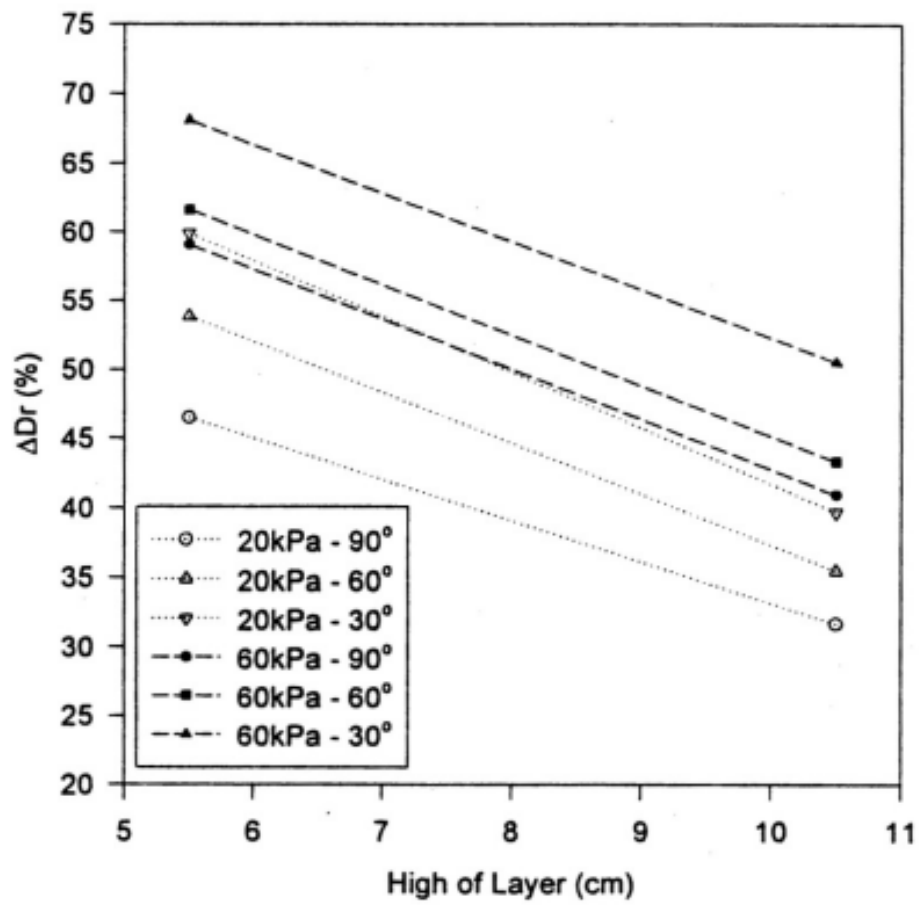
Fig. 2.13. Change of relative density due to cyclic disc shear at different depths with

high of layer (after Ren, 2006)
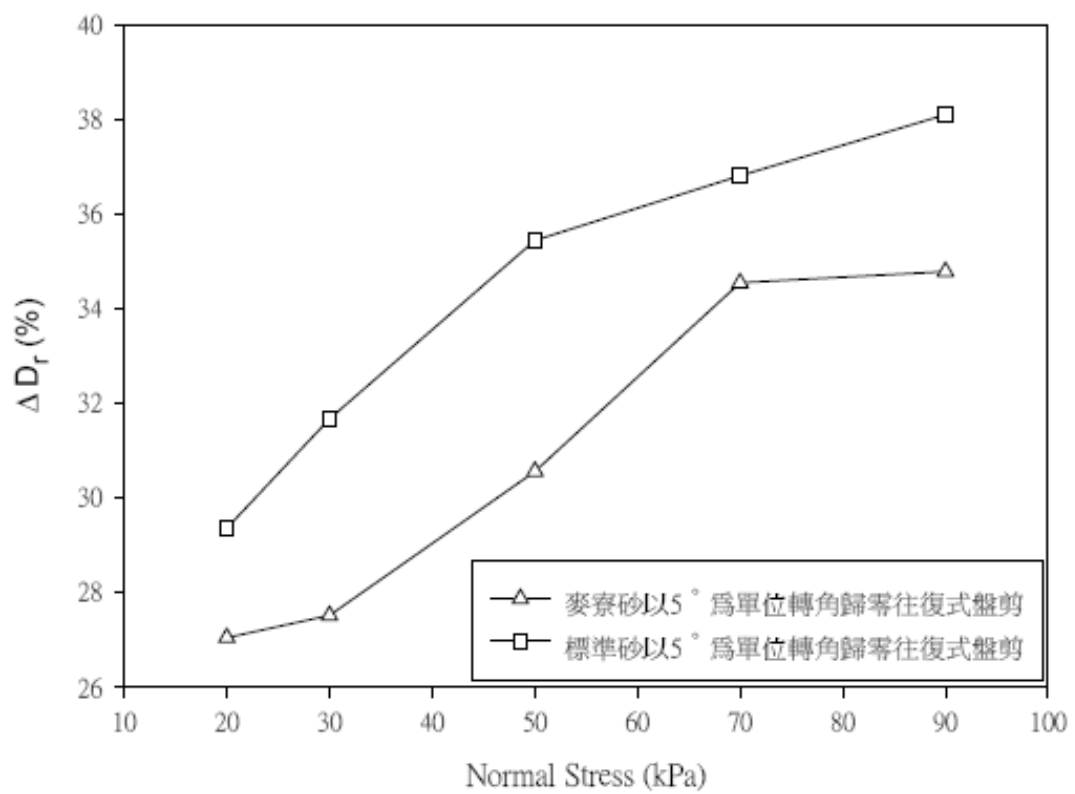
Fig. 2.14. Change of relative density due to cyclic disc shear with normal stress

(after Huang, 2008)
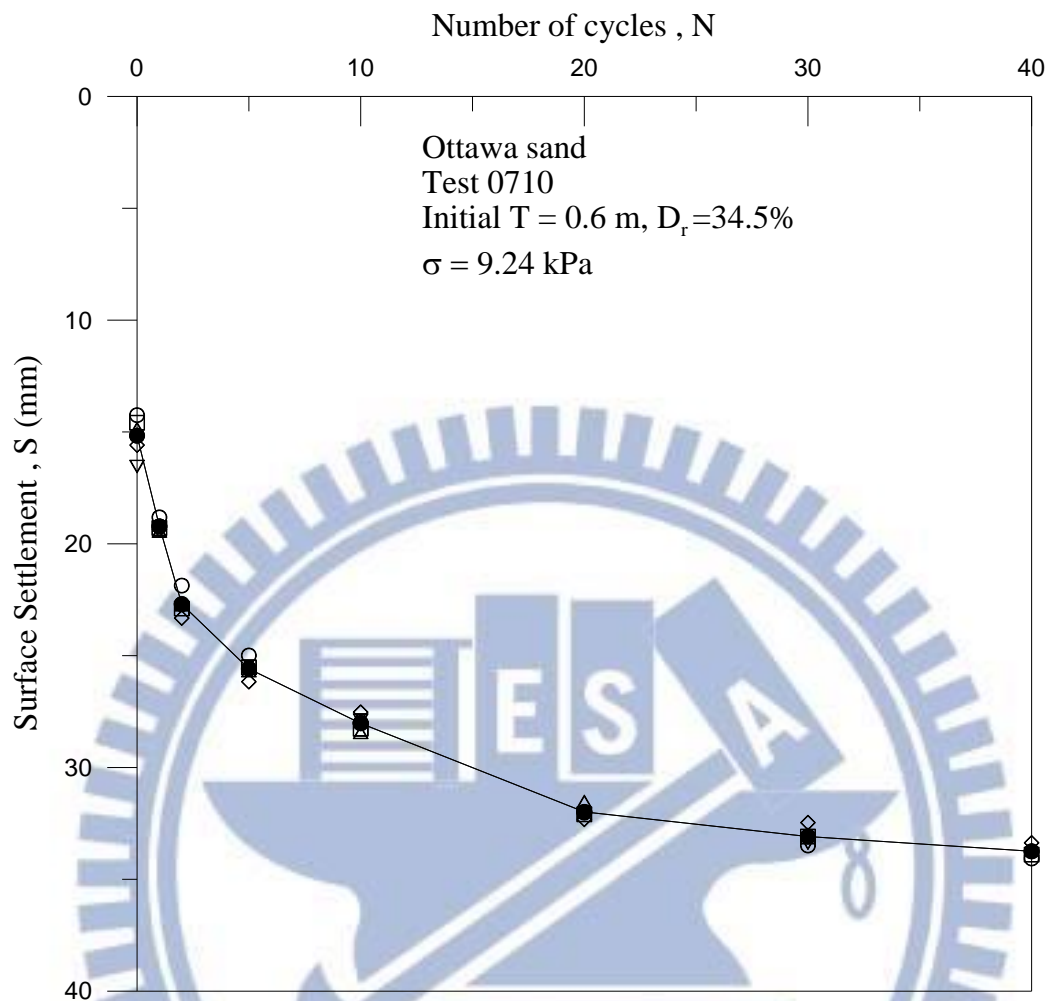
Fig. 2.15. Surface settlement due to static vertical load at N = 0 to N = 40 (after

Chen, 2011)
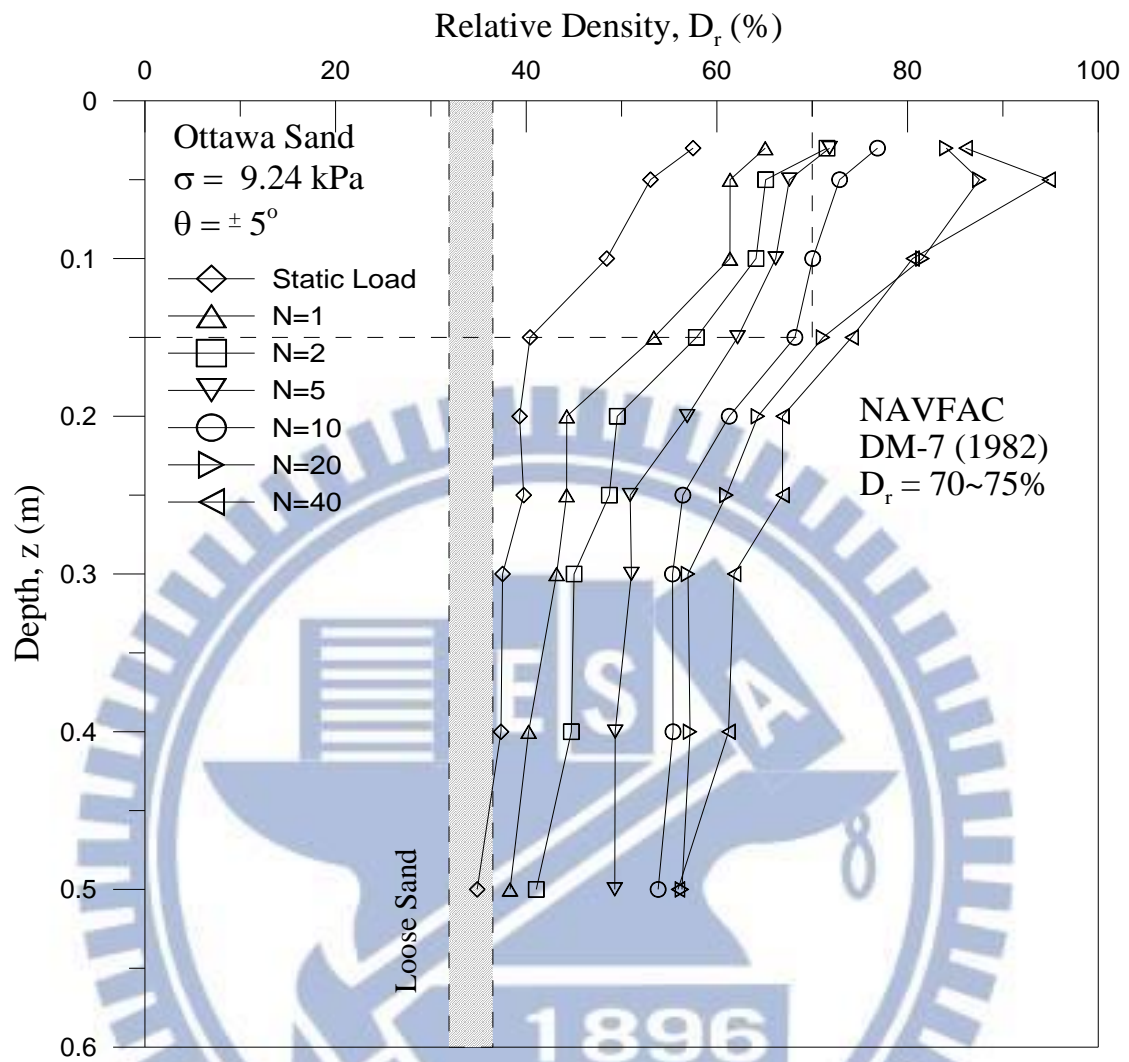
Fig. 2.16. Distribution of relative density due to cyclic torsional shearing (after Chen, 2011)

66
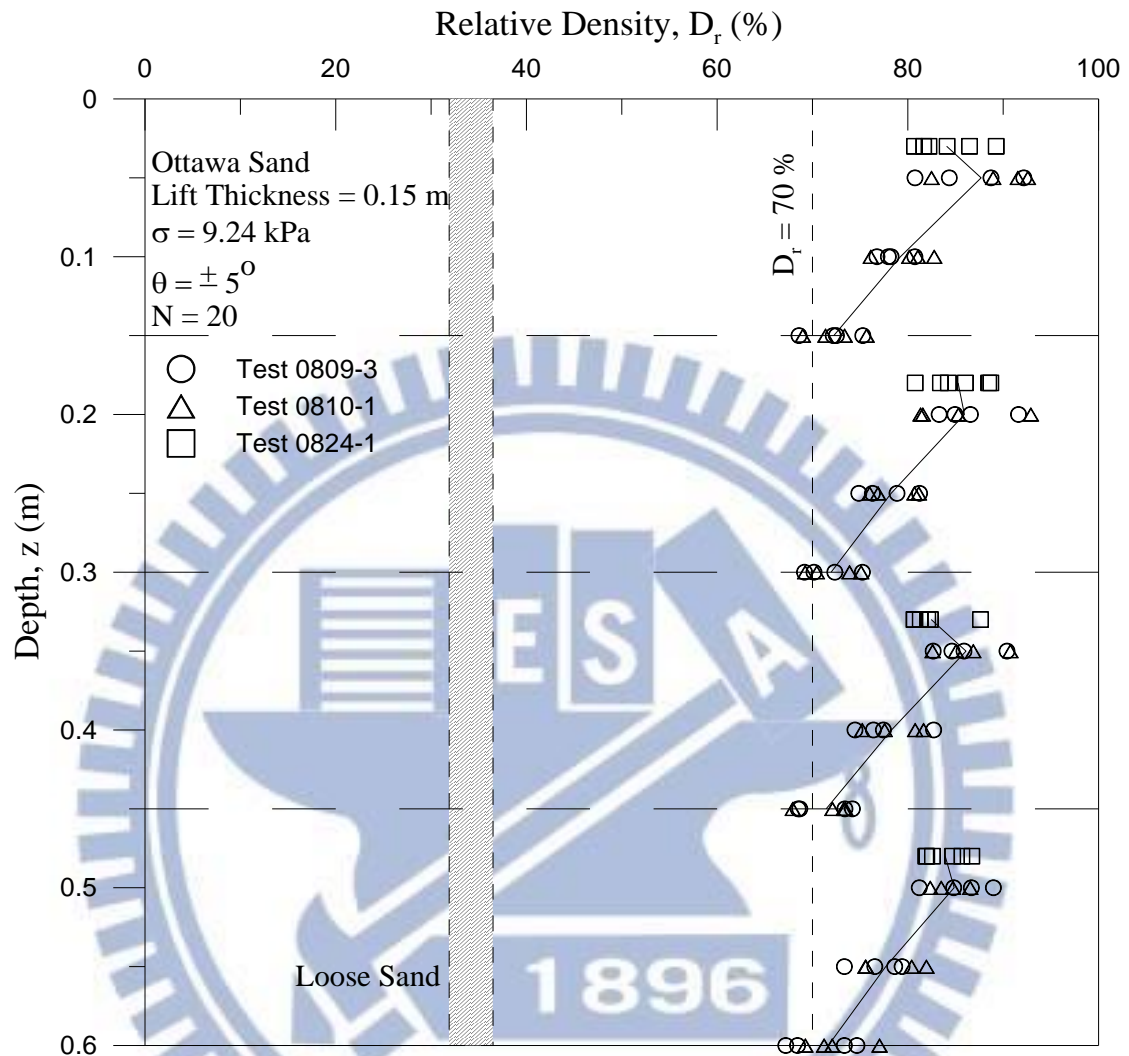
Fig. 2.17. Distribution of relative density in lift 1 to 4 (after Chen, 2011)

67
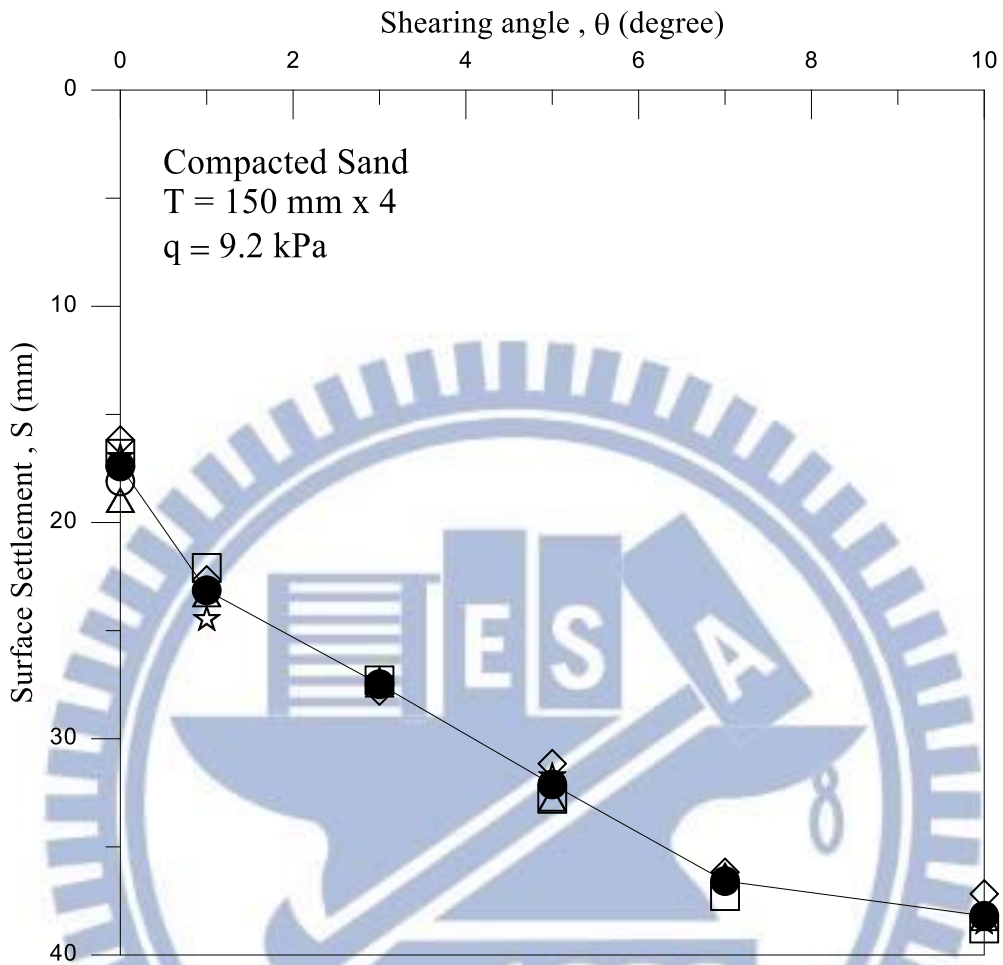
Fig. 2.18. Surface settlement as a function of shearing angle (after Liu, 2012)
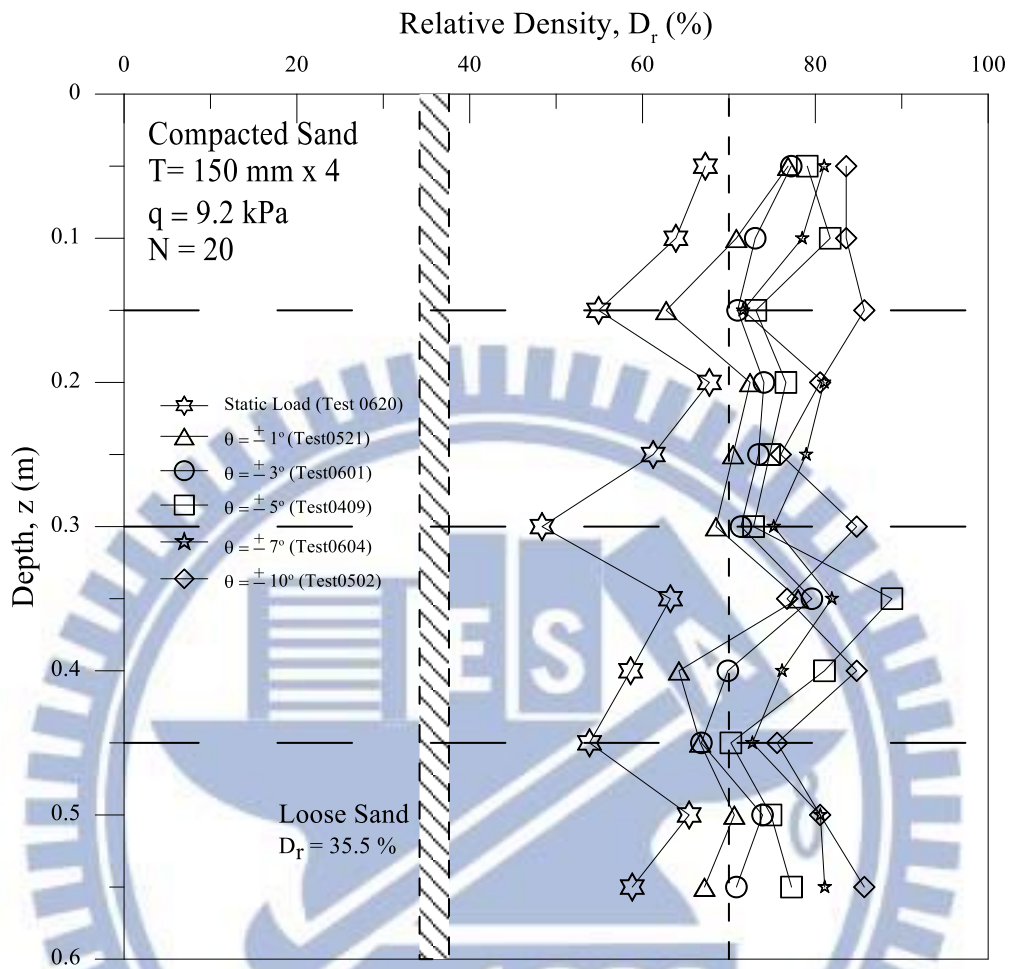
Fig. 2.19. Distribution of relative density after cyclic torsional shearing (after Liu, 2012)
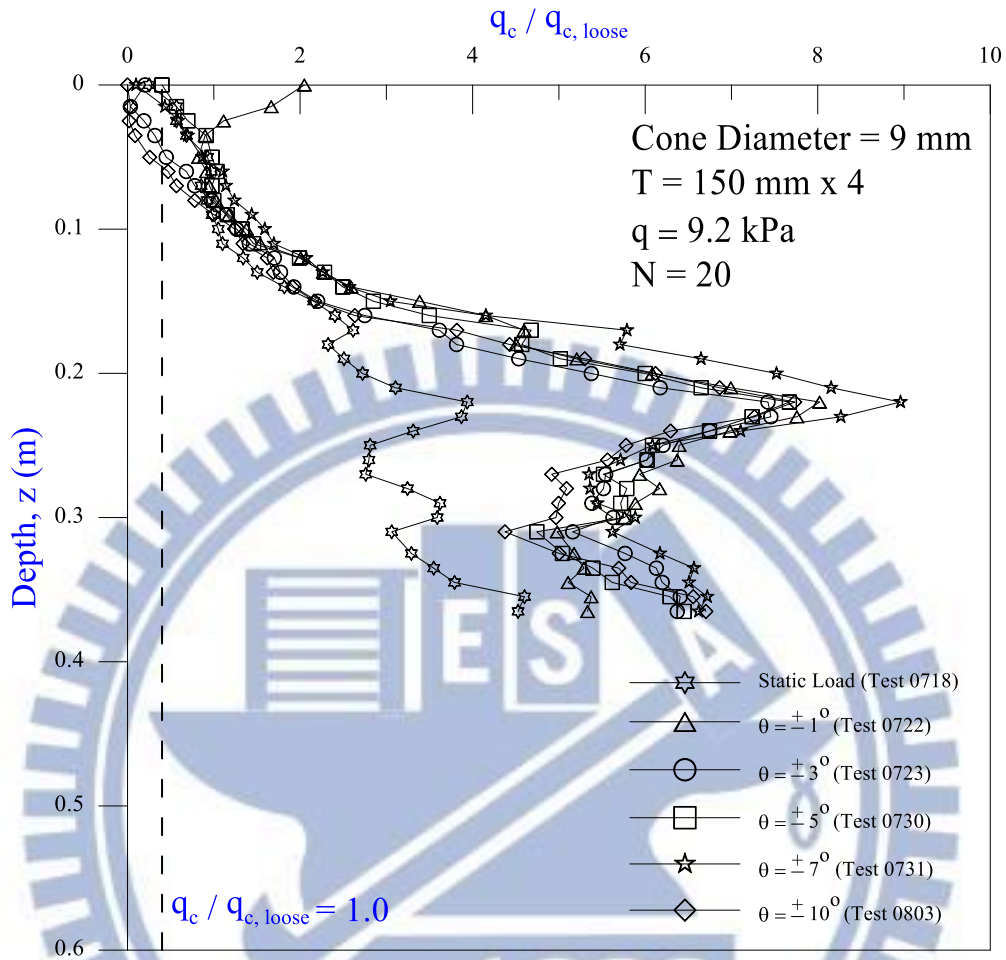
Fig. 2.20. Distribution of $q_c / q_{c,loose}$ after cyclic torsional shearing (after Liu, 2012)
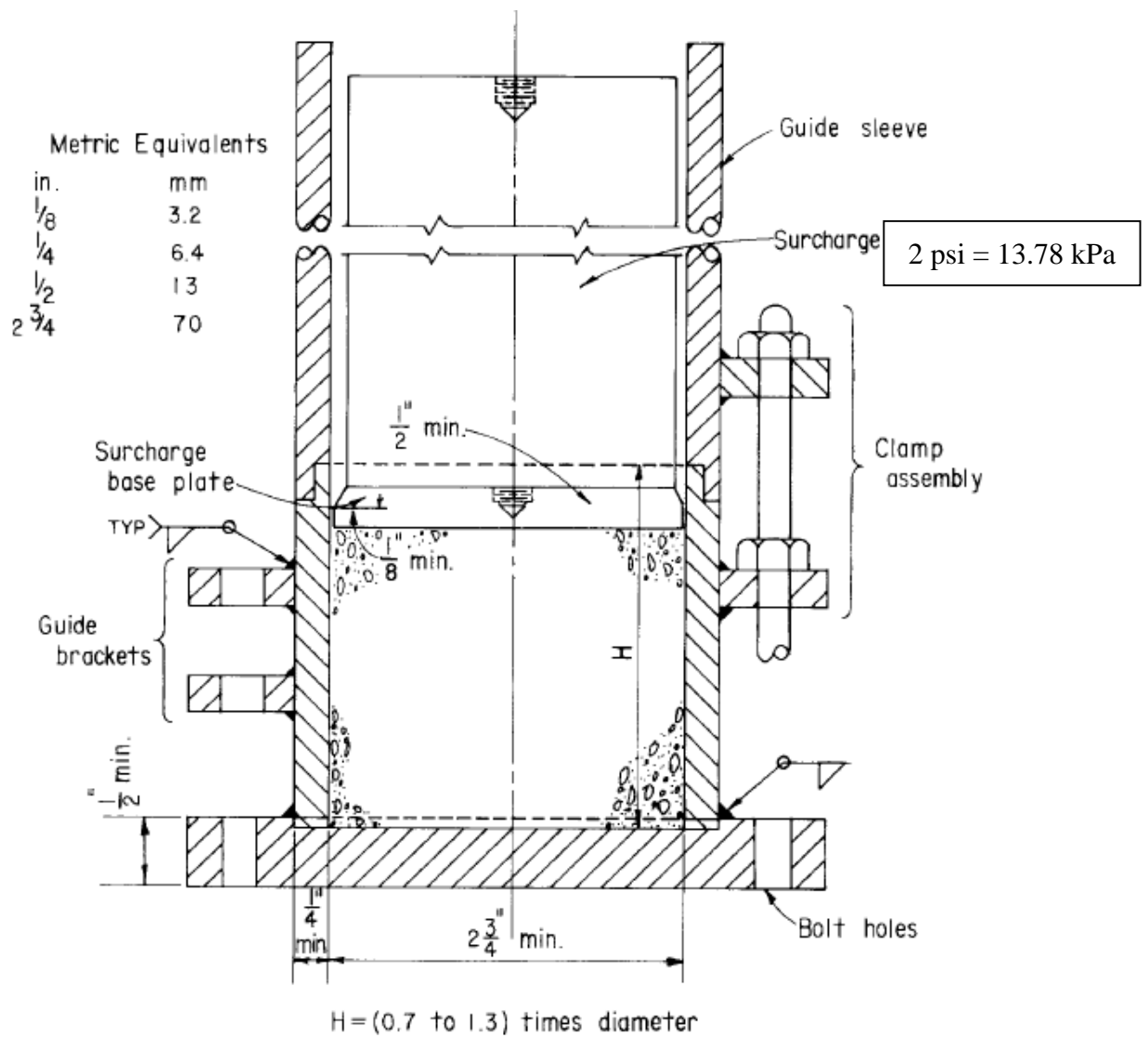
Fig 2.21 Special Cylindrical Metal Molds (after, ASTM D 4253)

Model Wall

1500

Sidewall

45

1500

Footboard

End
Wall

1600

20

Steel Base Plate

Steel Column
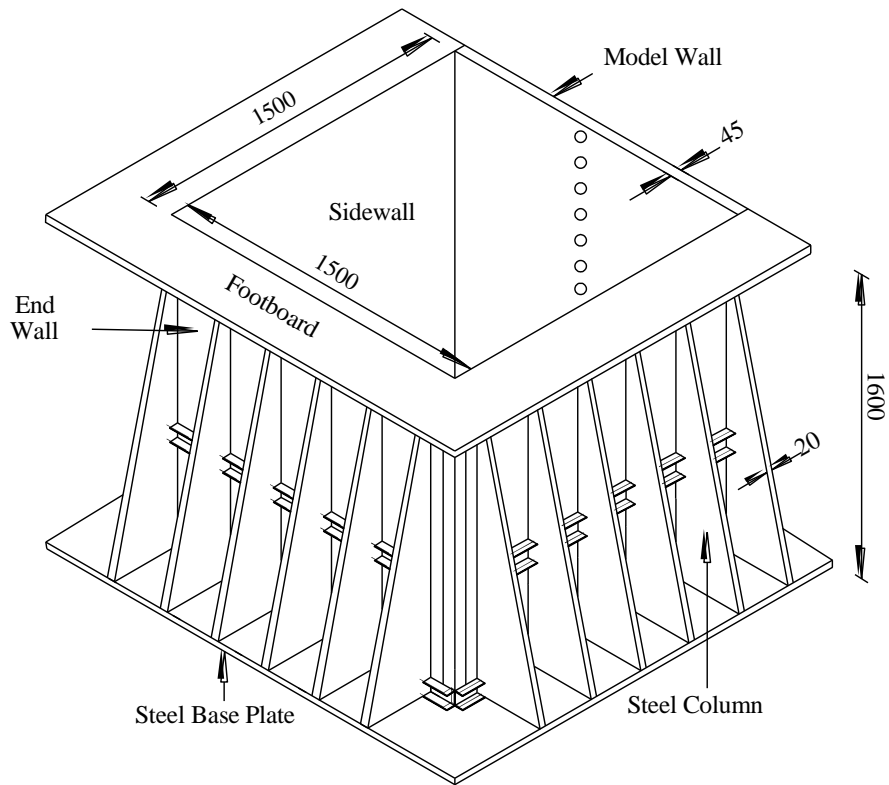
Unit : mm

Fig. 3.1. NCTU non-yielding model retaining wall and soil bin

(after Chen and Fang, 2008)
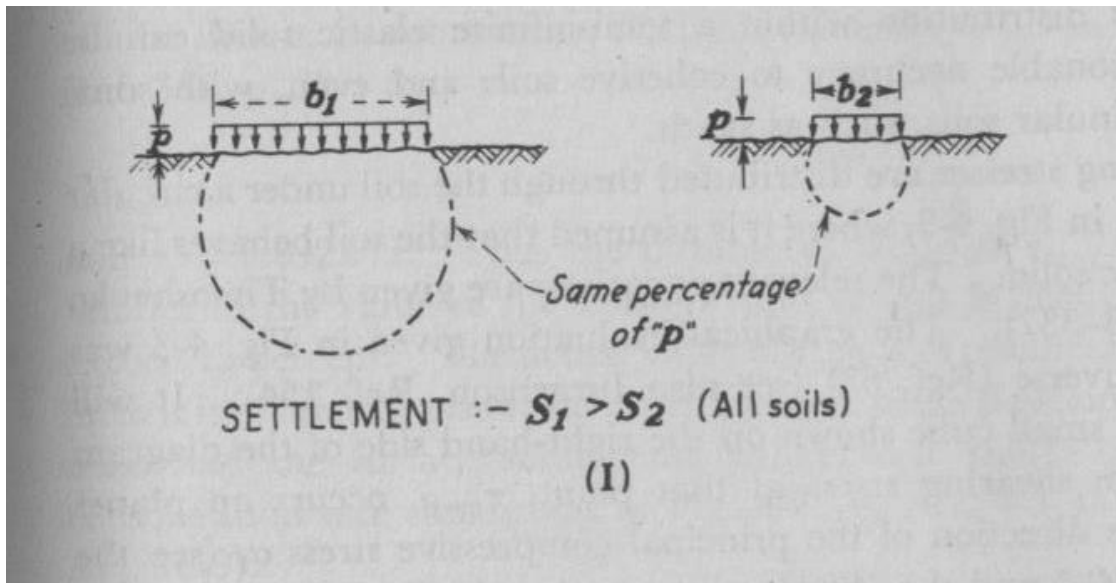
Fig. 3.2 Relationship between footing width and influenced depth (afte

Tschebotarioff, 1973)
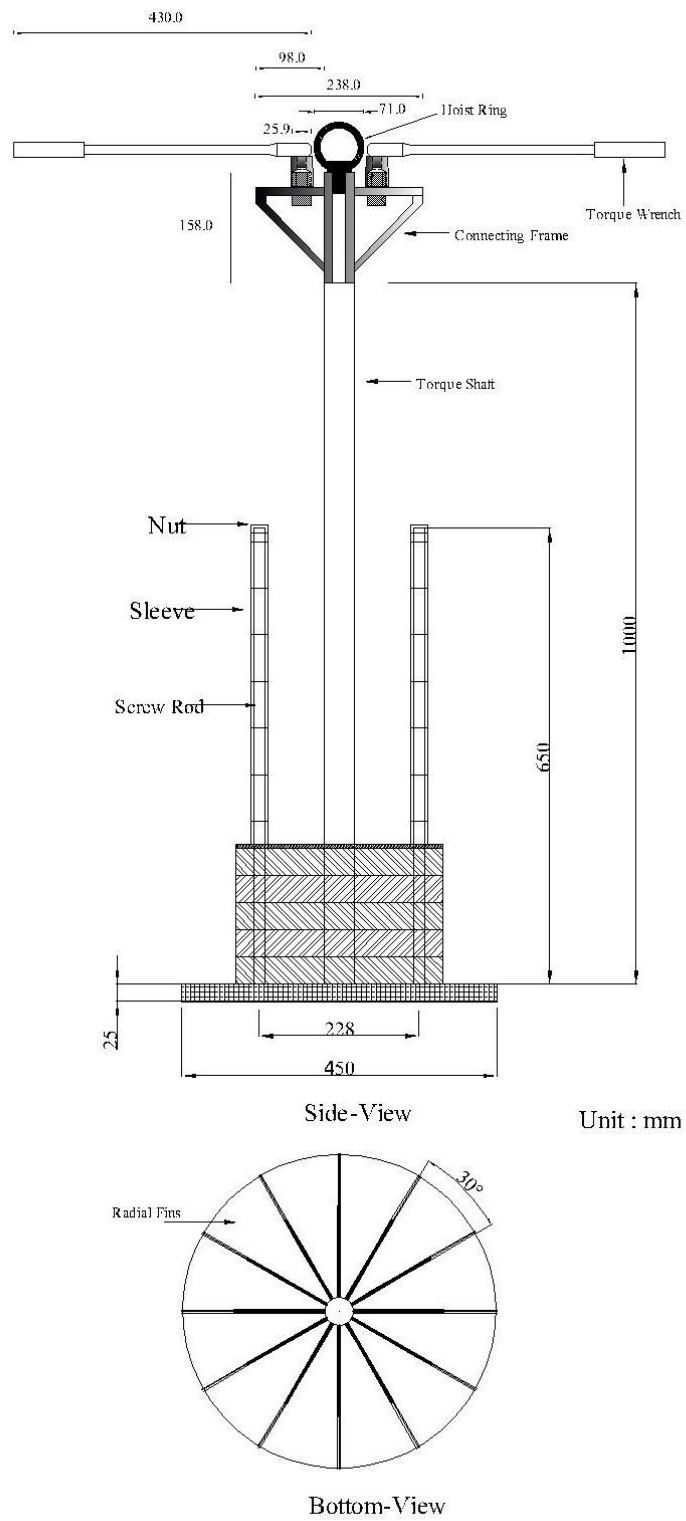
Fig. 3.3. Dimensions of cyclic torsional shear compactor
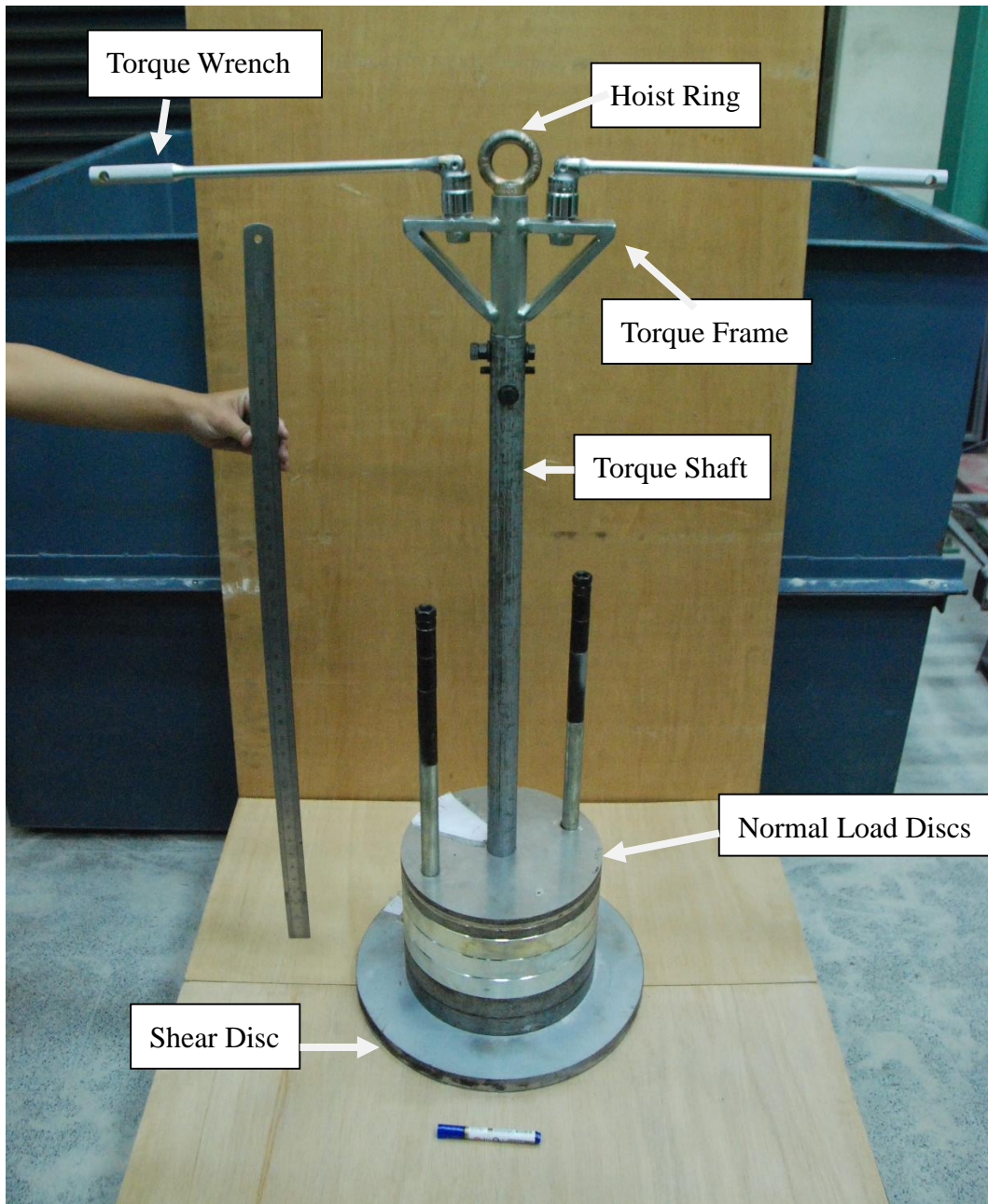
Fig. 3.4. Cyclic torsional shear compactor

Fig. 3.5. Bottom of shearing disc with radial fins
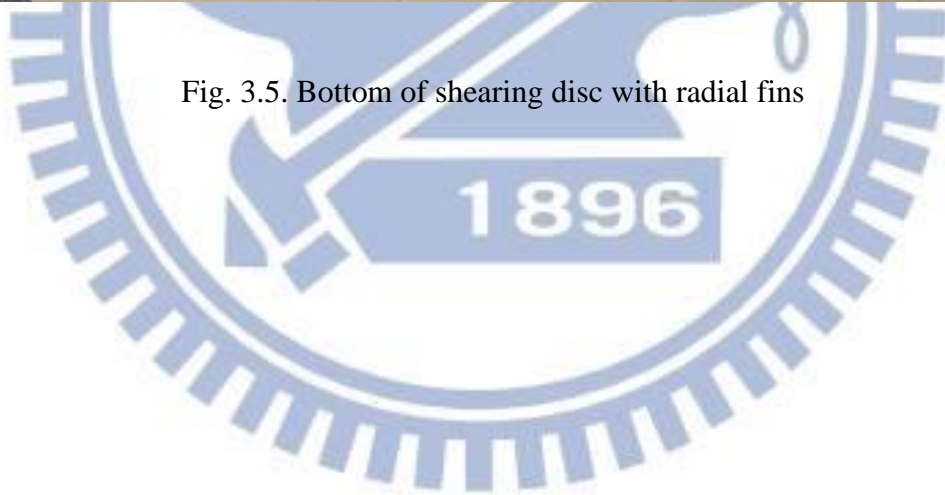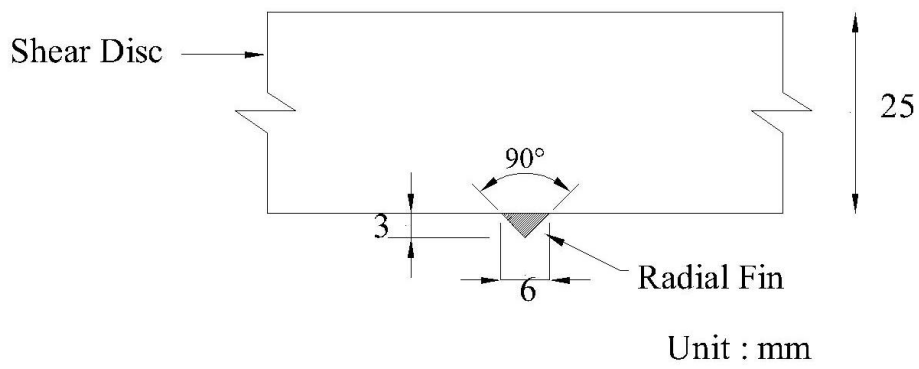
(a)

(b)

Fig. 3.6. Dimensions of a radial fin
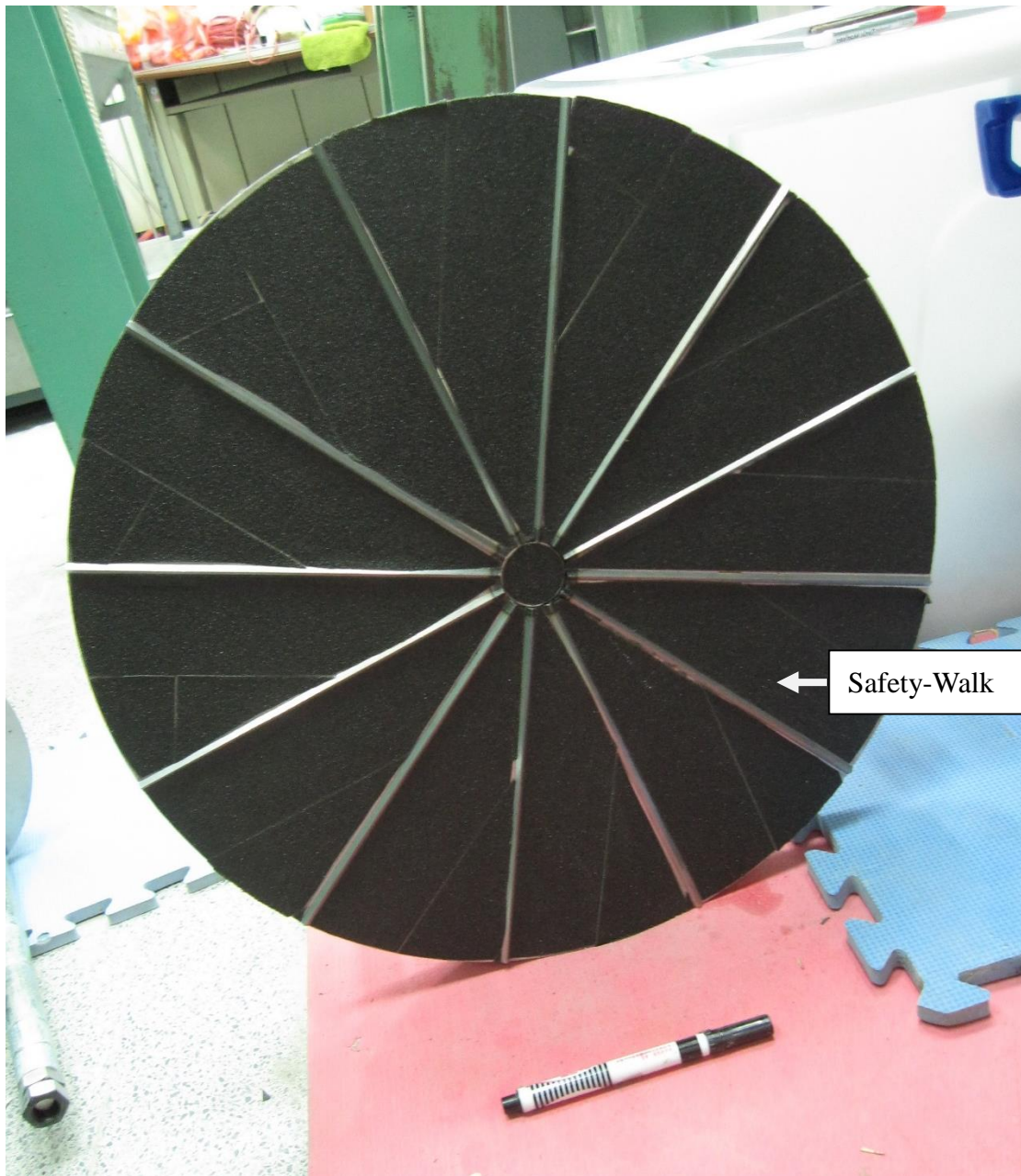
Fig. 3.7. Bottom of shearing disc with Safety-Walk
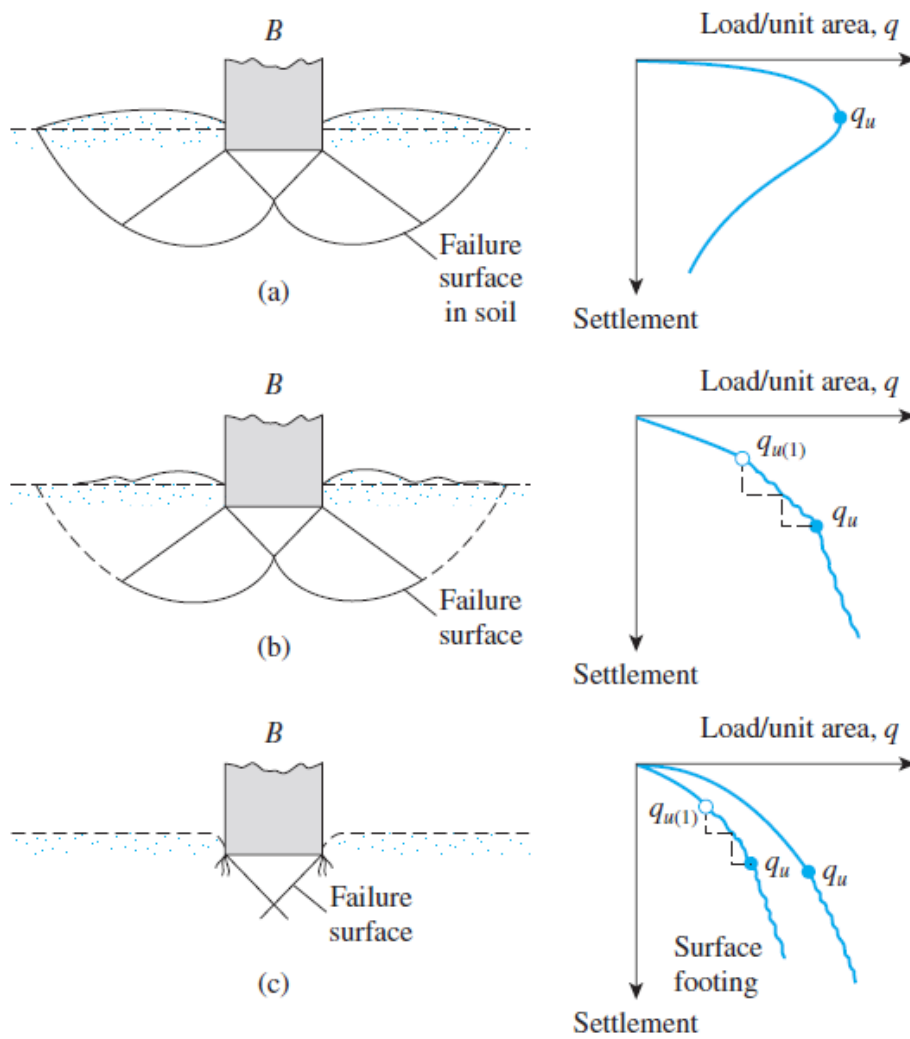
Fig. 3.8. Nature of bearing capacity failure in soil: (a) general shear failure; (b) local

shear failure; (c) punching shear failure (Radrawn after Vesic, 1973)
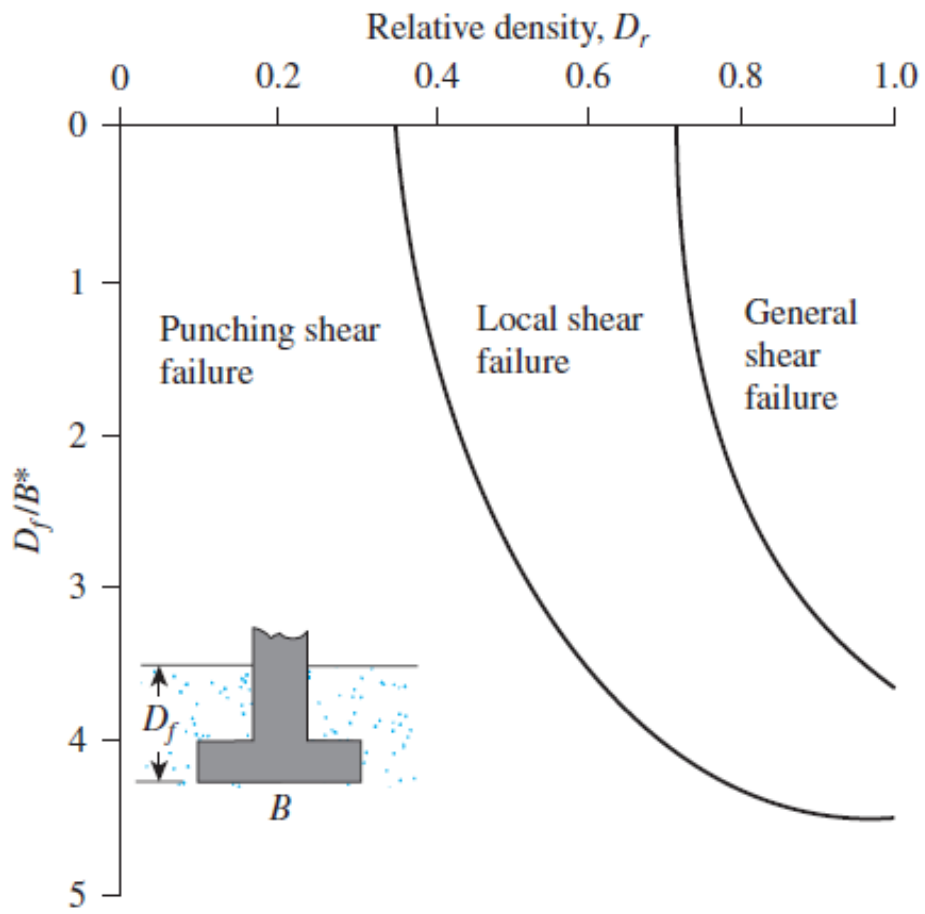
Fig. 3.9. Modes of foundation failure in sand (after Vesic, 1973)
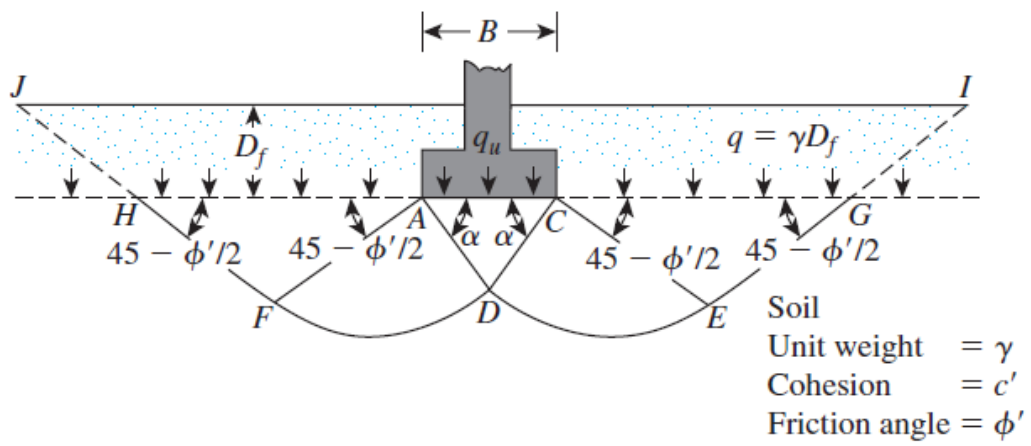
Fig. 3.10. Bearing capacity failure in soil under a rough rigid continuous foundation

(after Terzaghi, 1943)
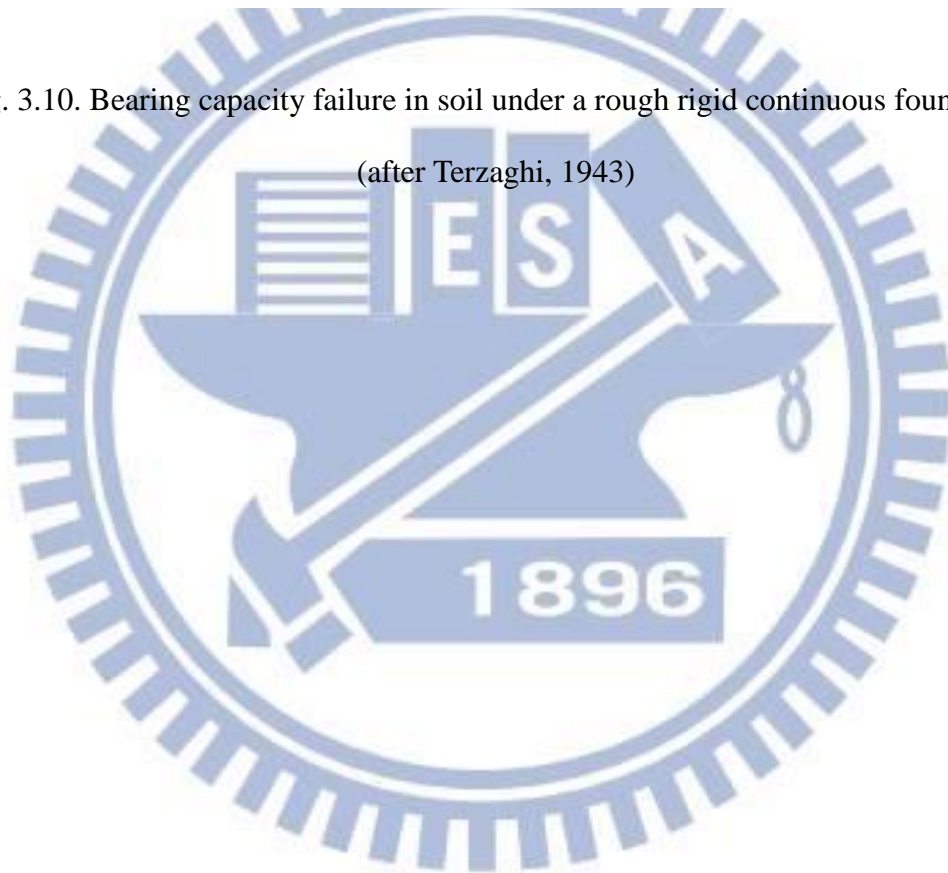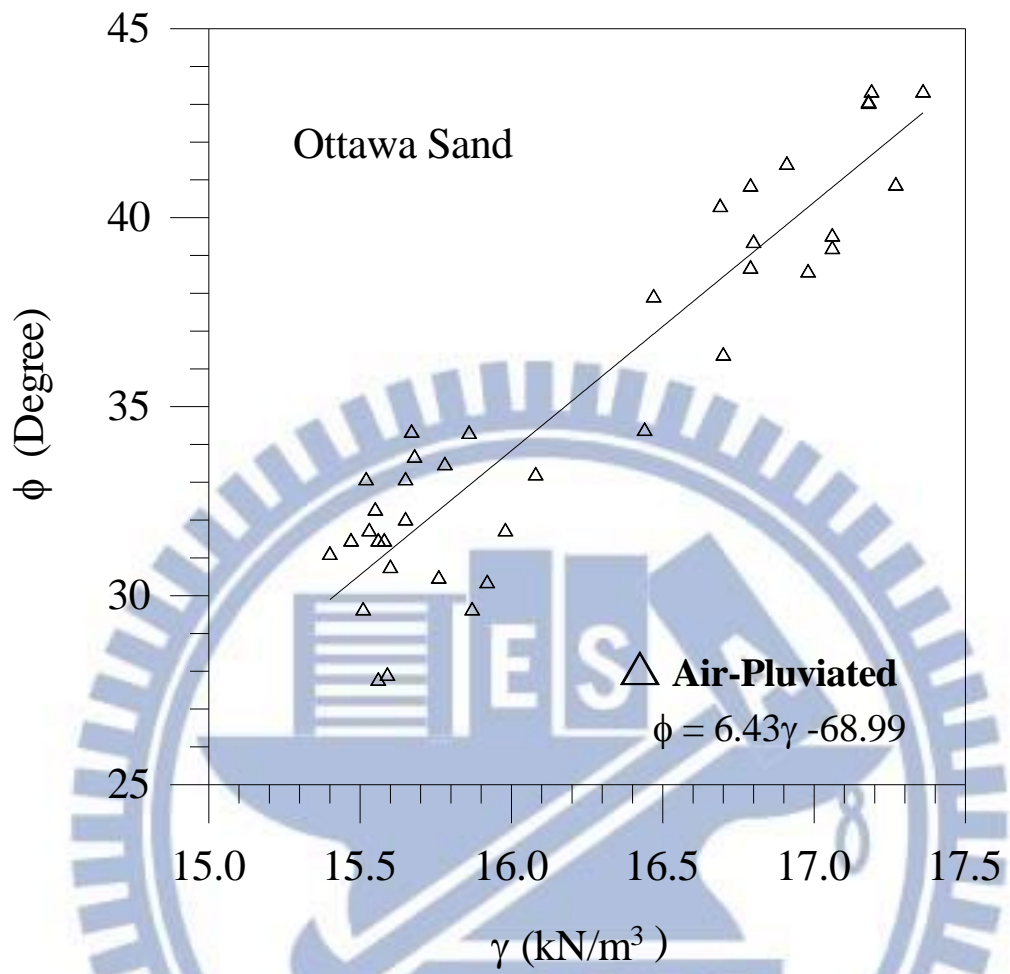
Fig. 3.11 Relationship between Unit Weight γ and Internal Friction Angle φ

(after Chang, 2000)

Top-View

Side-View
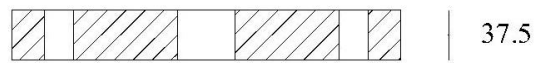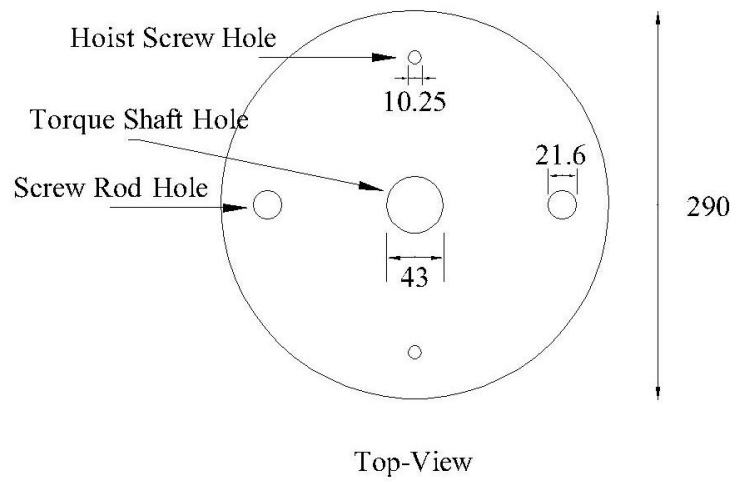
Unit : mm

(a)

(b)

Fig. 3.12. Dimensions of normal loading disc for mass = 19.80 kg
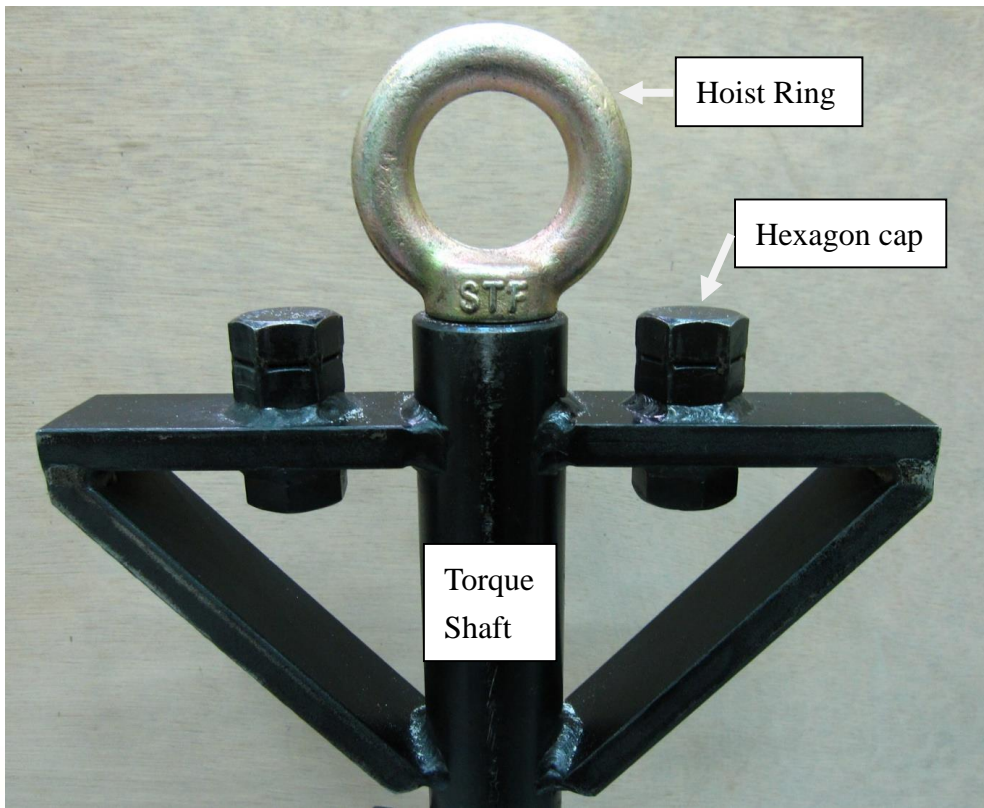
Fig. 3.13. Torque loading frame (after Chen, 2011)

Hoist Ring

Hexagon cap
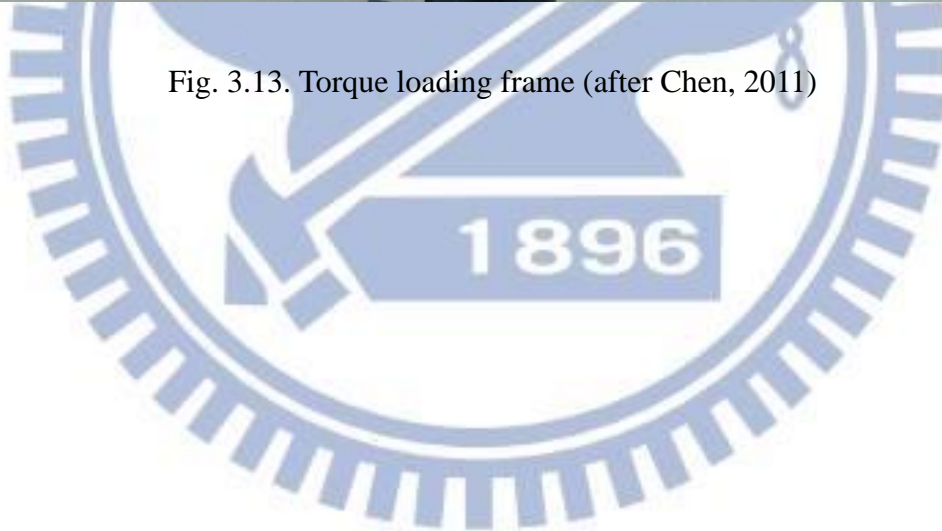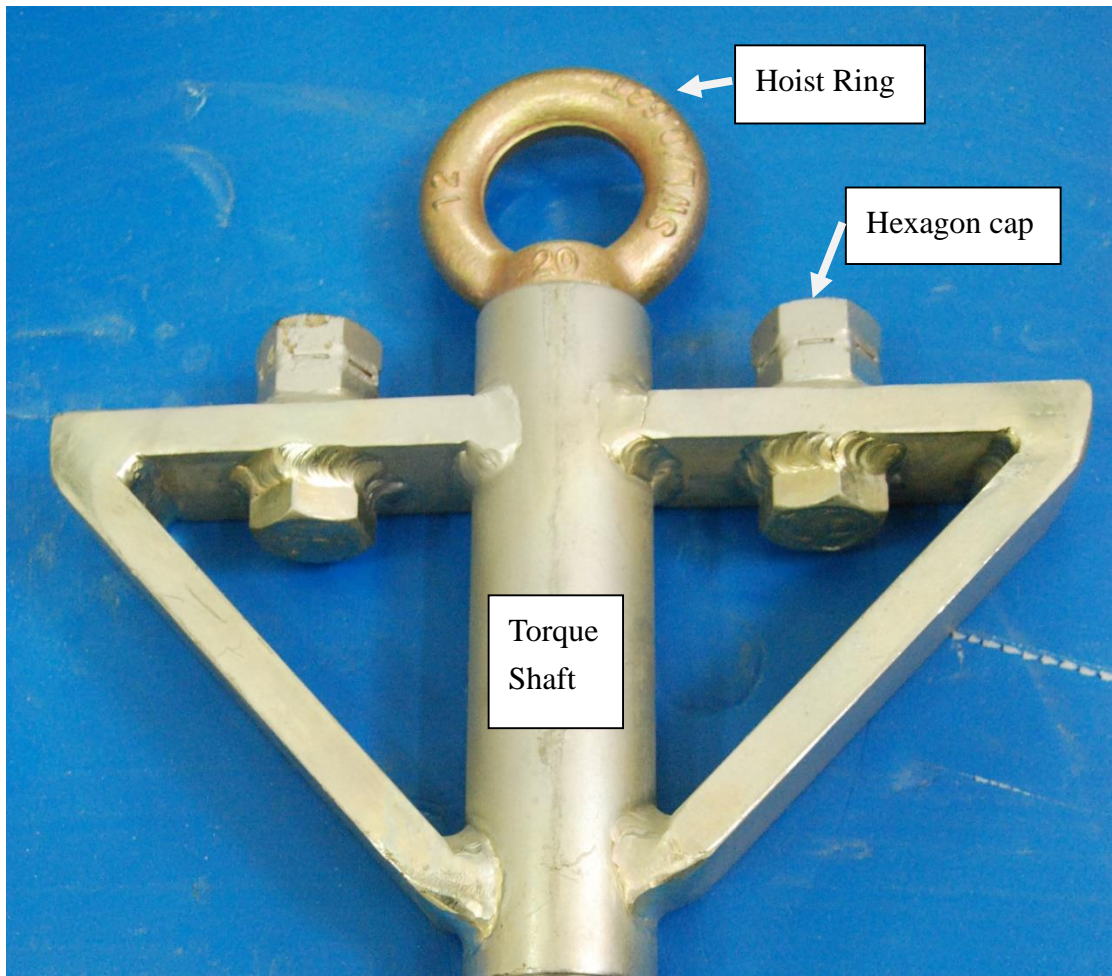
Torque
Shaft

Fig. 3.14. Torque loading frame
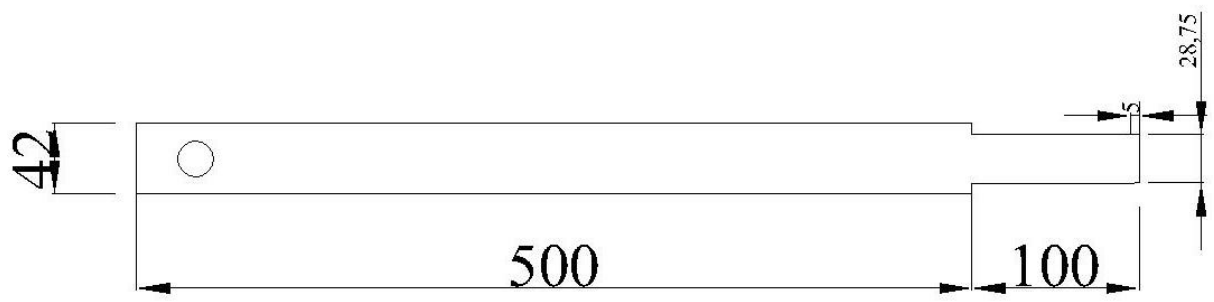
Unit: mm

(a)
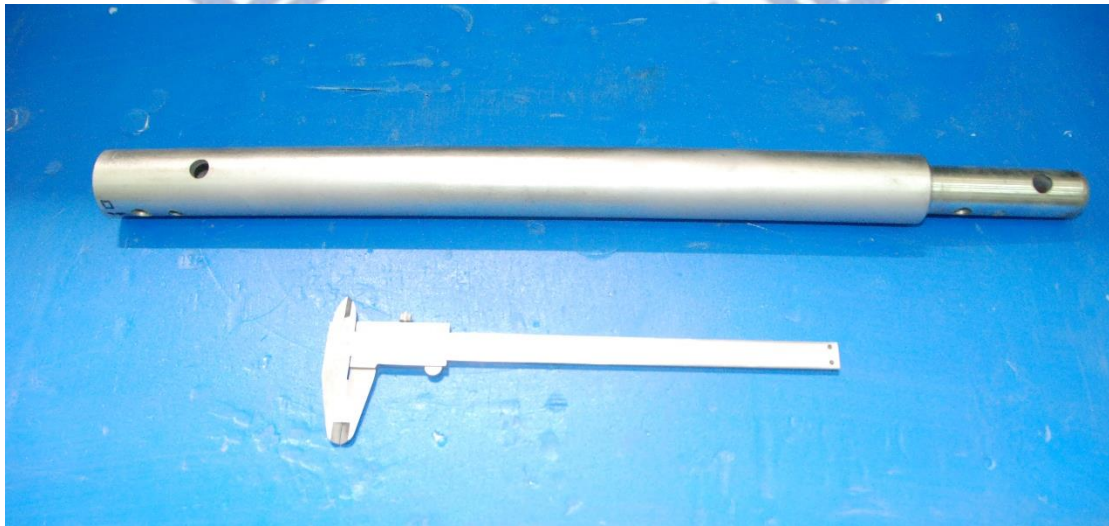
(b)

Fig. 3.15. Dimensions of extension tube
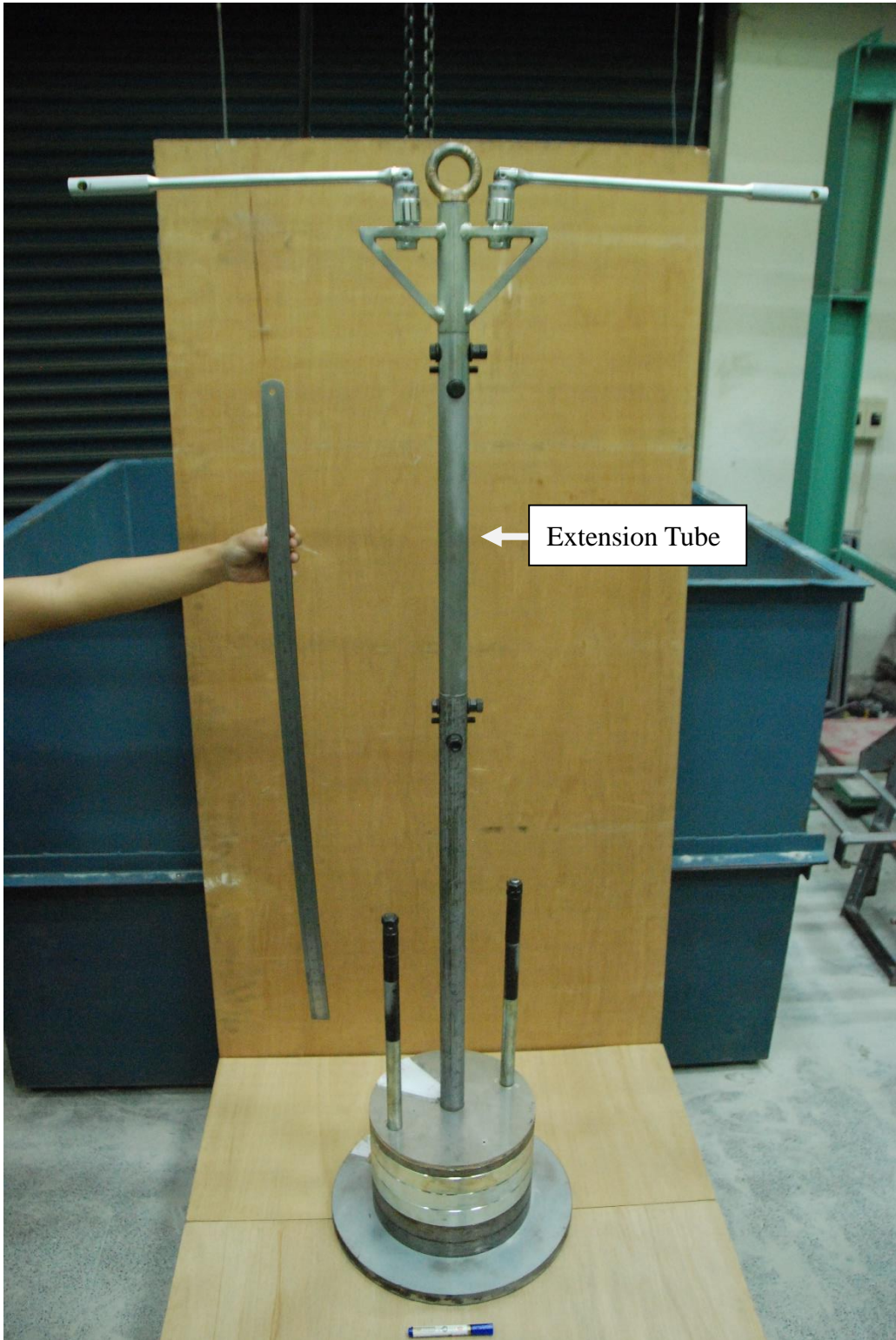
Fig. 3.16. CTSC and torque loading frame are connected by extension tube

430
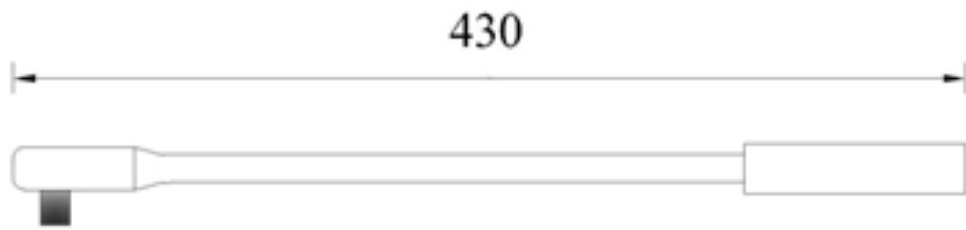
Unit : mm

(a)

(b)

Fig. 3.17. Dimensions of torque wrench (after Chen, 2011)
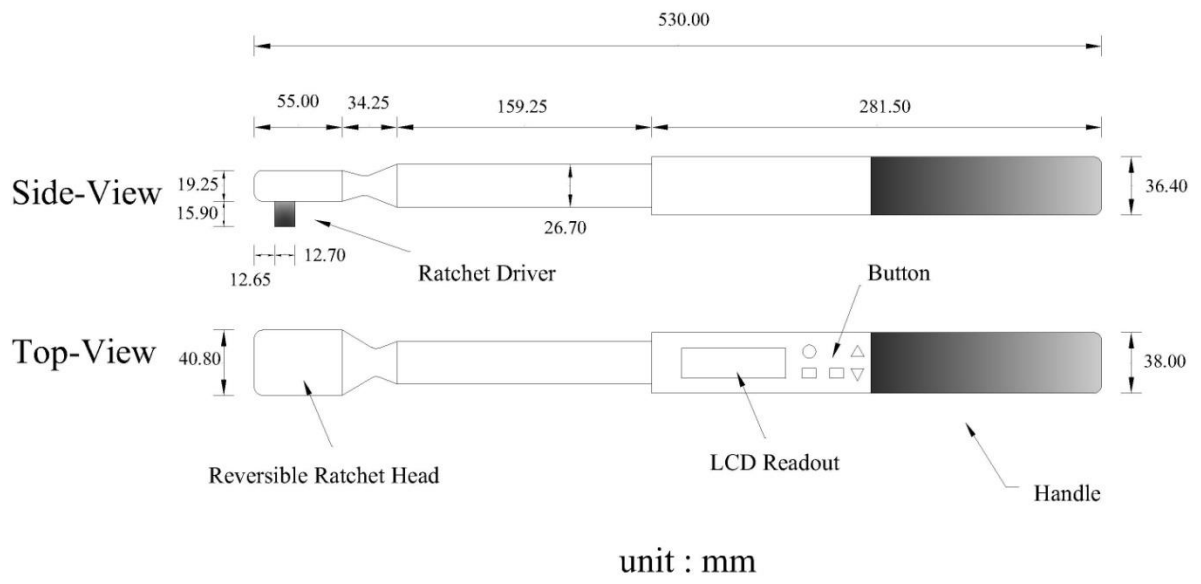
(a)

(b)

Fig. 3.18. Dimensions of digital torque wrench (after Chen, 2011)
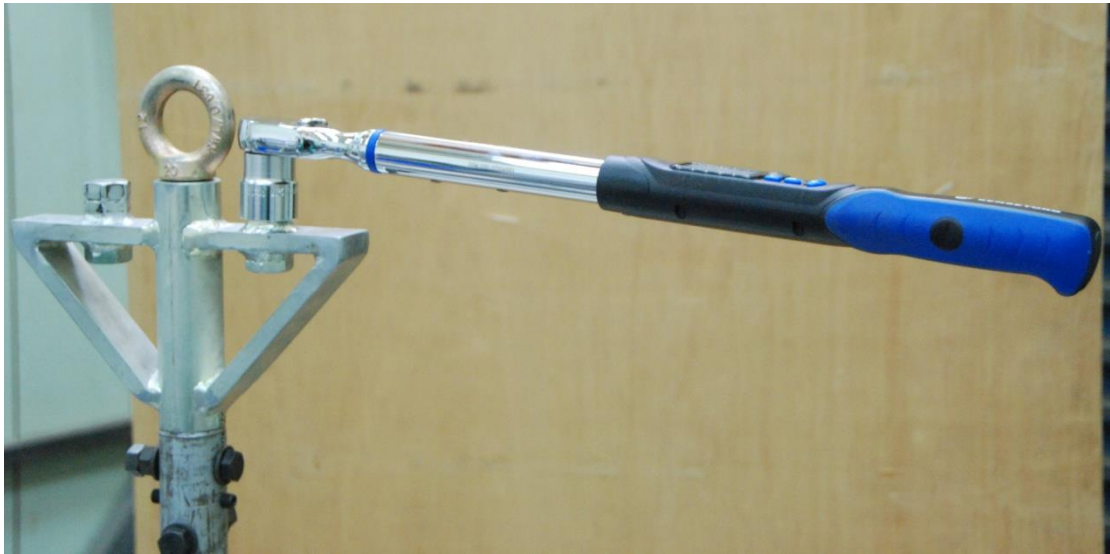
Fig. 3.19. Digital torque wrench are installed on the connecting frame
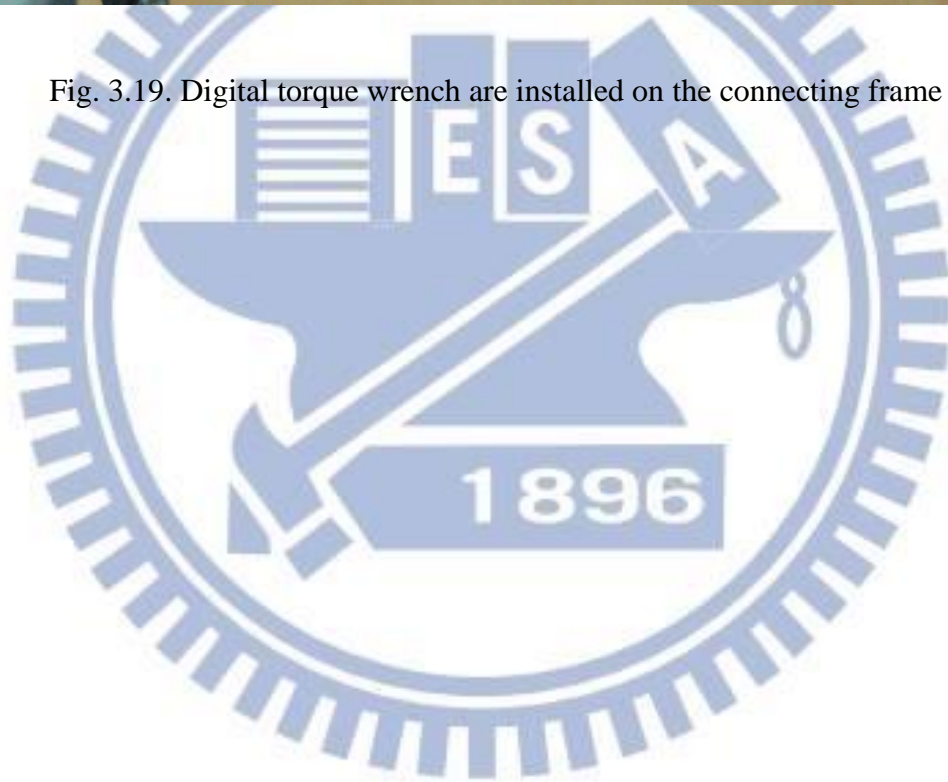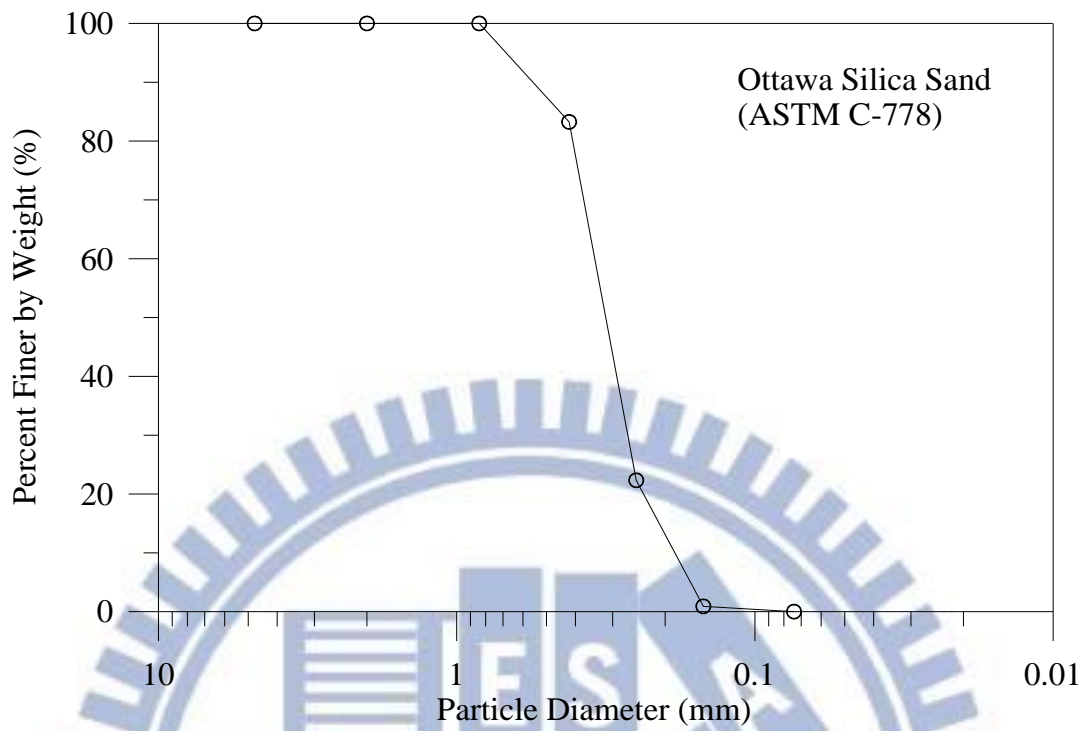
Fig. 4.1. Grain size distribution of Ottawa sand (after Chen, 2003)
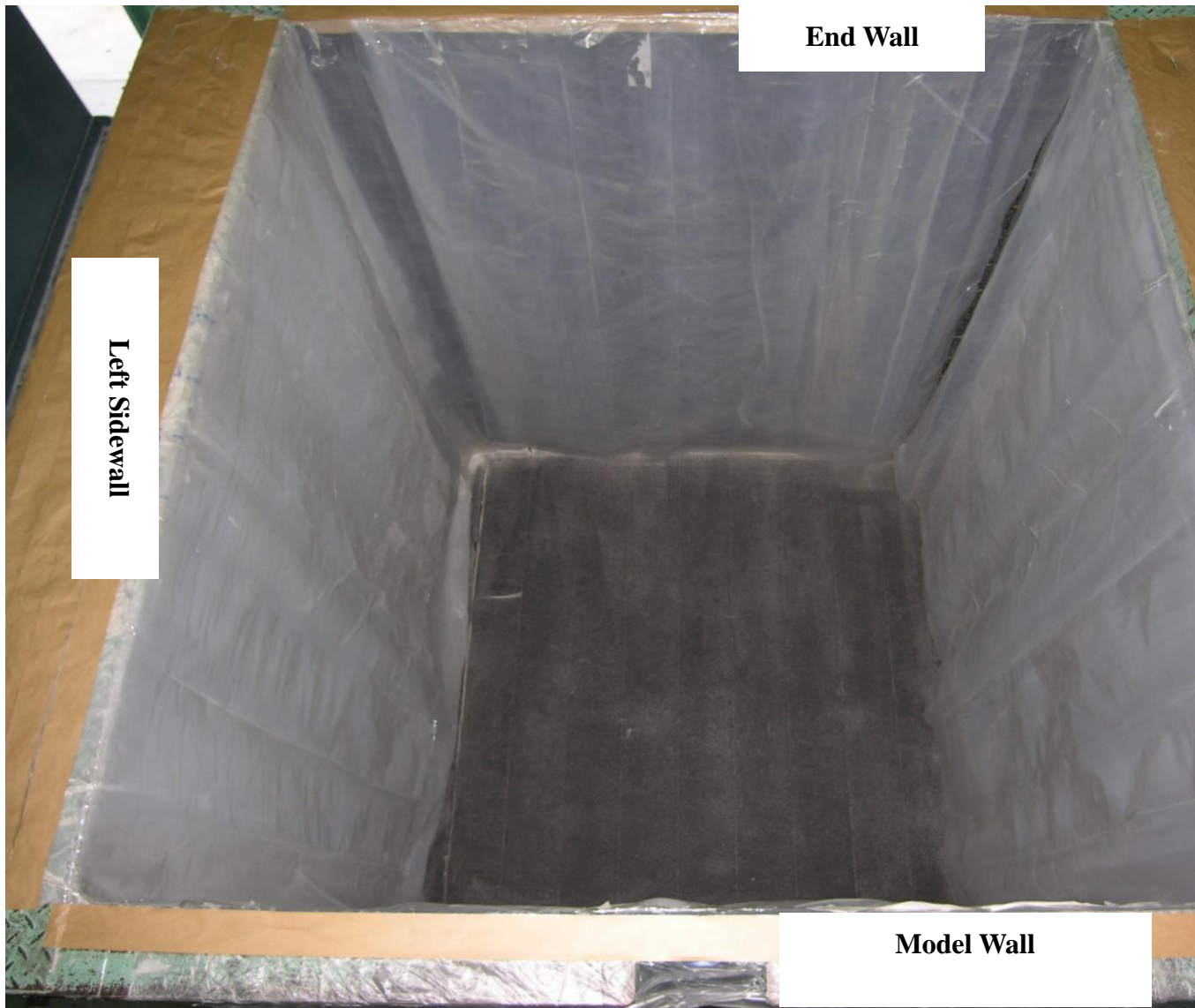
Fig. 4.2. Lubrication layers on the side walls (after Chen, 2011)
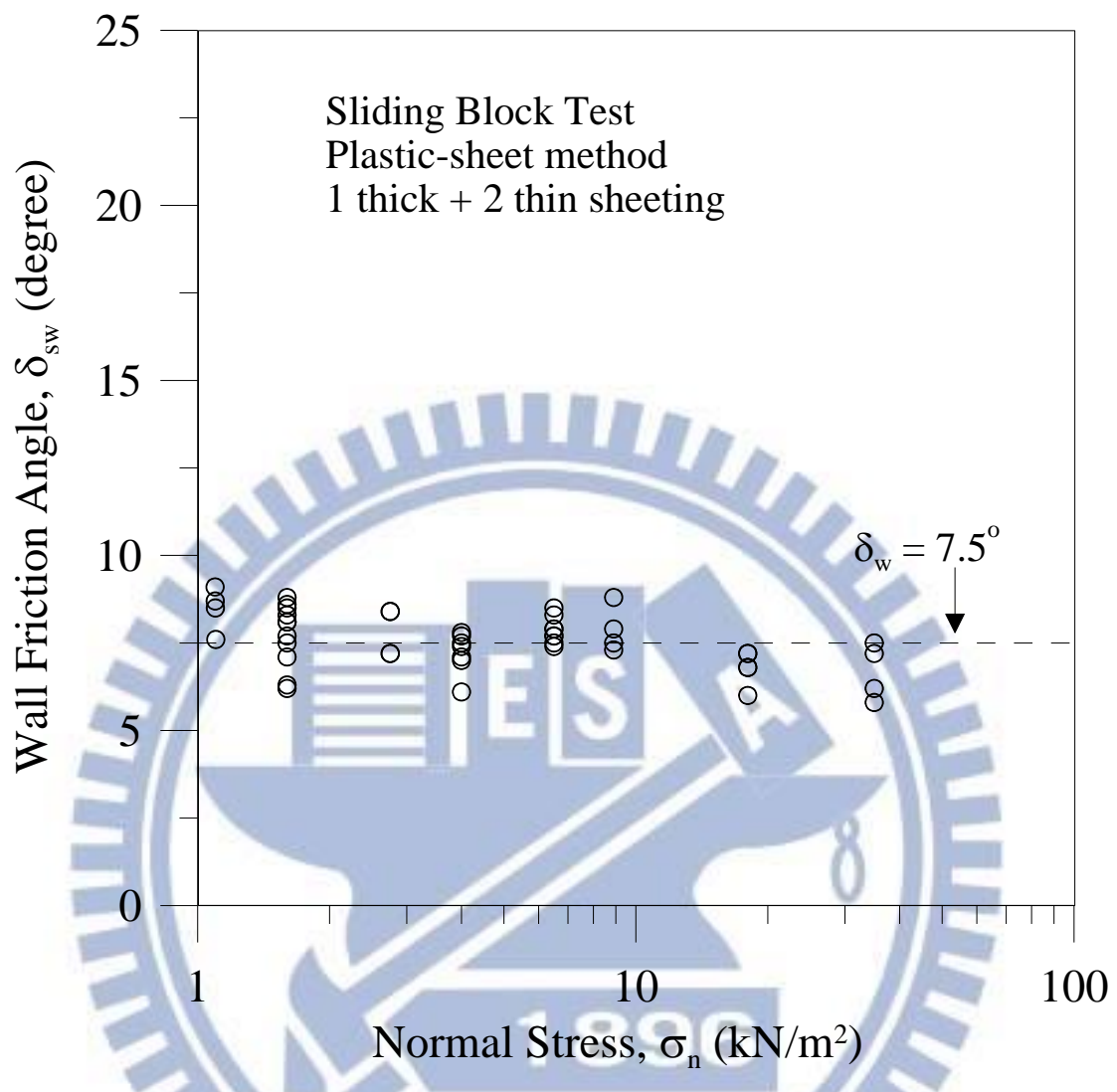
Fig. 4.3. Variation of friction angle with normal stress (after Fang et al., 2004)

940

500

800

500

430

120

Slot Opening

Slot Control Handle
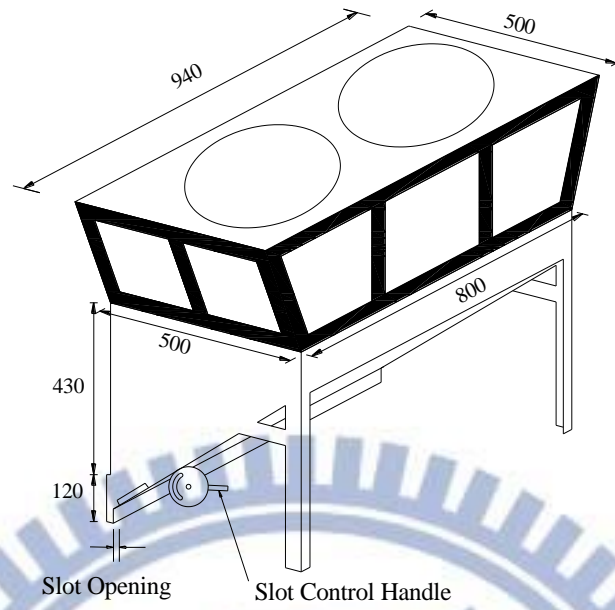
<u>Unit:mm</u>

Fig. 4.4. Soil hopper

Opening = 15 mm
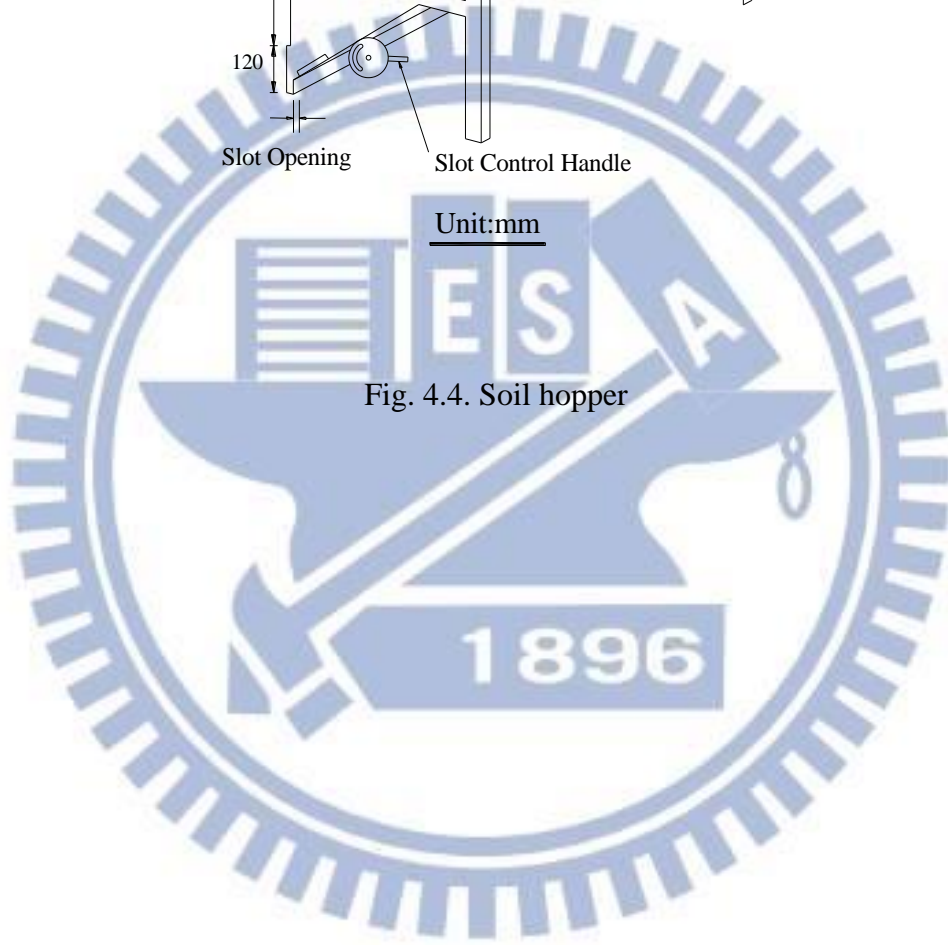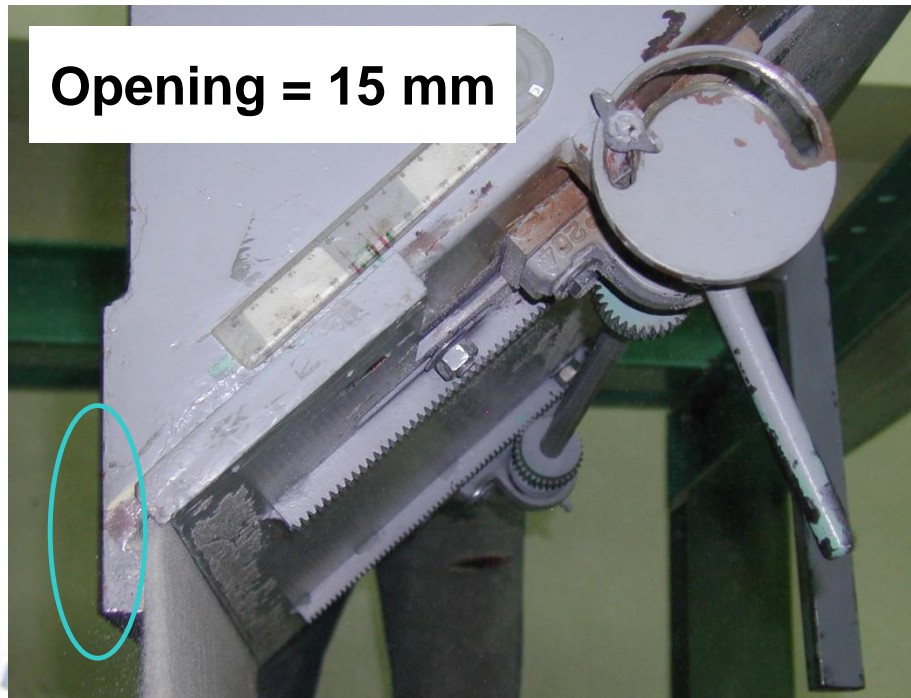
Drop Height = 1.0m

Fig. 4.5 Pluviation of Ottawa sand into soil bin (after Chen, 2011)
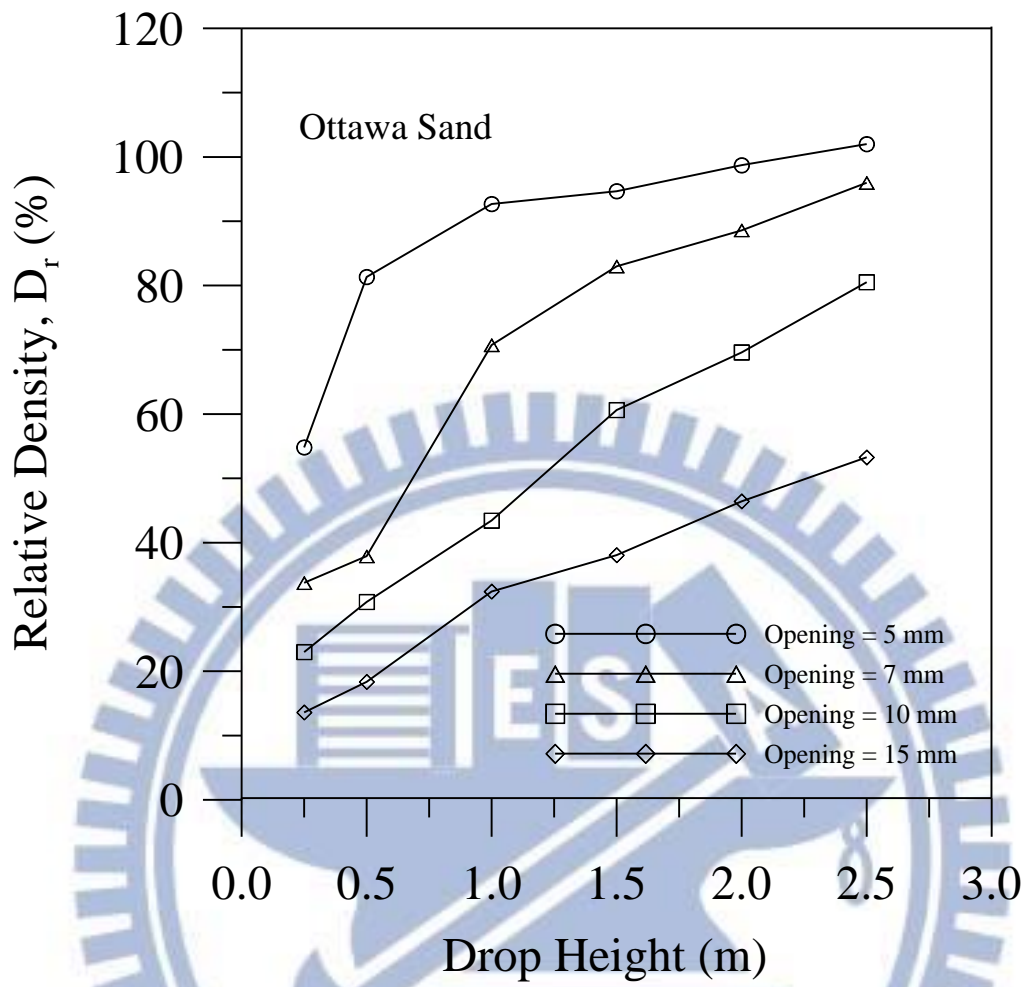
Fig. 4.6 Relationship among slot opening, drop height, and relative density
(after Ho, 1999)
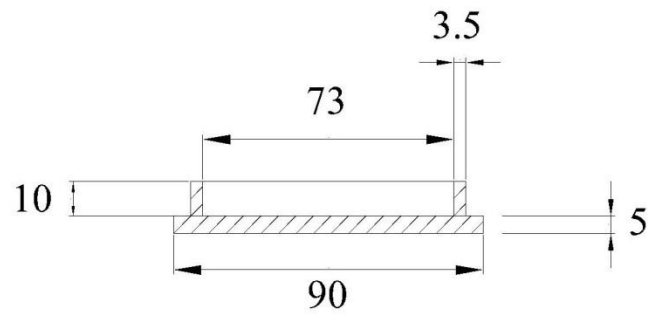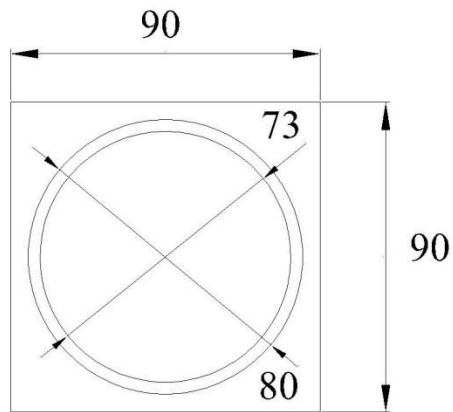
Fig. 4.7. Dimensions of soil density cup (after Chen, 2011)
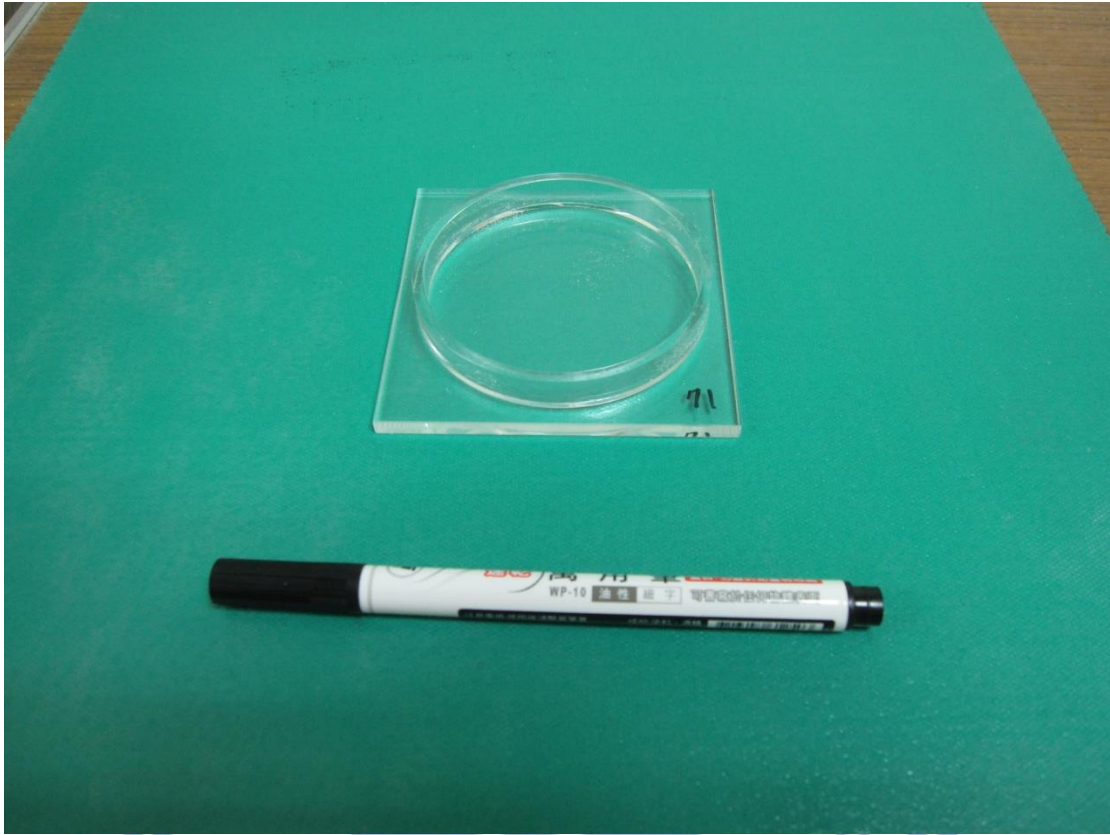
Fig. 4.8. Soil density cup
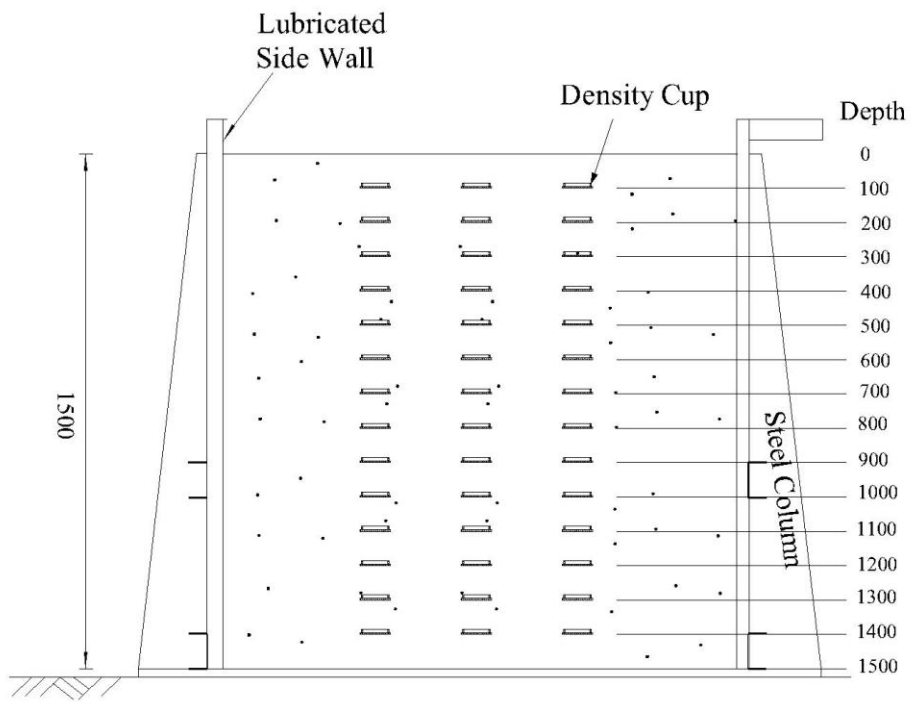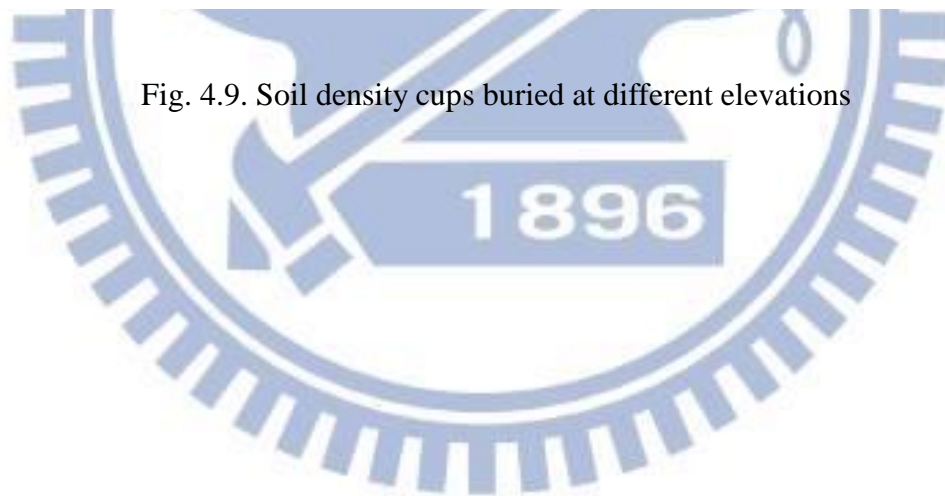
Fig. 4.9. Soil density cups buried at different elevations
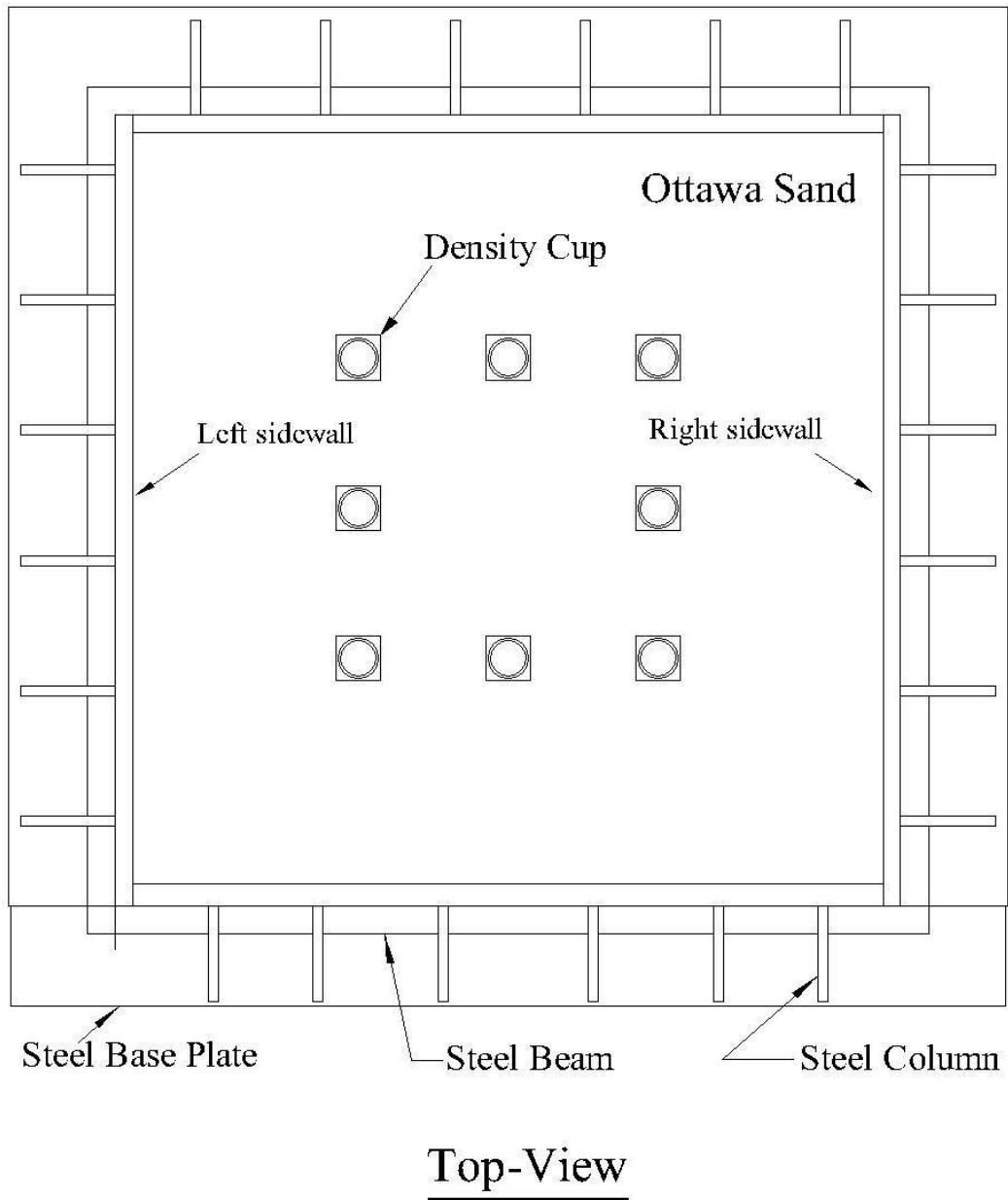
Fig. 4.10. Arrangement of soil density cups at same elevation

Fig. 4.11. Measurement of soil mass in density cup
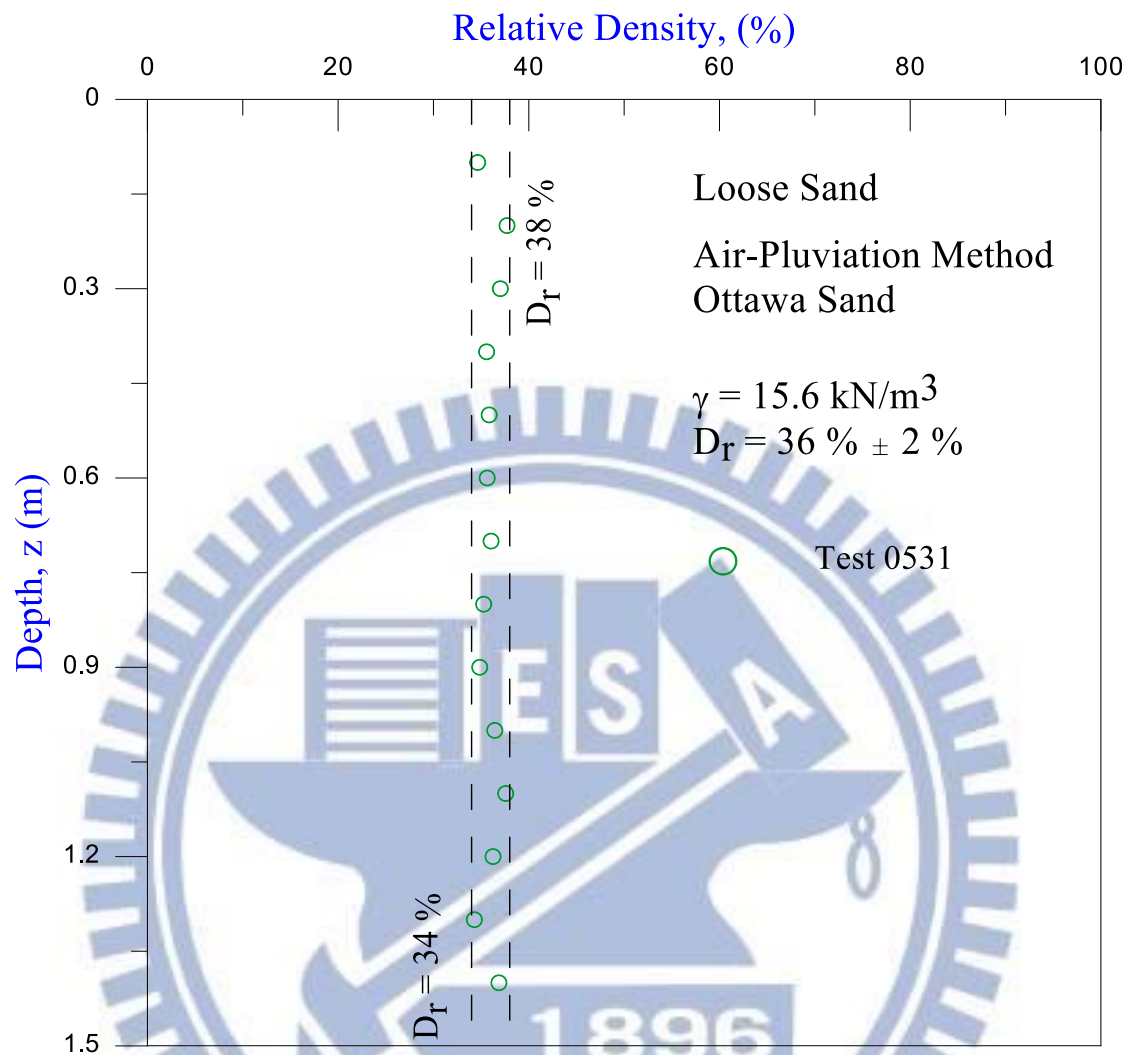
Fig. 4.12. Distribution of relative density with depth

Fig. 5.1. Soil storage
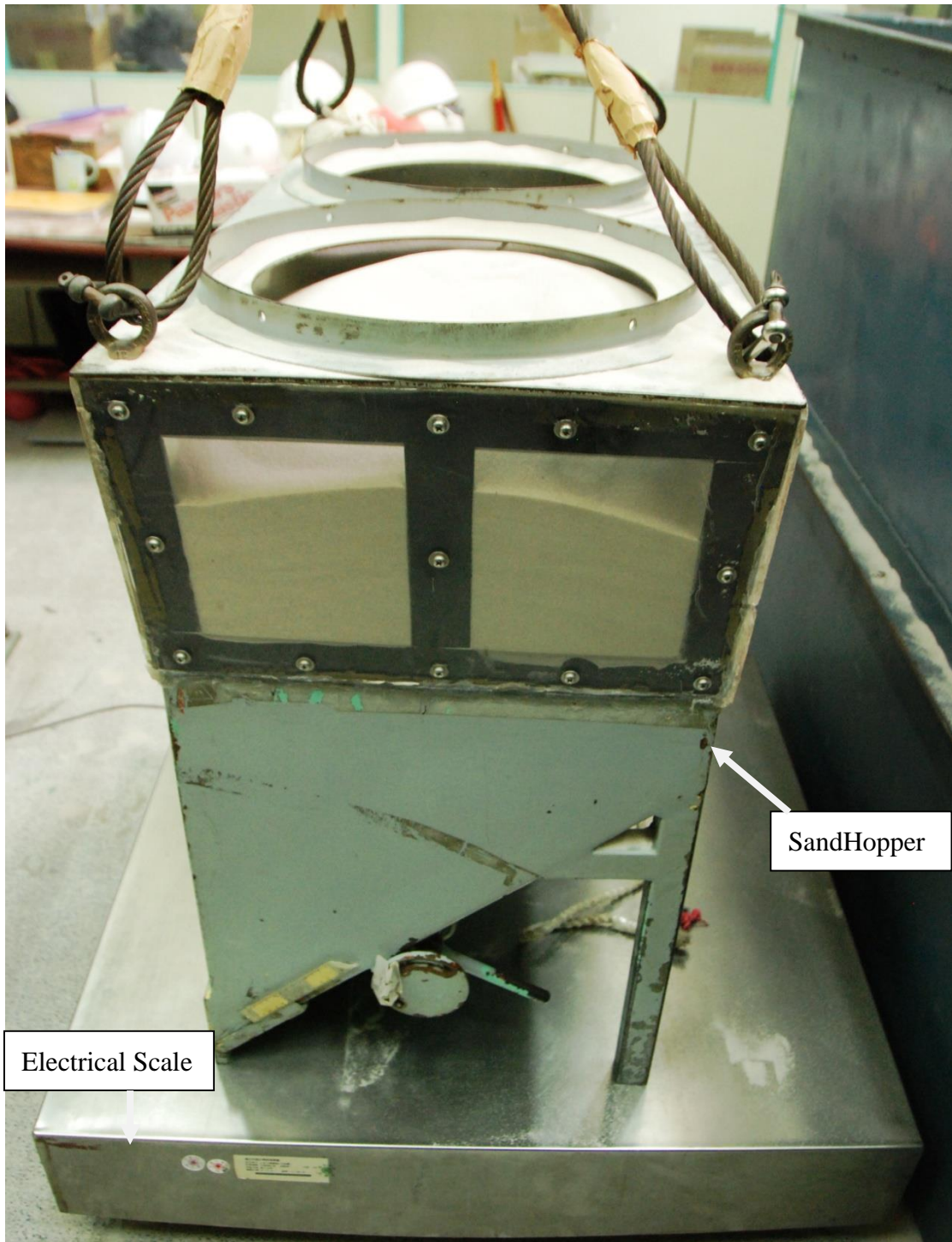
Fig. 5.2. Sand hopper and electrical scale

Fig. 5.3. Sand hopper lifted by overhead crane (after Chen, 2011)

Fig. 5.4. Air-pluviation of Ottawa sand into soil bin

(a)

(b)

Fig. 5.5. Portable ladders and bridge board hung on side walls

Fig. 5.6. Leveling of soil surface with a brush
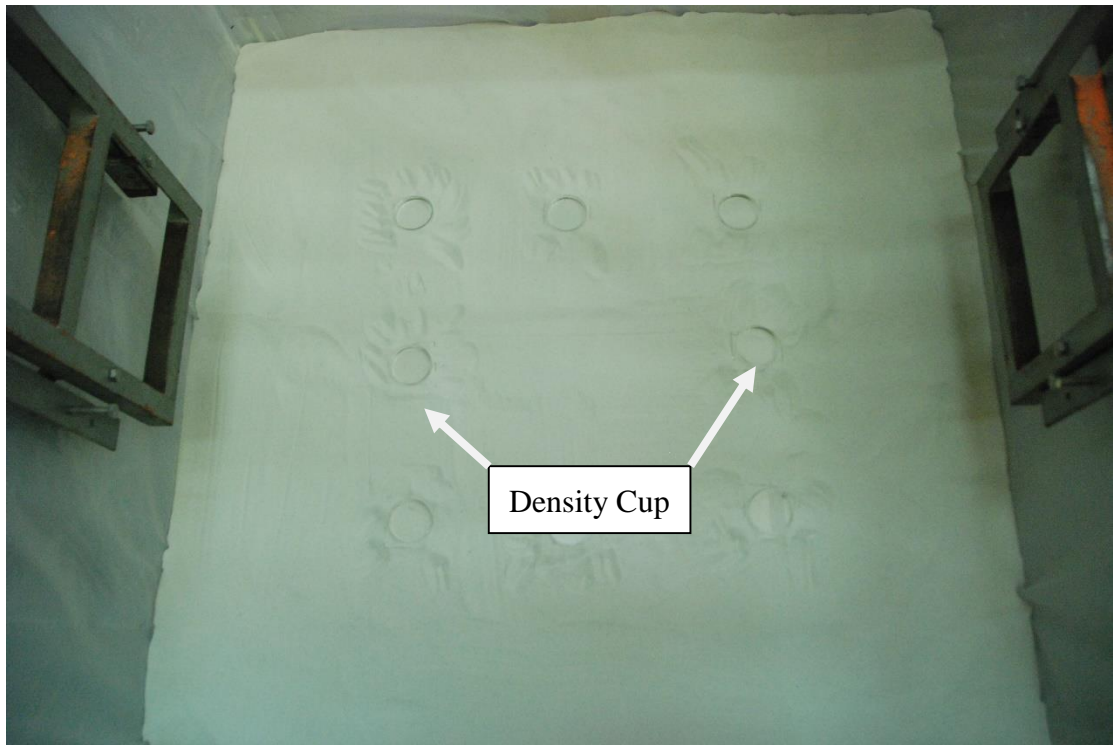
Fig. 5.7. Soil density cup placed on soil surface
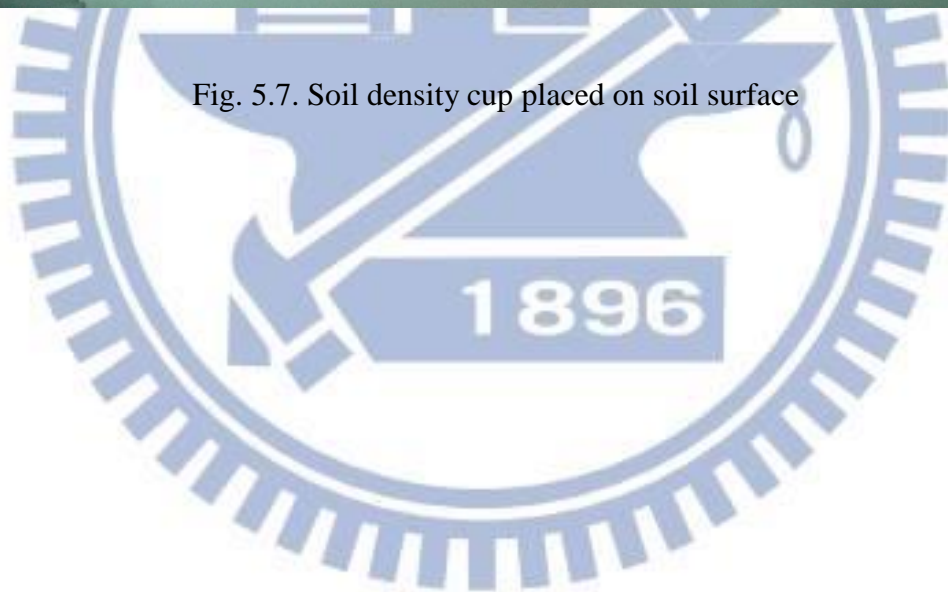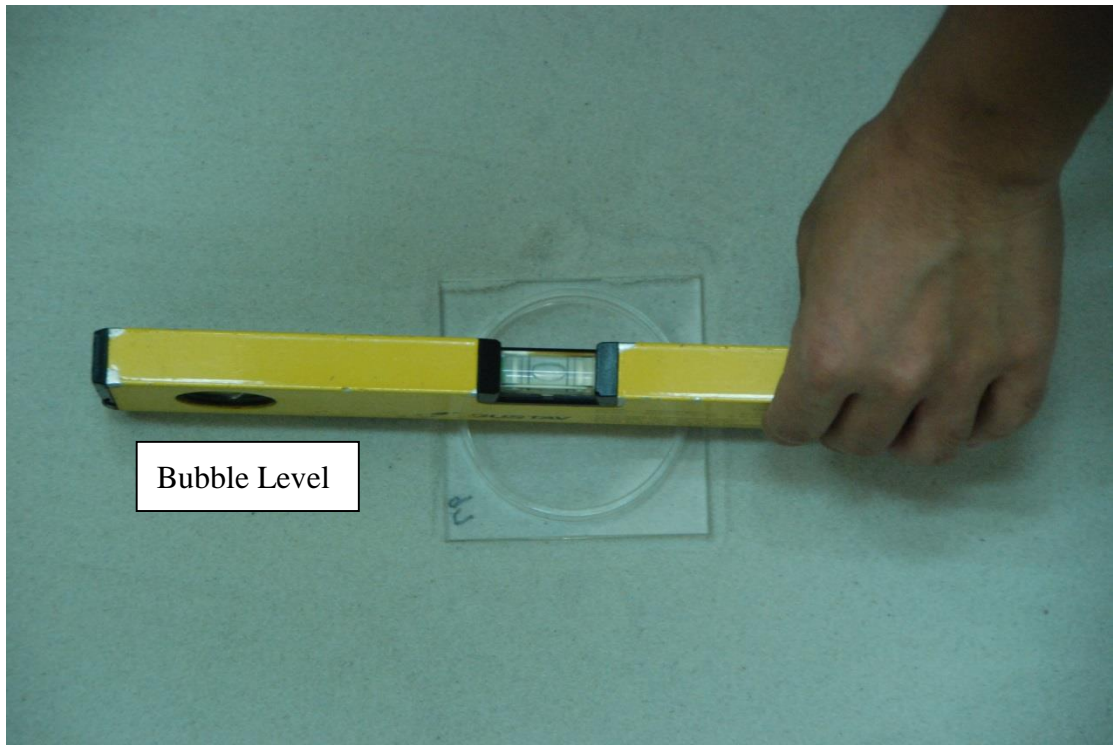
(a)
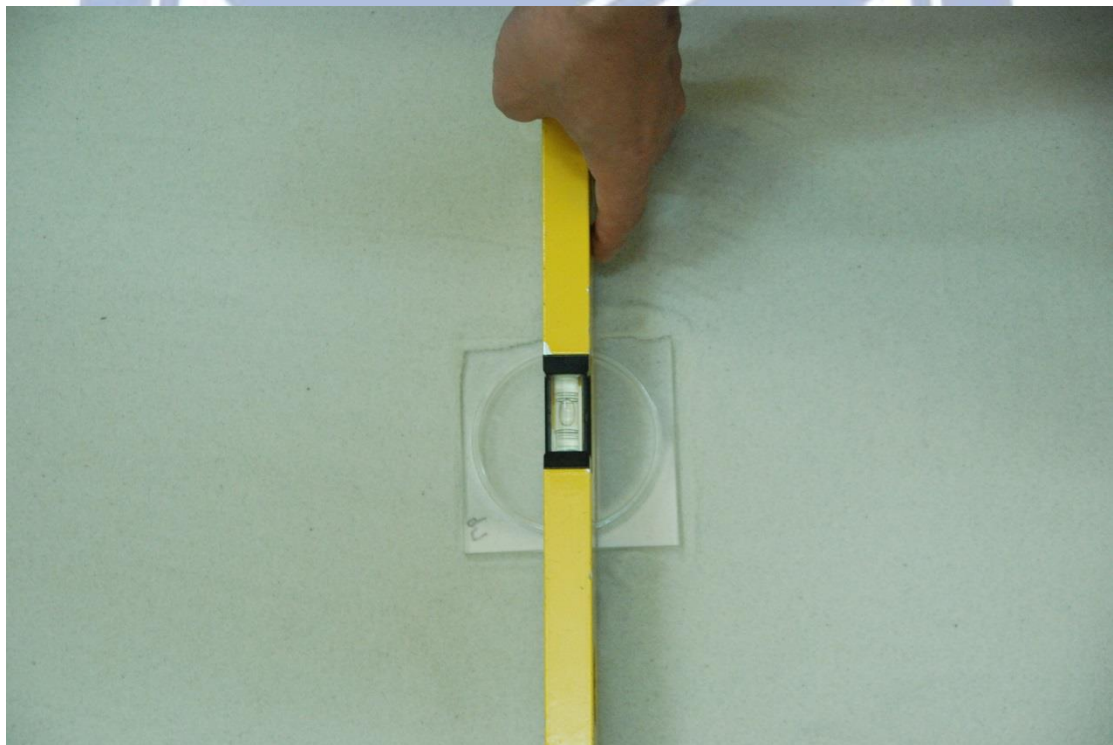
(b)

Fig. 5.8. Horizontal check of density cup with a bubble level

(a) N = 1~5

(b) N = 6~10

(c) N = 11~15

(d) N = 16~20
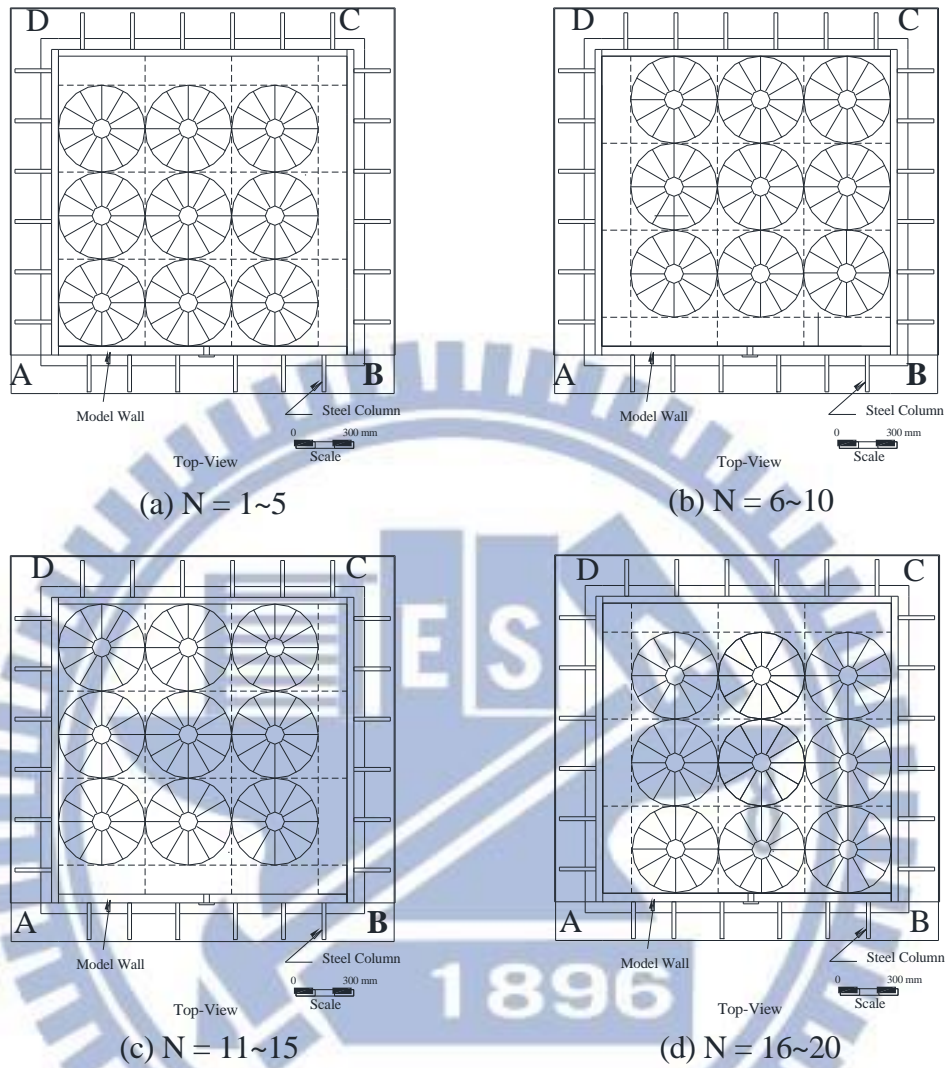
Fig. 5.9 Loading pattern on soil surface

111
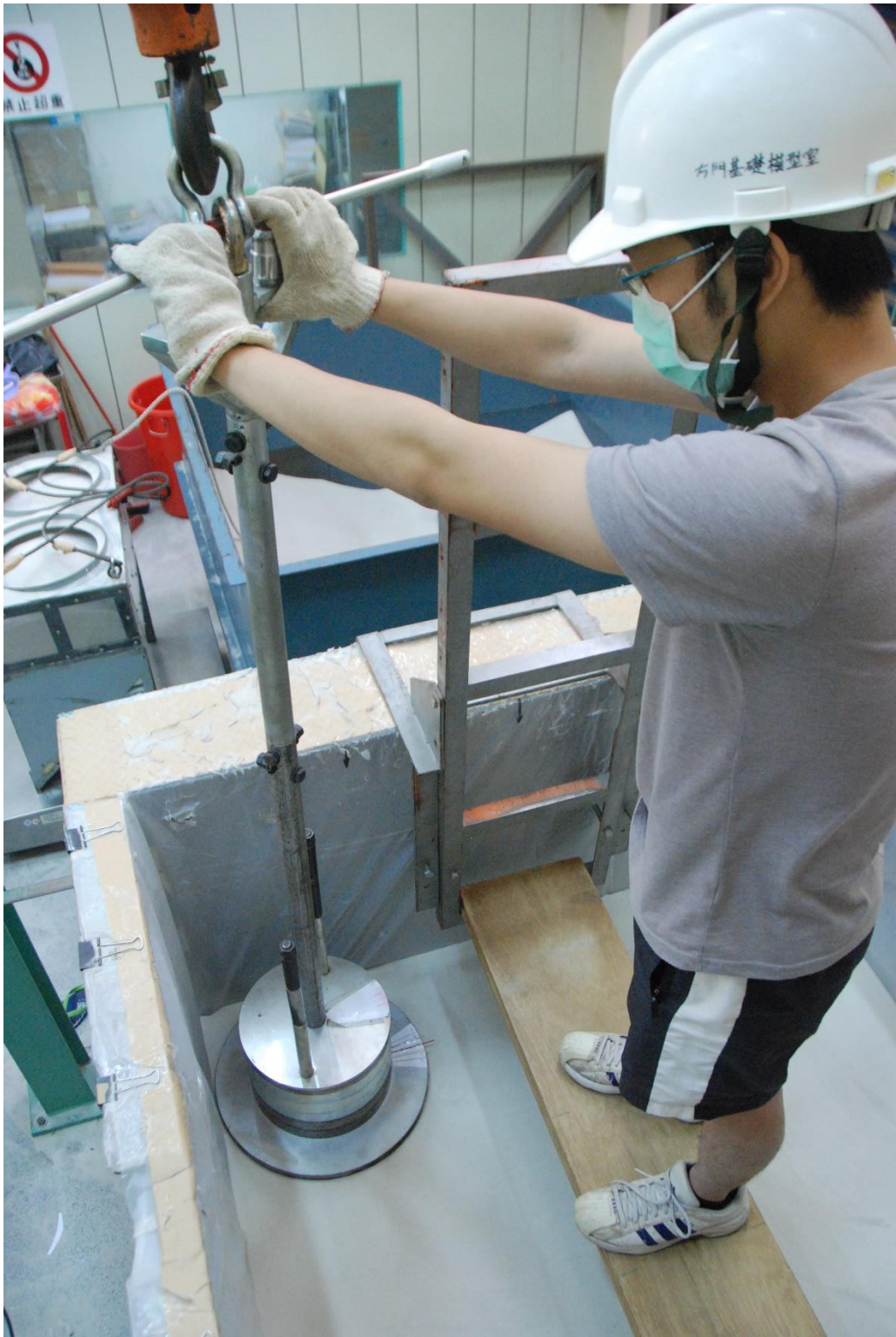
Fig. 5.10. Hoist of CTSC into the soil bin

Fig. 5.11. Apply vertical static load on loose sand
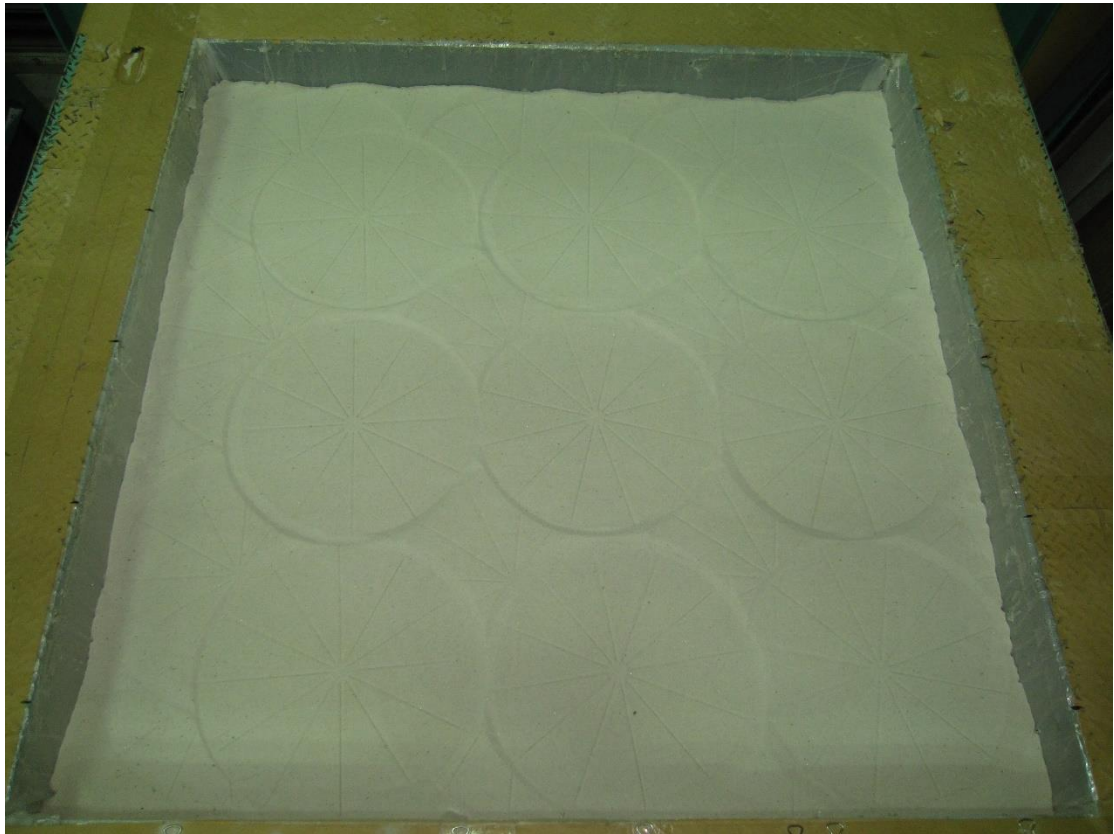
Fig. 5.12 Soil surface after a patterns of vertical static load
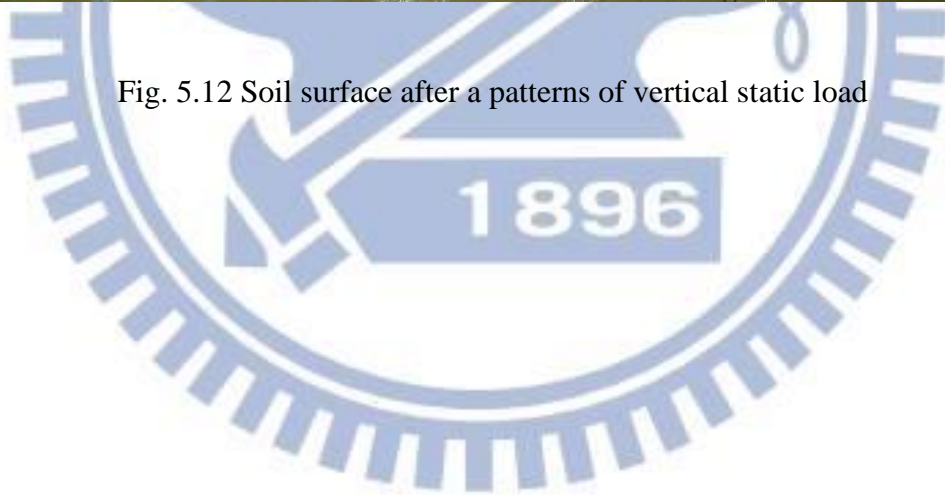
Fig. 5.13. Cyclic torsional shear compactor with rotation angle indicator and

controller
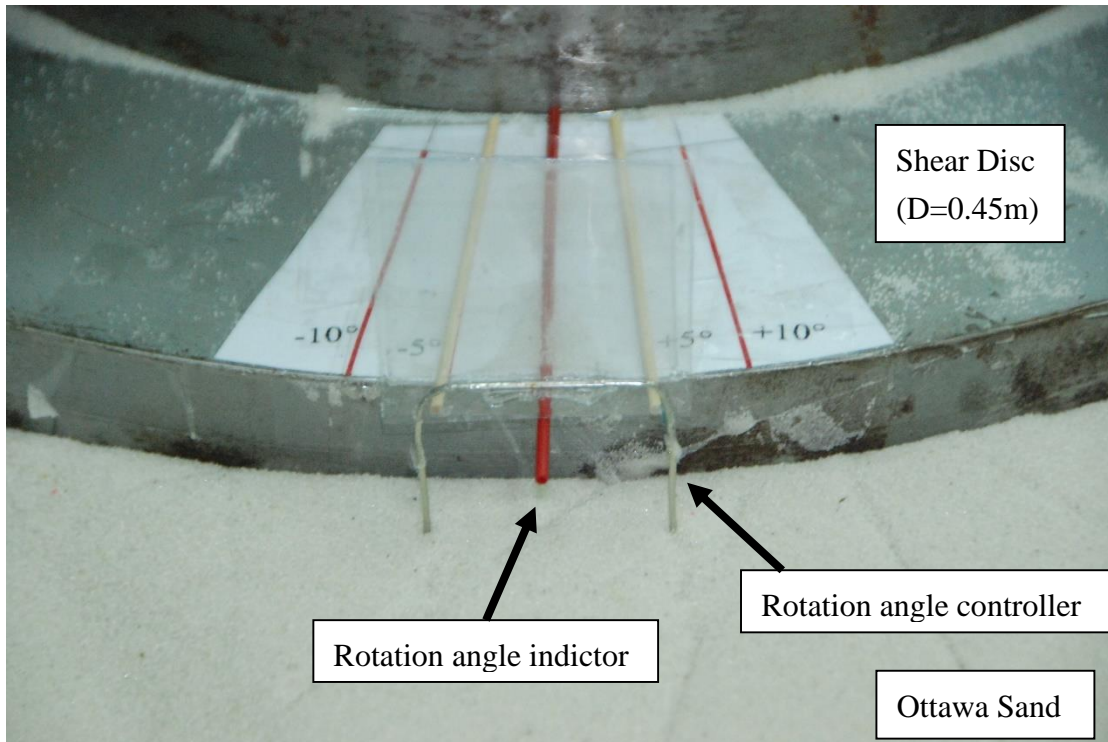
Fig. 5.14. Shearing disc at initial position θ = 0°
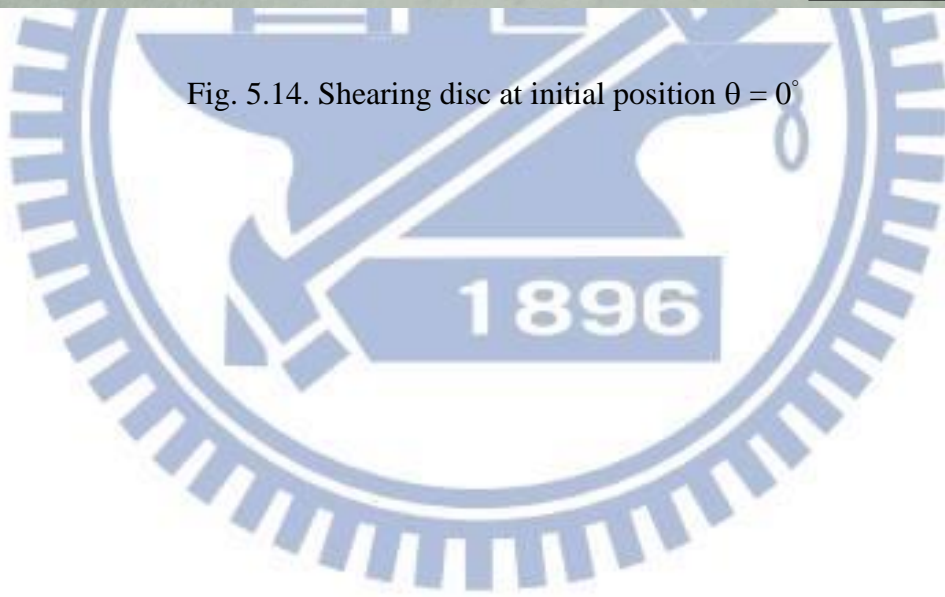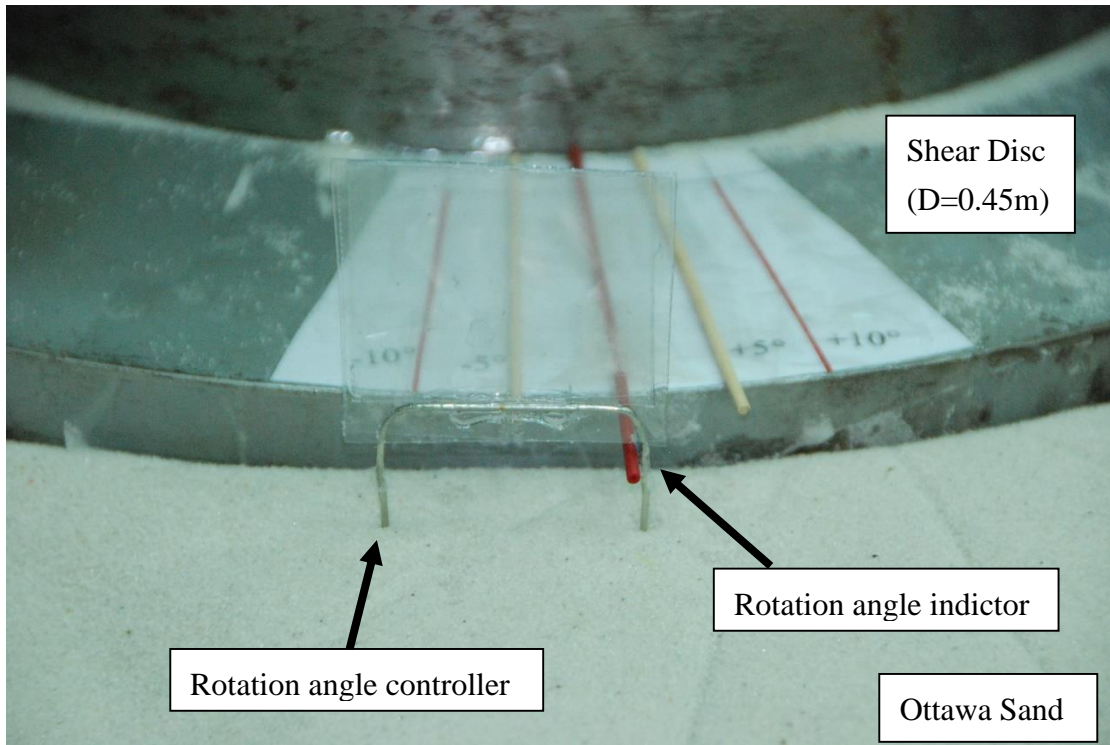
Fig. 5.15. Shearing disc rotated to θ= +5°
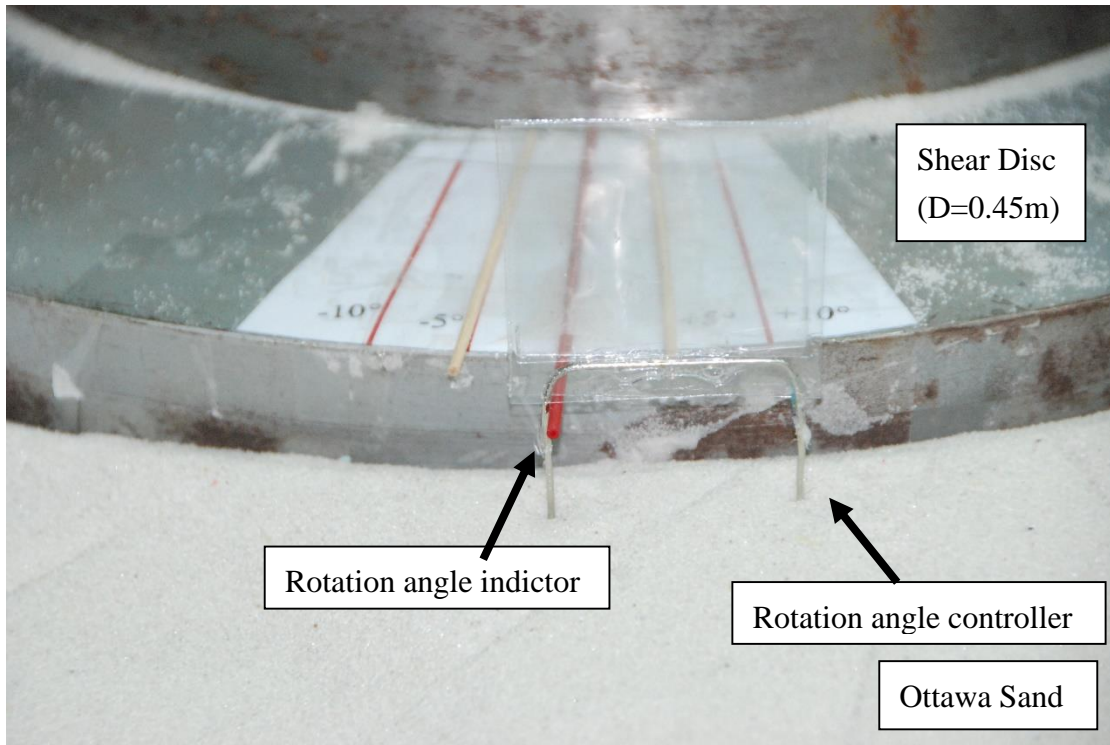
Fig. 5.16. Shearing disc rotated to θ= - 5°

Fig. 5.17. The application of cyclic torsional shear to loose sand
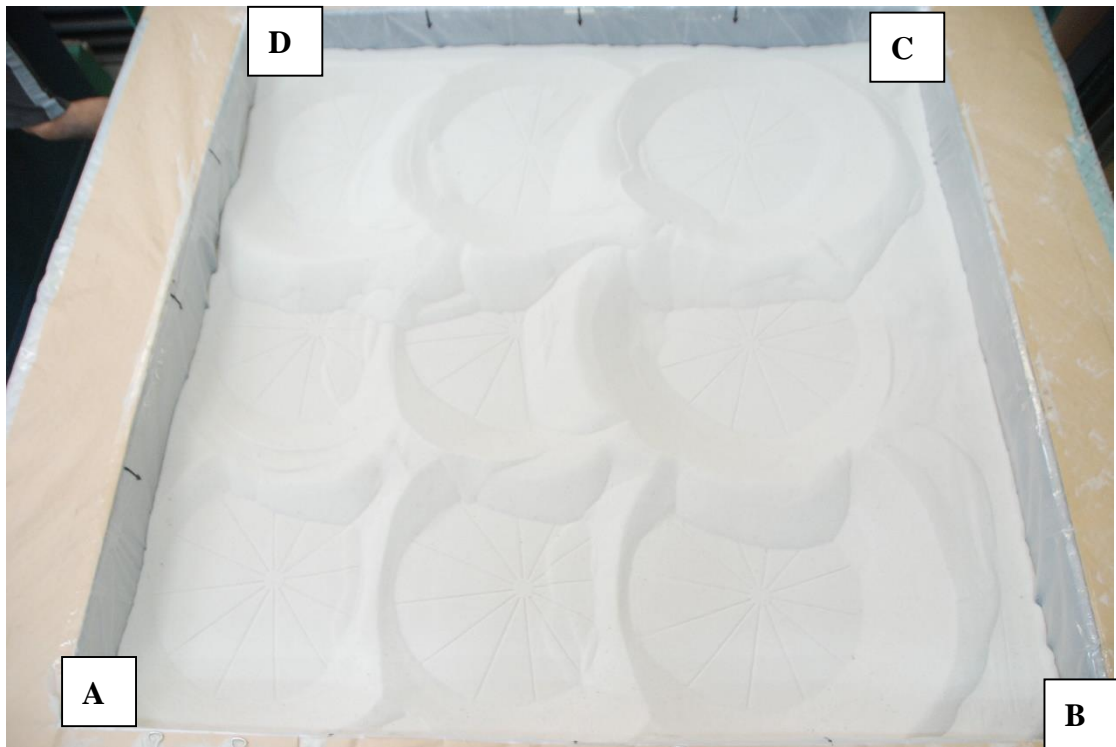
(a) N=1~5
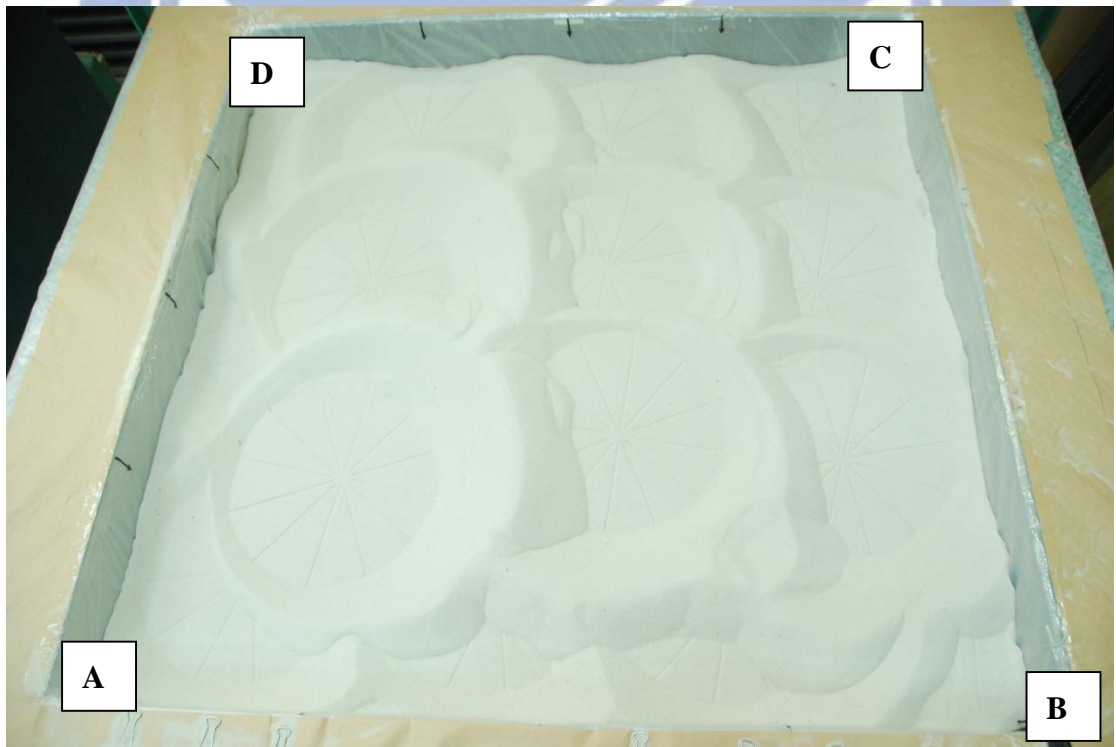
(b) N=6~10

Fig. 5.18. Compacted soil surface after 3×3 formation of cyclic torsional shear

Fig. 5.19. Soil density cup dug out of compacted soil mass

(a)

(b)

(c)

Fig. 5.20. Scraping of soils toward edge of density cup with a spatula

(a)

(b)

(c)

Fig. 5.21. Brush away soil particles from base plate of density cup

Top-View
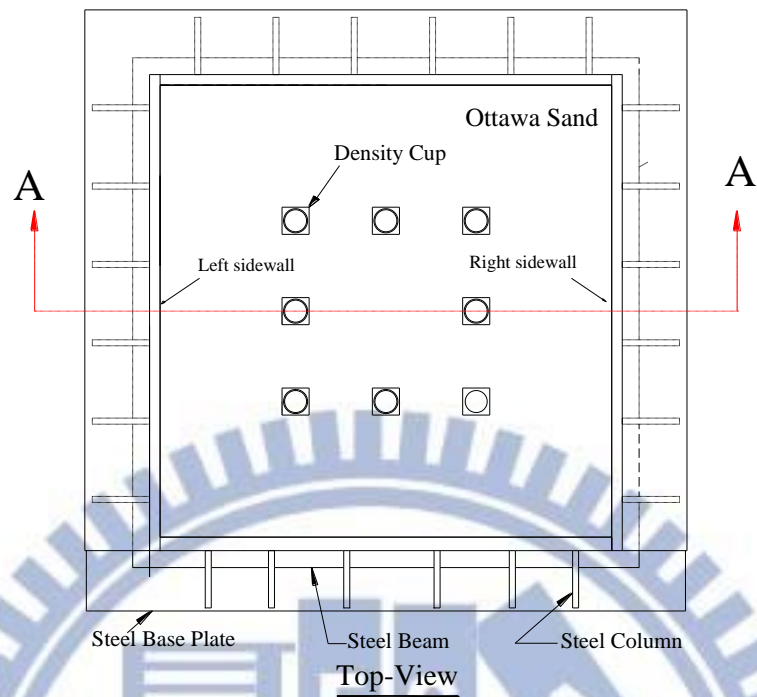
(a)
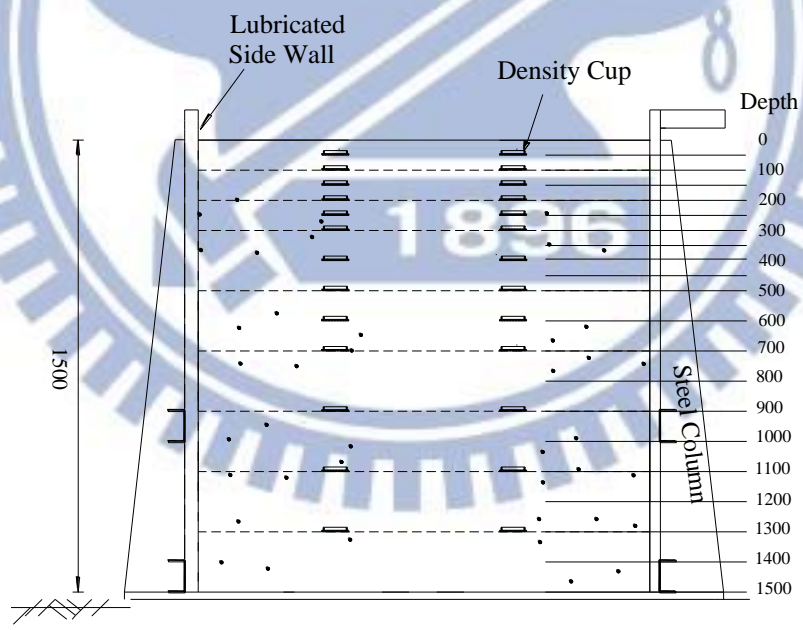
Side-View

Unit : mm

(b)

Fig. 6.1 Density cups buried in soil mass at different elevations and locations

Left Sidewall

Right Sidewall

A

A   B   C

D   E   F

G   H   I

Steel Column

○   center of shear disc

+   settlement measurement point

0 ⊢———⊣ 300 mm
Scale

3 x 3 loading formation

Top-View
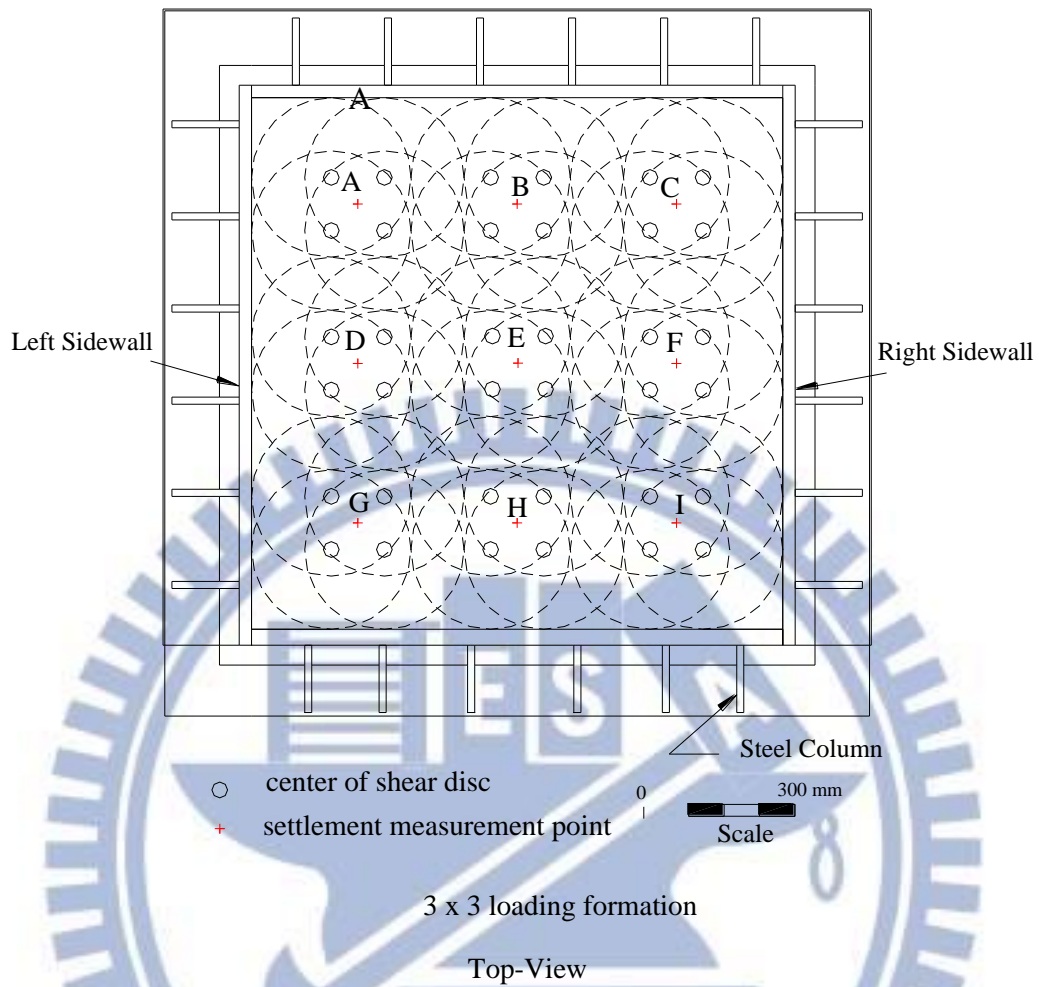
Fig 6.2. The application of vertical static loading formation

125
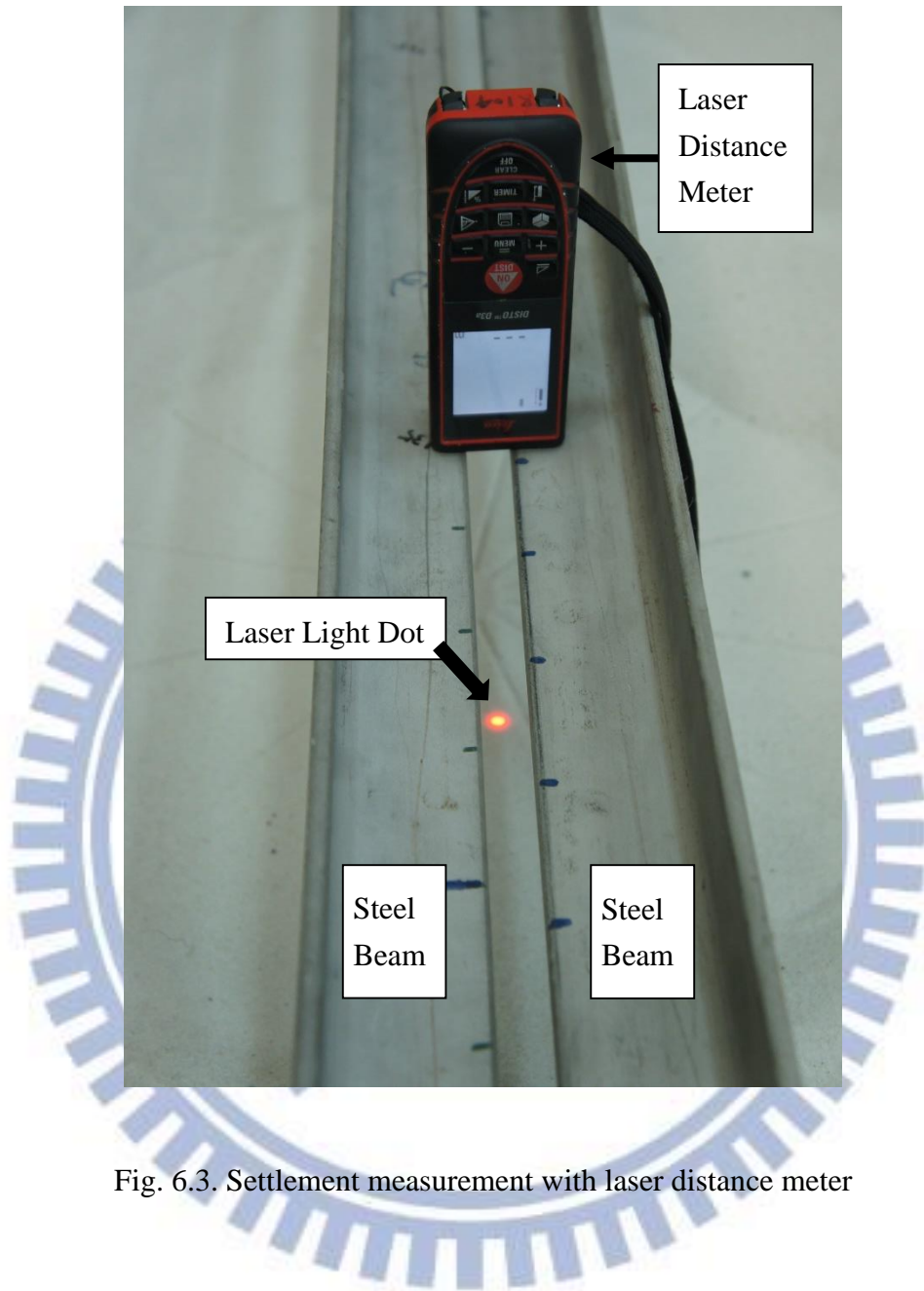
Fig. 6.3. Settlement measurement with laser distance meter
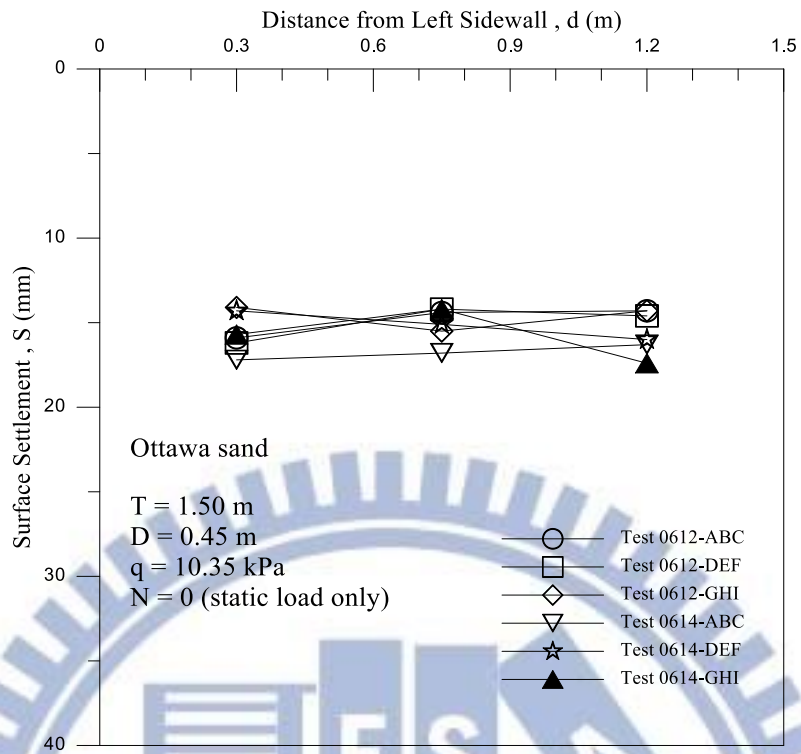
(a) Surface settlement
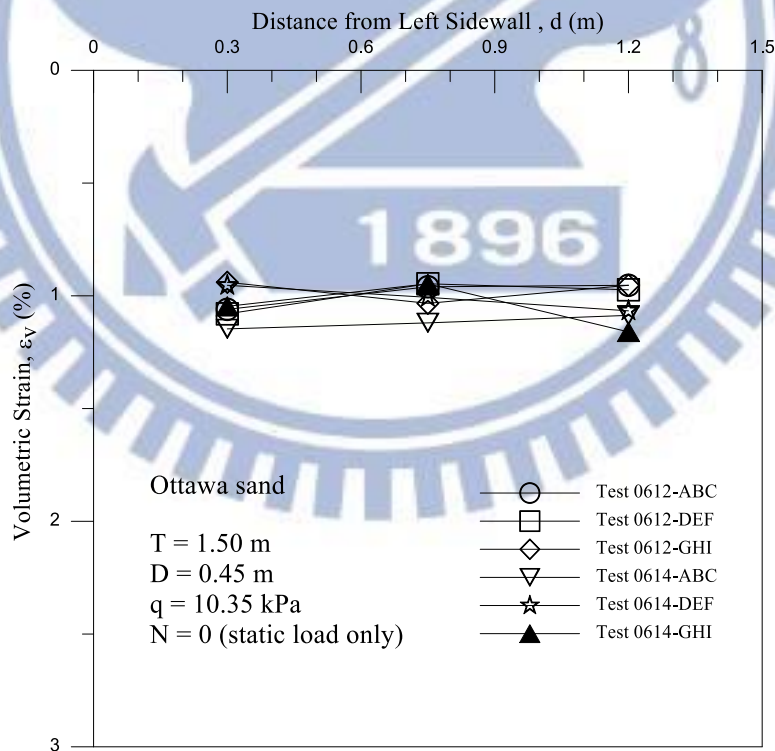
(b) Volumetric strain

Fig. 6.4. Surface settlement and Volumetric strain due to static vertical load
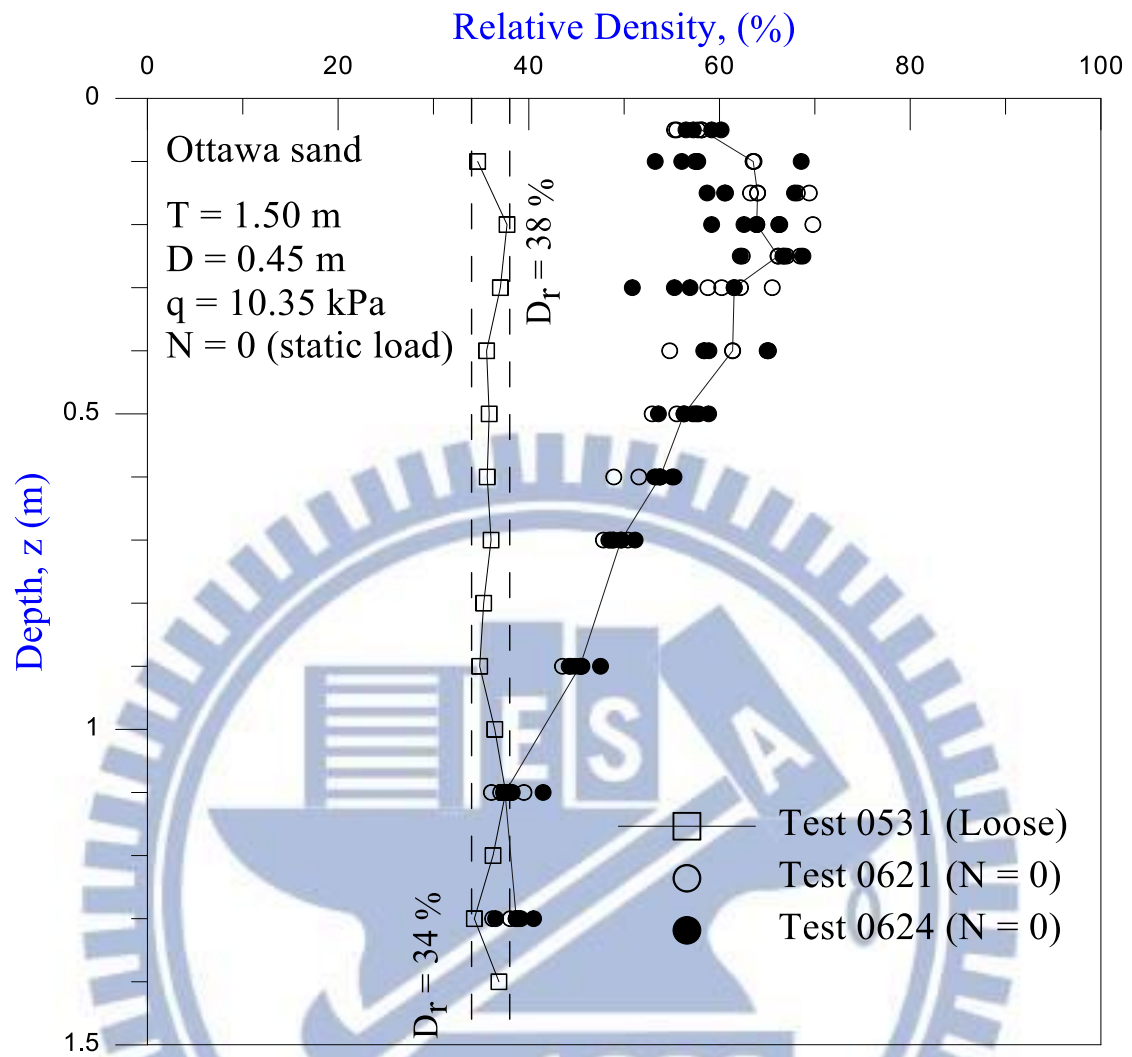
Fig. 6.5. Distribution of relative density after vertical static load
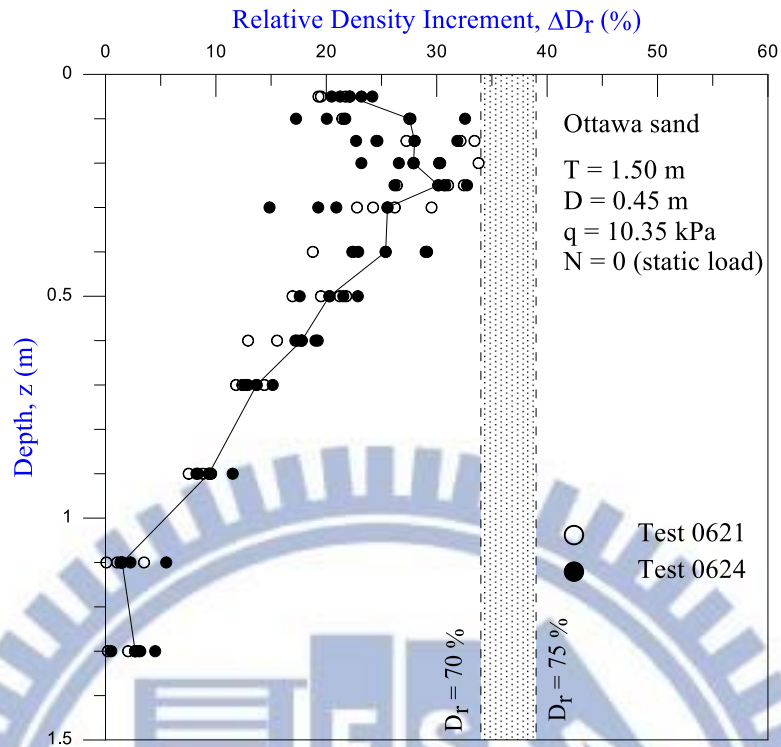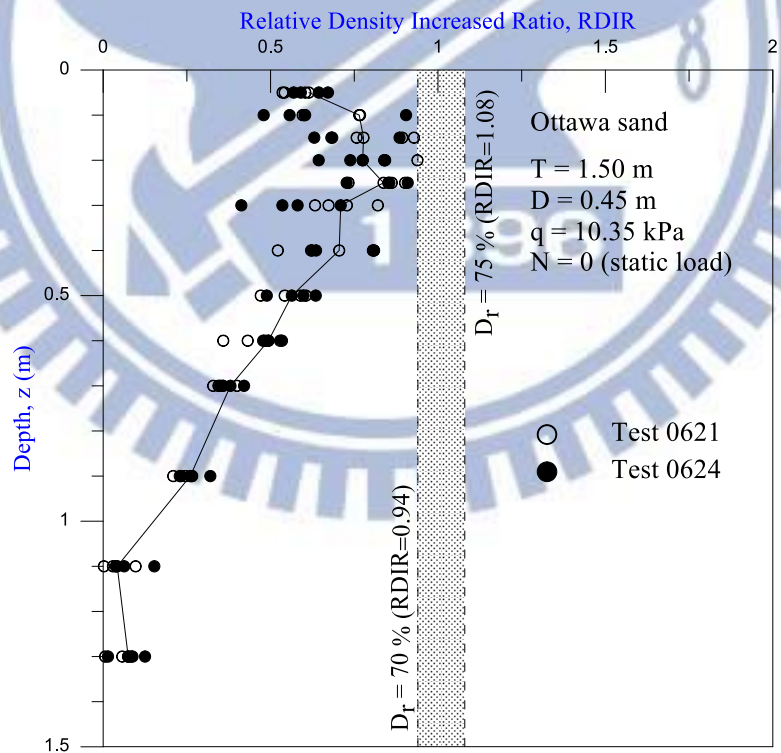
Fig. 6.6. Change of density due to vertical static load (N = 0)

Fig. 6.7. Digital torque wrench on the connecting frame

$$\text{F} \times \text{L}' = T' \ ; \ \frac{T'}{L'} = F = \frac{T}{L} \ ; \ \text{T} = \frac{T'}{L'} \times L$$
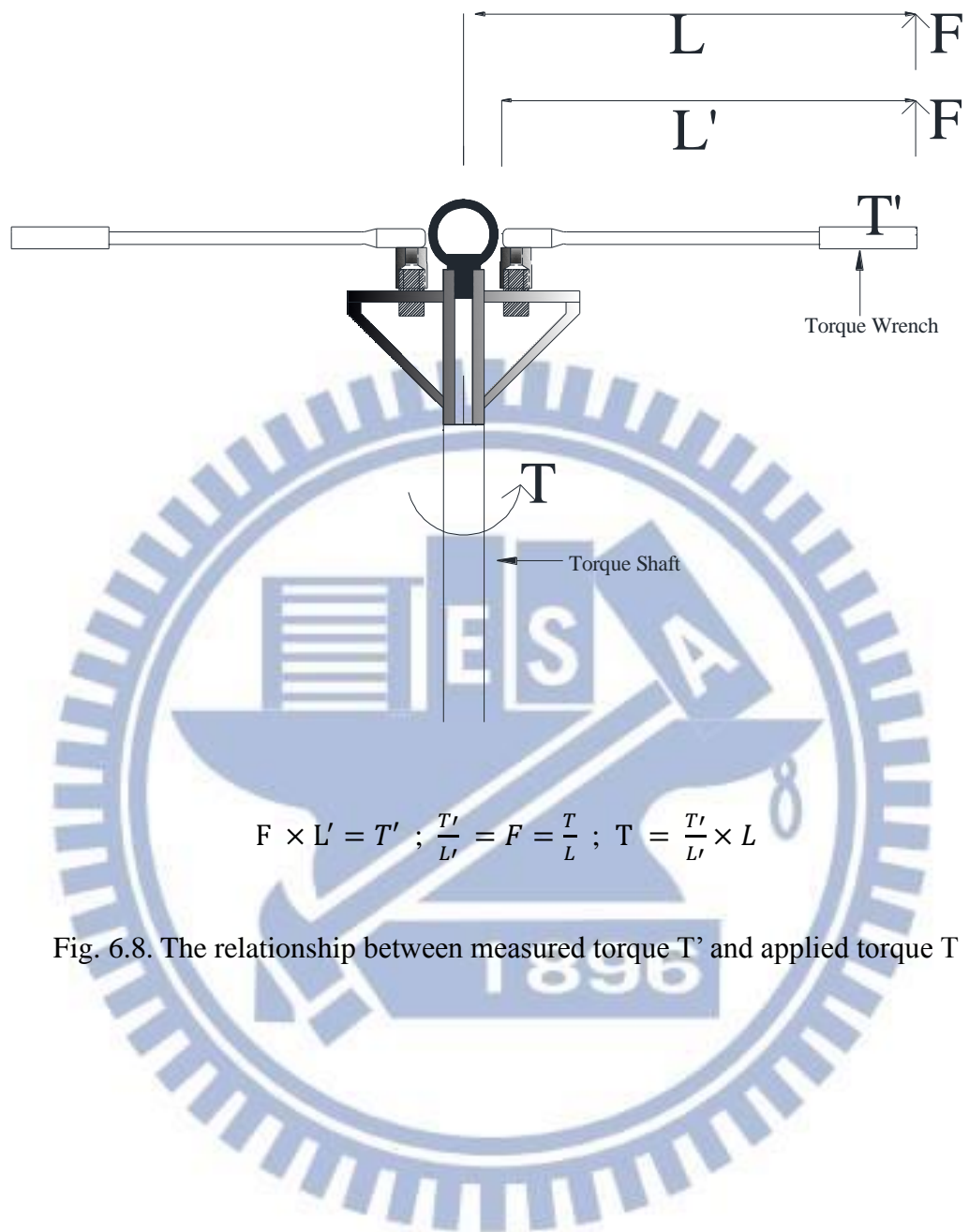
Fig. 6.8. The relationship between measured torque T' and applied torque T

Without extension tube

With extension tube

Extension tube

Fig. 6.9. The cyclic torsional shear compactor
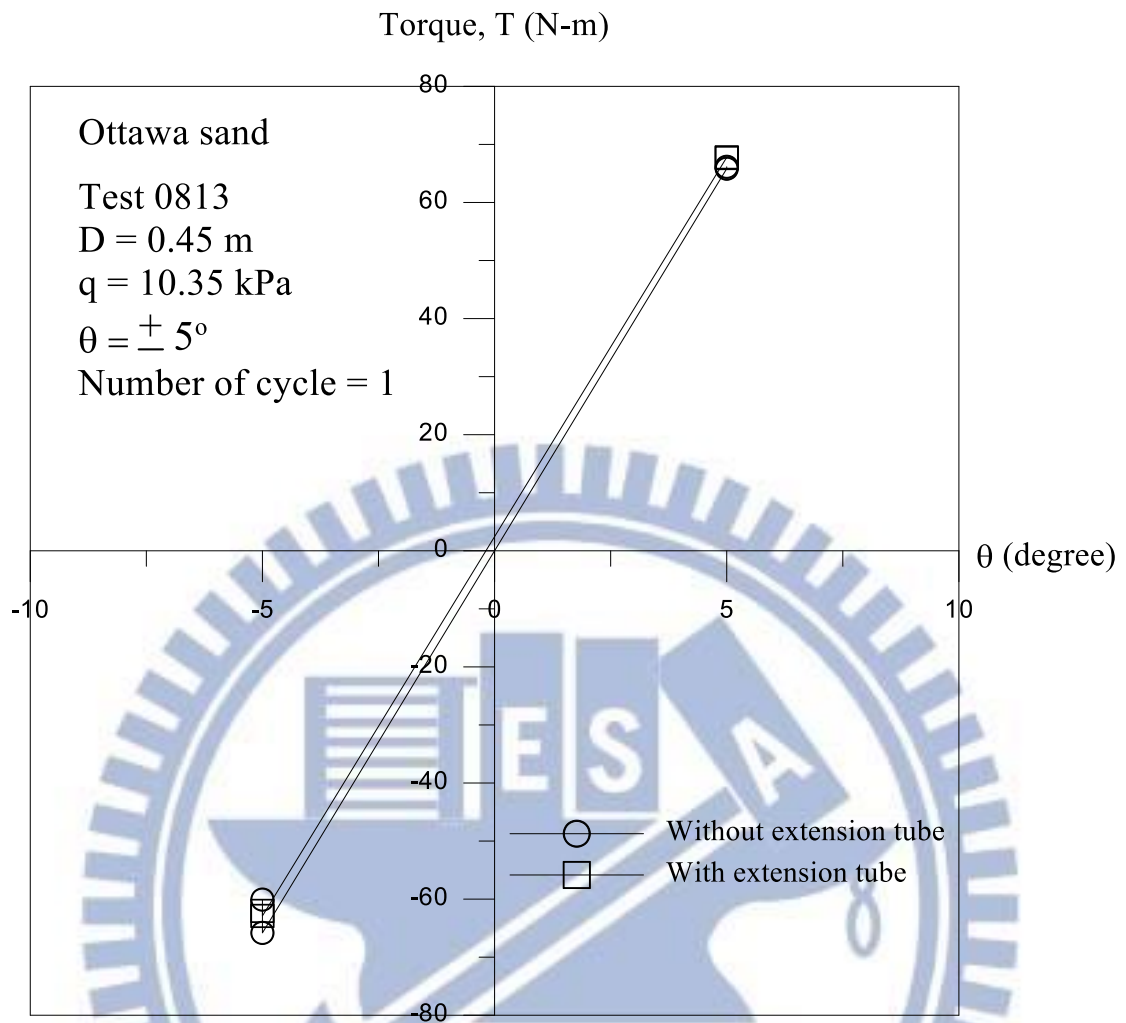
Torque, T (N-m)

Fig. 6.10. Variation of torque T with shearing disc angle θ for Number of cycle = 1
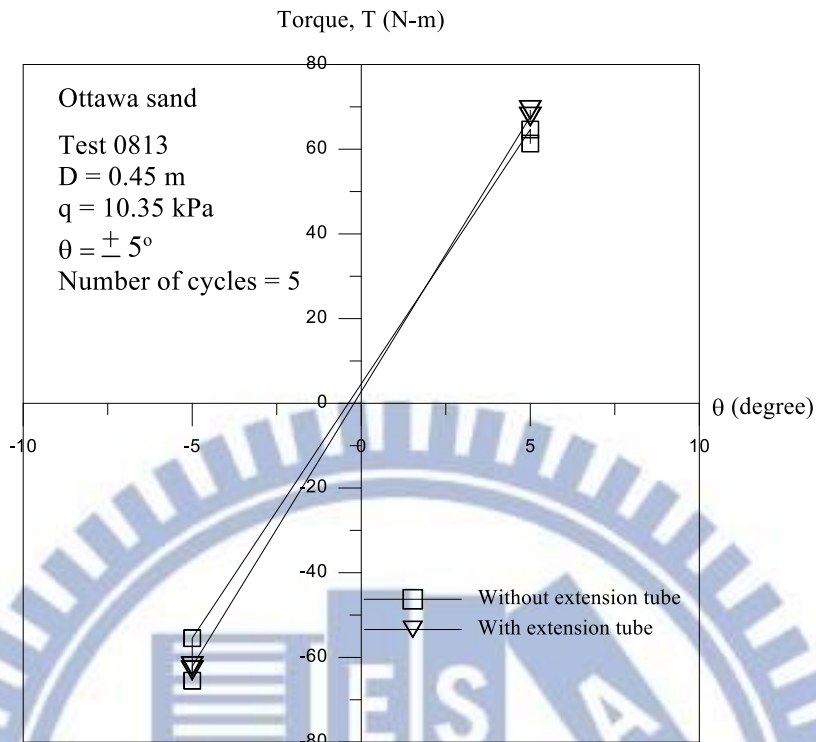
Torque, T (N-m)

Ottawa sand

Test 0813
D = 0.45 m
q = 10.35 kPa
θ = $\pm$ 5º
Number of cycles = 5

□ —— Without extension tube
▽ —— With extension tube

θ (degree)

(a) Variation of torque T with shearing disc angle θ for Number of cycles = 5

Torque, T (Newton-m)

Ottawa sand

Test 0813
D = 0.45 m
q = 10.35 kPa
θ = $\pm$ 5º
Number of cycles = 10

○ —— Without extension tube
□ —— With extension tube

θ (degree)
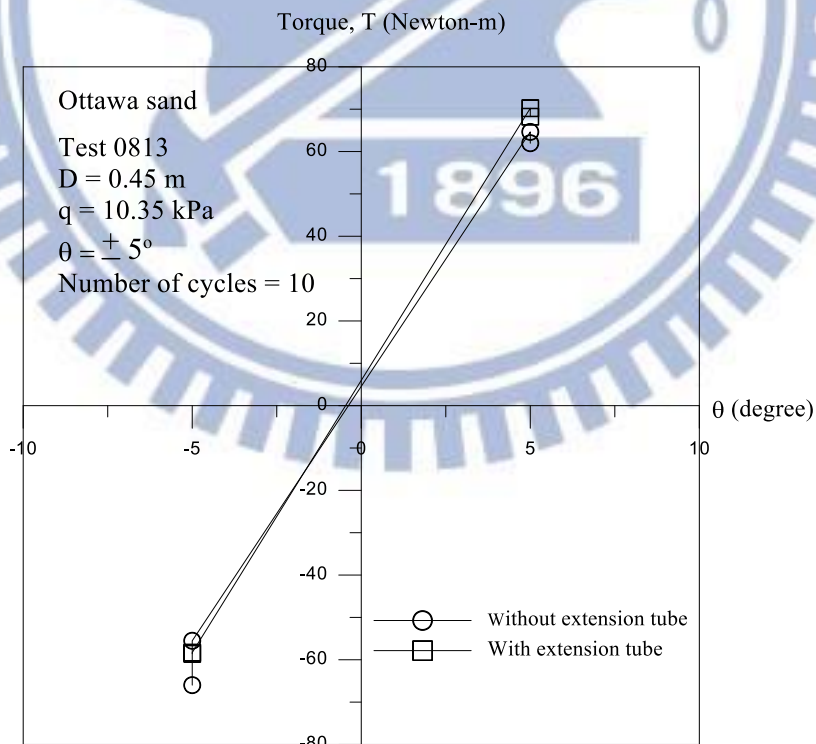
(b) Variation of torque T with shearing disc angle θ for Number of cycles =10

Fig. 6.11. Variation of torque T with shearing disc angle θ
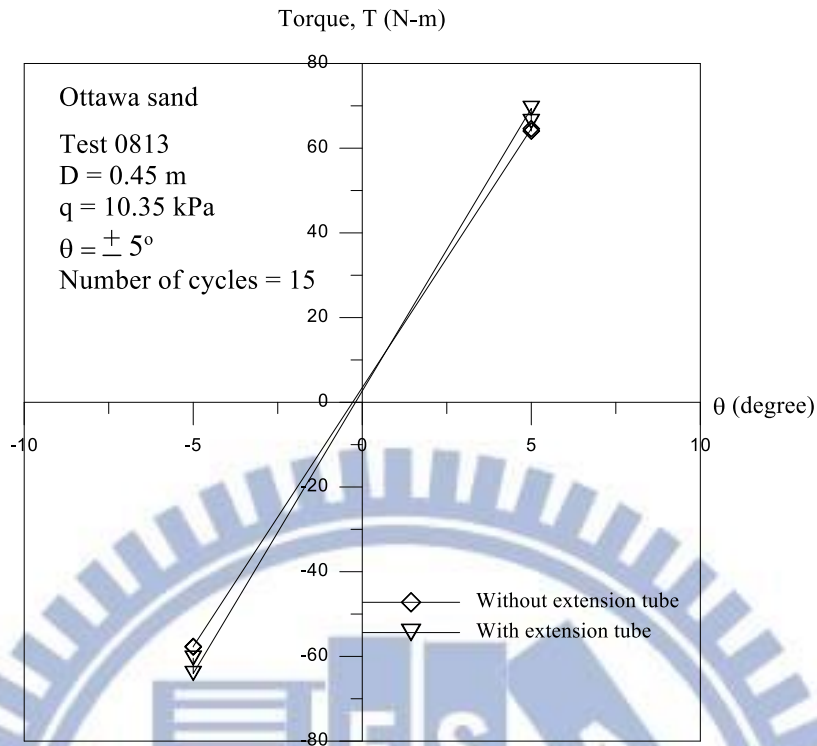
134

Torque, T (N-m)

Ottawa sand

Test 0813
D = 0.45 m
q = 10.35 kPa
$\theta = \pm 5^{o}$
Number of cycles = 15

◇ Without extension tube
▽ With extension tube

θ (degree)

(a) Variation of torque T with shearing disc angle θ for Number of cycles = 15

Torque, T (N-m)

Ottawa sand

Test 0813
D = 0.45 m
q = 10.35 kPa
$\theta = \pm 5^{o}$
Number of cycles = 20

○ Without extension tube
□ With extension tube

θ (degree)
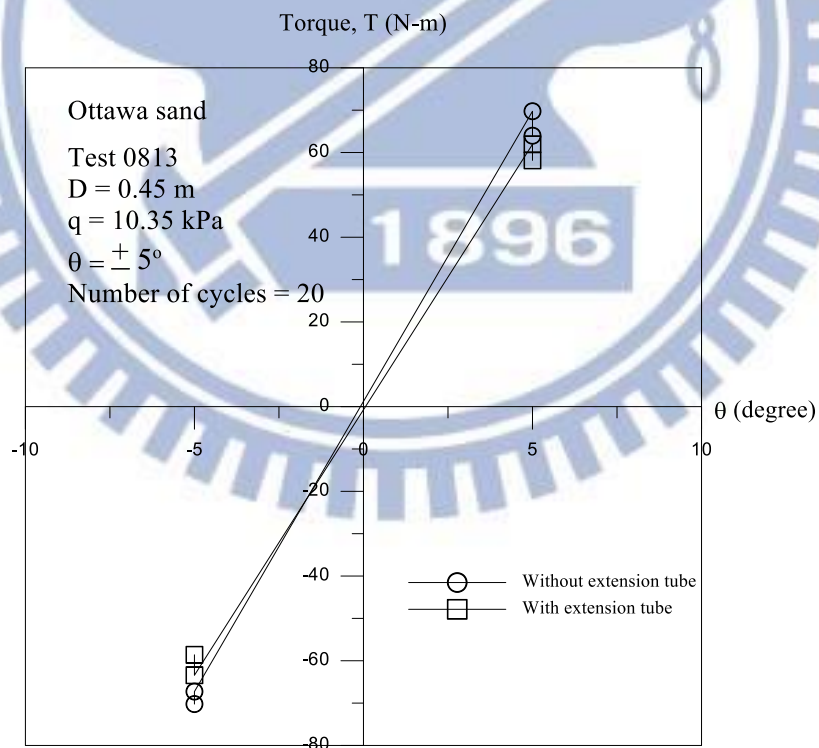
(b) Variation of torque T with shearing disc angle θ for N = 20

Fig. 6.12. Variation of torque T with shearing disc angle θ

135
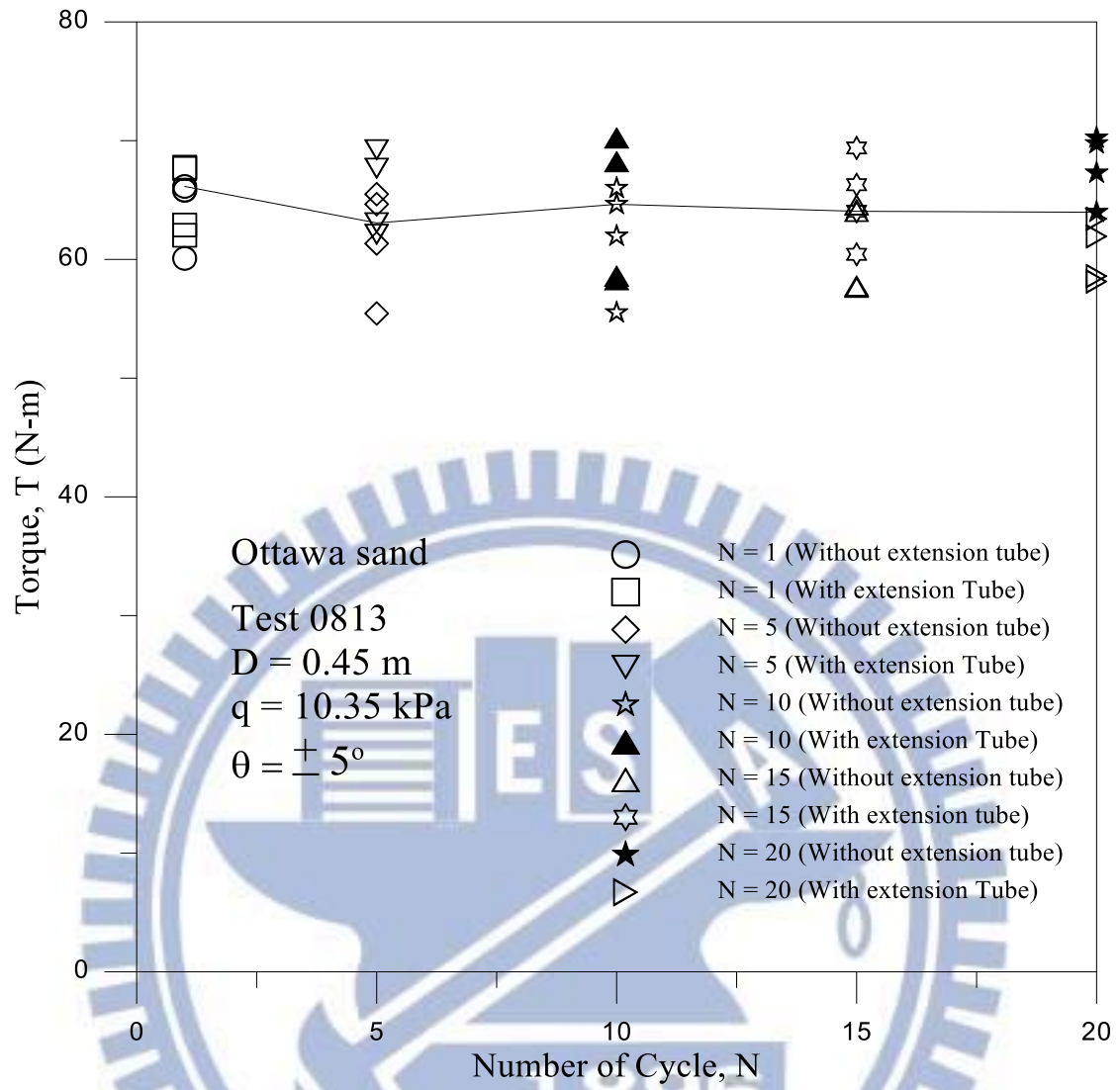
Fig. 6.13. Variation of Torque T with number of cycle of cyclic torsional shearing
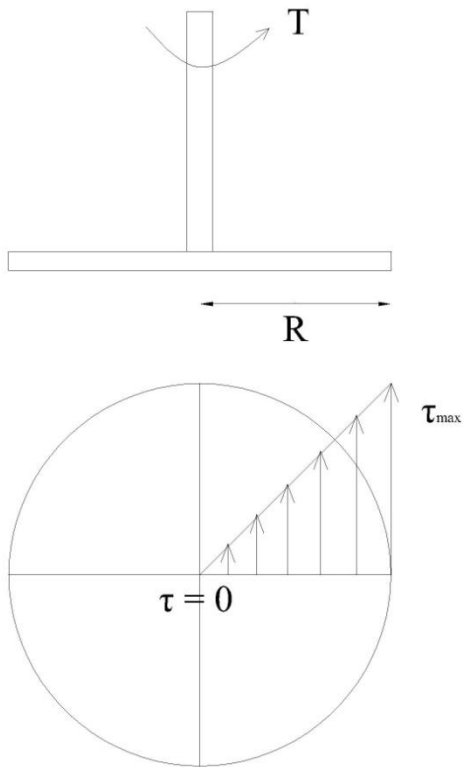
Maximum shear stress torsion for a solid circular shaft :

$$\tau_{max} = \frac{TR}{J}$$

T = Torsion
R = Radial of circular disc
J = Polar moment of inertia of the circular cross section

$$J = \frac{\pi}{32} D^4$$

Fig. 6.14. Determine the maximum torsional shear stress at the edge of the shearing disc due to the applied torque

137
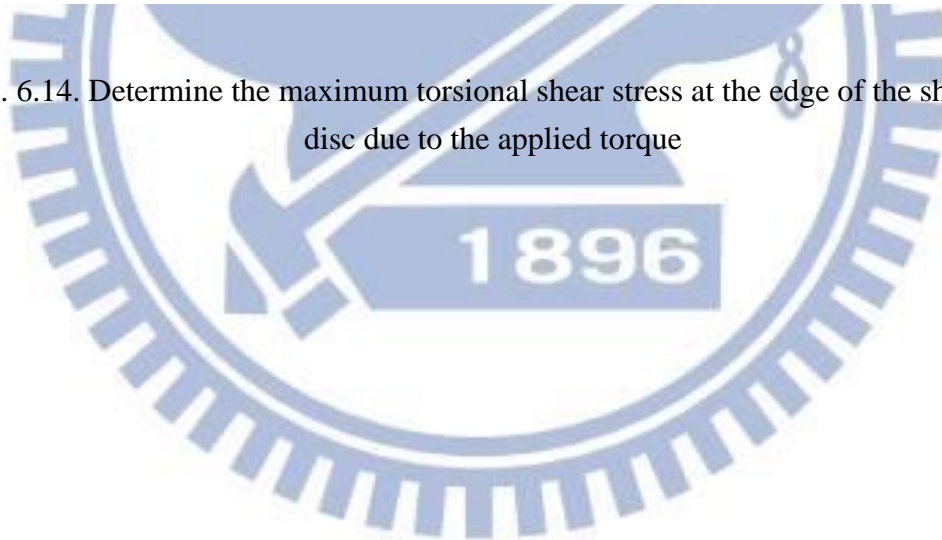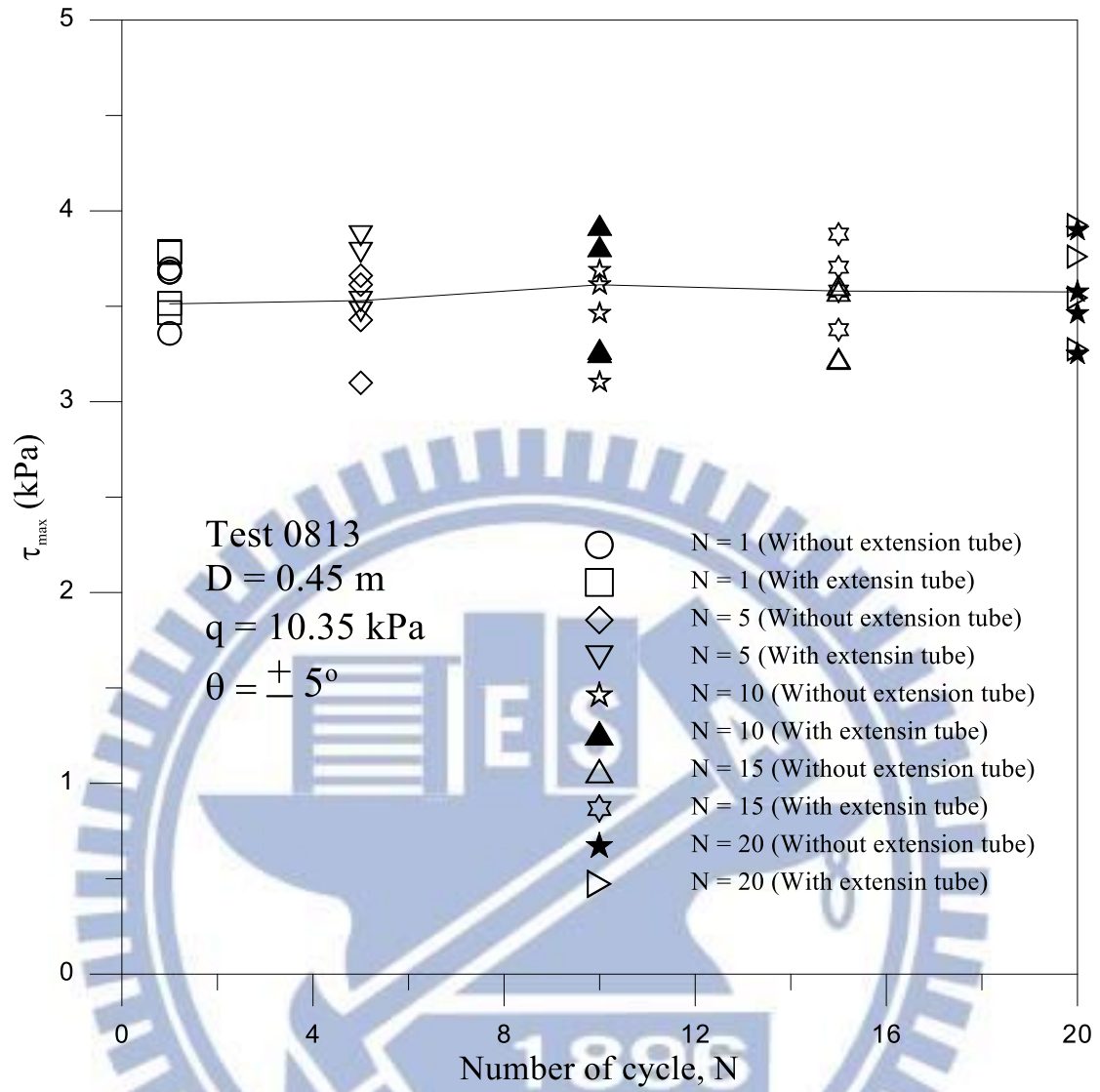
Fig. 6.15. Maximum shear stress with number of cycle, N

Model Wall

+ settlement measurement point

Steel Column

0   300 mm

Scale

3 x 3 loading formation

Top-View
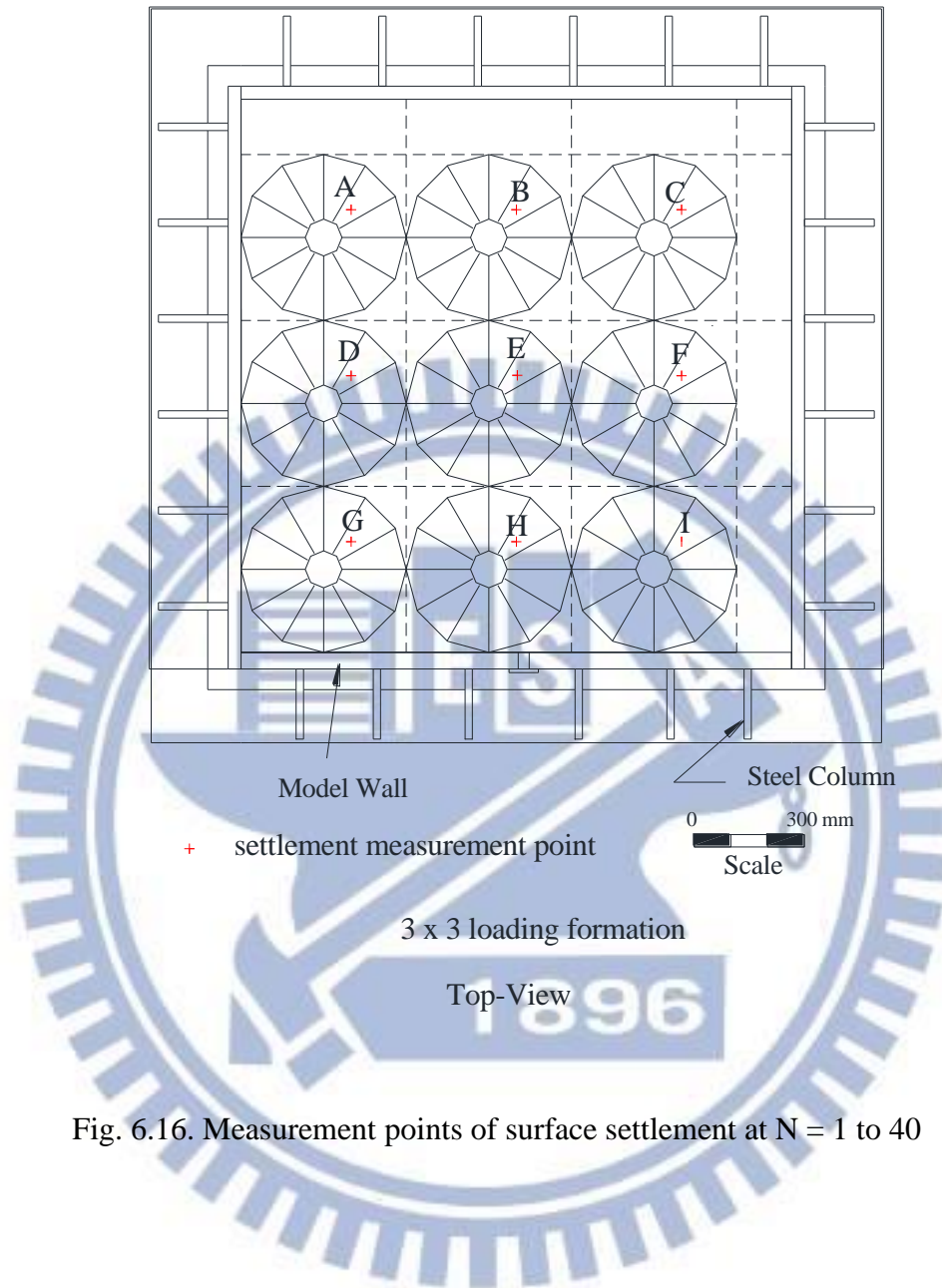
Fig. 6.16. Measurement points of surface settlement at N = 1 to 40

Distance from Left Sidewall , d (m)

Ottawa sand

T = 1.50 m
D = 0.45 m
q = 10.35 kPa
θ = ± 5º
N = 1

○ Test 0612-ABC
□ Test 0612-DEF
◇ Test 0612-GHI
▽ Test 0614-ABC
☆ Test 0614-DEF
▲ Test 0614-GHI

(a) Surface settlement

Distance from Left Sidewall , d (m)

Ottawa sand

T = 1.50 m
D = 0.45 m
q = 10.35 kPa
θ = ± 5º
N = 1

○ Test 0612-ABC
□ Test 0612-DEF
◇ Test 0612-GHI
▽ Test 0614-ABC
☆ Test 0614-DEF
▲ Test 0614-GHI
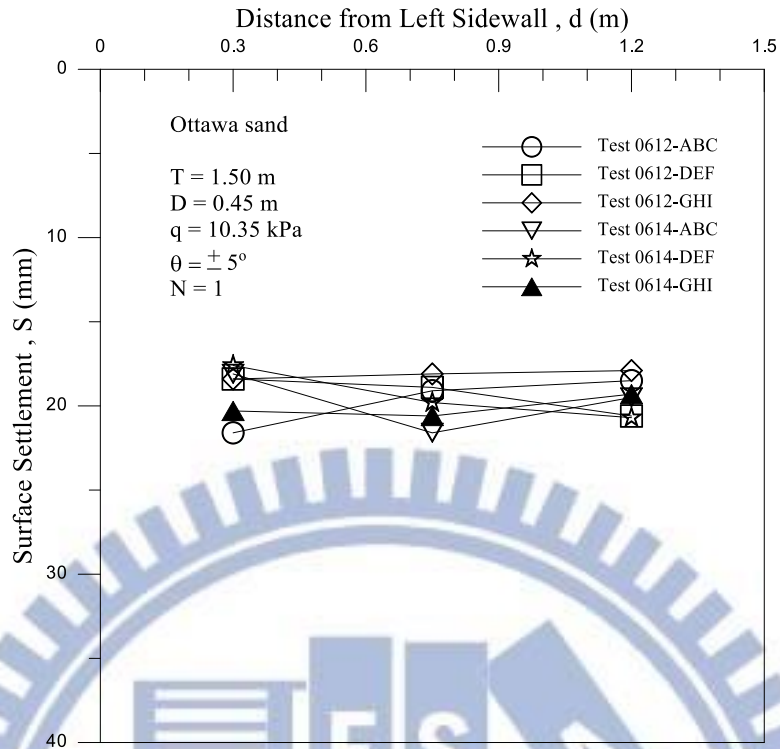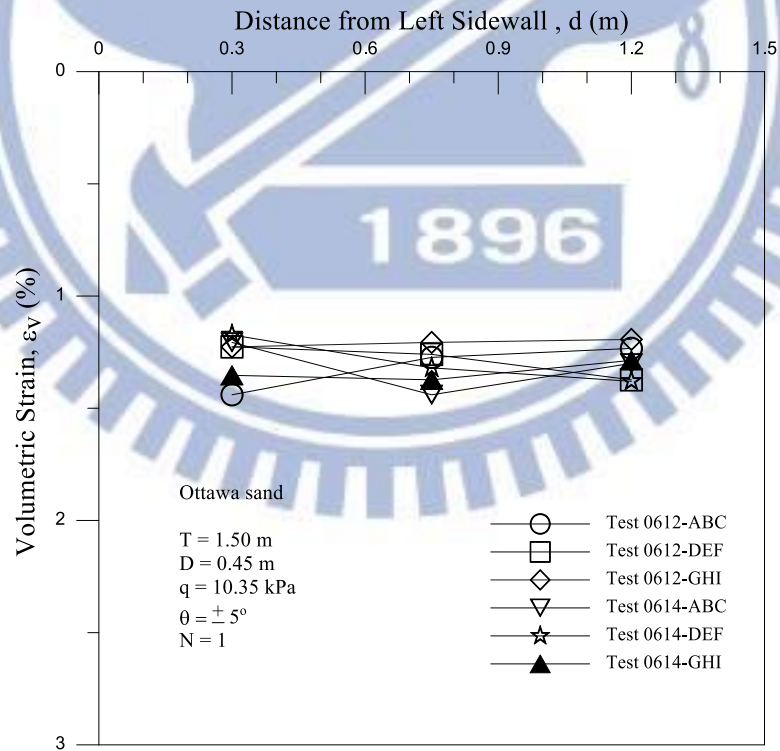
(b) Volumetric strain

Fig. 6.17. Surface settlement and Volumetric strain due to cyclic torsional shear at N = 1
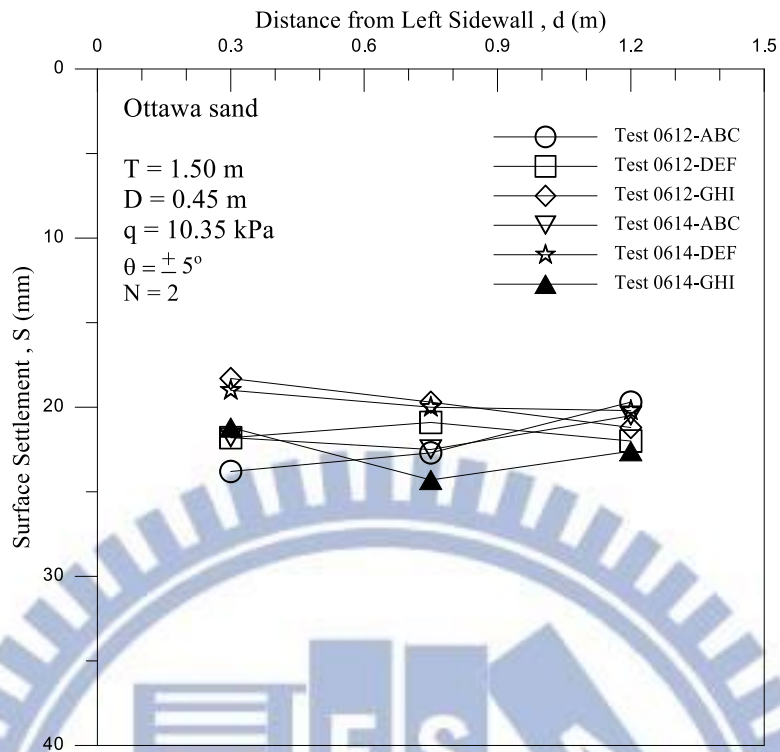
(a) Surface settlement
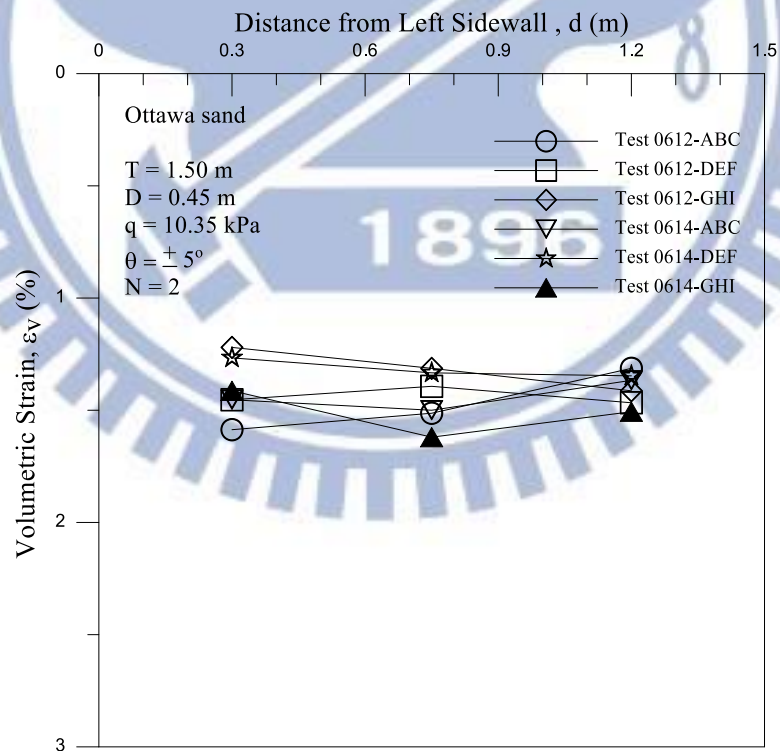
(b) Volumetric strain

Fig. 6.18. Surface settlement and Volumetric strain due to cyclic torsional shear at N = 2

141
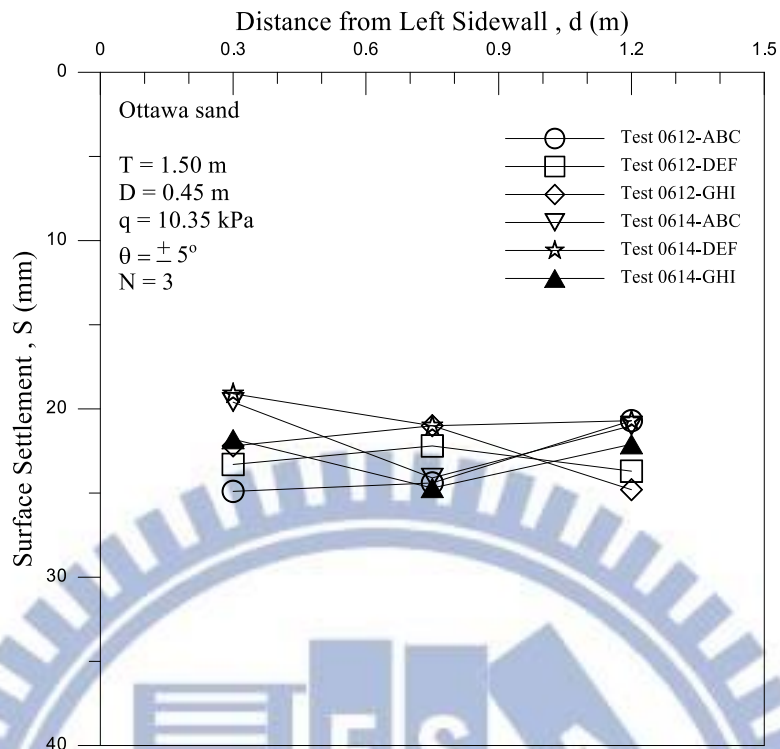
(a) Surface settlement
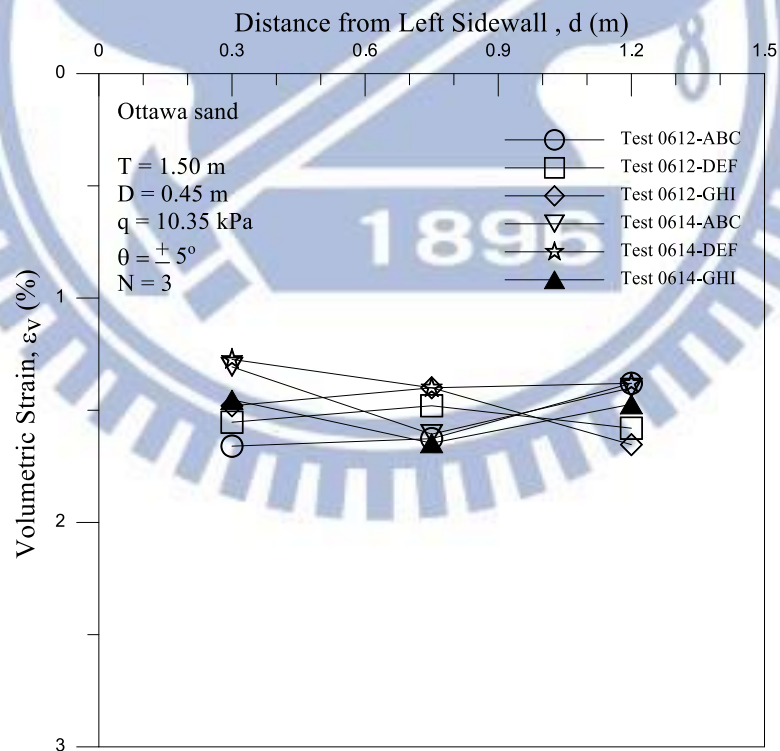
(b) Volumetric strain

Fig. 6.19. Surface settlement and Volumetric strain due to cyclic torsional shear at N = 3
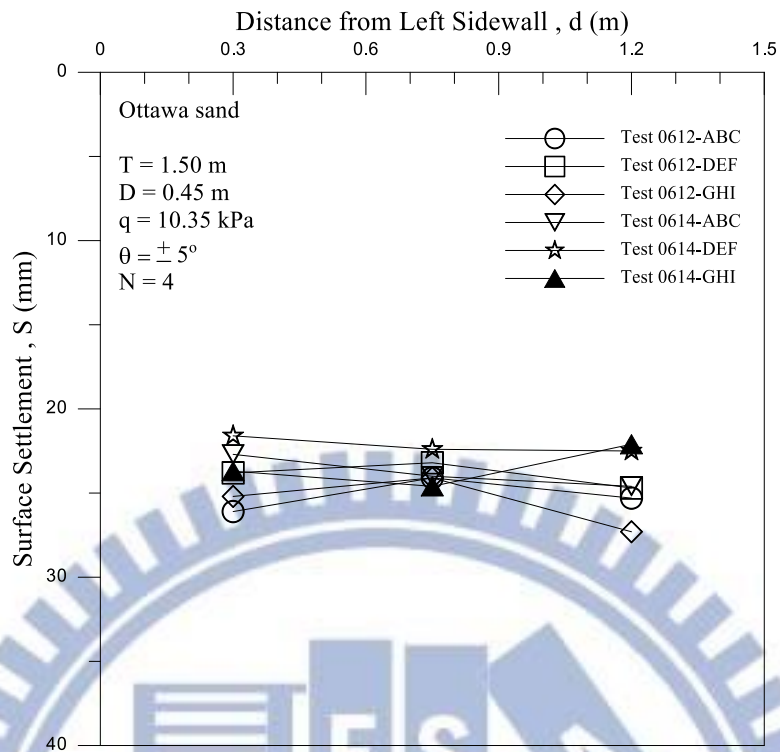
(a) Surface settlement
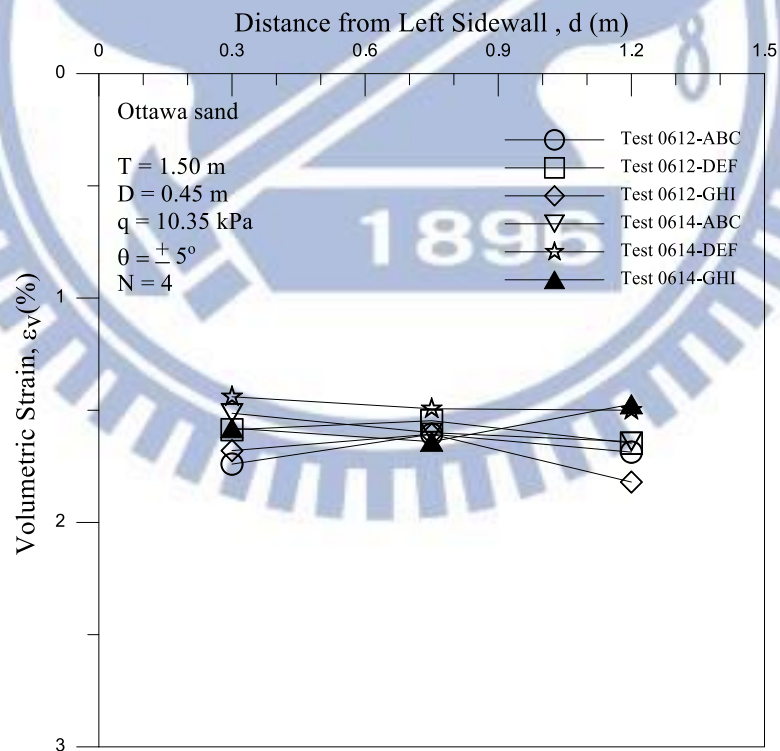
(b) Volumetric strain

Fig. 6.20. Surface settlement and Volumetric strain due to cyclic torsional shear at N = 4

143
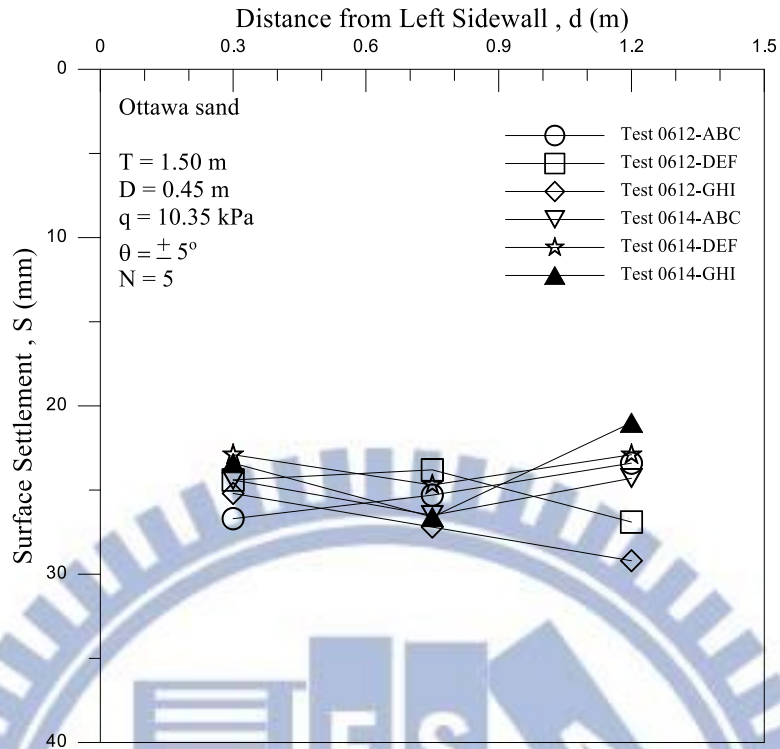
(a) Surface settlement
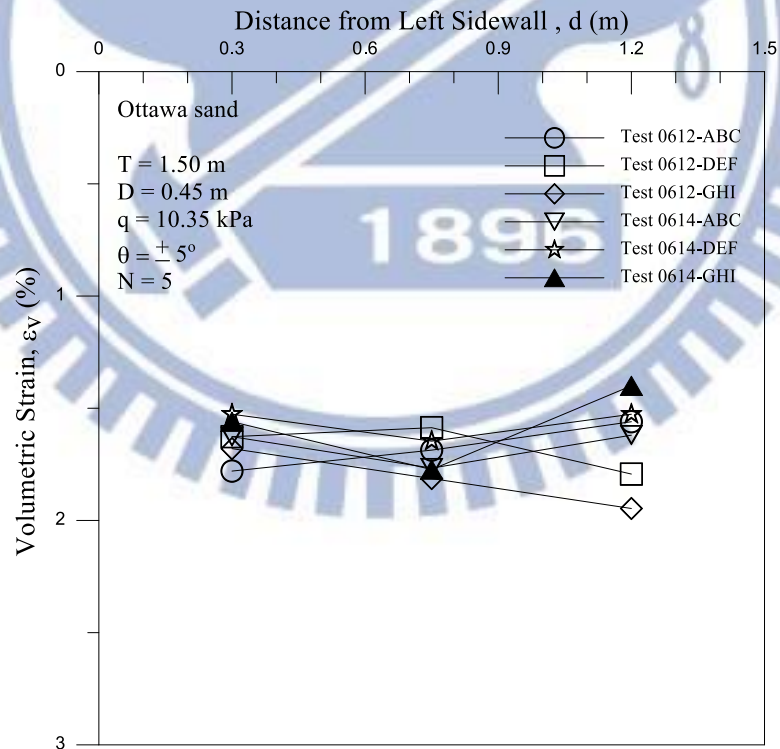
(b) Volumetric strain

Fig. 6.21. Surface settlement and Volumetric strain due to cyclic torsional shear at N = 5

144
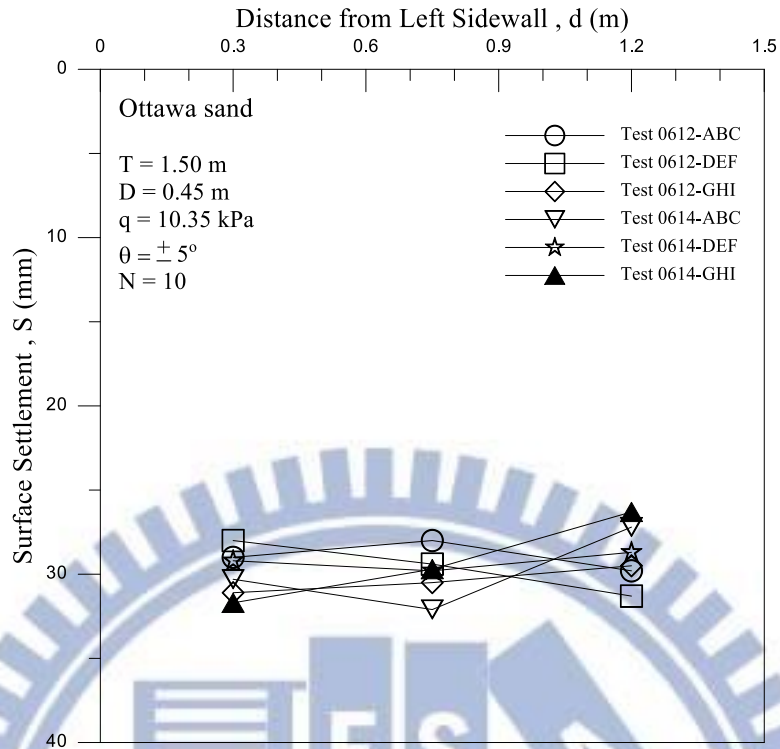
(a) Surface settlement
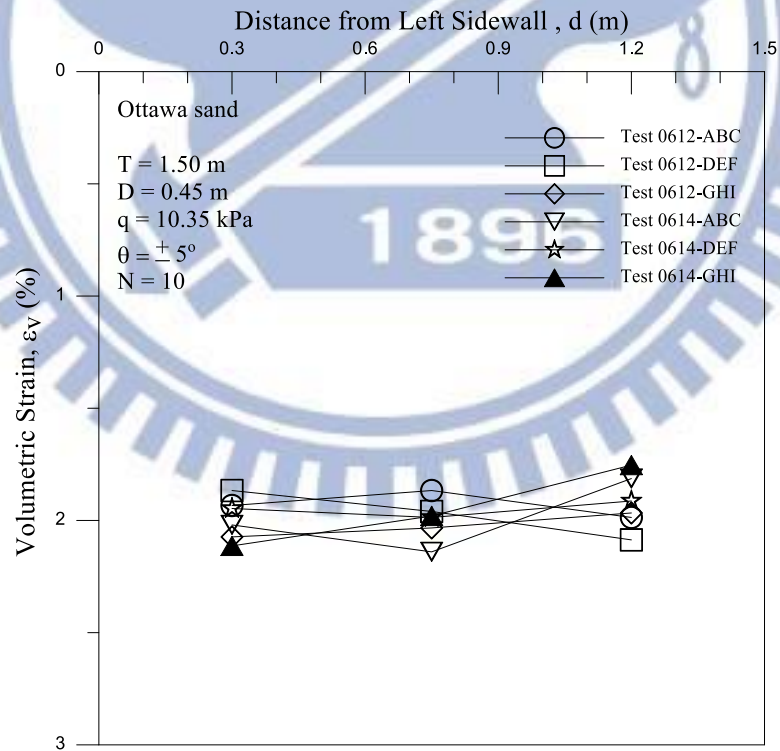
(b) Volumetric strain

Fig. 6.22. Surface settlement and Volumetric strain due to cyclic torsional shear at N = 10

145
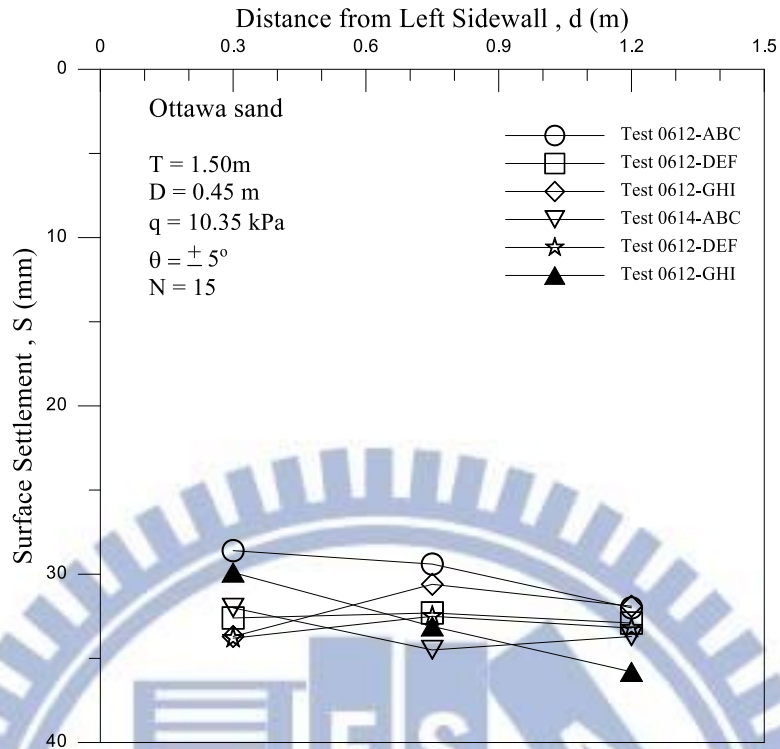
(a) Surface settlement
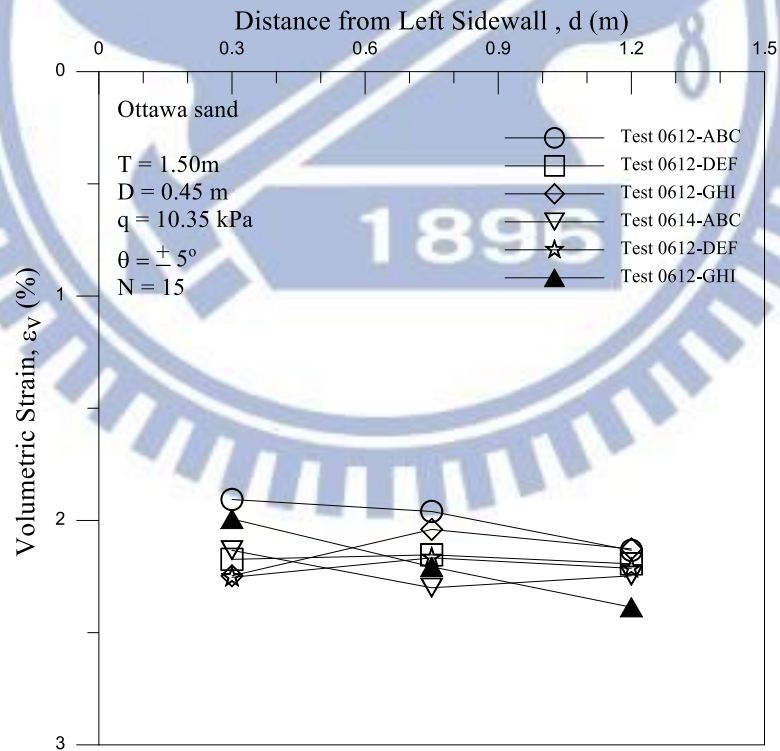
(b) Volumetric strain

Fig. 6.23. Surface settlement and Volumetric strain due to cyclic torsional shear at N = 15

146
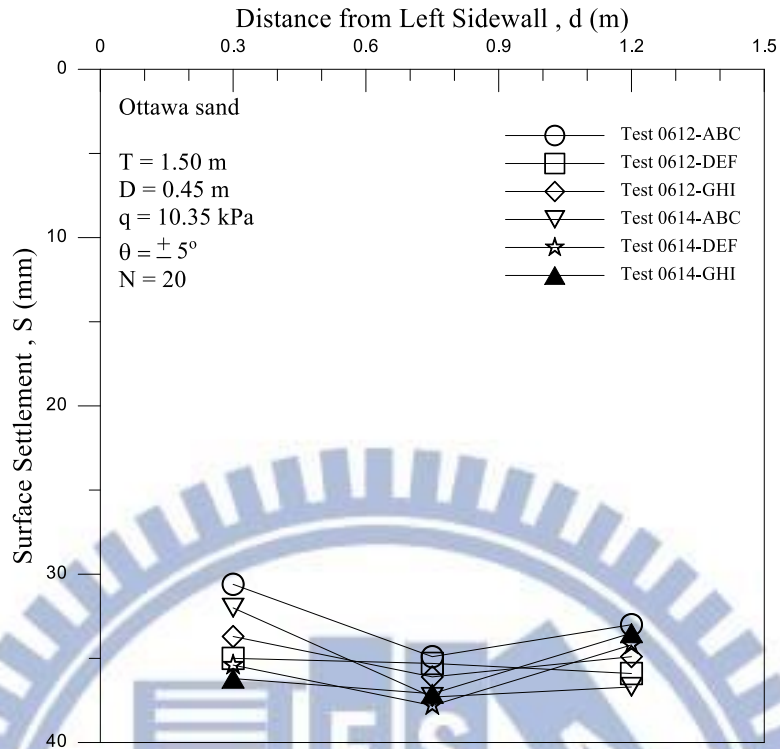
(a) Surface settlement
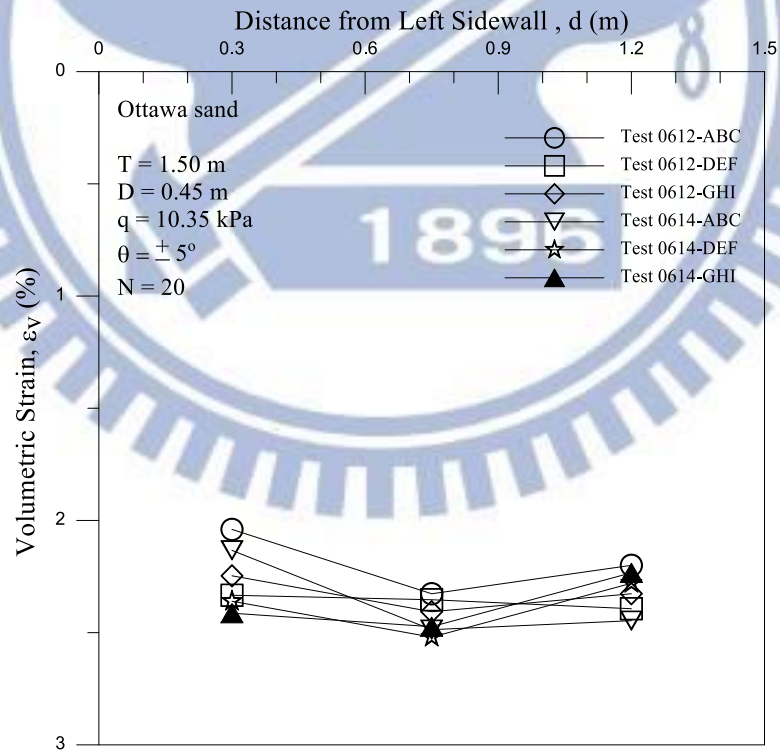
(b) Volumetric strain

Fig. 6.24. Surface settlement and Volumetric strain due to cyclic torsional shear at N = 20

147

Distance from Left Sidewall , d (m)

Ottawa sand

T = 1.50 m
D = 0.45 m
q = 10.35 kPa
θ = ± 5º
N = 30

Surface Settlement , S (mm)

Test 0612-ABC
Test 0612-DEF
Test 0612-GHI
Test 0614-ABC
Test 0614-DEF
Test 0614-GHI

(a) Surface settlement

Distance from Left Sidewall , d (m)

Ottawa sand

T = 1.50 m
D = 0.45 m
q = 10.35 kPa
θ = ± 5º
N = 30

Volumetric Strain, ε$_v$ (%)

Test 0612-ABC
Test 0612-DEF
Test 0612-GHI
Test 0614-ABC
Test 0614-DEF
Test 0614-GHI
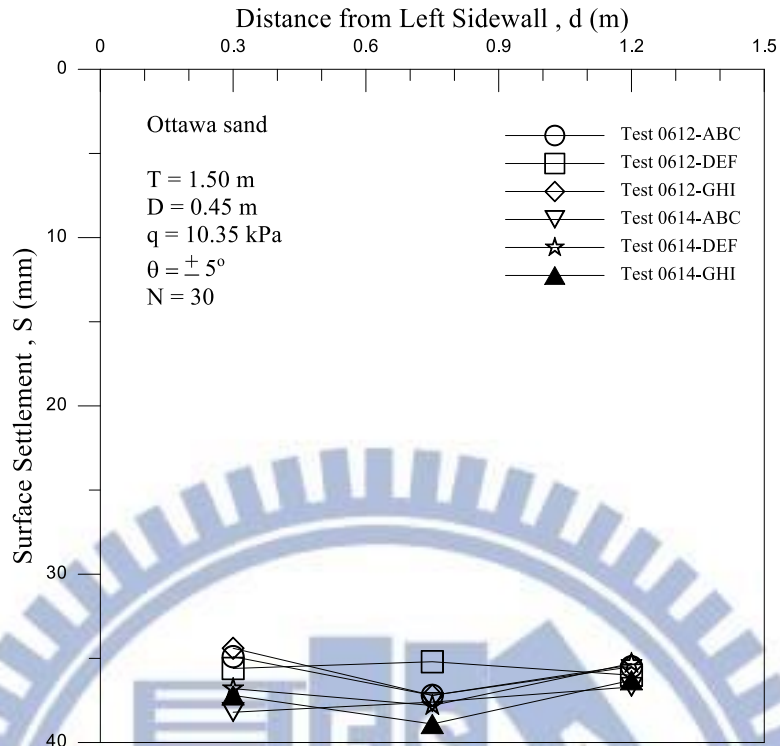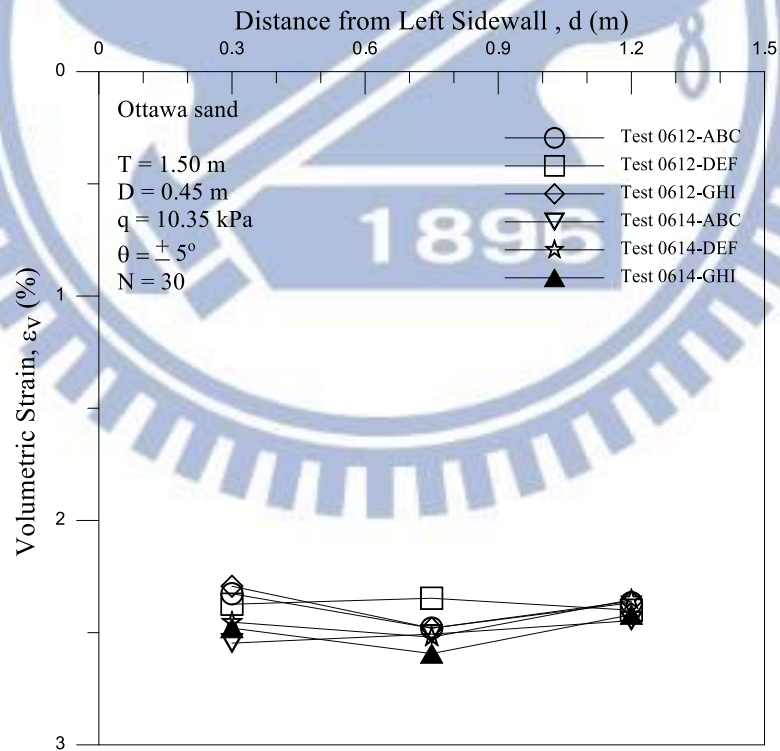
(b) Volumetric strain

Fig. 6.25. Surface settlement and Volumetric strain due to cyclic torsional shear at N = 30

148
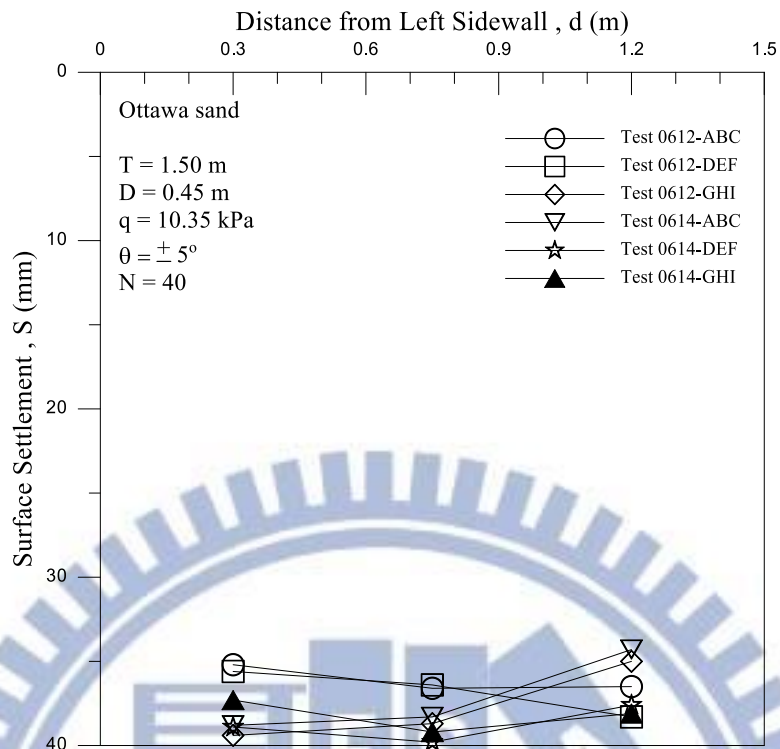
(a) Surface settlement
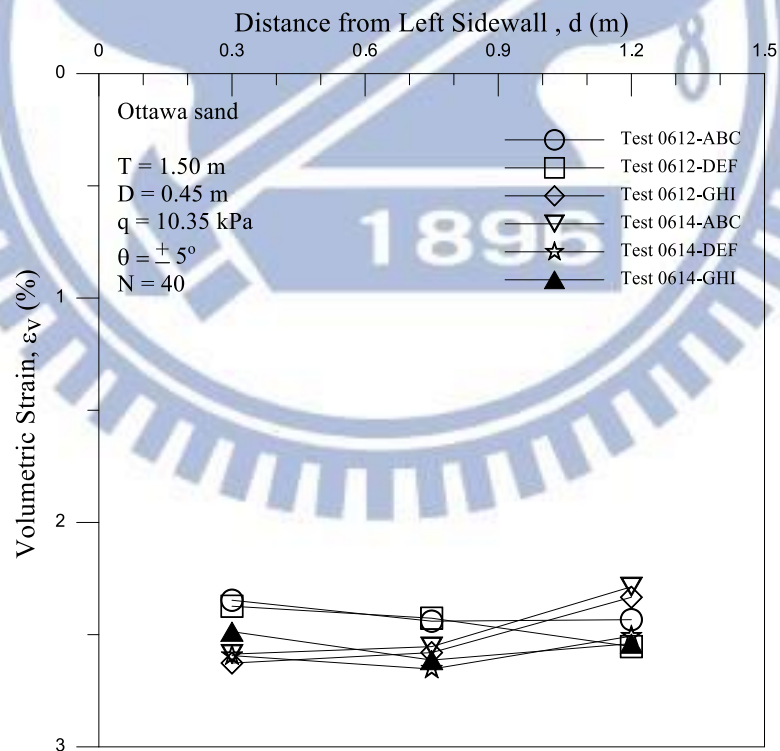
(b) Volumetric strain

Fig. 6.26. Surface settlement and Volumetric strain due to cyclic torsional shear at N = 40

149

(a) Surface settlement
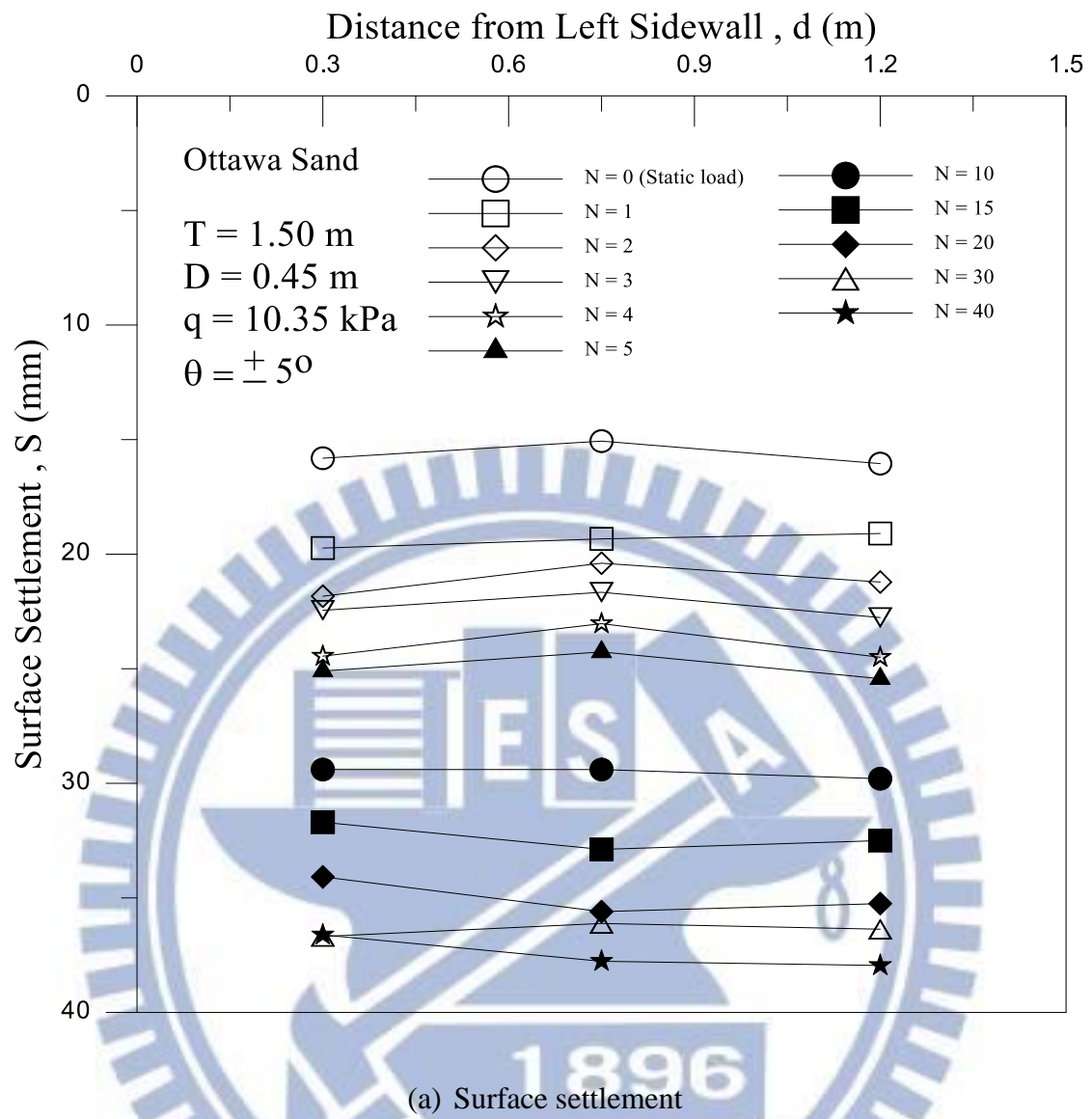
Fig. 6.27. Variation of surface settlement and volumetric strain for N = 1 to 40
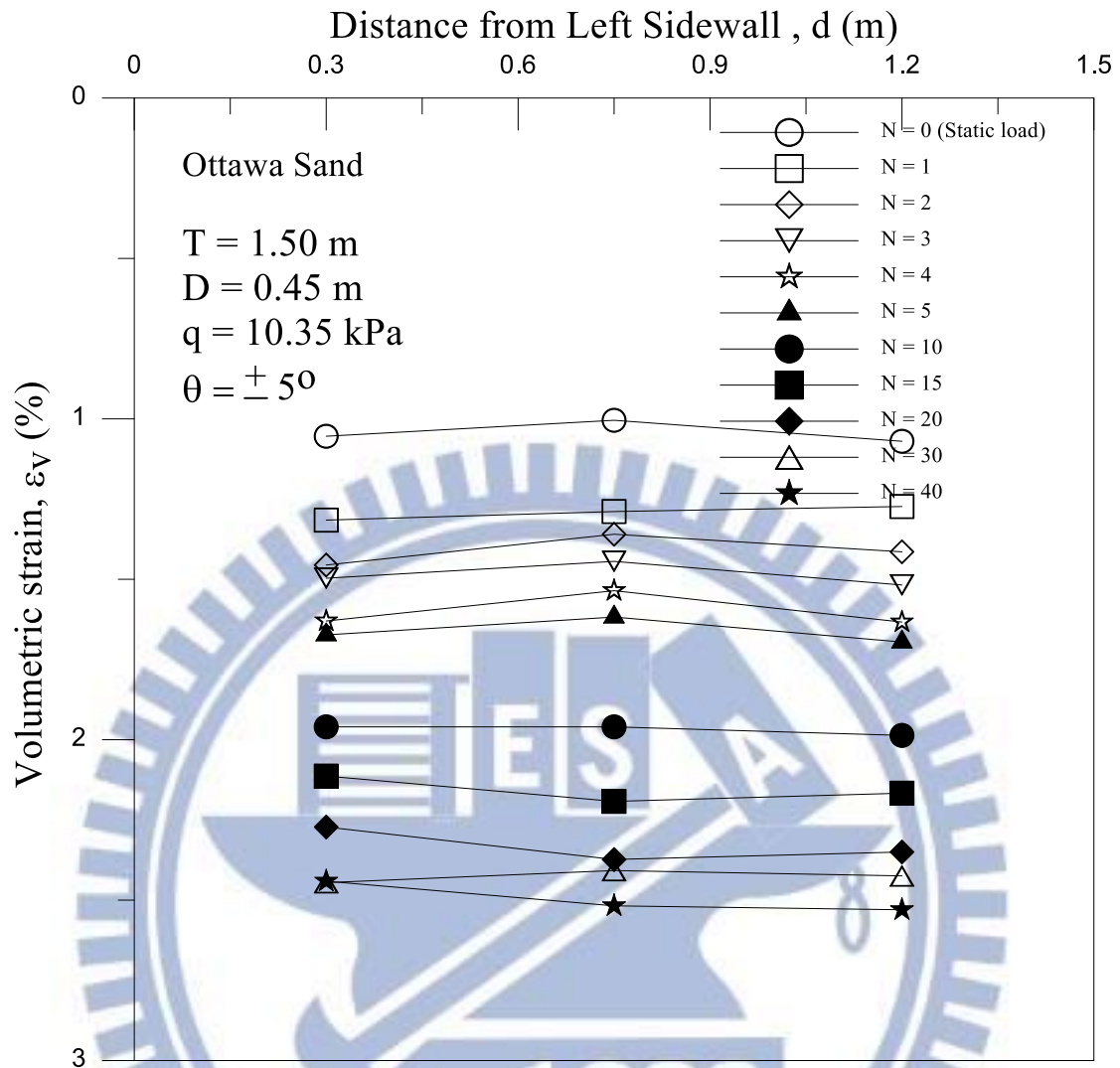
(b) Volumetric strain

Fig. 6.27. Variation of surface settlement and volumetric strain for N = 1 to 40
(cont'd))
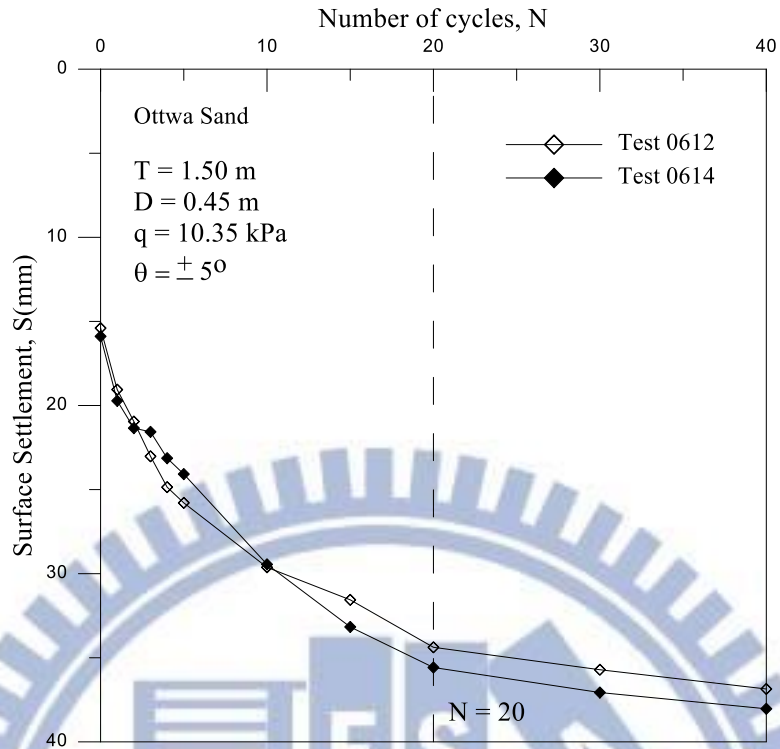
(a) Surface settlement for N = 1~40
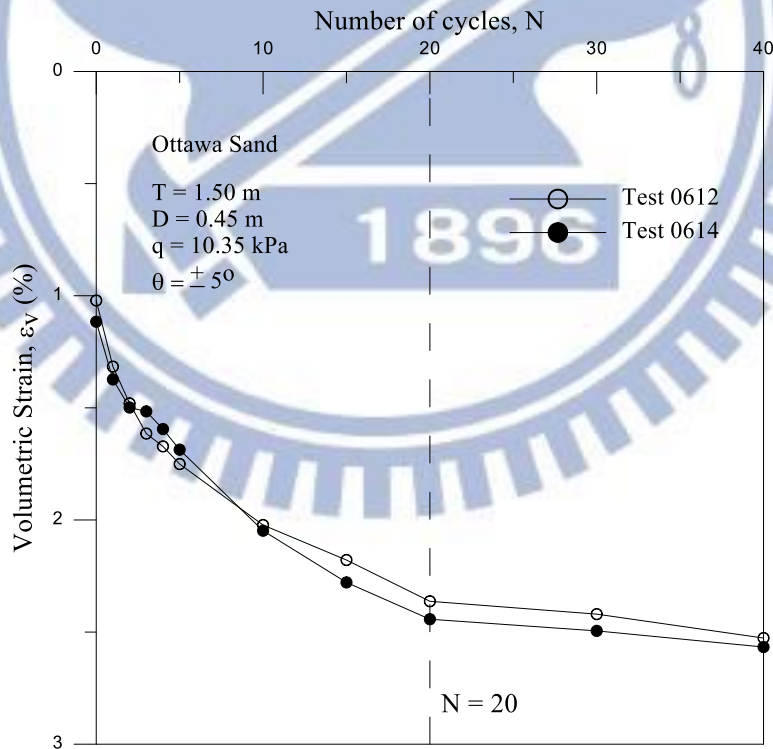
(b) Volumetric strain for N = 1~40

Fig. 6.28. Variation of surface settlement and volumetric strain for N = 1 to 40

Fig. 6.29. Distribution of relative density after cyclic torsional shearing at N = 5

The figure shows a plot of Relative Density, D_r (%) on the x-axis (0 to 100) versus Depth, z (m) on the y-axis (0 to 1.5).

Ottawa sand

T = 1.50 m
D = 0.45 m
q = 10.35 kPa
$\theta = \pm 5^{\circ}$
N = 5

D_r = 38 %
D_r = 75 %
D_r = 70 %
D_r = 34 %

Test 0531 (Loose)
Test 0621 (static)
Test 0708 (N = 5)
Test 0715 (N = 5)

Fig. 6.30. Distribution of relative density after cyclic torsional shearing at N = 10

Relative Density, D_r (%) — horizontal axis (0 to 100)

Depth, z (m) — vertical axis (0 to 1.5)

Ottawa sand

T = 1.50 m
D = 0.45 m
q = 10.35 kPa
$\theta = \pm 5^o$
N = 10

$D_r = 38\%$
$D_r = 34\%$
$D_r = 75\%$
$D_r = 70\%$

Test 0531 (Loose)
Test 0621 (static)
Test 0703 (N = 10)
Test 0705 (N = 10)

Relative Density, D_r (%)

Ottawa sand

T = 1.50 m
D = 0.45 m
q = 10.35 kPa
θ = ± 5°
N = 20

D_r = 38 %

D_r = 75 %

D_r = 70 %

D_r = 34 %

Depth, z (m)

□ Test 0531 (Loose)
○ Test 0621 (static)
◇ Test 0626 (N = 20)
◆ Test 0701 (N = 20)
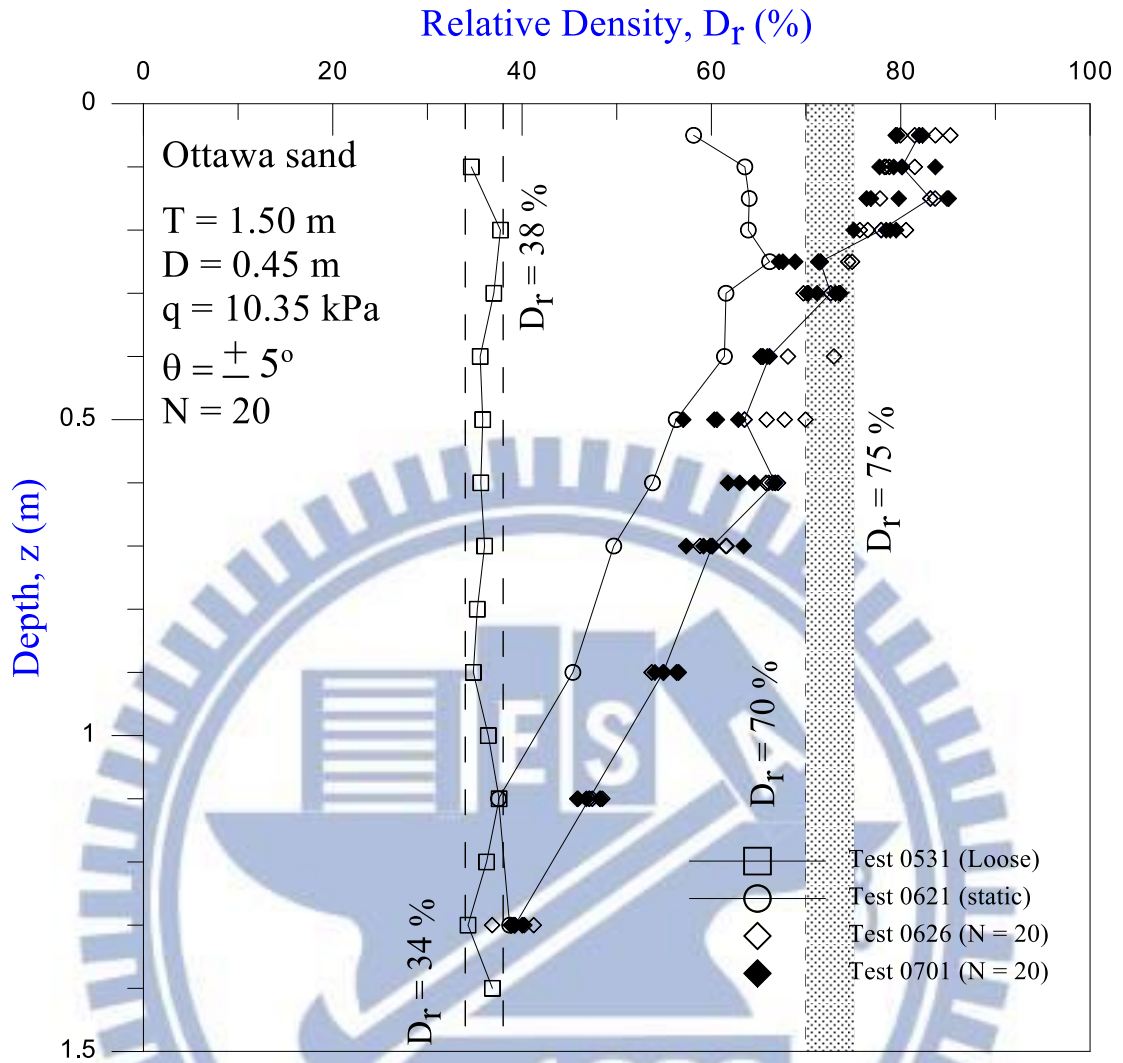
Fig. 6.31. Distribution of relative density after cyclic torsional shearing at N = 20
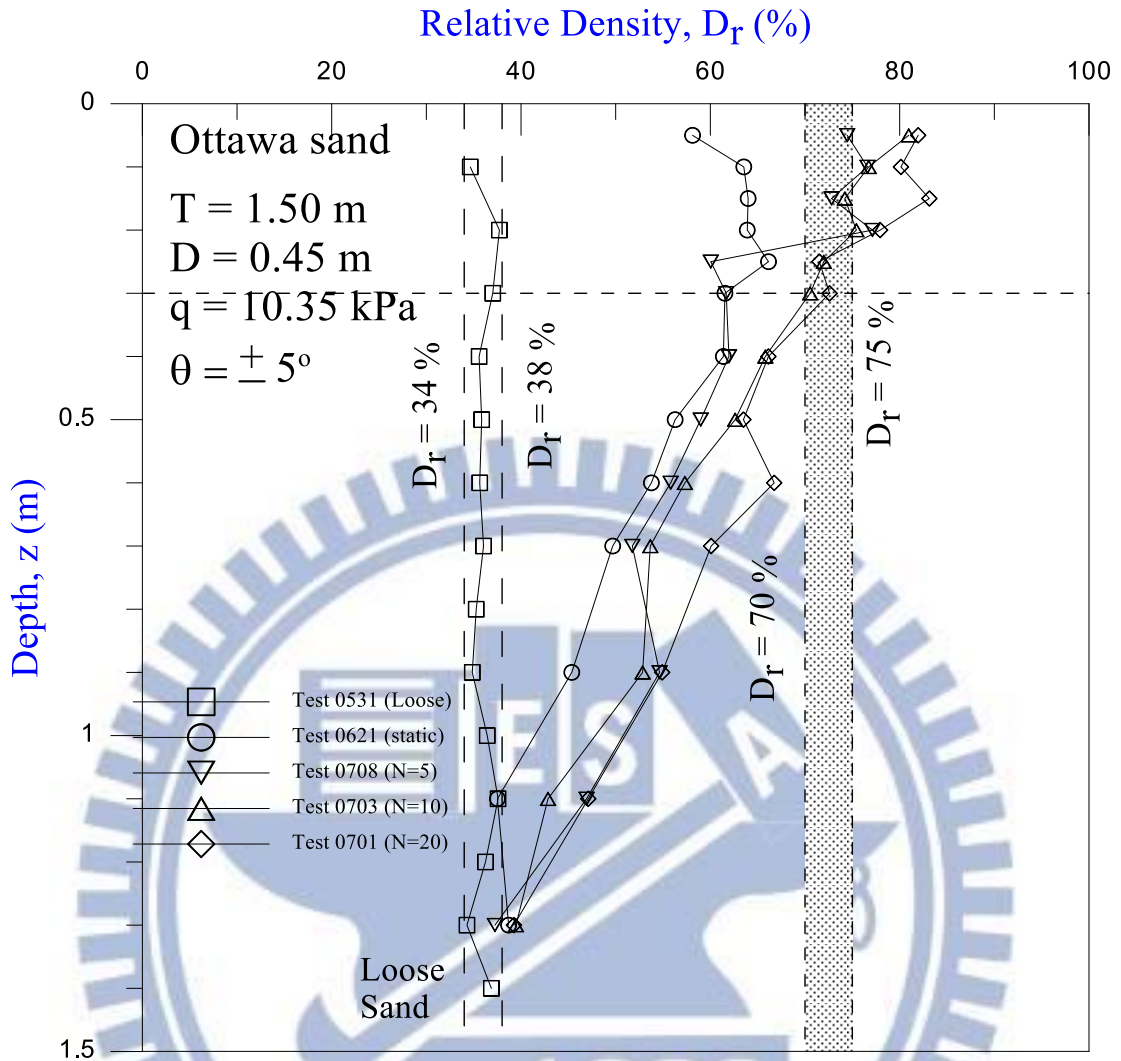
Fig. 6.32. Distribution of relative density after cyclic torsional shearing
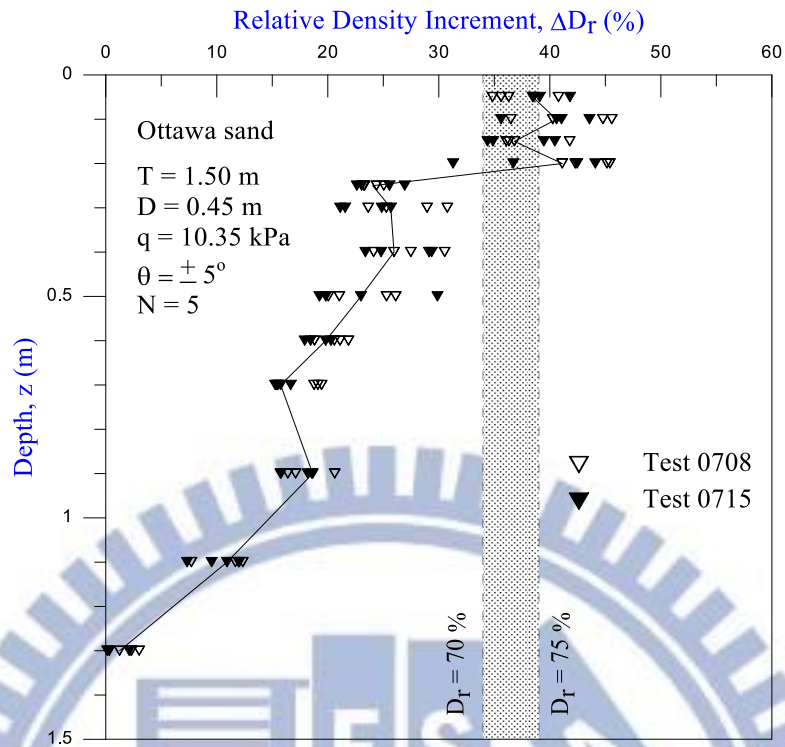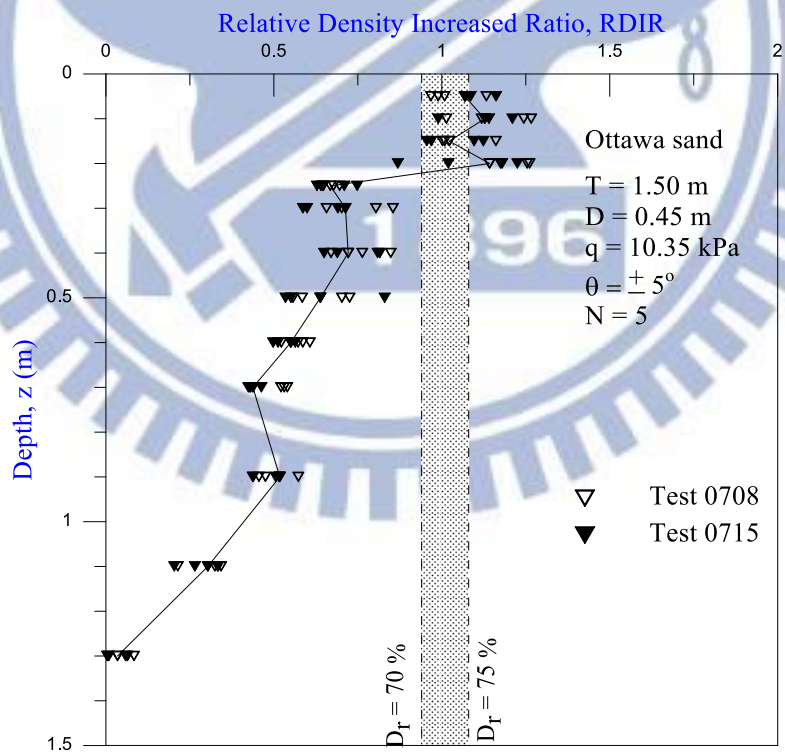
Fig. 6.33. Change of density due to cyclic torsional shearing at N = 5
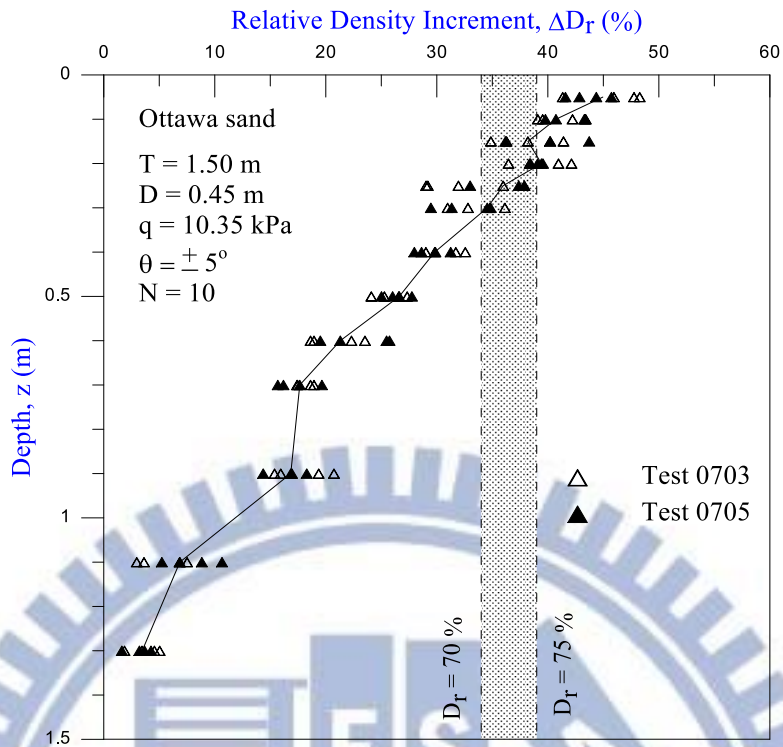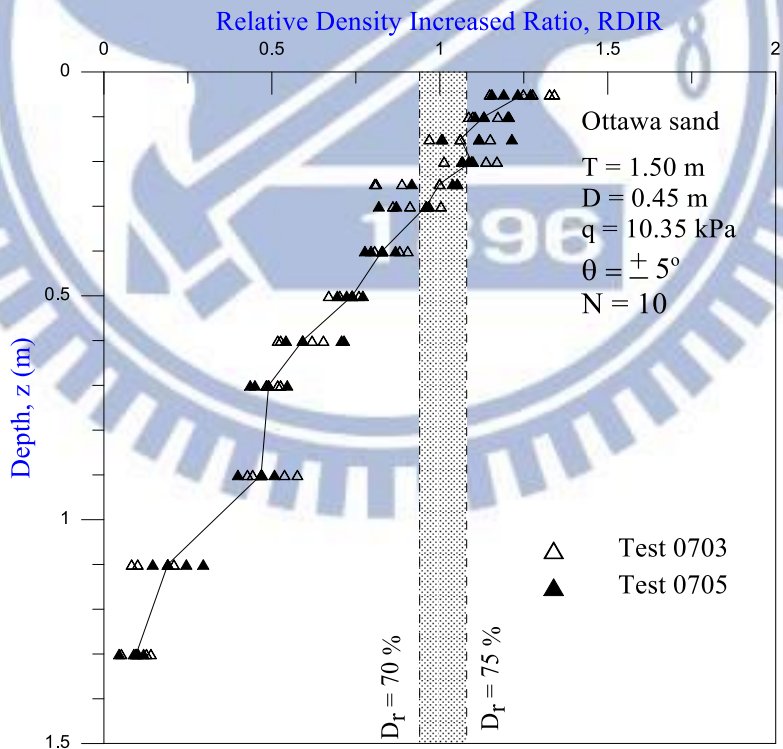
Fig. 6.34. Change of density due to cyclic torsional shearing at N = 10
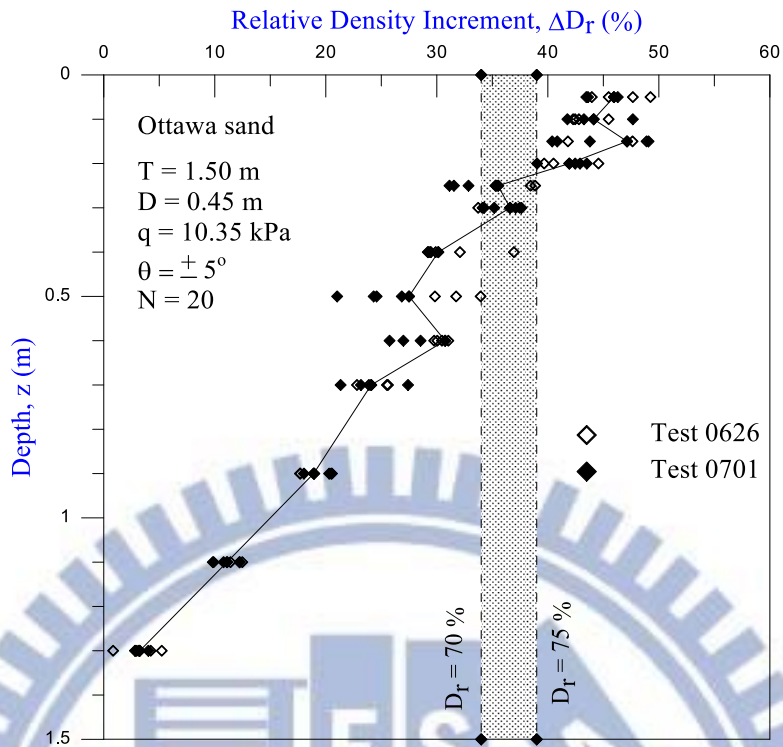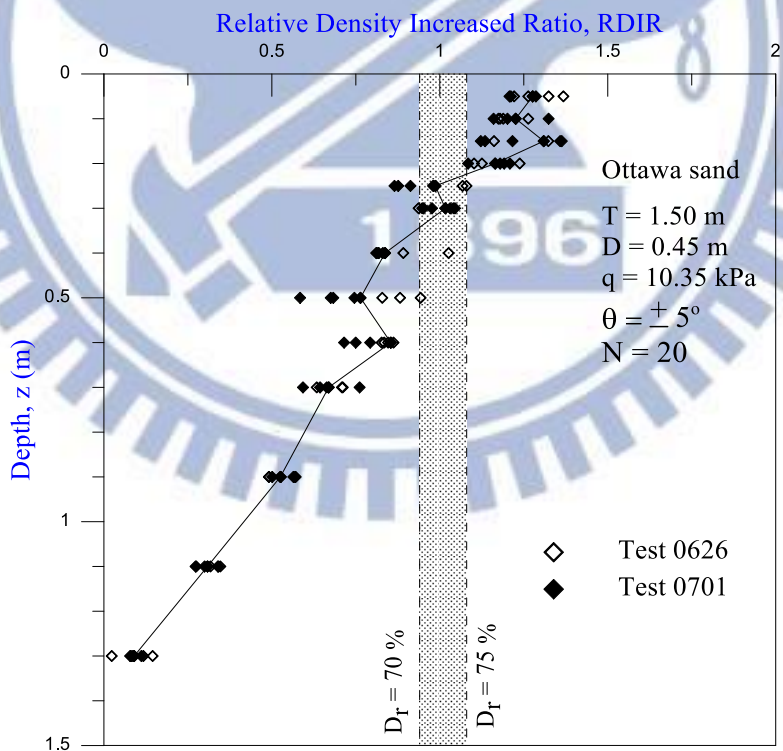
Fig. 6.35. Change of density due to cyclic torsional shearing at N = 20
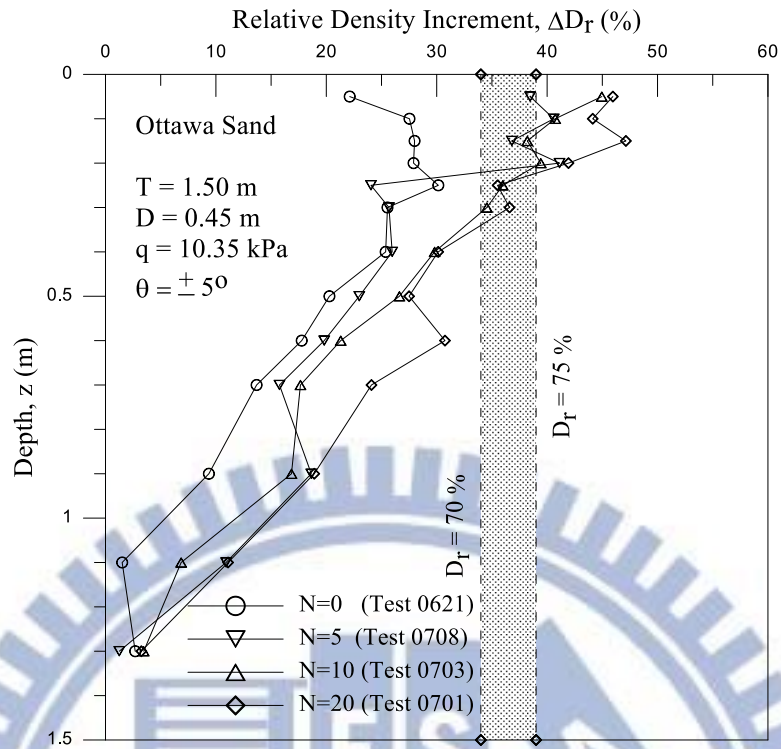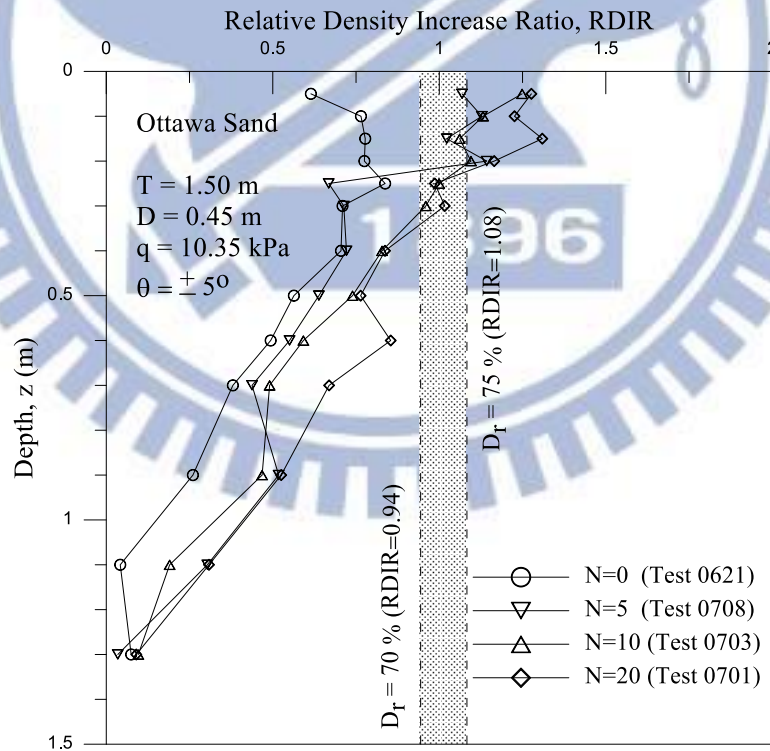
Fig. 6.36. Change of density due to cyclic torsional shearing
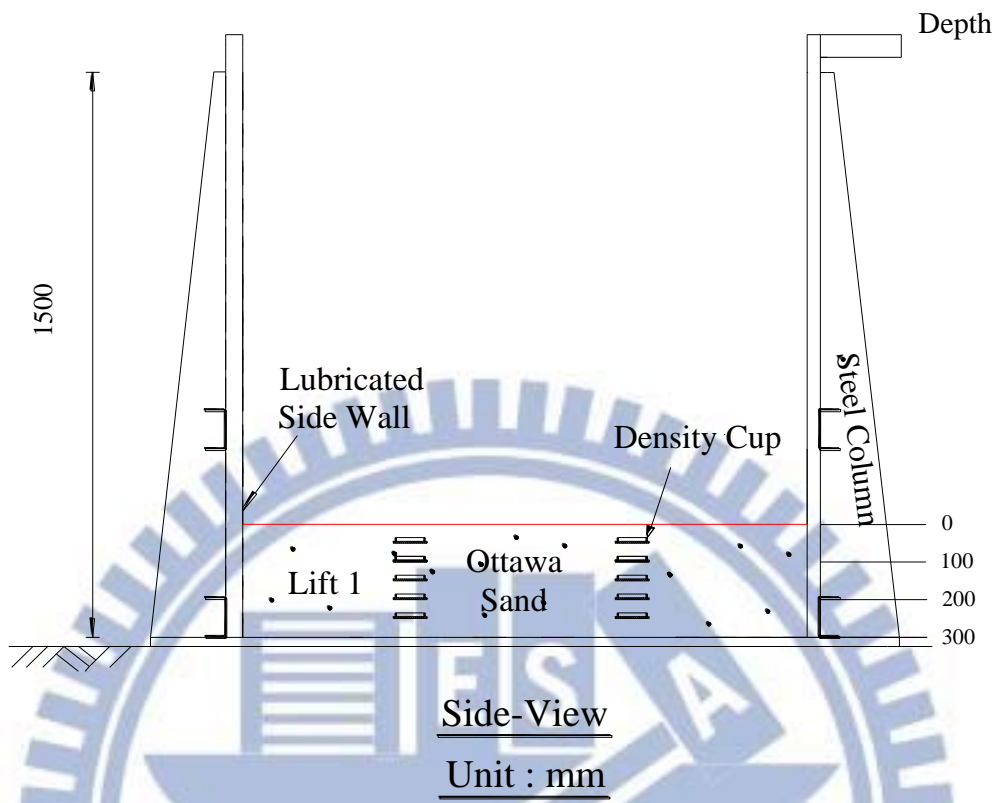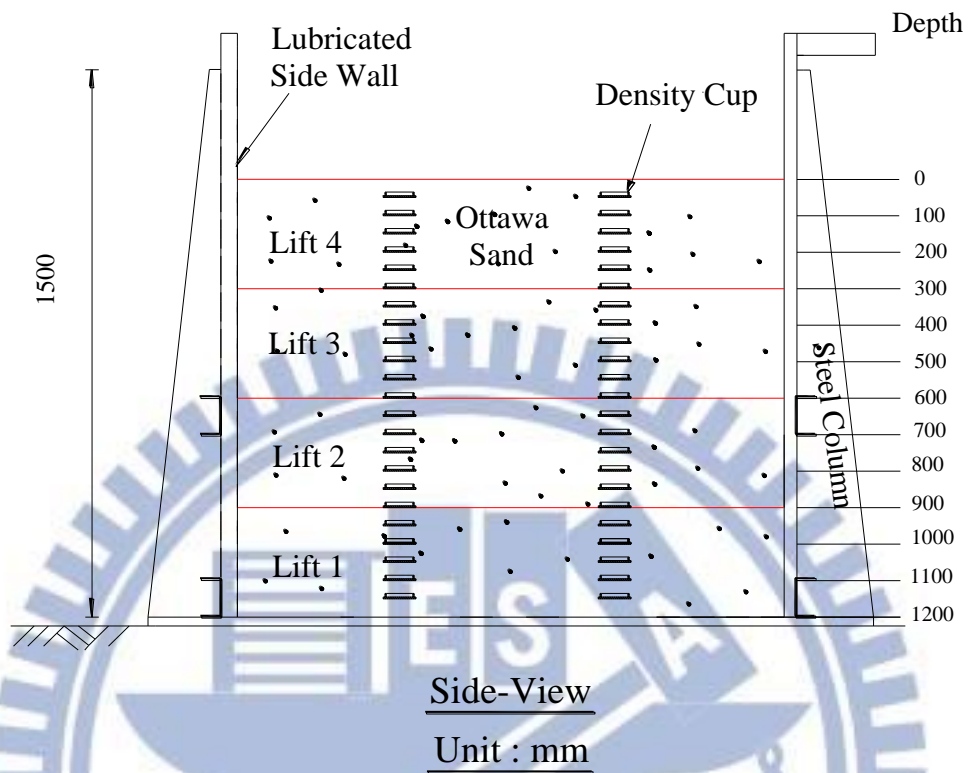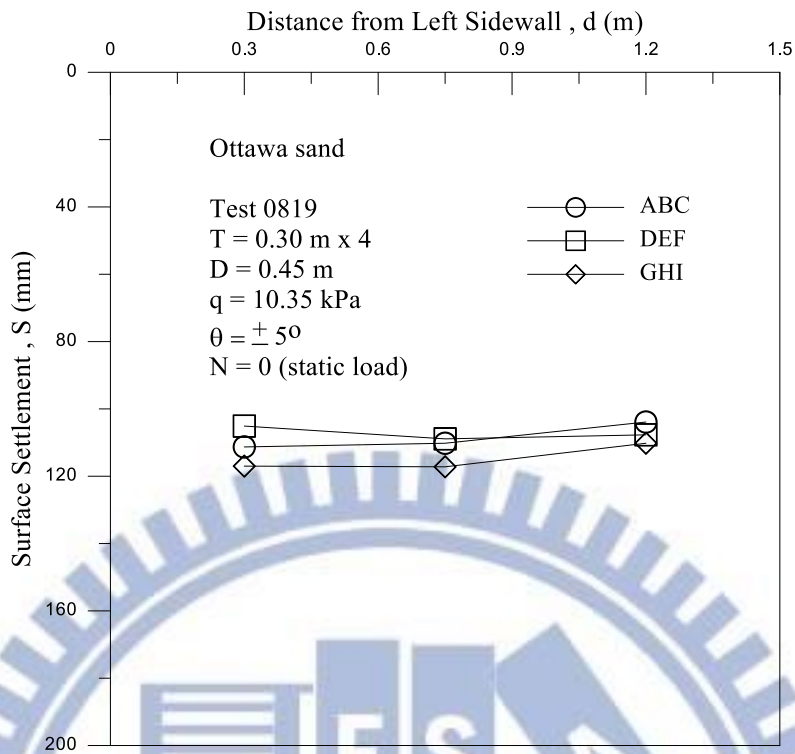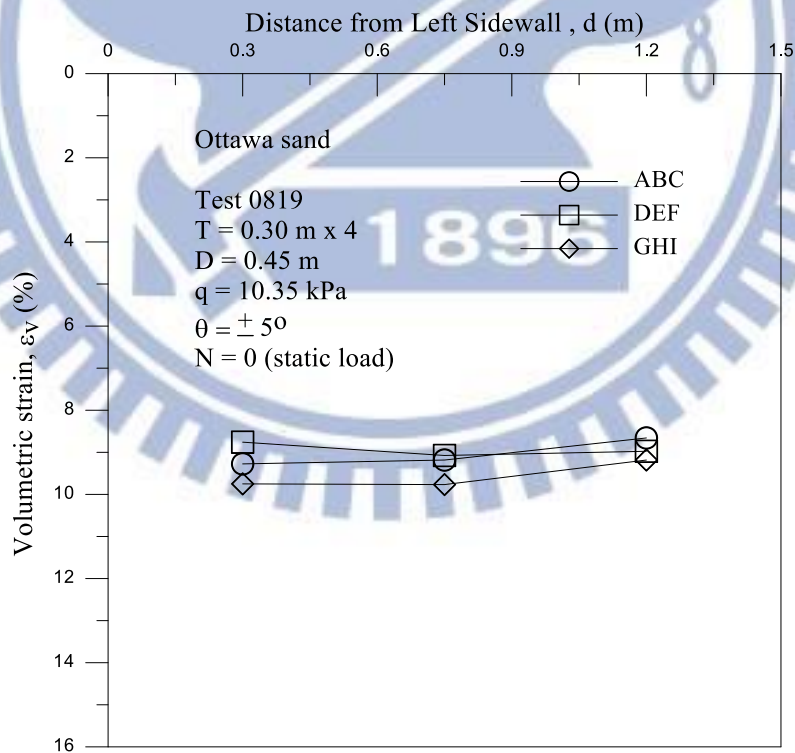
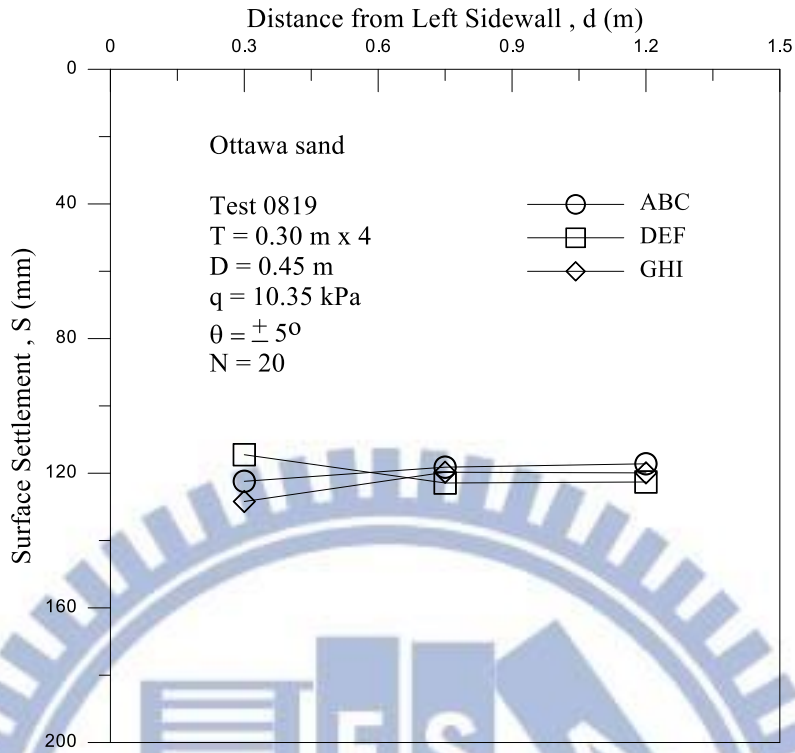Fig. 6.37. Soil density cups buried at different elevations in Lift 1
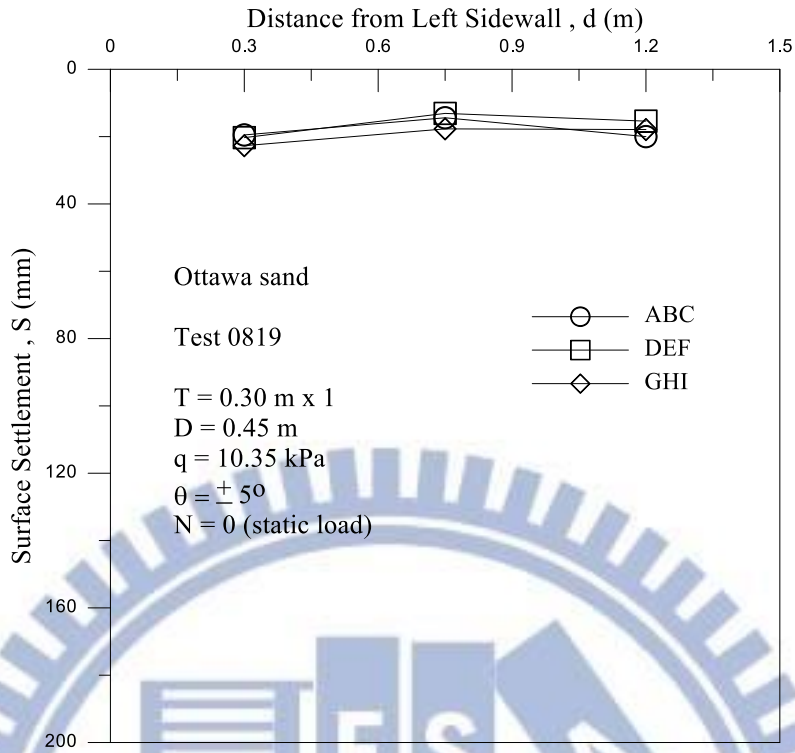
(a) Surface settlement after static load on Lift 1
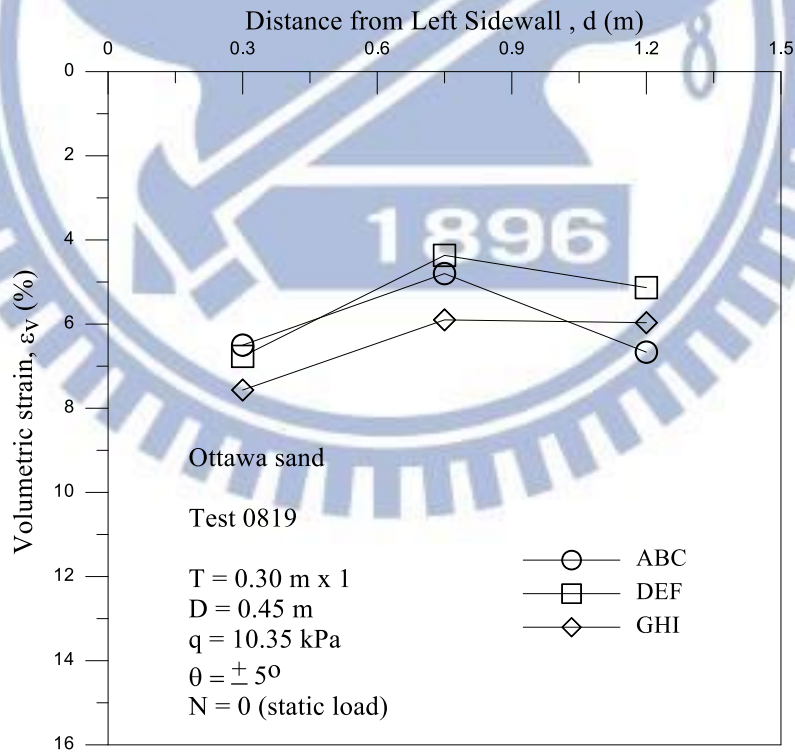
(b) Volumetric strain after static load on Lift 1

Fig. 6.38. Surface settlement and Volumetric strain after static load on Lift 1

Distance from Left Sidewall , d (m)

Ottawa sand

Test 0819

T = 0.30 m x 1
D = 0.45 m
q = 10.35 kPa
θ = $\pm$ 5º
N = 20

○——— ABC
□——— DEF
◇——— GHI
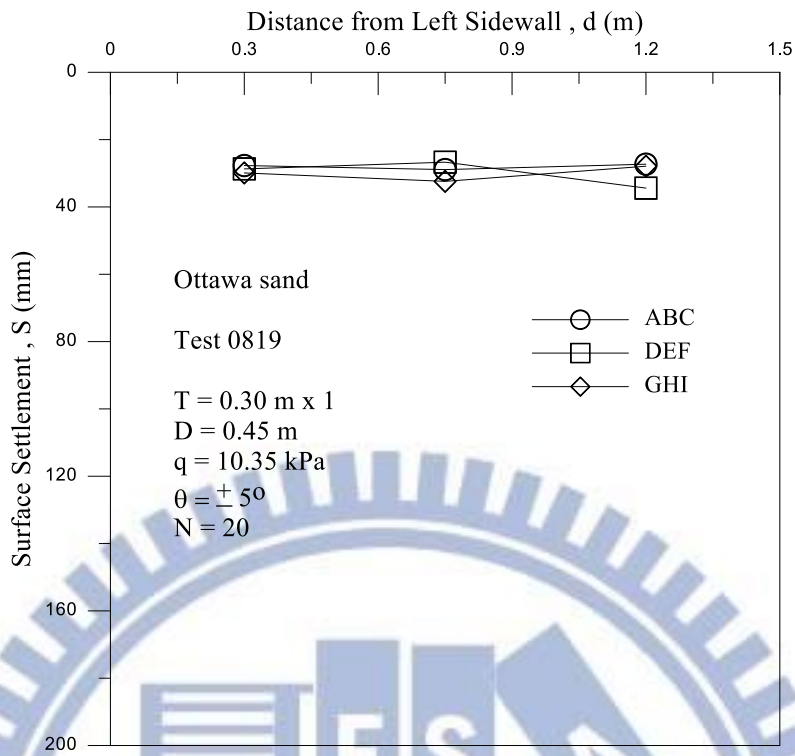
(a) Surface settlement after compaction for N = 20 on Lift 1

Distance from Left Sidewall , d (m)

Ottawa sand

Test 0819
T = 0.30 m x 1
D = 0.45 m
q = 10.35 kPa
θ = $\pm$ 5º
N = 0 (static load)

○——— ABC
□——— DEF
◇——— GHI
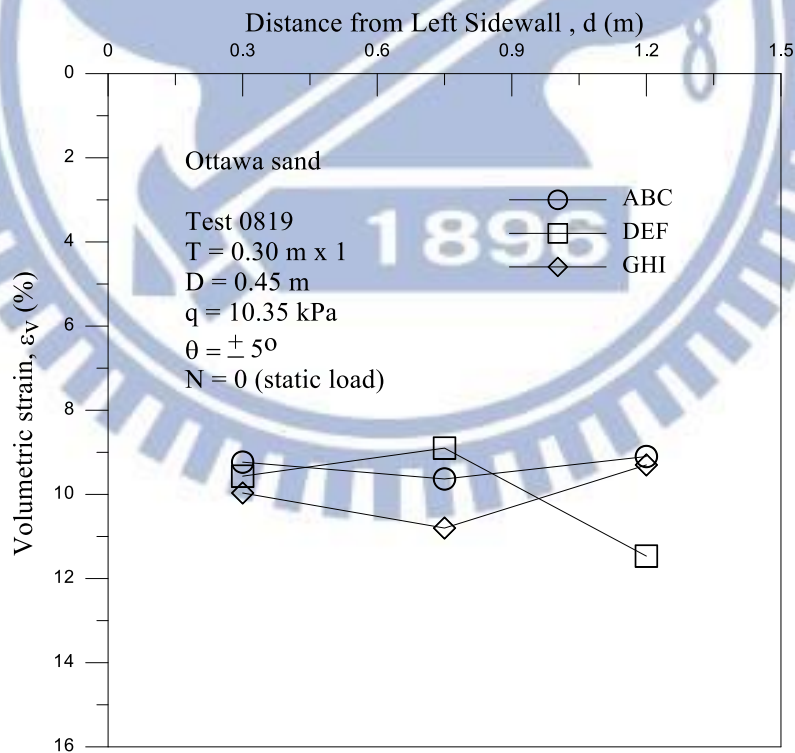
(b) Volumetric strain after compaction for N = 20 on Lift 1

Fig. 6.39. Surface settlement and Volumetric strain after shearing compaction for N = 20 on Lift 1

163
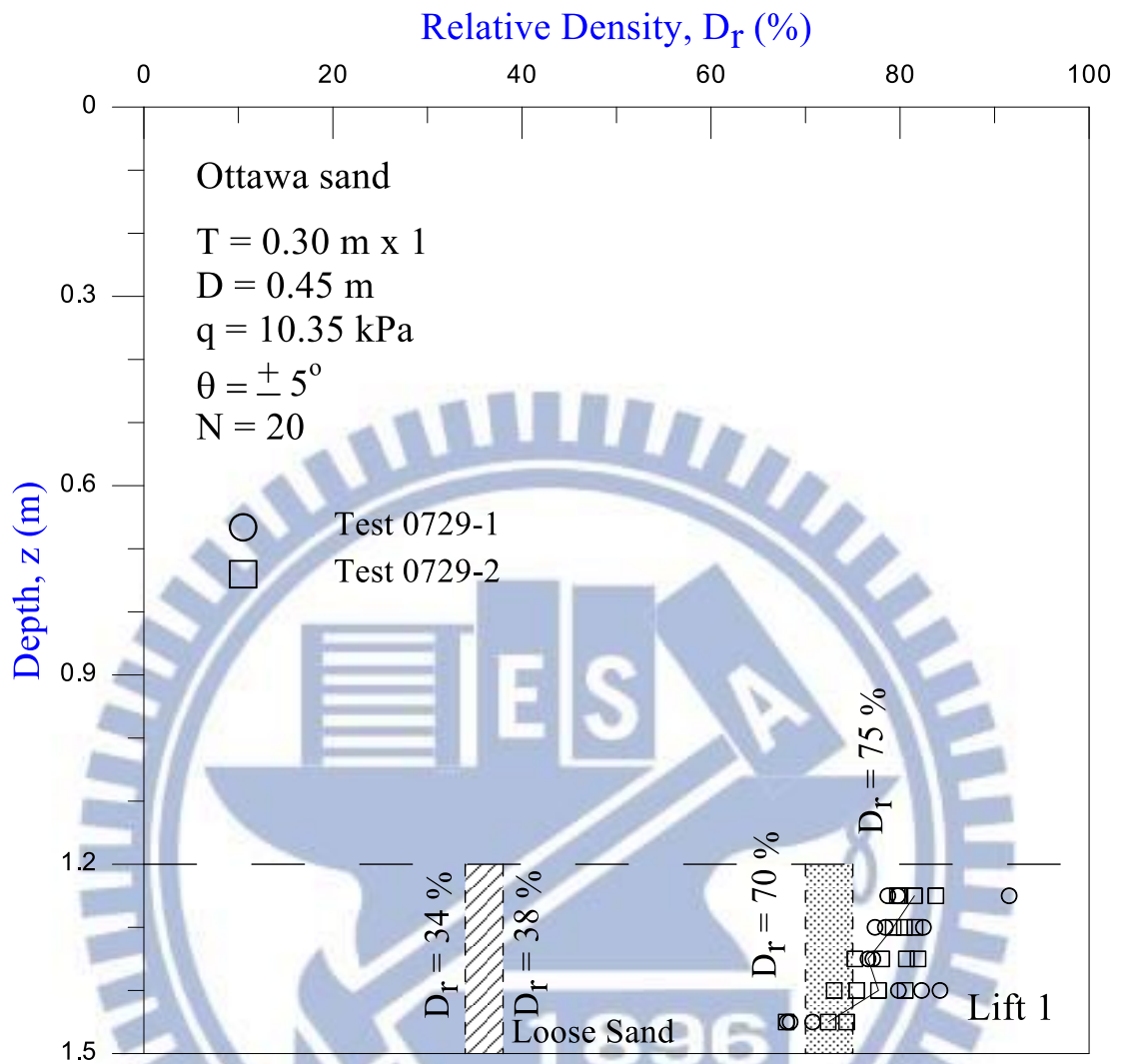
Fig. 6.40. Distribution of relative density in Lift 1
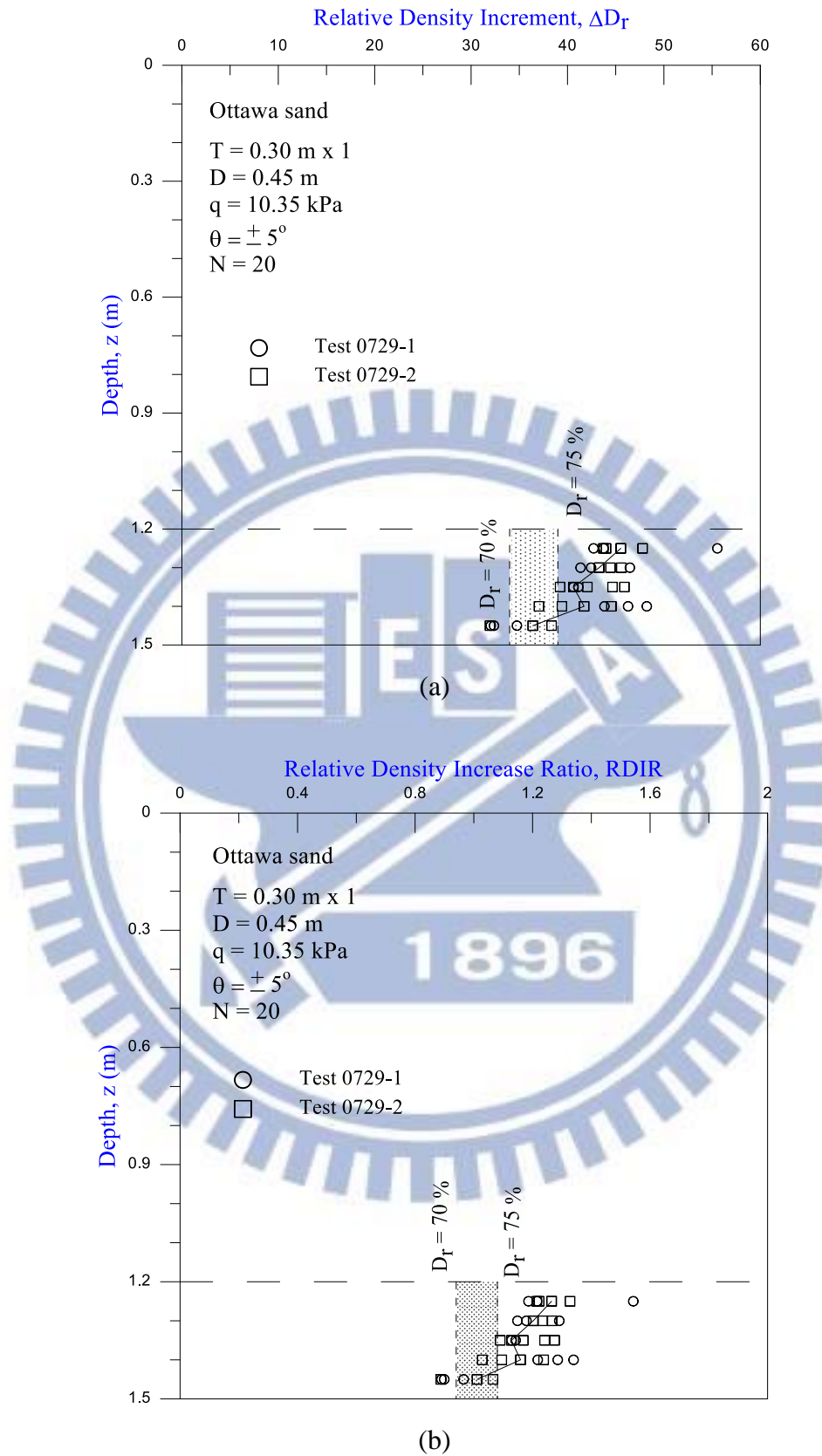
Fig. 6.41. Change of density after shearing compaction for N = 20 in lift 1
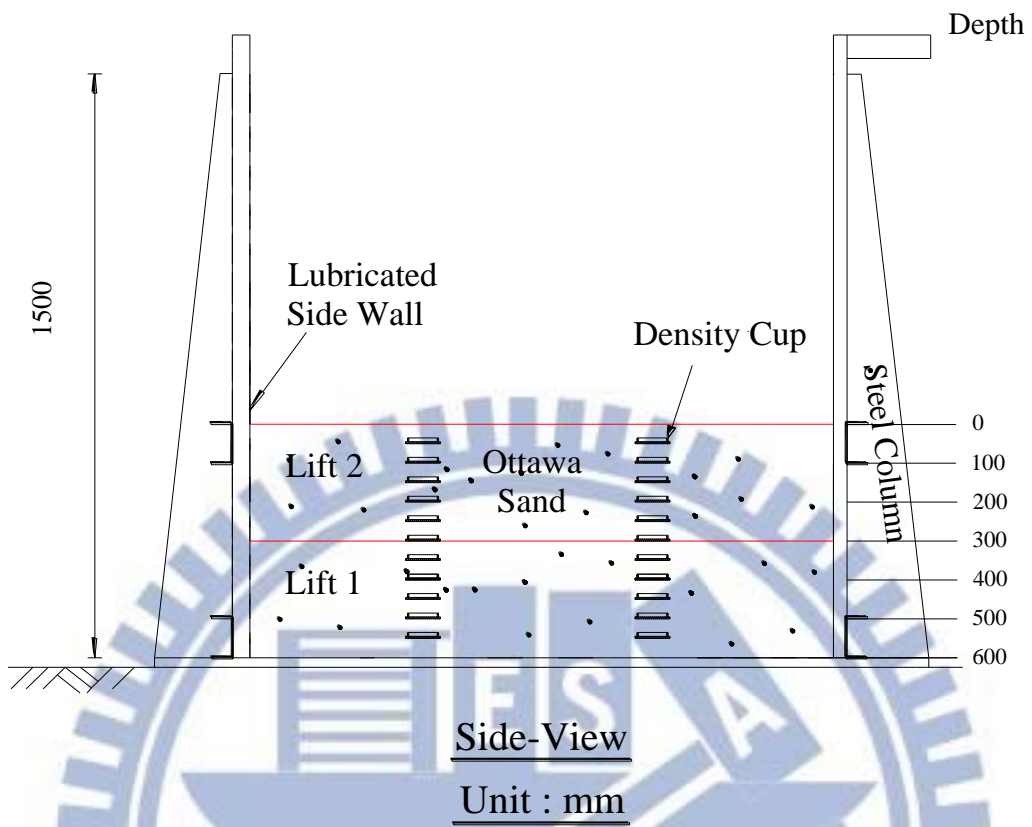
Fig. 6.42. Soil density cups buried at different elevations in Lifts 1 and 2
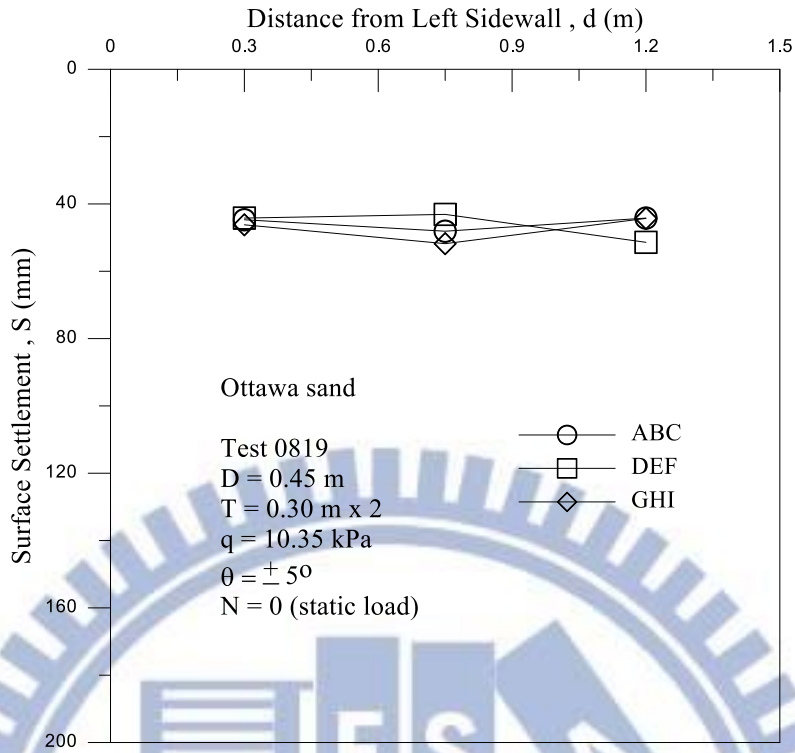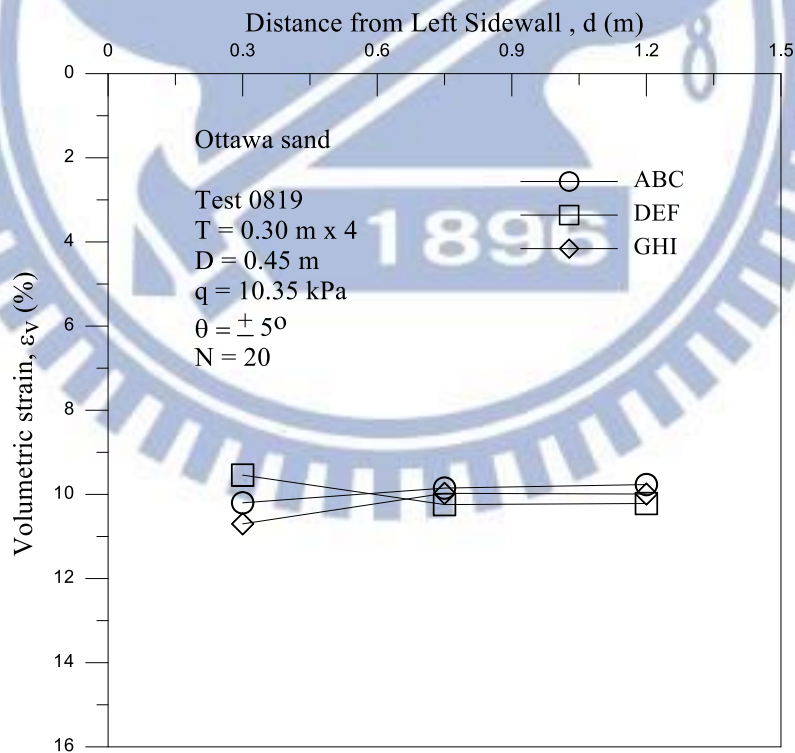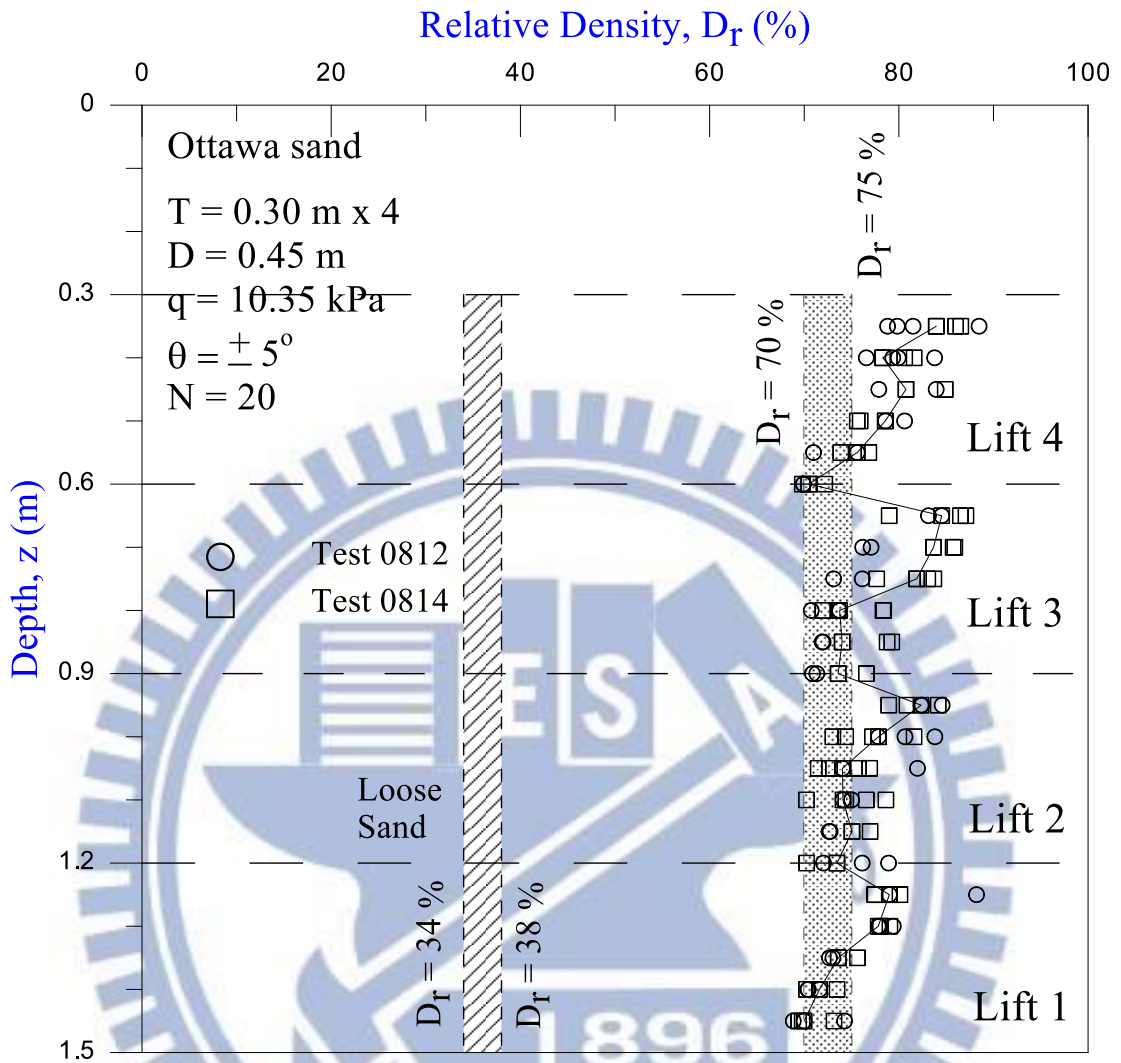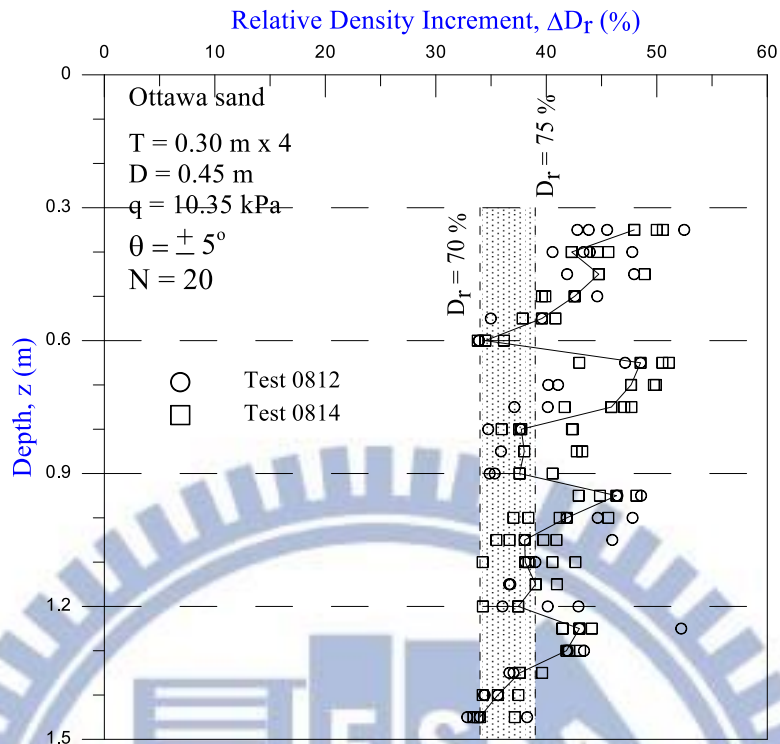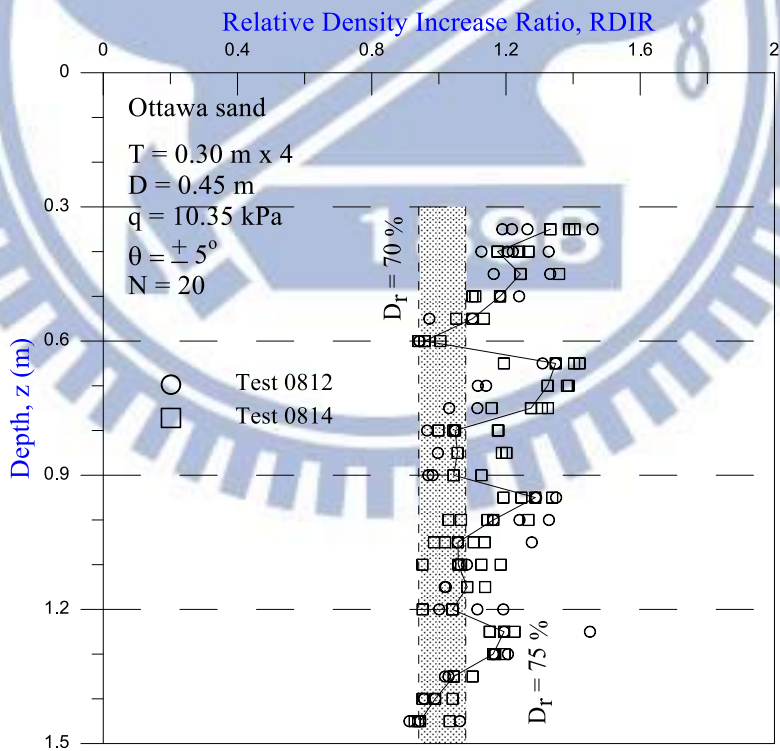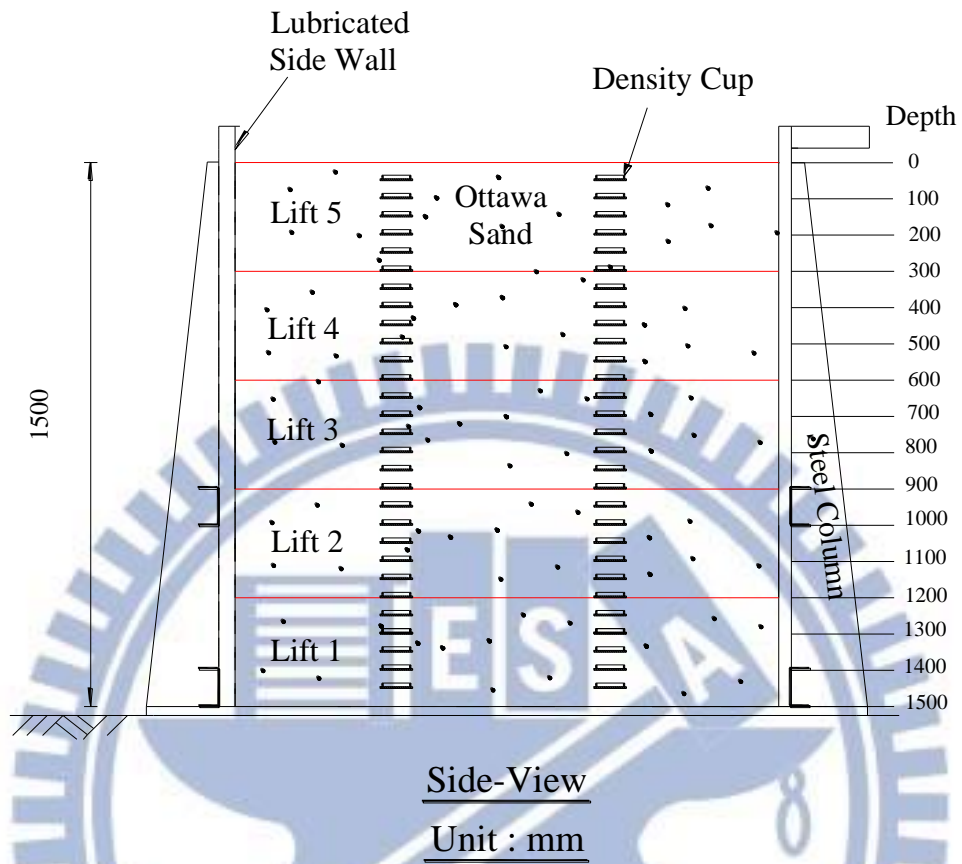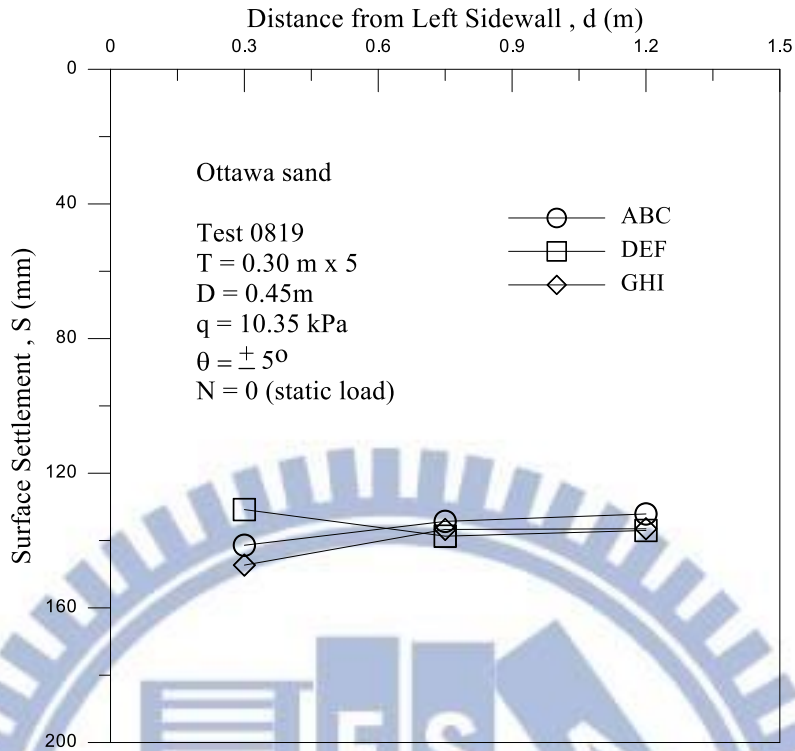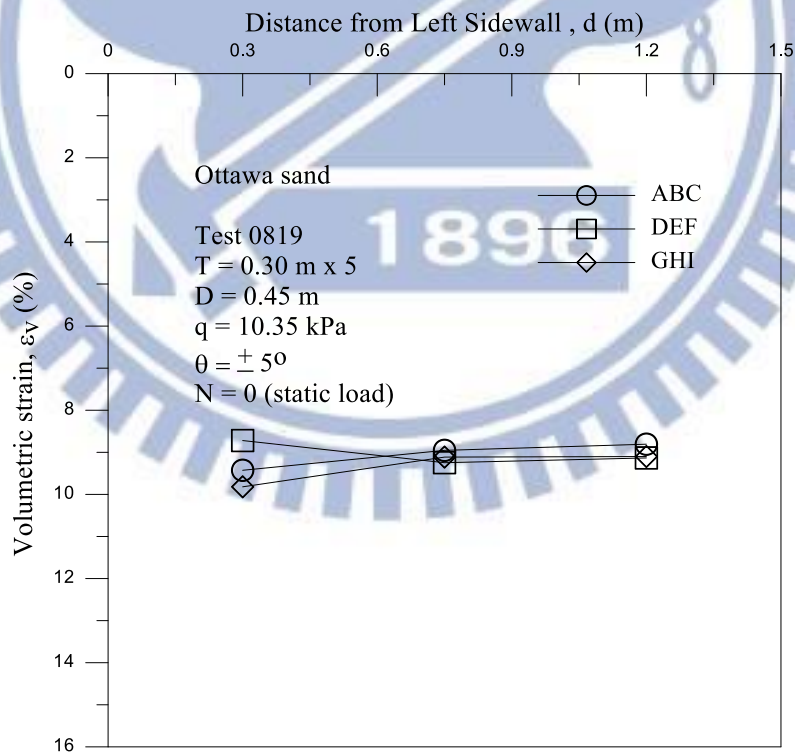
(a) Surface settlement after static load on Lift 2
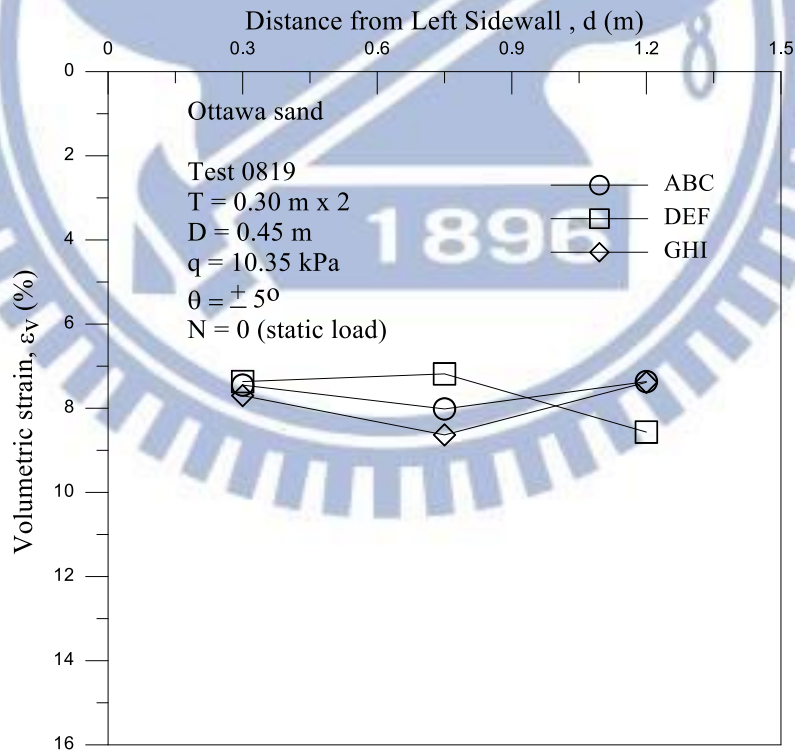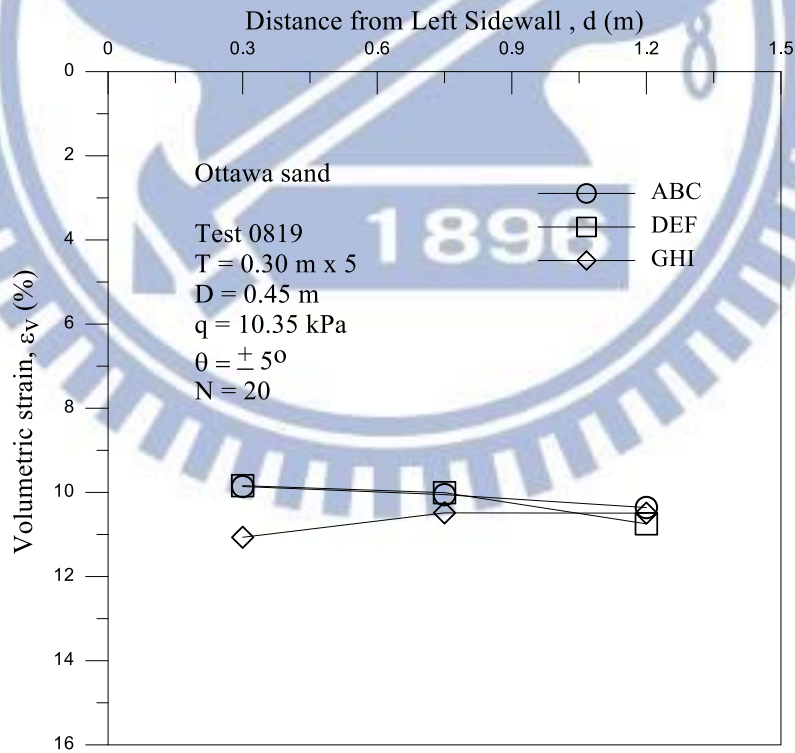

(b) Volumetric strain after static loa on Lift 2

Fig. 6.43. Surface settlement and Volumetric strain after static load on Lift 2
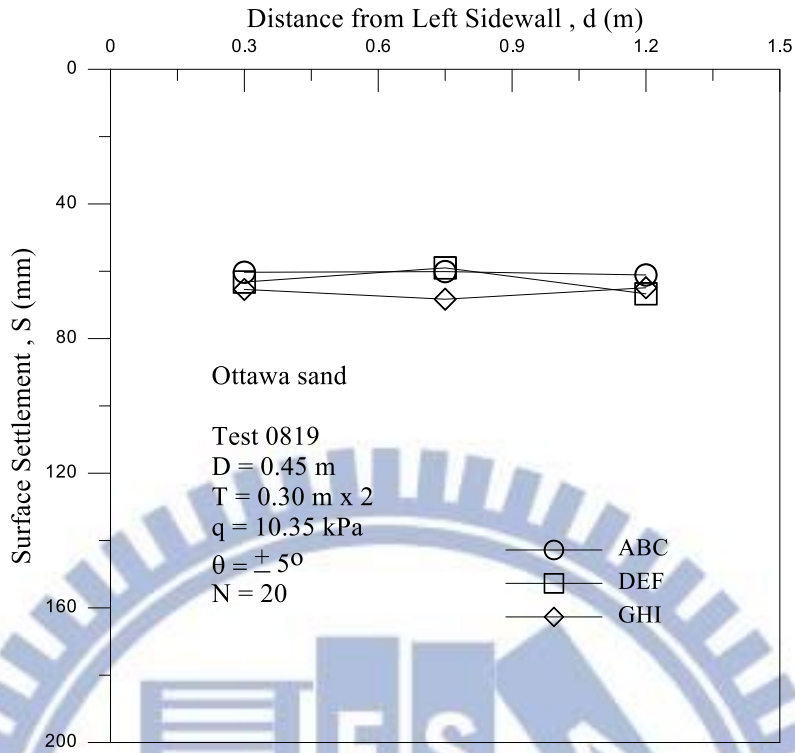
(a) Surface settlement after shearing compaction for N = 20 on Lift 2
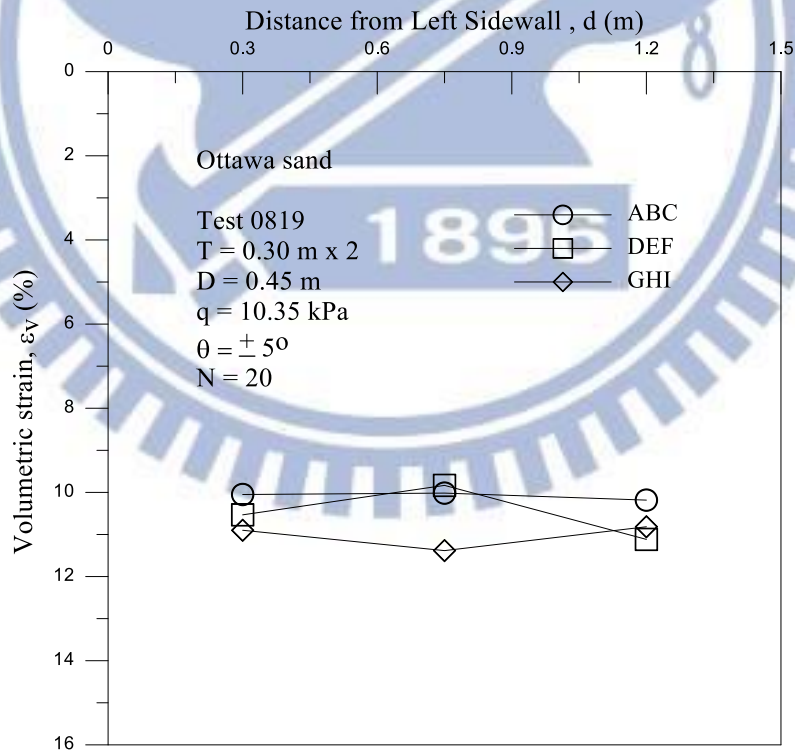
(b) Volumetric strain after shearing compaction for N = 20 on Lift 2

Fig. 6.44. Surface settlement and Volumetric strain after shearing compaction for N = 20 on Lift 2

Relative Density, D_r (%)

Depth, z (m)

Ottawa sand

T = 0.30 m x 2
D = 0.45 m
q = 10.35 kPa
$\theta = \pm 5^o$
N = 20

○   Test 0731
□   Test 0801

Loose Sand

$D_r = 34\ \%$

$D_r = 38\ \%$

$D_r = 70\ \%$

$D_r = 75\ \%$

Lift 2
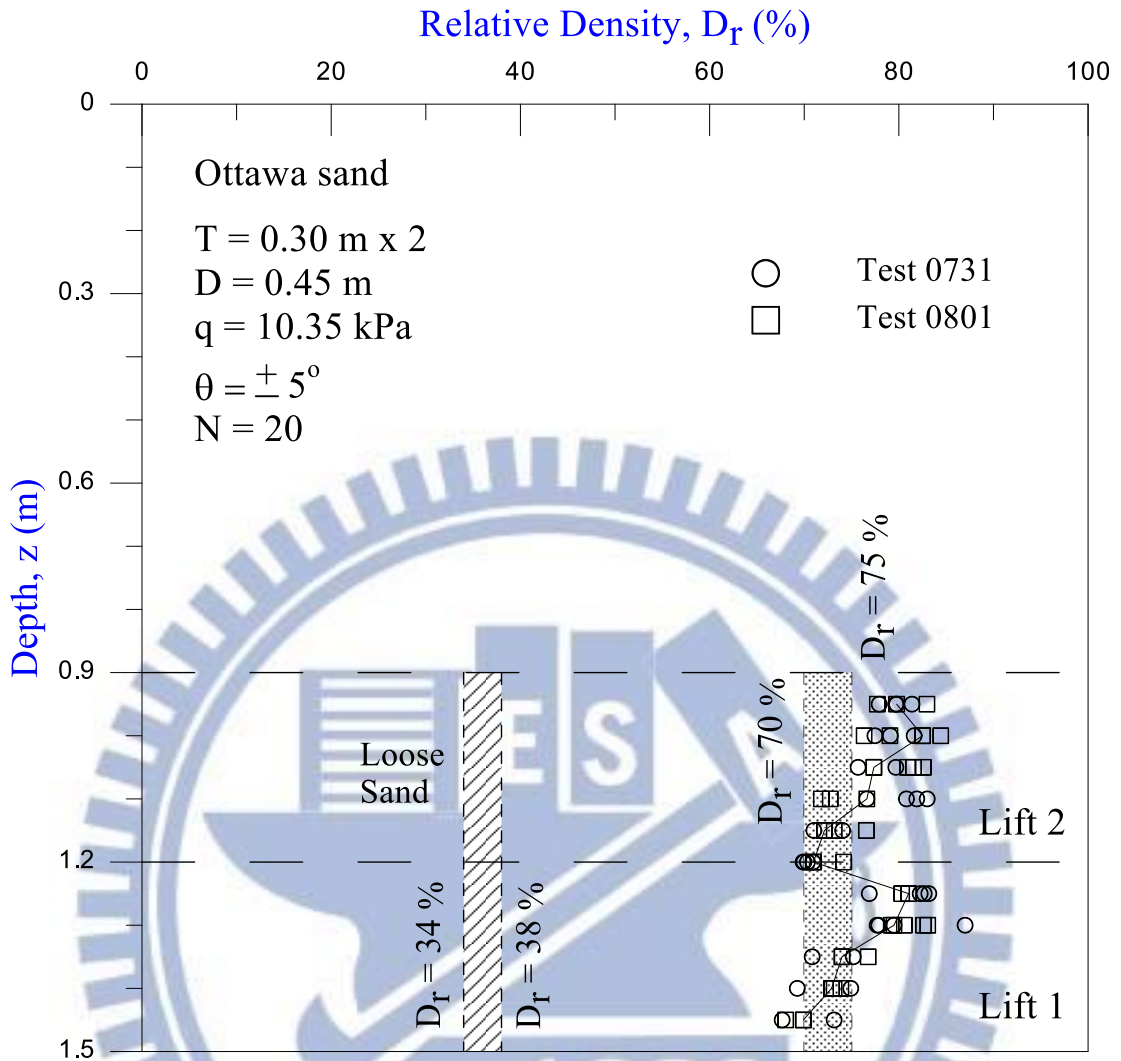
Lift 1

Fig. 6.45 Distribution of elevation density in Lift 1 and 2

169

Relative Density Increment, ΔD_r

Ottawa sand

T = 0.30 m x 2
D = 0.45 m
q = 10.35 kPa
$\theta = \pm 5°$
N = 20

○ Test 0731
□ Test 0801

$D_r = 70\%$

$D_r = 75\%$

(a)

Relative Density Increase Ratio, RDIR

Ottawa sand

T = 0.30 m x 2
D = 0.45 m
q = 10.35 kPa
$\theta = \pm 5°$
N = 20

○ Test 0731
□ Test 0801

$D_r = 70\%$

$D_r = 75\%$

(b)
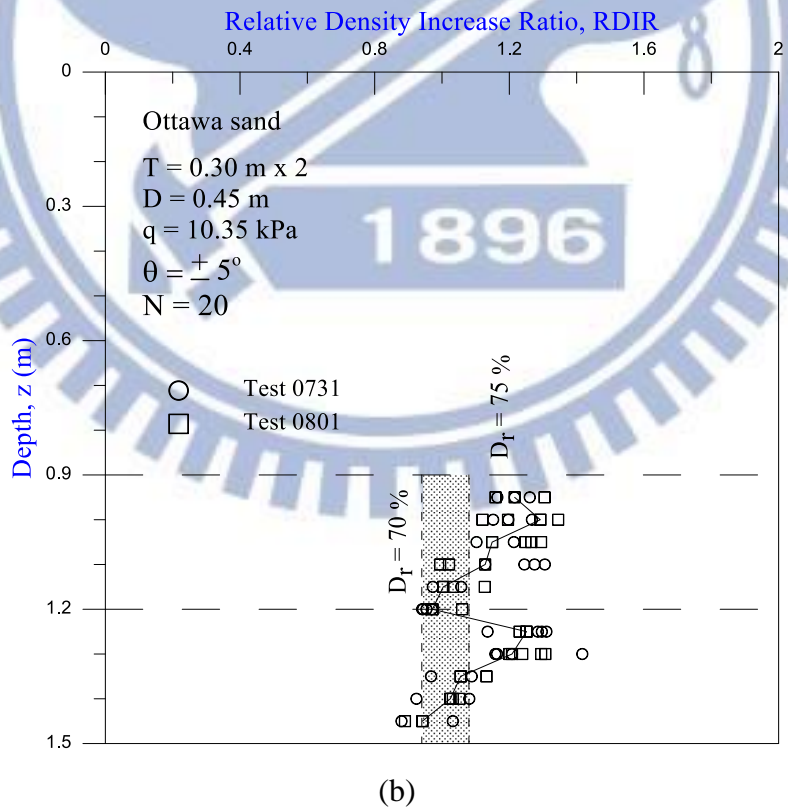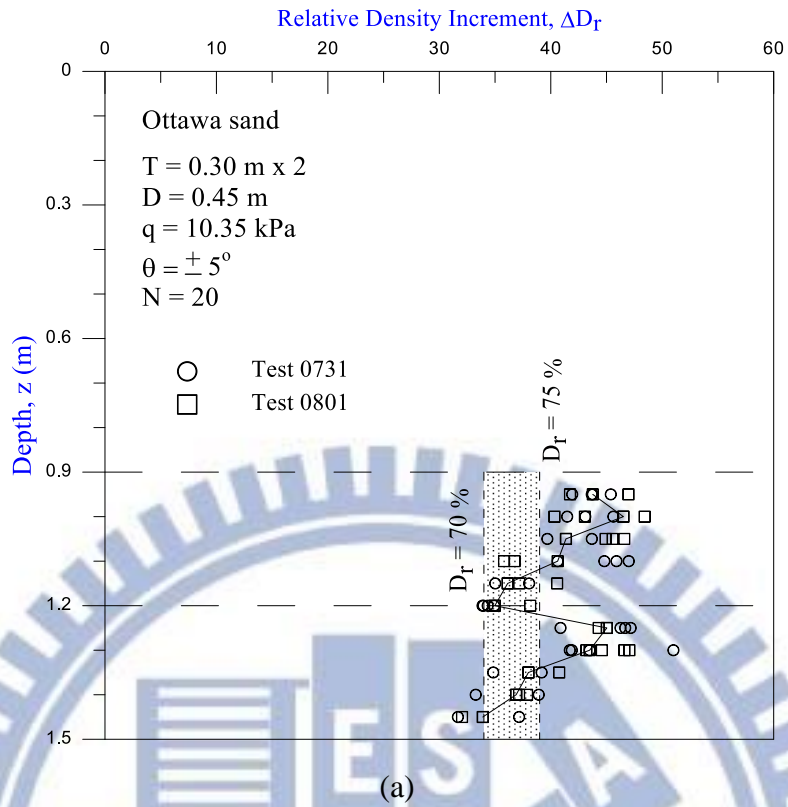
Fig. 6.46. Change of density after shearing compaction for N = 20 in Lift 1 and 2
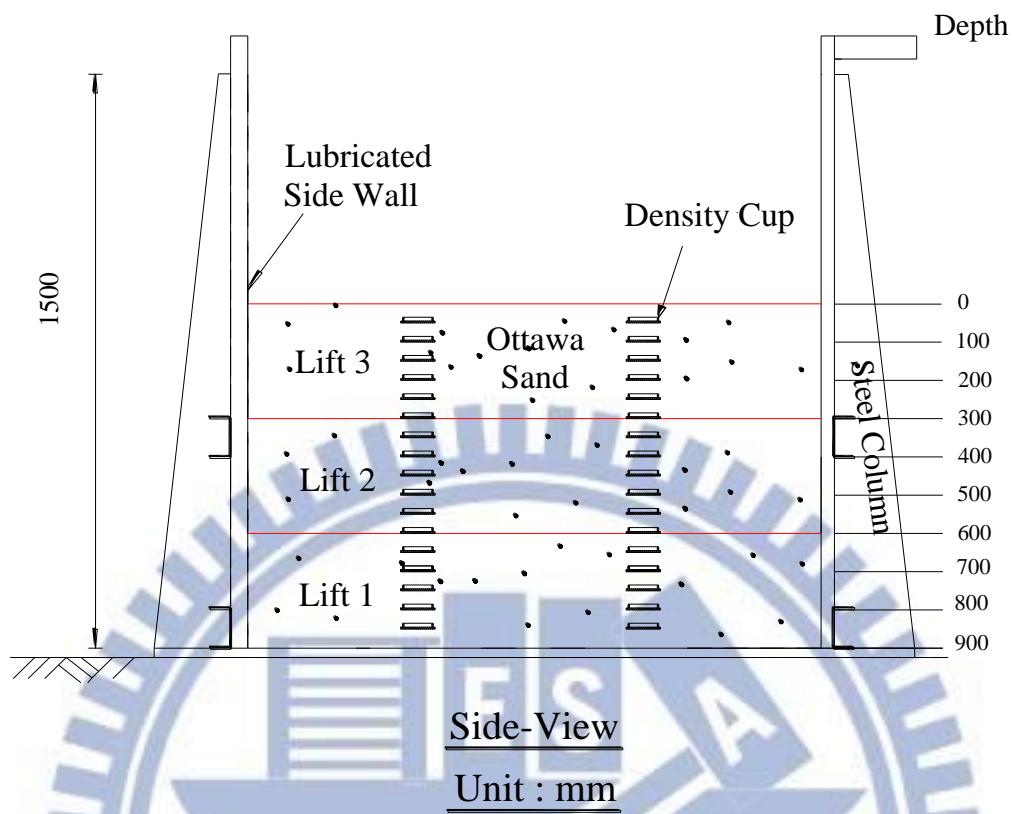
Fig. 6.47. Soil density cups buried at different elevations in Lifts 1 to 3

171
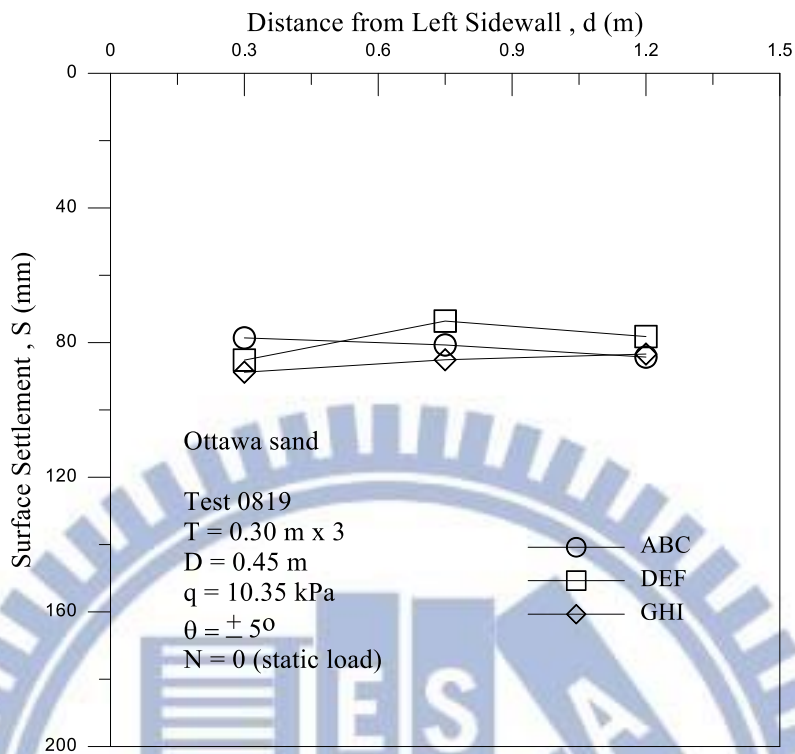
(a) Surface settlement after static load on Lift 3
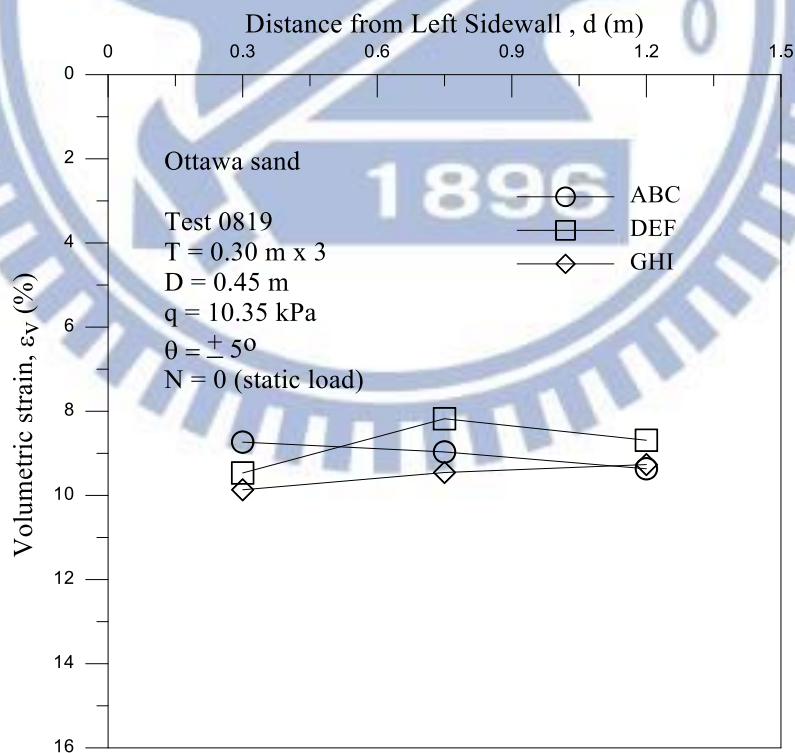
(b) Volumetric strain after static load on Lift 3

Fig. 6.48. Surface settlement and Volumetric strain after static load on Lifts 3

172
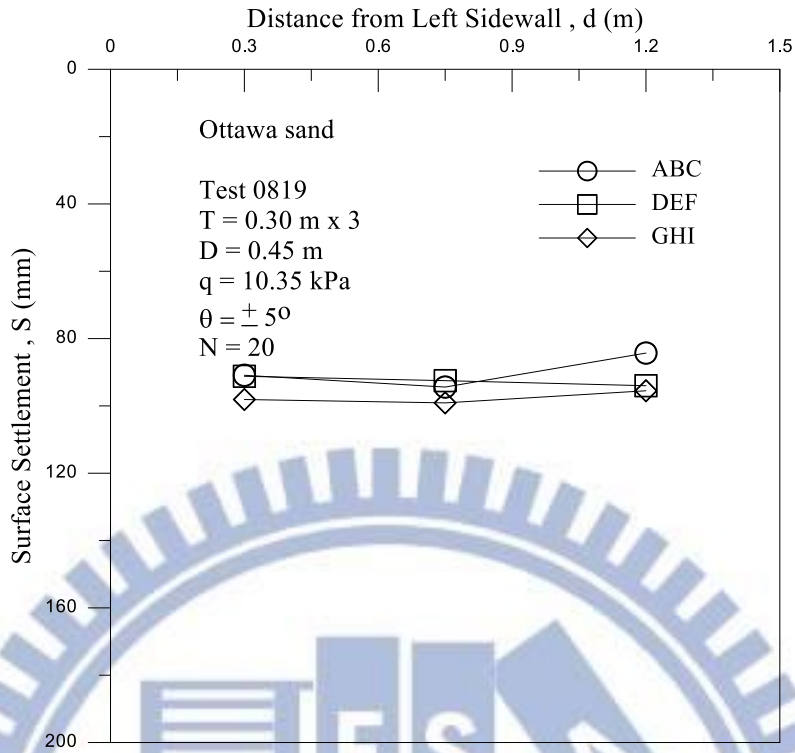
(a) Surface settlement after shearing compaction for N = 20 on Lift 3
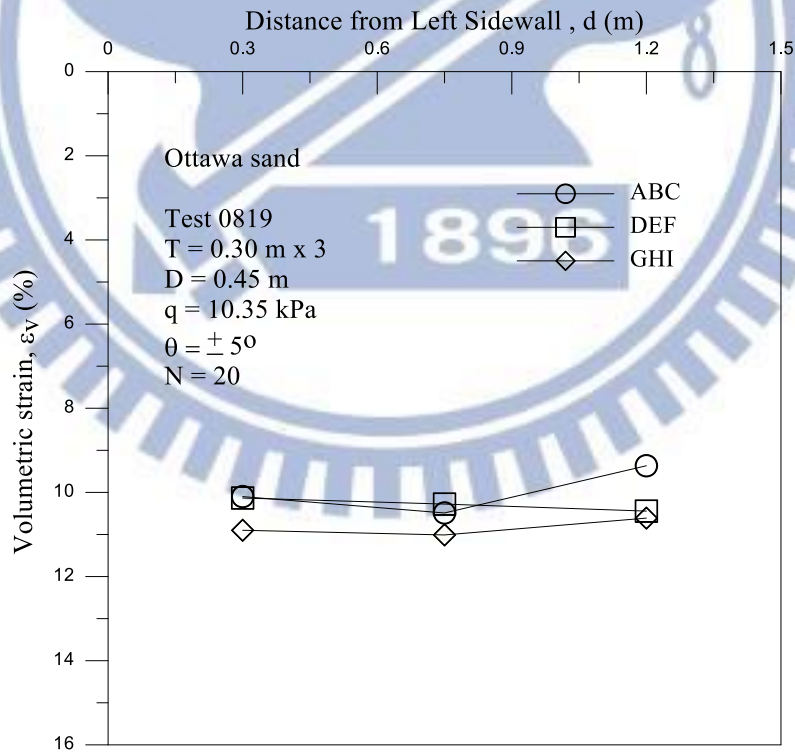
(b) Volumetric strain after shearing compaction for N = 20 on Lift 3

Fig. 6.49. Surface settlement and Volumetric strain after shearing compaction for N = 20 on Lift 3
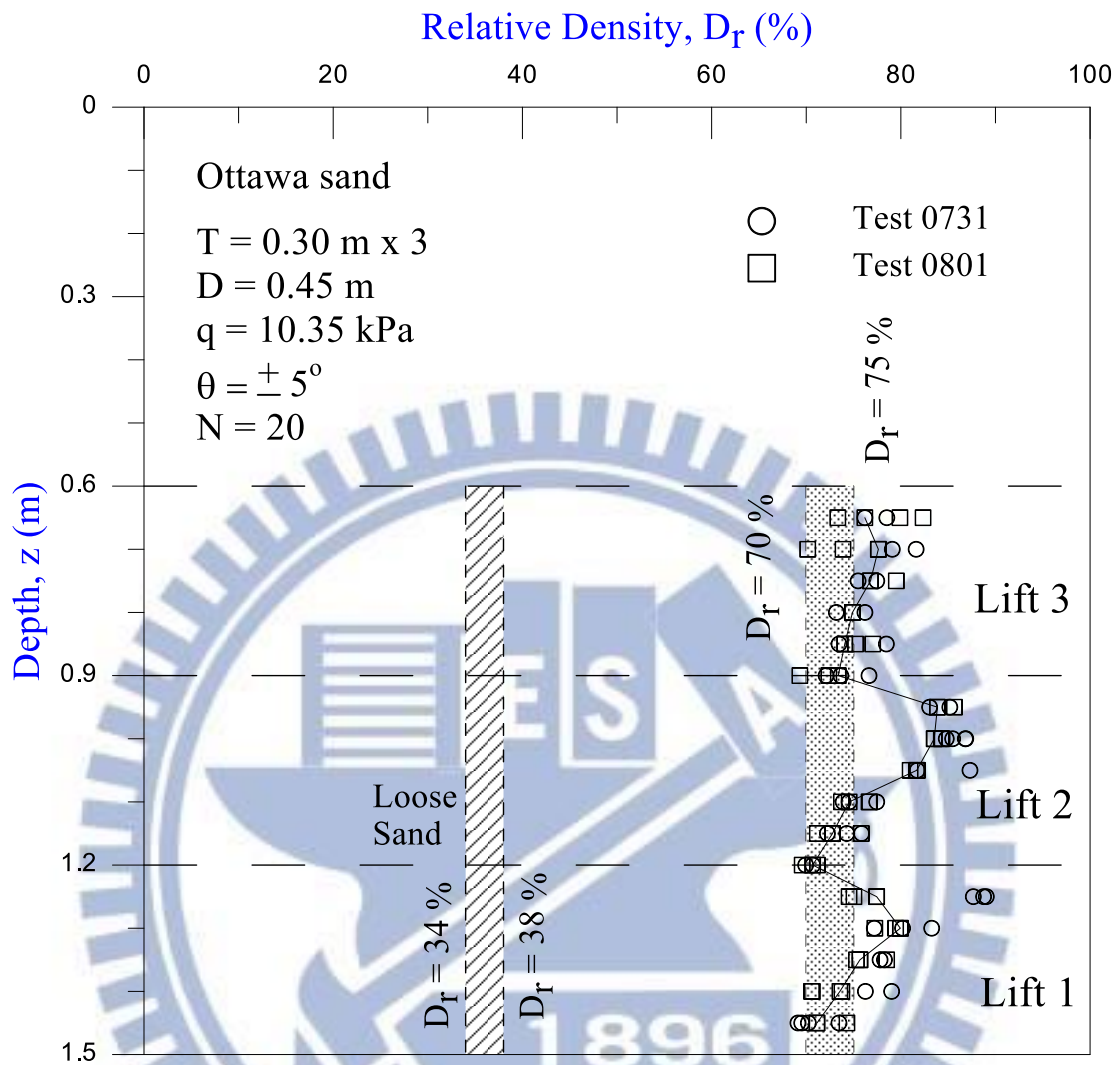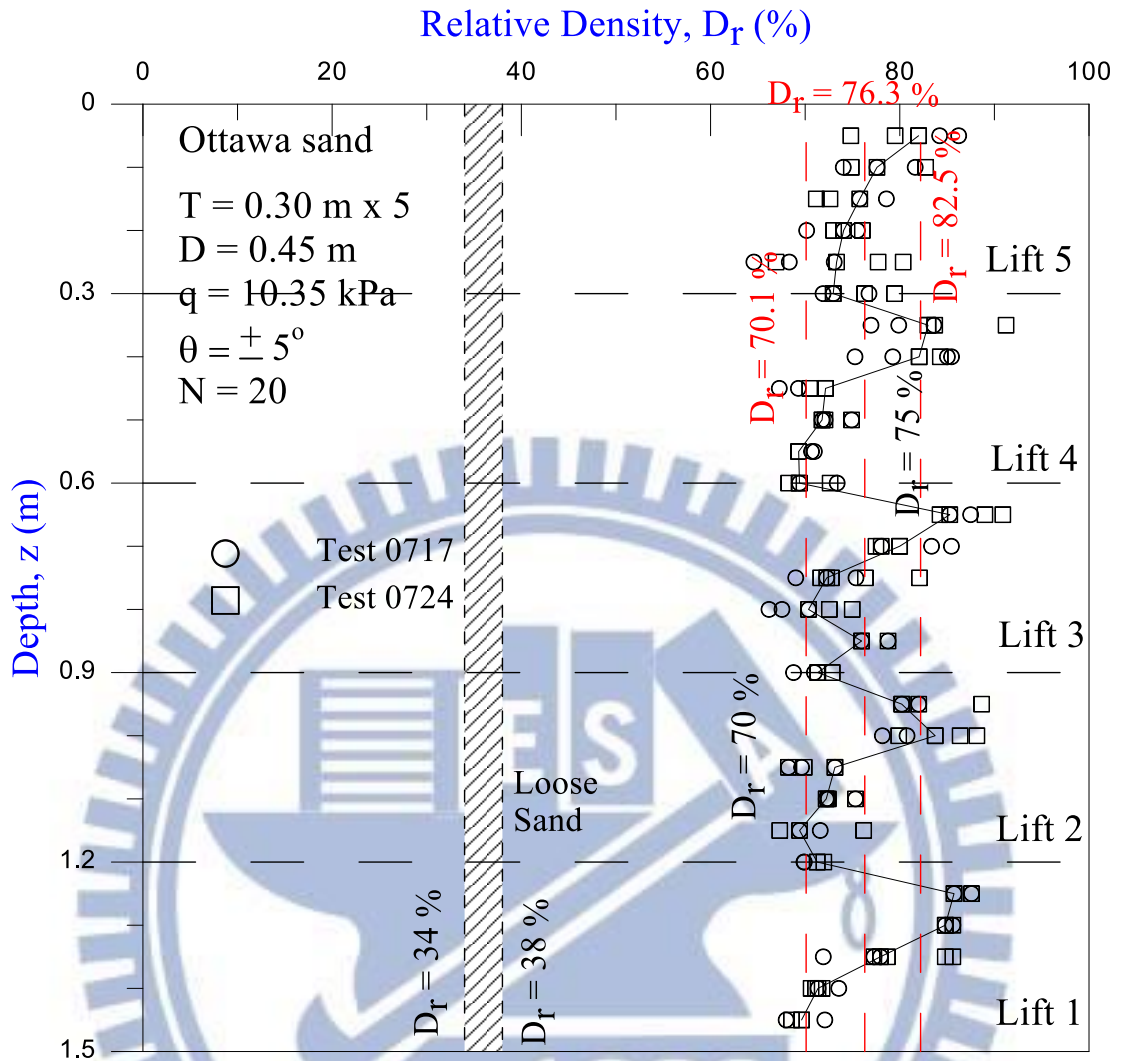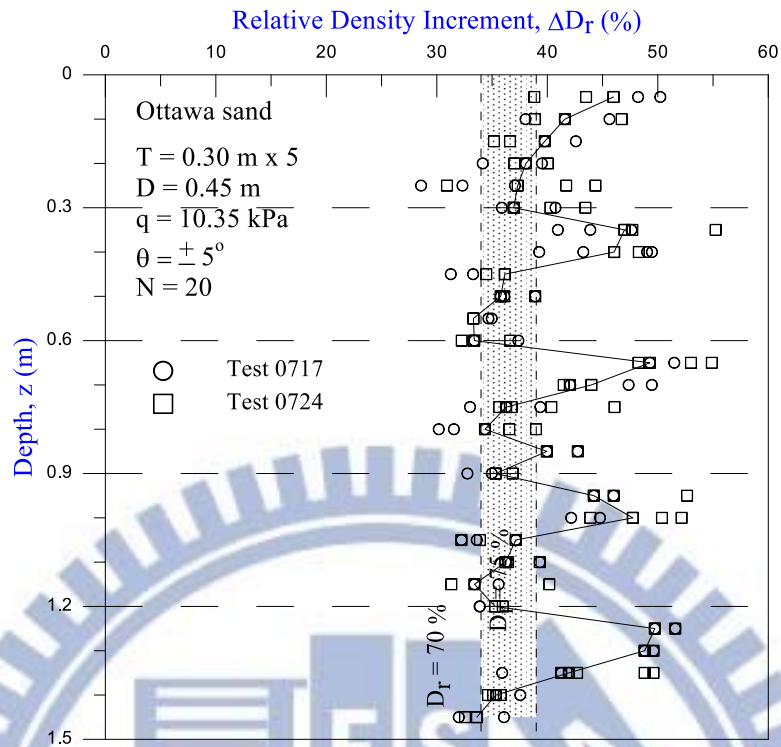
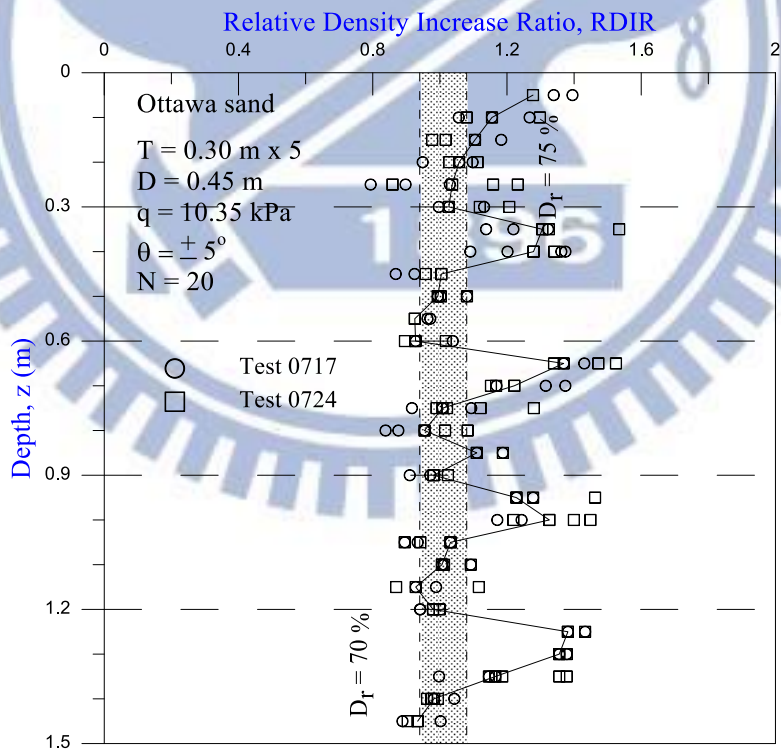Fig. 6.50. Distribution of relative density in Lift 1 to 3

174
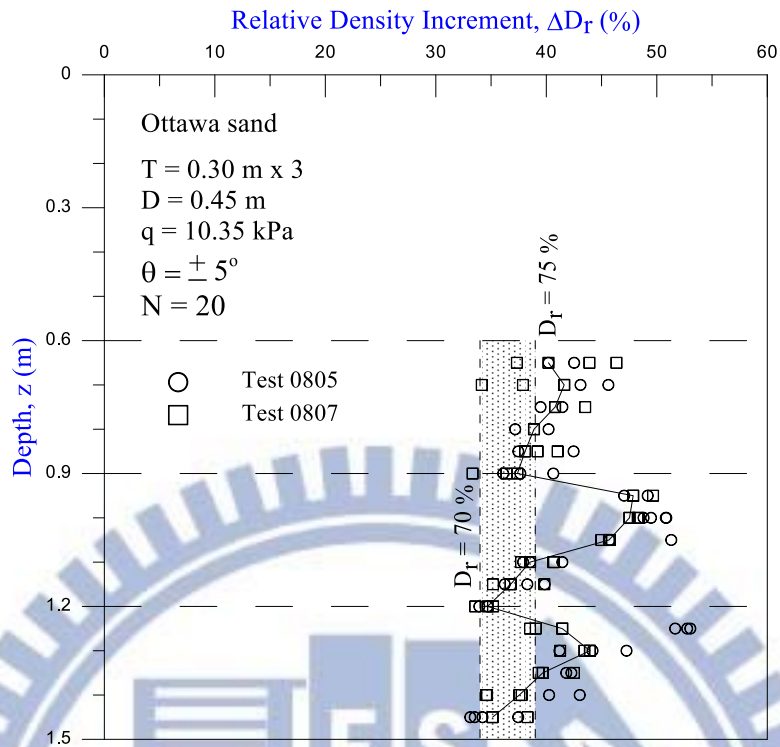
(a)
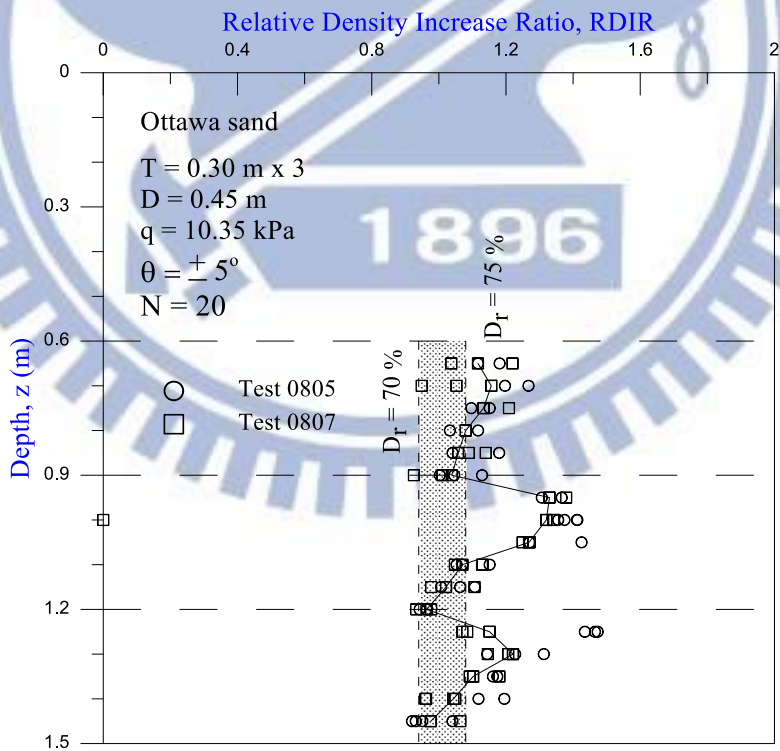
(b)

Fig. 6.51. Change of density after shearing compaction for N = 20 in Lift 1 and 3

Fig. 6.52. Soil density cups buried at different elevations in Lifts 1 to 4

176

(a) Surface settlement after static load on Lift 4

(b) Volumetric strain after static load on Lift 4

Fig. 6.53. Surface settlement and Volumetric strain after static load on Lift 4

(a) Surface settlement after shearing compaction for N = 20 on Lift 4

(b) Volumetric strain after shearing compaction for N = 20 on Lift 4

Fig. 6.54. Surface settlement and Volumetric strain after compaction for N = 20 on Lift 4

Fig. 6.55. Distribution of relative density in Lift 1 to 4

(a)

(b)

Fig. 6.56. Change of density after shearing compaction for N = 20 in Lift 1 to 4

Fig. 6.57. Soil density cups buried at different elevations in Lift 1 to 5

(a) Surface settlement after static load on Lift 5

(b) Volumetric strain static load on Lift 1 to Lift 5

Fig. 6.58. Surface settlement and Volumetric strain after static load on Lift 5
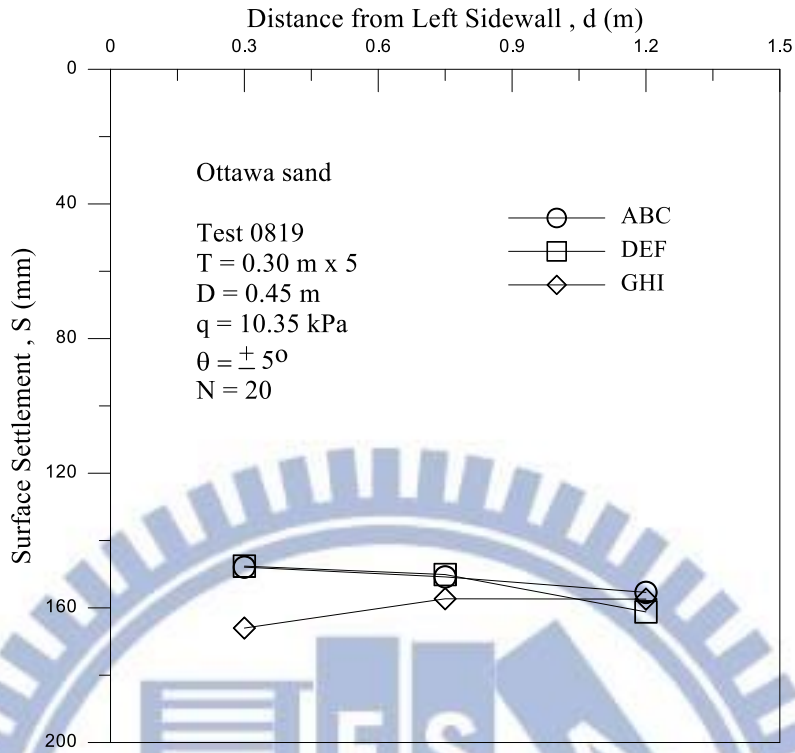
(a) Surface settlement after shearing compaction for N = 20 on Lift 5

(b) Volumetric strain after shearing compaction for N = 20 on Lift 5

Fig. 6.59. Surface settlement and Volumetric strain after shearing compaction for N = 20 on Lift 5
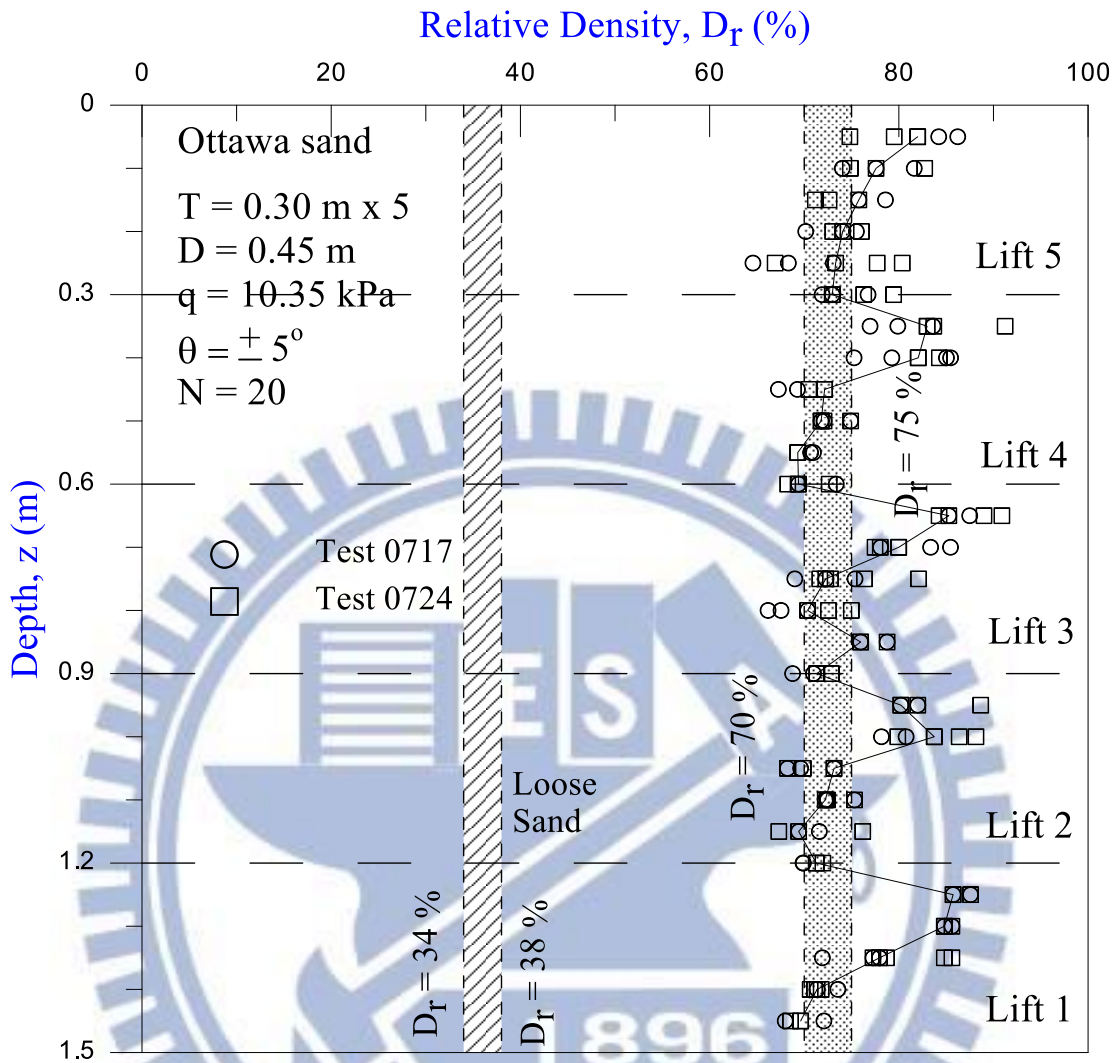
Fig. 6.60. Distribution of relative density in Lift 1 to 5

Fig. 6.61 Distribution of relative density with mean and standard deviation

Ottawa sand

T = 0.30 m x 5
D = 0.45 m
q = 10.35 kPa
θ = ± 5°
N = 20

Depth, z (m)

○ Test 0717
□ Test 0724

$D_r = 70\%$

(a)

Relative Density Increase Ratio, RDIR

Ottawa sand

T = 0.30 m x 5
D = 0.45 m
q = 10.35 kPa
θ = ± 5°
N = 20

Depth, z (m)

○ Test 0717
□ Test 0724

$D_r = 70\%$

(b)

Fig. 6.62. Change of density due to cyclic torsional shearing in Lift 1 to 5
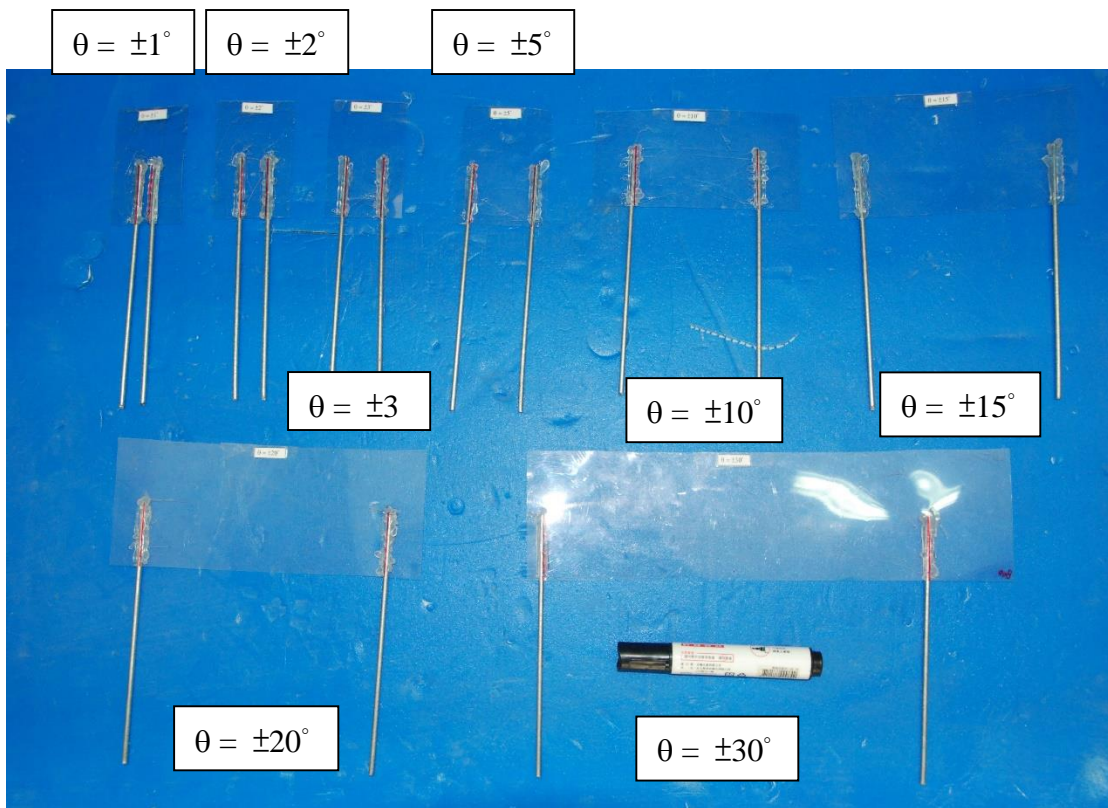
Fig. 6.63. Controllers for different shearing angles
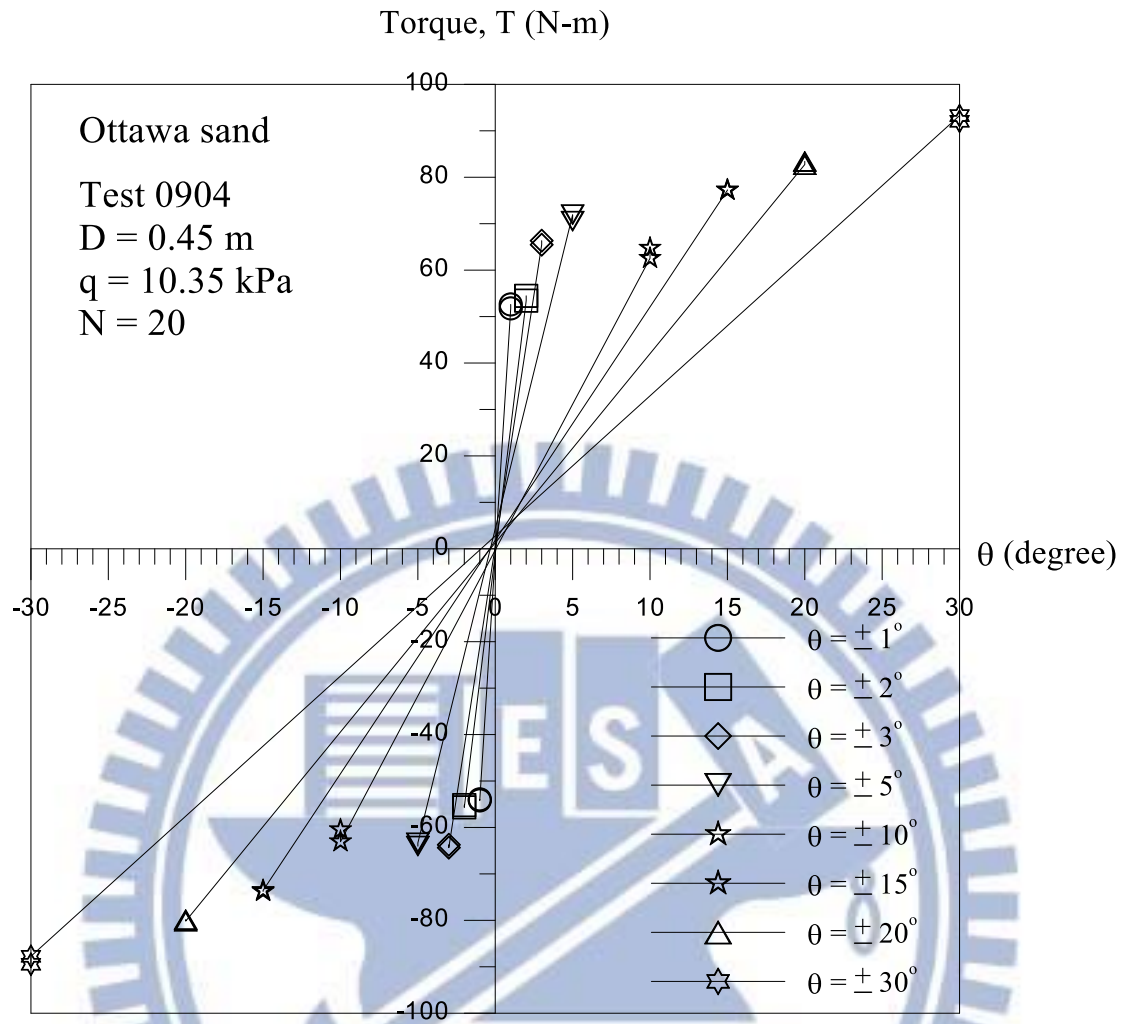
Fig. 6.64. Variation of torque T for different shearing angles
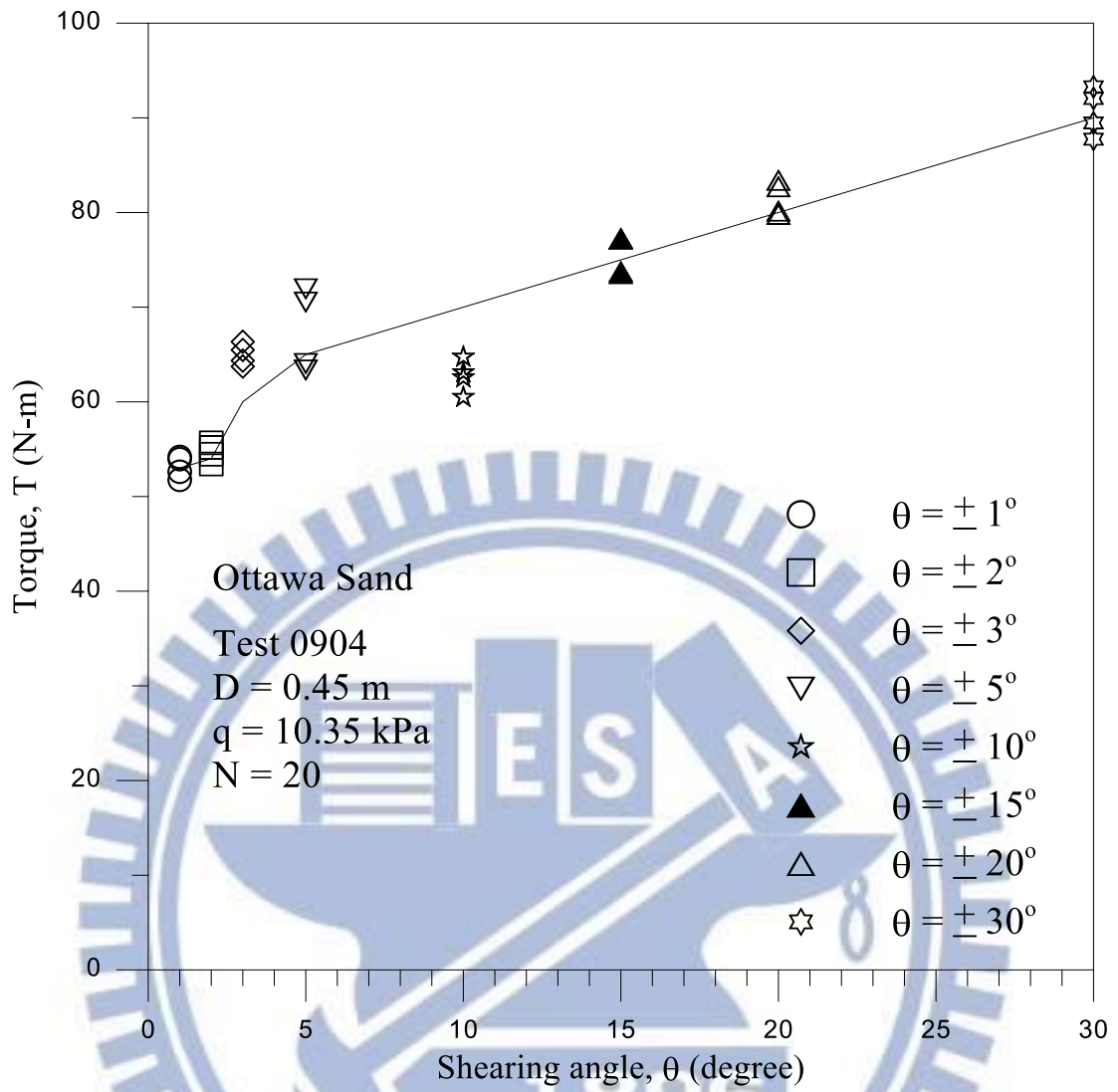
Fig. 6.65. Variation of torque T for different shearing angles
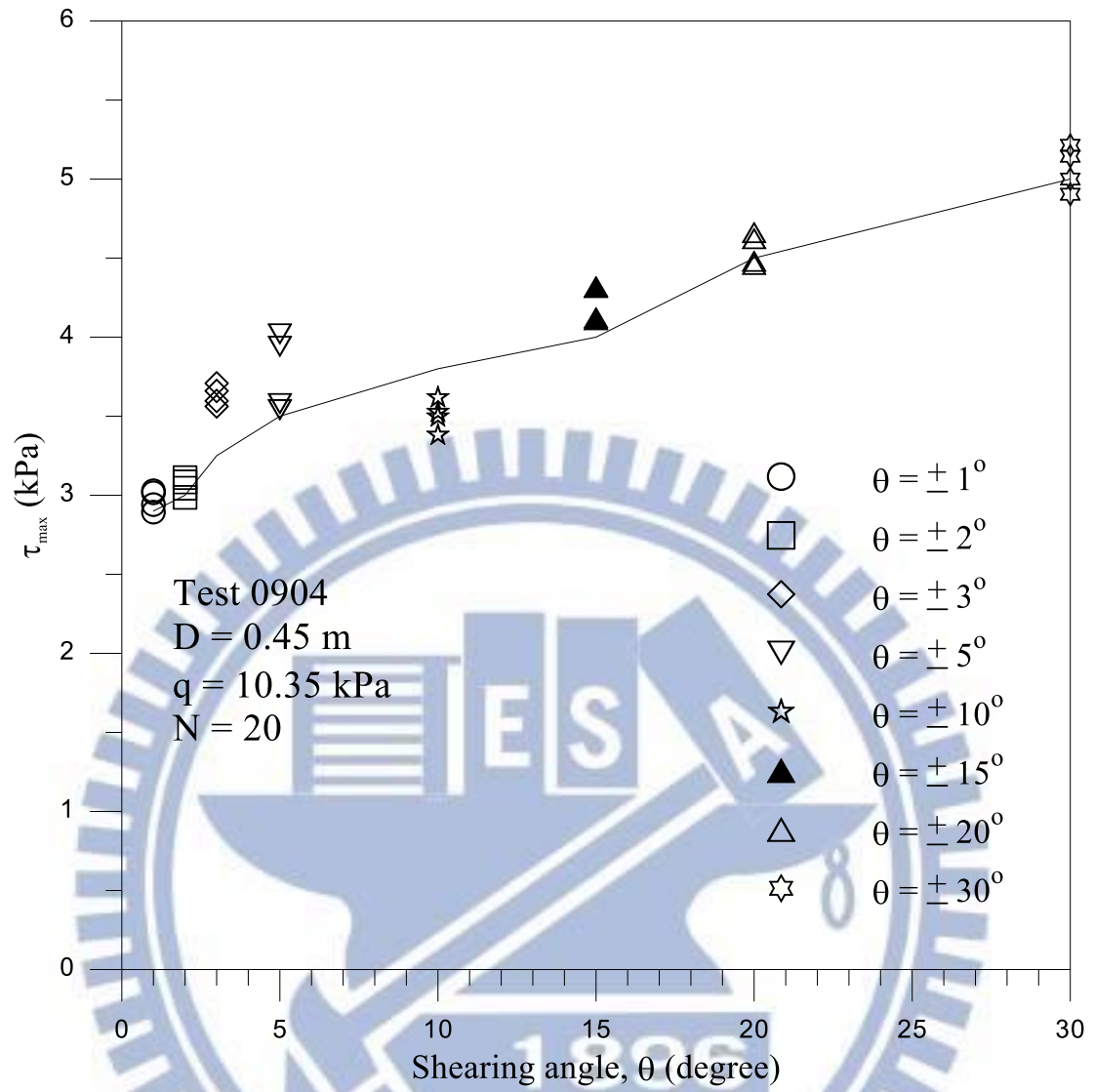
Fig. 6.66. Maximum shear stress for shearing angles

Distance from Left Sidewall , d (m)

Surface Settlement , S (mm)

Ottawa sand

T = 1.50 m
D = 0.45 m
q = 10.35 kPa
static load only

○ Test 0902-ABC
□ Test 0902-DEF
◇ Test 0902-GHI
▽ Test 0904-ABC
☆ Test 0904-DEF
▲ Test 0904-GHI

(a) Surface settlement

Distance from Left Sidewall , d (m)

Volumetric strain, ε_V (%)

Ottawa sand

T = 1.50 m
q = 10.35 kPa
static load only

○ Test 0902-ABC
□ Test 0902-DEF
◇ Test 0902-GHI
▽ Test 0904-ABC
☆ Test 0904-DEF
▲ Test 0904-GHI
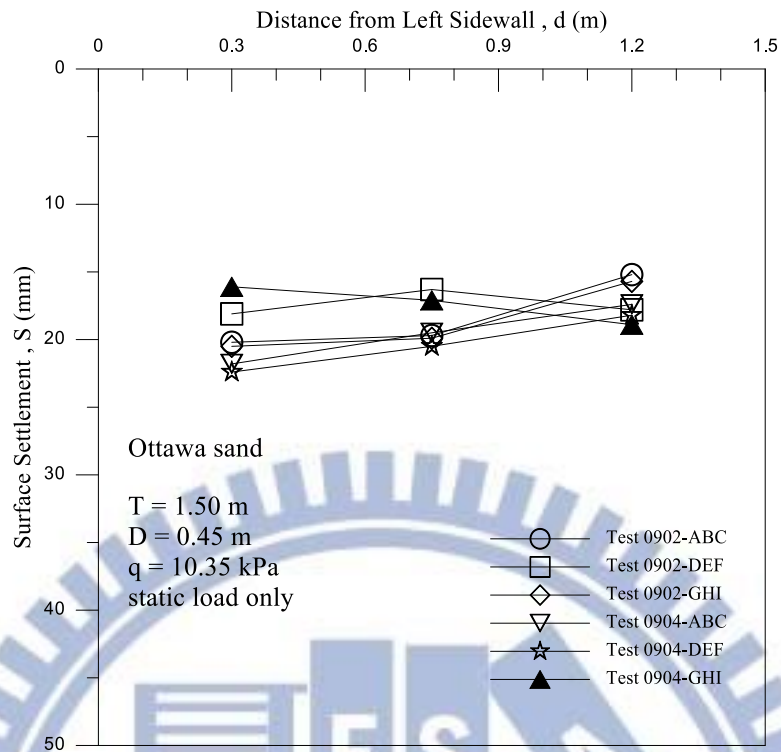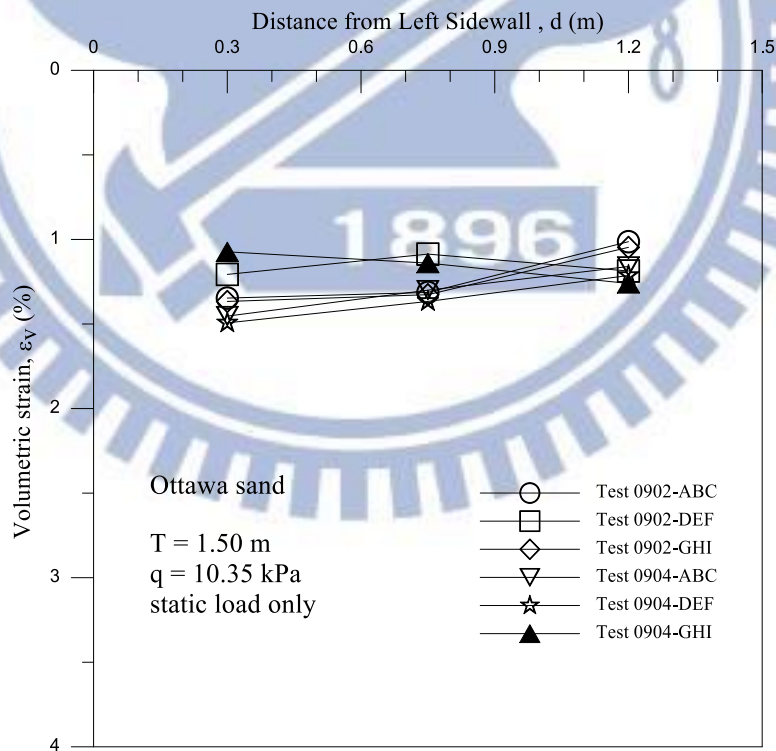
(b) Volumetric strain

Fig. 6.67. Surface settlement and Volumetric strain due to static vertical load
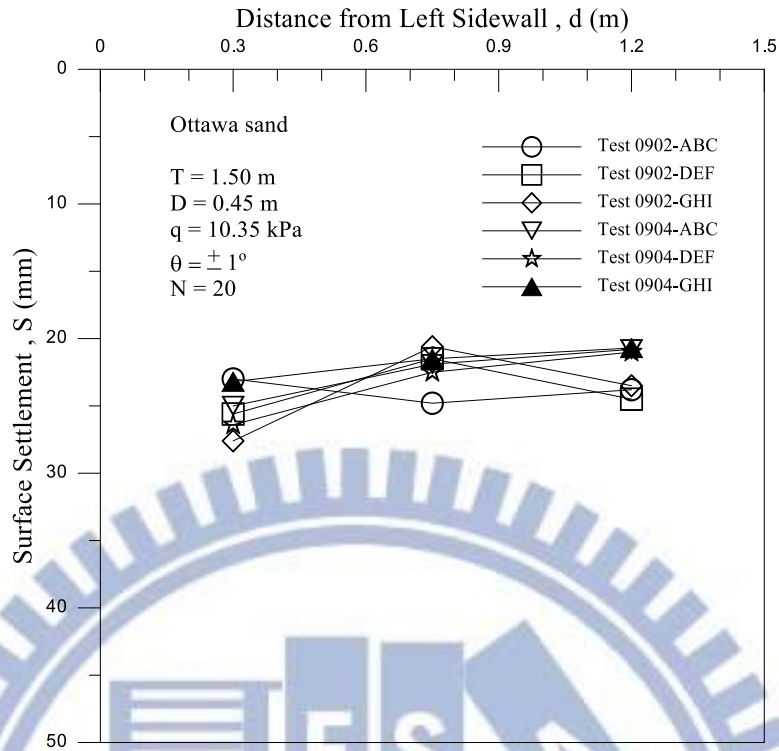
(a) Surface settlement
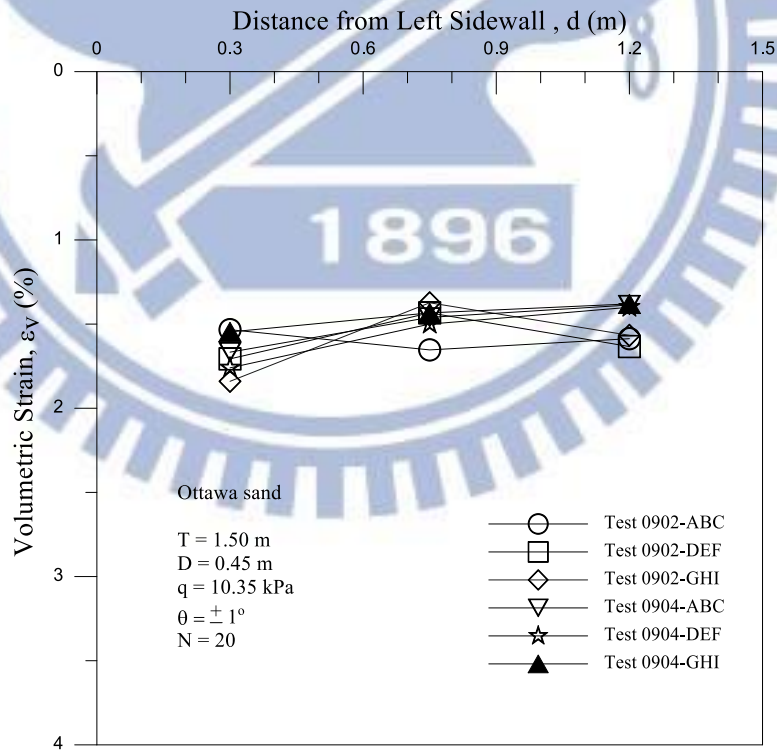
(b) Volumetric strain

Fig. 6.68. Surface settlement and Volumetric strain due to shearing angle
$\theta = \pm 1°$

192
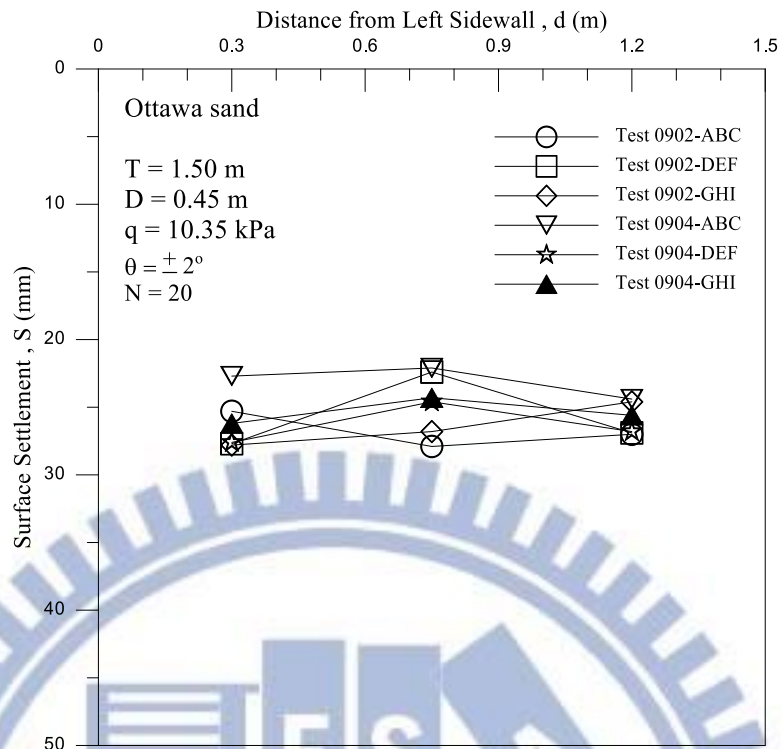
(a) Surface settlement
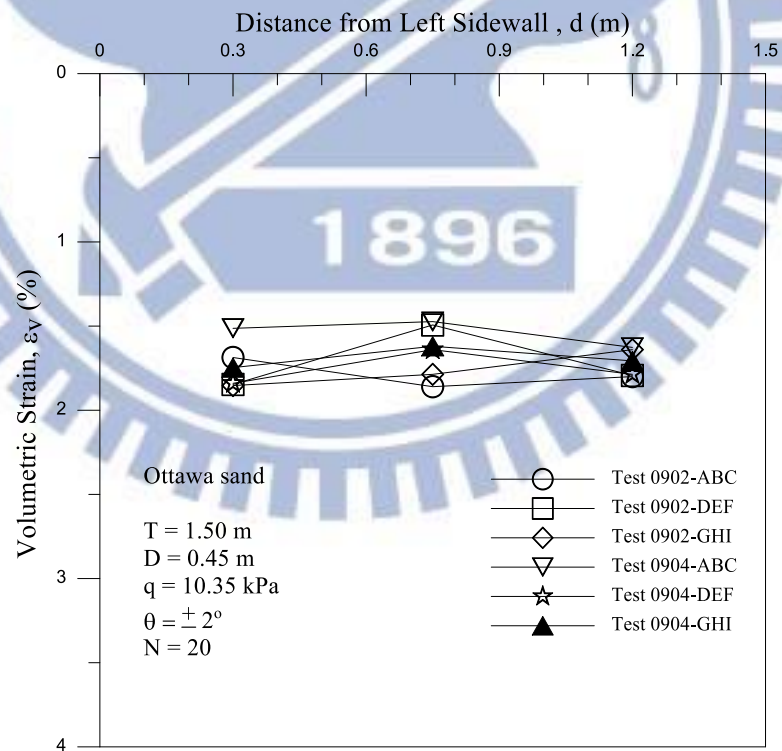
(b) Volumetric strain

Fig. 6.69. Surface settlement and Volumetric strain due to shearing angle $\theta = \pm 2°$

193
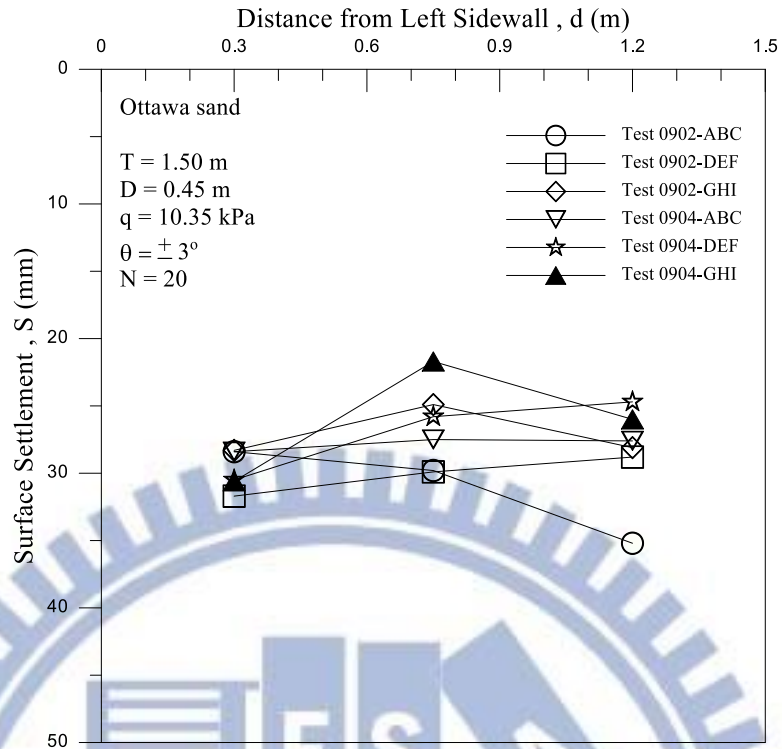
(a) Surface settlement
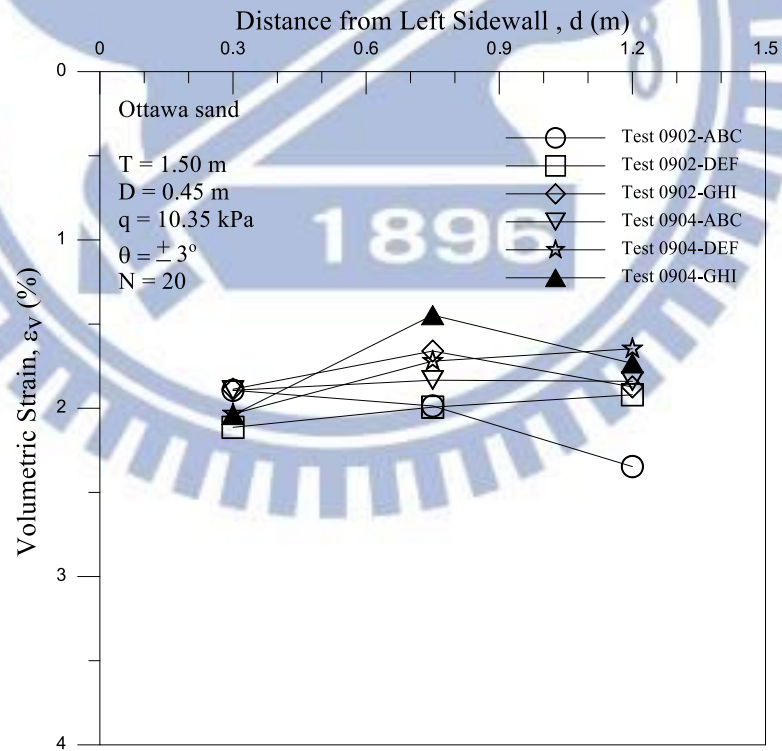
(b) Volumetric strain

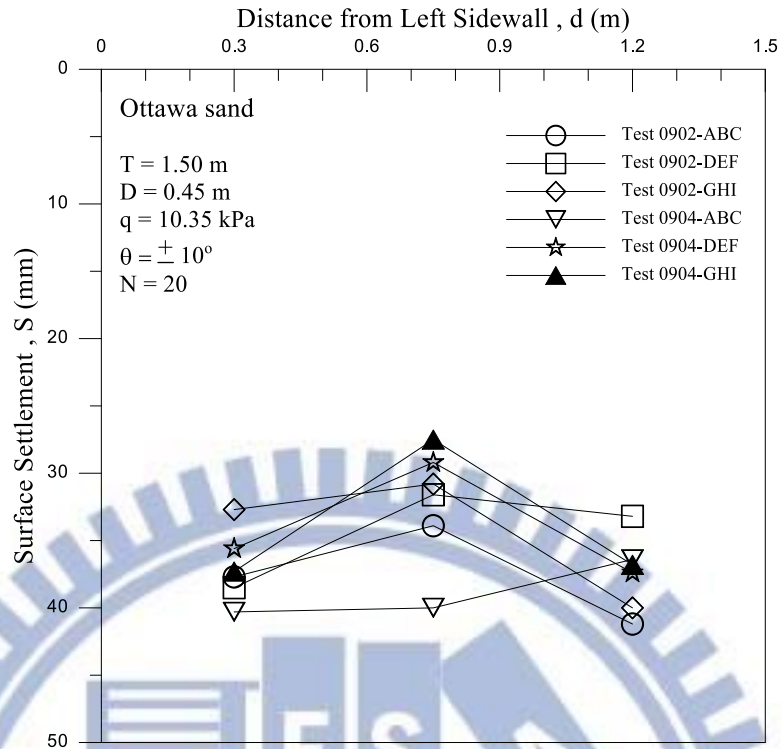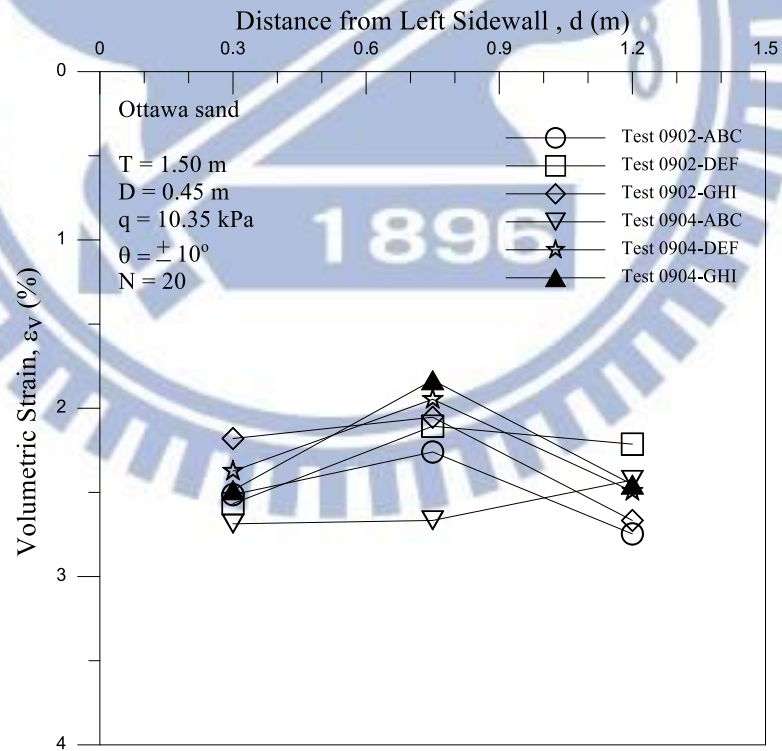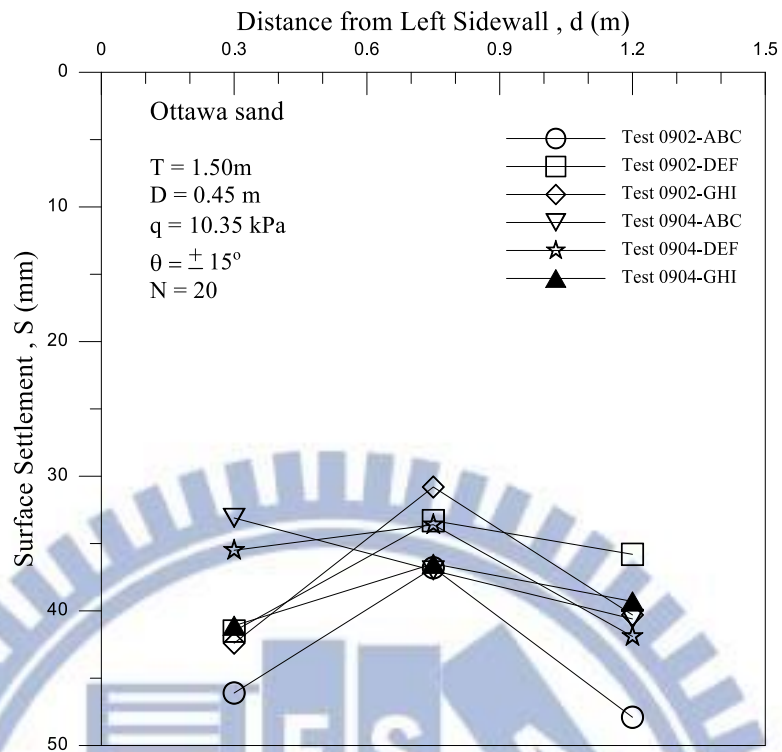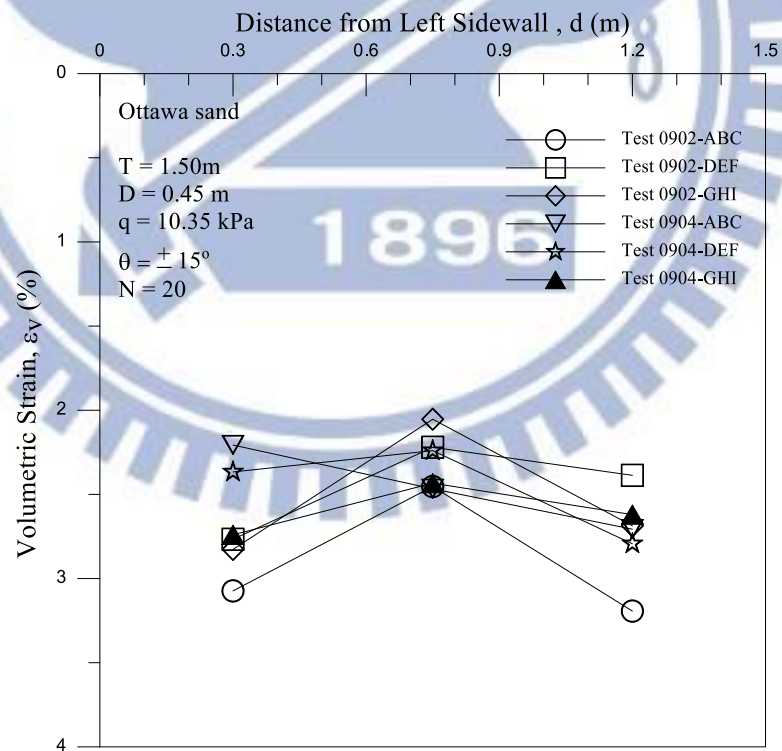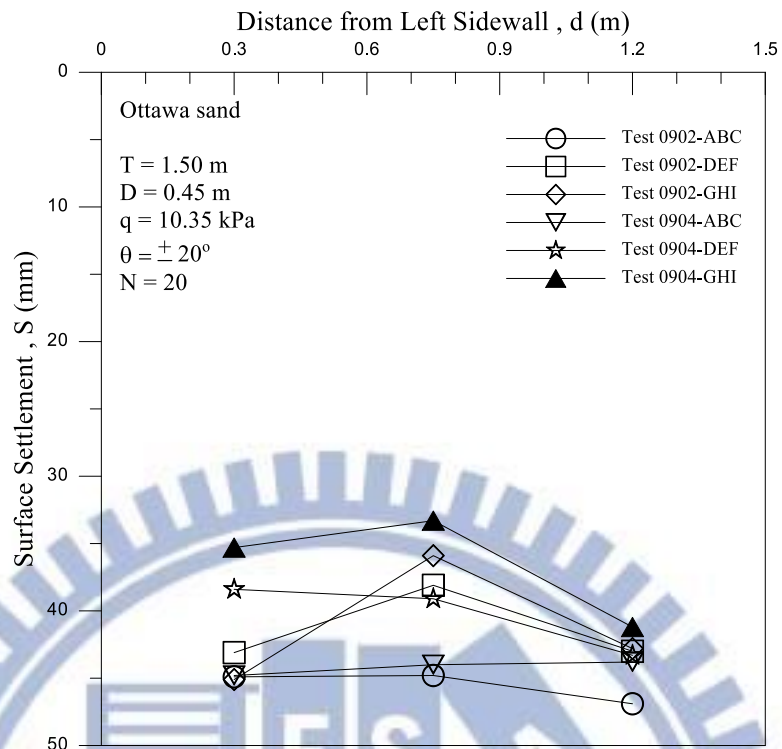Fig. 6.70. Surface settlement and Volumetric strain due to shearing angle
$\theta = \pm 3°$

Distance from Left Sidewall , d (m)

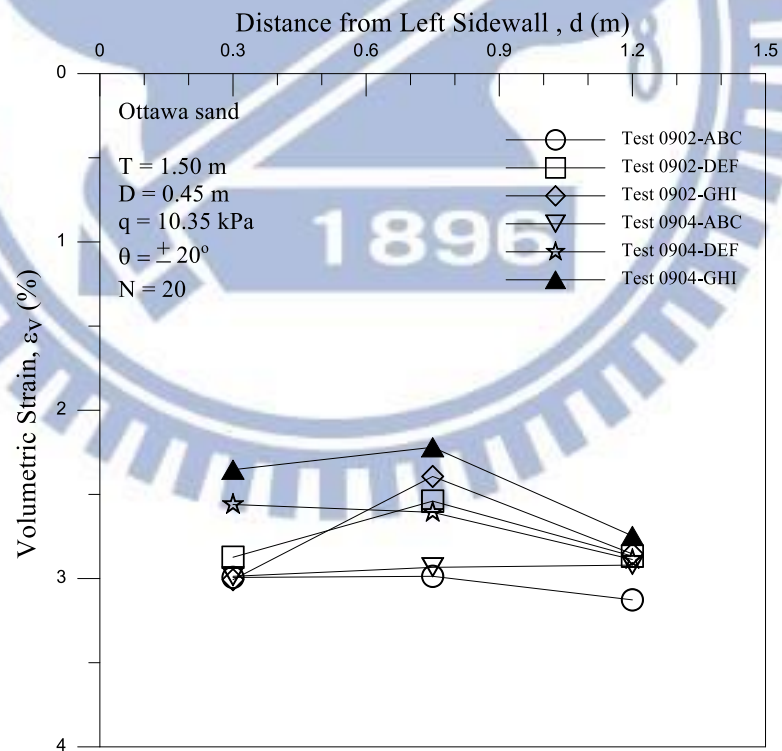(a) Surface settlement

Distance from Left Sidewall , d (m)
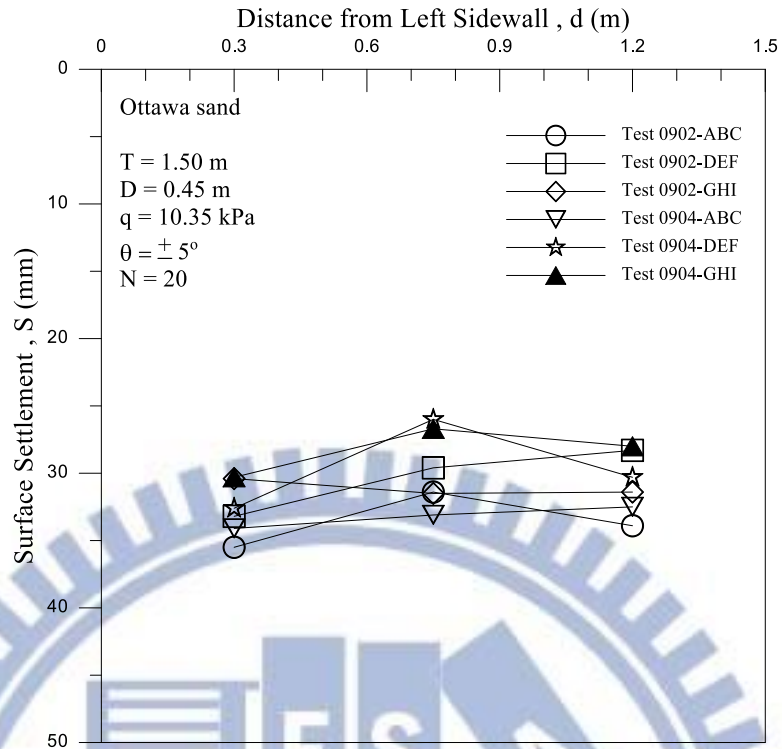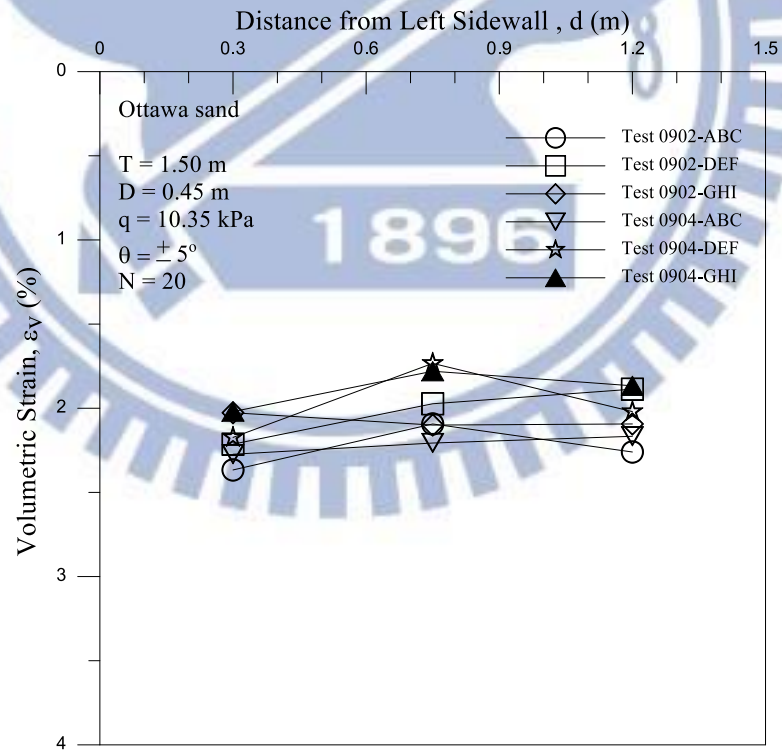
(b) Volumetric strain

Fig. 6.71. Surface settlement and Volumetric strain due to shearing angle

$\theta = \pm 5°$

195

(a) Surface settlement

(b) Volumetric strain

Fig. 6.72. Surface settlement and Volumetric strain due to shearing angle
$\theta = \pm 10°$

196

(a) Surface settlement

(b) Volumetric strain

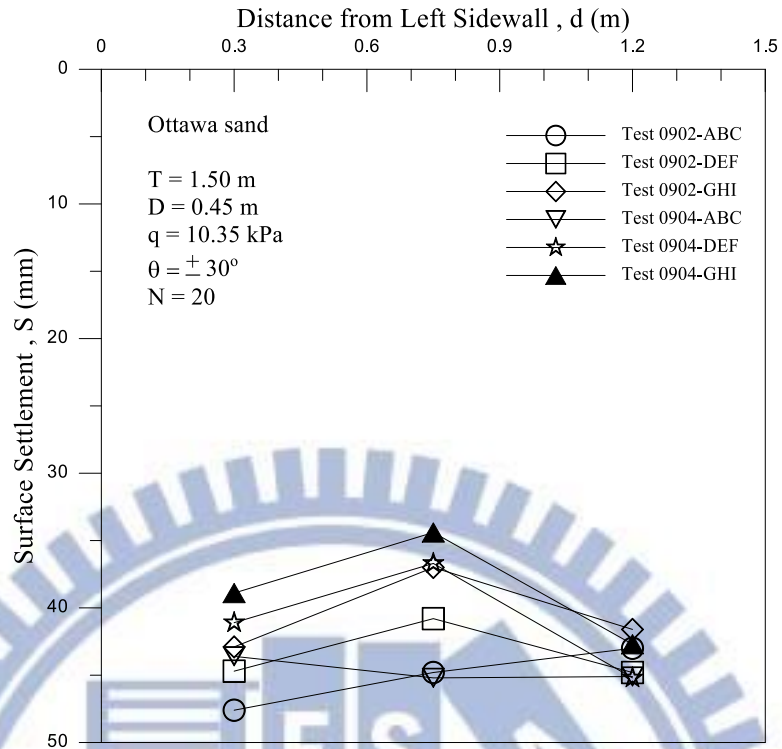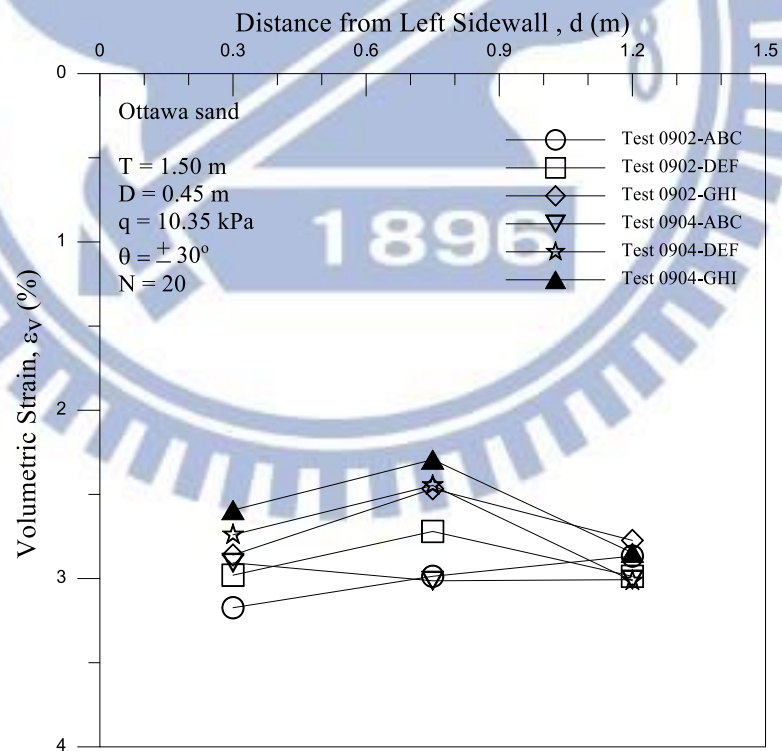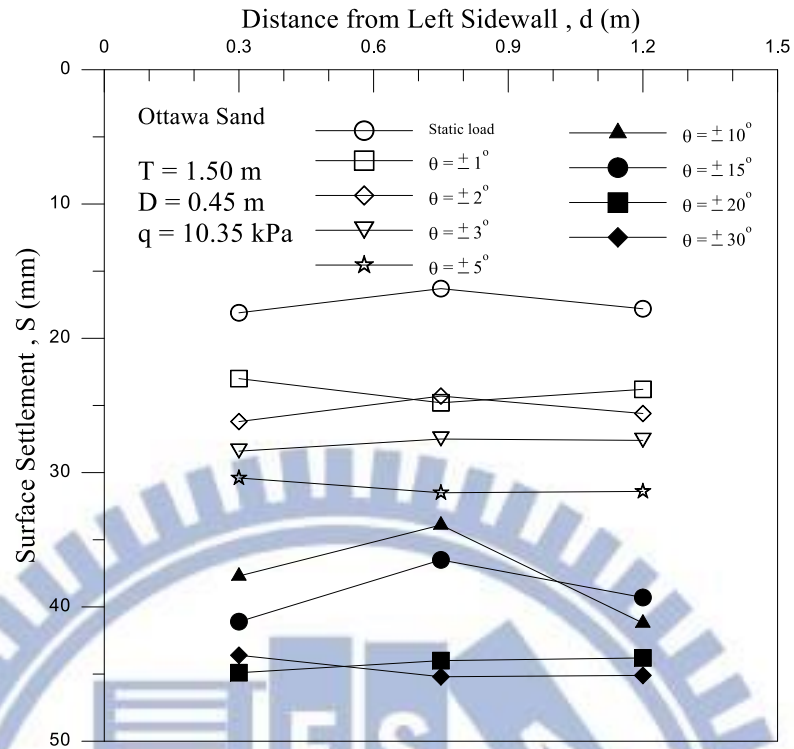Fig. 6.73. Surface settlement and Volumetric strain due to shearing angle
$\theta = \pm 15°$

197

Distance from Left Sidewall , d (m)

(a) Surface settlement

Distance from Left Sidewall , d (m)

(b) Volumetric strain

Fig. 6.74. Surface settlement and Volumetric strain due to shearing angle
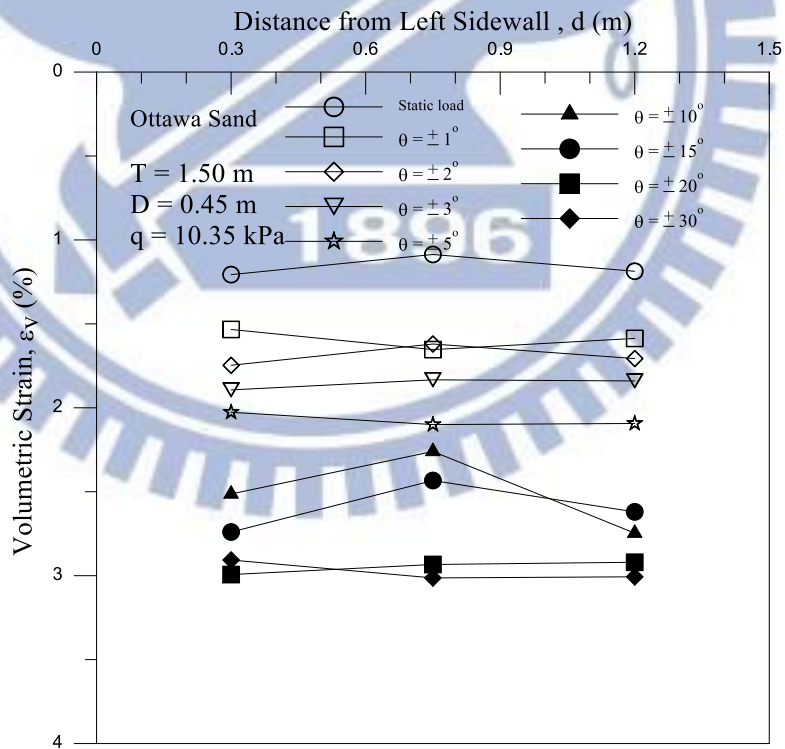
$\theta = \pm 20°$

(a) Surface settlement

(b) Volumetric strain

Fig. 6.75. Surface settlement and Volumetric strain due to shearing angle
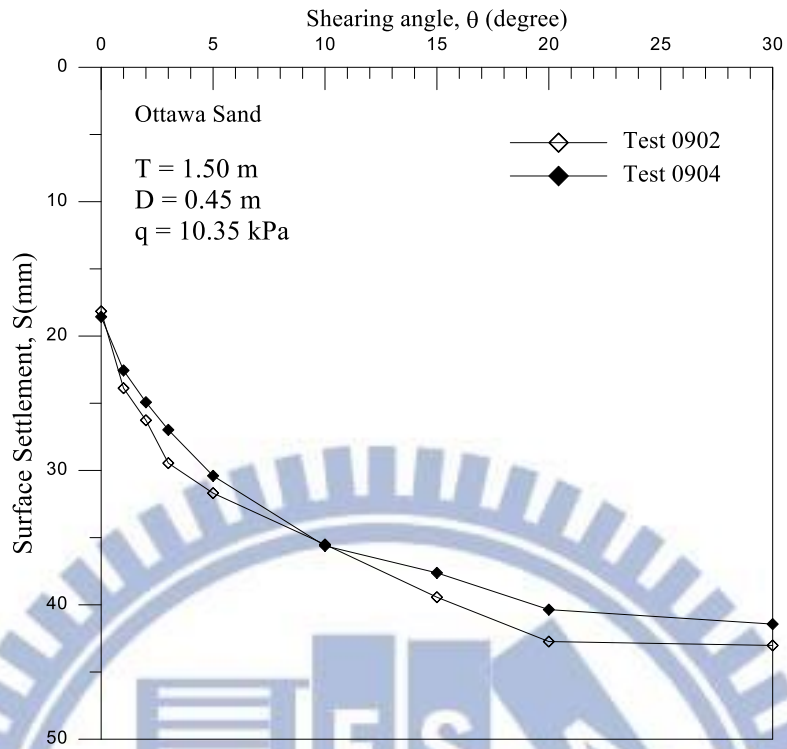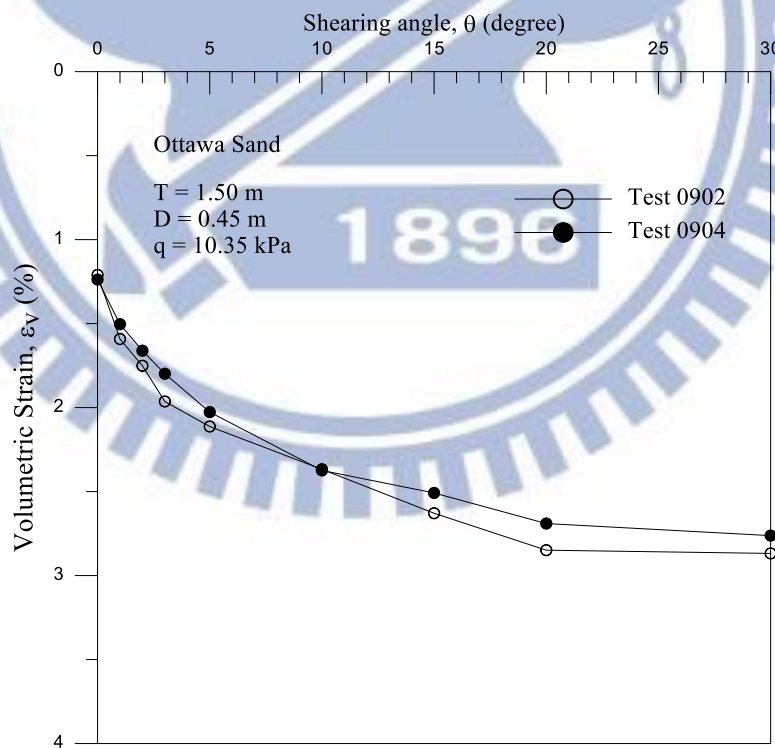$\theta = \pm 30°$

199

(a) Surface settlement

(b) Volumetric strain

Fig. 6.76. Variation of surface settlement and volumetric strain for θ = 1 to 30

200

(a) Surface settlement for θ = 1 to 30

(b) Volumetric strain for θ = 1 to 30

Fig. 6.77. Variation of surface settlement and volumetric strain for θ = 1 to 30